Dehydration of Methanol and Ethanol over Silica-Supported Heteropoly Acids in the Gas Phase

Thesis submitted in accordance with the requirements of the University of Liverpool for the degree of Doctor in Philosophy by

Rawan Abdullah Al-Faze

April 2022

Abstract

Dehydration of Methanol and Ethanol over Silica-Supported Heteropoly Acids in the Gas Phase

PhD thesis by Rawan Abdullah Al-Faze

Dehydration of methanol (MeOH) to dimethyl ether (DME) and of ethanol (EtOH) to diethyl ether (DEE) and ethene is of significant interest in relation to sustainable development. DME is a multimarket product that has attracted attention as a supplement to liquefied petroleum gas (LPG) and as a clean alternative to diesel. Ethene is the raw material for approximately 30% of all petrochemical products, and DEE is considered an eco-friendly transportation fuel as well as a valuable chemical.

This thesis aims to investigate MeOH and EtOH dehydration over Brønsted solid-acid catalysts based on tungsten Keggin heteropoly acids (HPAs). Dehydration of MeOH to DME and of EtOH to DEE and ethene was investigated at the gas-solid interface in the presence of bulk and SiO_2-supported HPAs ($H_3PW_{12}O_{40}$, (HPW) and $H_4SiW_{12}O_{40}$, (HSiW)) as catalysts. The acid strength, texture and structural integrity of these catalysts were characterised by use of ammonia adsorption calorimetry (NH_3-MC), Brunauer-Emmett-Teller method (BET), X-ray diffraction (XRD) and diffuse reflectance infrared Fourier transform spectroscopy (DRIFTS). The strength of the acid sites in the HPA/SiO_2 catalysts was demonstrated to increase monotonically with the HPA loading up to 100% loading, and HPW catalysts were stronger than HSiW catalysts at any loading. In the dehydration of MeOH and EtOH, the turnover reaction rate for HPW catalysts was higher than for HSiW catalysts, which agrees with their acid strength. Upon increasing HPA loading, alcohol conversion passed a maximum and scaled with the number of HPA surface proton sites rather than with the HPA loading. This

indicated that alcohol dehydration occurred via a mechanism of surface-type HPA catalysis at the gas-solid interface rather than a bulk-type (pseudo-homogeneous) mechanism.

In addition, the conversion of DEE to ethene and EtOH, which is a step in the dehydration of EtOH to ethene, was studied at the gas-solid interface in the presence of bulk and supported HPA catalysts at 130–250 °C and ambient pressure. The catalysts involved HSiW and HPW supported on SiO_2, TiO_2 and ZrO_2, as well as the bulk acidic heteropoly salt CsPW ($Cs_{2.5}H_{0.5}PW_{12}O_{40}$). The DEE elimination process was demonstrated to be of zero order in the DEE partial pressure within the range of 6–24 kPa. The ethene yield increased as the temperature of reaction was increased, reaching 98% at 220–250 °C and weight hourly space velocity (WHSV) of 2.2 h^{-1}. The most active HPA catalysts were silica-supported HPW and HSiW and bulk CsPW salt. The HPA catalysts outperformed zeolites HZSM-5 and ultra stable Y (USY), which have been reported elsewhere. A correlation between catalyst acid strength and catalyst activity was established. This correlation indicates that Brønsted acid sites played a vital role in the elimination of DEE over HPA catalysts. The results suggest that the reaction occurred through consecutive reaction pathways: DEE → C_2H_4 + EtOH followed by EtOH → C_2H_4 + H_2O. In this scheme, ethene is both a primary product of DEE elimination and a secondary product via dehydration of the primary product EtOH. The work provided evidence that DEE elimination over bulk HPA and high-loaded HPA/SiO_2 catalysts proceeded via a surface-type mechanism.

List of publications

Published articles

- R. Al-Faze, A. Finch, E.F. Kozhevnikova, I.V. Kozhevnikov, Dehydration of methanol and ethanol over silica-supported heteropoly acids in the gas phase: Surface-type versus bulk-type catalysis mechanism, Appl. Catal. A: Gen. 597 (2020) 117549.
- R. Al-Faze, E.F. Kozhevnikova, I.V. Kozhevnikov, Diethyl ether conversion to ethene and ethanol catalysed by heteropoly acids, ACS Omega 6 (2021) 9310–9318.

Conference presentations

- R. Al-Faze, E.F. Kozhevnikova, I.V. Kozhevnikov, The 7th EuCheMS Chemistry Congress, ACC Liverpool, United Kingdom, August 2018.
- R. Al-Faze, E.F. Kozhevnikova, I.V. Kozhevnikov, The 6th UK Catalysis Conference 2019 (UKCC2019), Loughborough, United Kingdom, January 2019.
- R. Al-Faze, E.F. Kozhevnikova, I.V. Kozhevnikov, PhD Symposium Day, Liverpool, United Kingdom, January 2019.
- R. Al-Faze, E.F. Kozhevnikova, I.V. Kozhevnikov, Poster Day of the Faculty of Science & Engineering Research, University of Liverpool, United Kingdom, March 2019.
- R. Al-Faze, E.F. Kozhevnikova, I.V. Kozhevnikov, The 14th International Conference on Materials Chemistry (MC14), University of Birmingham, United Kingdom, July 2019.
- R. Al-Faze, E.F. Kozhevnikova, I.V. Kozhevnikov, The Catalysis: Fundamentals and Practice Summer School, University of Liverpool, United Kingdom, July 2019.
- R. Al-Faze, E.F. Kozhevnikova, I.V. Kozhevnikov, The 5th Edition of Global Conference on Catalysis, Chemical Engineering & Technology, London, United Kingdom, September 2019.

- R. Al-Faze, E.F. Kozhevnikova, I.V. Kozhevnikov, The 7th UK Catalysis Conference 2021 (UKCC2021), Virtual Conference, January 2021.

Acknowledgements

I would like to take this opportunity to offer my gratitude to those who have contributed to the success of this work. The achievement of this work is down to my beloved father. It was his dream to see me succeed in getting the degree, but, unfortunately, he passed away before it came true. At that moment, I felt broken, and it made my journey more challenging to make him sure that I was strong as always by his soul! RIP, my beloved Hero, I have achieved your goal!!

Special thanks go to my principal supervisor, Professor Ivan Kozhevnikov, for his support and encouragement during my research. He offered me unforgettable support and advice. I cannot find words to express my thanks to him. I would also like to give a special thanks to Dr. Elena Kozhevnikova. Thanks go to her for her support and her constructive discussions and comments, which deeply encouraged me towards success.

For considerable support in carrying out this research, I am deeply grateful to the Government of Saudi Arabia, represented by the Ministry of Higher Education, to Taibah University, represented by the College of Science, and to the University of Liverpool. I would also like to give special thanks to my mother, sisters, brothers, and husband for their encouragement, love, support, and prayers-especially to my mother, who always prays for my success. I would also like to thank my colleagues for every moment spent in the lab, seminars, and workshops.

List of abbreviations

BET	Brunauer-Emett-Teller method
BJH	Barrett-Joyner-Halenda method
CHN	Carbon, Hydrogen and Nitrogen microanalysis
CsPW	$Cs_{2.5}H_{0.5}PW_{12}O_{40}$
DEE	Diethyl ether
DME	Dimethyl ether
DRIFTS	Diffuse Reflectance Infrared Fourier Transform Spectroscopy
DSC	Differential Scanning Calorimetry
DTBP	2,6-di-tert-butylpyridine
ECN	Effective Carbon Number
EtOH	Ethanol
FID	Flame Ionisation Detector
FTIR	Fourier Transform Infrared Spectroscopy
GC	Gas Chromatography
HPA	Heteropoly acid
HPW	$H_3PW_{12}O_{40}$
HSiW	$H_4SiW_{12}O_{40}$
HZSM-5	Hydrogen Zeolite Socony Mobil-5
ICP-OES	Inductively Coupled Plasma Optical Emission Spectroscopy
IUPAC	International Union of Pure and Applied Chemistry
MAS NMR	Magic Angle Spinning Nuclear Magnetic Resonance
MC	Microcalorimetry
MeOH	Methanol

TGA	Thermogravimetric Analysis
TOF	Turnover Frequency
USY	Ultra Stable Y
XRD	X-Ray Diffraction

Table of contents

List of figures

List of tables

List of schemes

Chapter 1: Introduction

Chapter 1 : Introduction

1.1. Catalysis

The term catalysis derives from the combination of the Greek prefix "cata" and "lysein", which mean down and split or break, respectively [1,2]. The term was coined by Berzelius in 1836 [1]. Catalysis is a phenomenon that occurs when small amounts of a substance, known as a catalyst, accelerates a chemical reaction without being consumed during the reaction [3–6]. Catalysts can increase the rate of a chemical reaction by providing a more efficient reaction route with a lower activation energy (E_a) (Figure 1.1) [1,3,4]. The use of catalysts does not alter reaction equilibrium or the thermodynamics of the system [1,3,4].

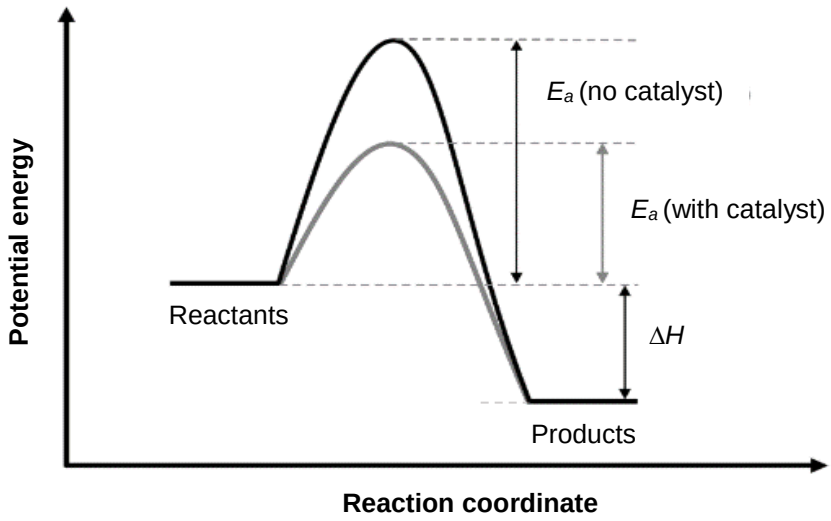

Figure 1.1. A potential energy profile that illustrates the influence of a catalyst on the activation energy of reaction [1].

Catalysis plays a fundamental role in manufacturing, particularly in the chemical and petrochemical industries [7]. In approximately 85% of chemical processes in these industries, catalysts are used to create products such as polymers, fuels, construction supplies, medicines, food and other materials in one or more steps [3,8–10]. In addition, catalysts mitigate the

potential environmental impact of chemical reactions as their involvement leads to removal of the need for hazardous chemicals, minimisation of reaction waste and a reduced demand for toxic or volatile solvents [11].

Generally, catalytic processes are categorised into two main types: heterogeneous and homogeneous [4,5]. In heterogeneous catalysis, the reactants and catalyst are in different phases, whereas in a homogeneous reaction, both the reactants and catalyst are in the same phase [4,8,12]. Numerous industrial processes rely on heterogeneous rather than homogeneous catalysis because the former allows for much easier catalyst treatment, recycling, and separation than the latter, which entails complicated and costly catalyst separation from the reaction mixture [12–15].

1.2. Heterogeneous catalysis

Heterogeneous catalysis occurs at a gas-solid or liquid-solid interface on the surface of a solid catalyst [16]. The first research on heterogeneous catalysis was conducted in the early 1800s [8]. Faraday, a pioneer in this field, studied the facilitation of oxidation reactions through the utilisation of platinum as a heterogeneous catalyst [1,2,8]. Later, various catalytic processes were developed to produce chemicals, pharmaceuticals, polymers and various materials, to generate energy and for other uses [8,17]. One of the most significant industrial applications of heterogeneous catalysis occurred at the beginning of the 20th Century with the development of industrial synthesis of ammonia from H_2 and N_2 through use of an iron catalyst [4,6,8]. Further industrial applications of heterogeneous catalysis are displayed in Table 1.1.

Table 1.1. Industrial processes involving heterogeneous catalytic systems [4,5,8].

Reactant	Catalyst	Product
CO, CO_2, H_2	$Cu/ZnO/Al_2O_3$	CH_3OH (bulk chemical)
CO, H_2	Co, Fe	C5–C11 hydrocarbons (fuel)
C3–C5 alkanes	Zeolites	C7–C9 isoalkanes (fuel)
Ethene	Organometallics	Polyethylene (polymer)
Xylenes, toluene	HZSM-5 zeolite	p-Xylene (bulk chemical)
Alkanes	Pt/Al_2O_3	Alkenes (bulk chemical)
Nitrobenzene, H_2	Pd/SiO_2	Aniline (bulk chemical)

The solid catalysts that are used in heterogeneous reactions are typically porous materials possessing specific surface areas 1–10^3 m^2g^{-1} [18]. The surface is an abrupt termination of a solid bulk structure, where atoms exist in an asymmetric environment in which they are lower coordinated than those in the bulk [3,15]. These low-coordinate atoms (or ions) are available for interaction with incoming reactant molecules as the catalyst active sites [3].

1.2.1. Reaction steps in heterogeneous catalysis

Catalytic processes on porous solid catalysts occur in seven consecutive steps (Figure 1.2) [3,8].

(1) Reactive molecules diffuse externally from the gas or liquid fluid phase towards the external surface of catalyst particle (film diffusion);

(2) Reactive molecules diffuse internally through the catalyst pores to reach the active sites on the internal surface of catalyst (pore diffusion);

(3) Reactant molecules adsorb to the active sites;

(4) The adsorbed molecules react at the catalyst's active sites;

(5) The product desorbs from the active sites;

(6) The product diffuses internally through the catalyst pores to the outer surface; and

(7) Product molecules diffuse externally to the fluid phase.

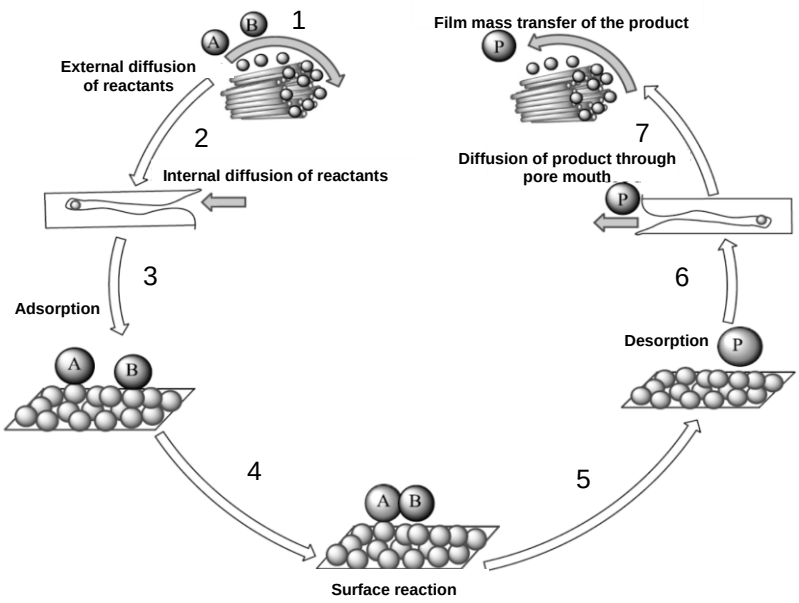

Figure 1.2. The seven steps of a heterogeneous catalysis reaction [8].

The surface of the catalyst plays a prominent role in heterogeneous catalysis [8]. The larger the catalyst surface area, the greater the number of active sites and the greater the contact between those sites and the reactant [3,8]. Thus, a catalytic reaction rate can be proportional to the number of active sites that are accessible on the catalyst surface during the process [3,9,19]. When these active sites have an acidic nature, the materials are considered to be solid acid catalysts [20]. This type of catalyst is covered in detail in the next sections of this Chapter.

1.3. Heterogeneous acid catalysis

1.3.1. Solid acid catalysts

Heterogeneous acid-catalysed reactions involve an acid-base interaction in which the surface of catalyst behaves as an acid towards reactant molecules that act as bases [20]. Solid acid catalysts play fundamental role in the development of large-scale chemical and petrochemical processes such as cracking, alkylation, isomerisation, hydration and polymerisation, etc. [8,20,21]. The chemical industry largely prefers solid acids as catalysts over liquid acids because the former offer significant advantages such as the easy separation of catalysts,

versatile process engineering, reduced reactor corrosion, continuous production, and elimination of waste [11,20–22].

Various materials with acidic properties have been applied as solid acid catalysts, including zeolites, mixed-metal oxides, metal salts, heteropoly acids (HPAs), cation exchange resins, etc. [20,23]. Table 1.2 shows various examples of solid acid catalysts.

Table 1.2. Types of solid acid catalysts [11,20,21].

Class	Example
Metal oxides	Al_2O_3, TiO_2, SiO_2, Nb_2O_5, WO_3.
Clays	Montmorillonite, Saponite.
Heteropoly compounds	$H_3PW_{12}O_{40}$, $H_4SiW_{12}O_{40}$, $H_3PMo_{12}O_{40}$, and their salts (e.g., $H_{0.5}Cs_{2.5}PW_{12}O_{40}$, etc.) (Keggin structure).
Metal salts	$AlPO_4$, $Nb_3(PO_4)_5$, $FePO_4$, $NiSO_4$.
Supported acids	H_3PO_4/SiO_2, $HClO_4/SiO_2$, H_2SO_4/SiO_2.
Sulfated oxides	SO_4^{2-}/ZrO_2, SO_4^{2-}/TiO_2, SO_4^{2-}/SnO_2.
Mixed metal oxides	SiO_2-Al_2O_3, SiO_2-ZrO_2, SiO_2-MgO, TiO_2-SiO_2 WO_3-ZrO_2.
Cation exchange resins	Amberlyst-15, Nafion, Nafion-silica composite.
Zeolites	Y-zeolites (faujasite), Beta-zeolite, Mordenite, HZSM-5.

1.3.1.1. Acid properties of solid acid catalysts

The acidity of solid acid catalysts depends on the nature, number and strength of acid sites on the catalyst surface [20,24–26]. In terms of the nature, solid acid catalysts can have Brønsted and/or Lewis acid sites [1,20,21]:

- Brønsted acid site is a donor of proton.
- Lewis acid site is an acceptor of electron pair.

Scheme 1.1. shows a fragment of metal oxide surface that possesses Brønsted acid sites (surface hydroxyl groups) and Lewis acid sites (coordinatively unsaturated surface metal cations) as well as base sites [12,20,26].

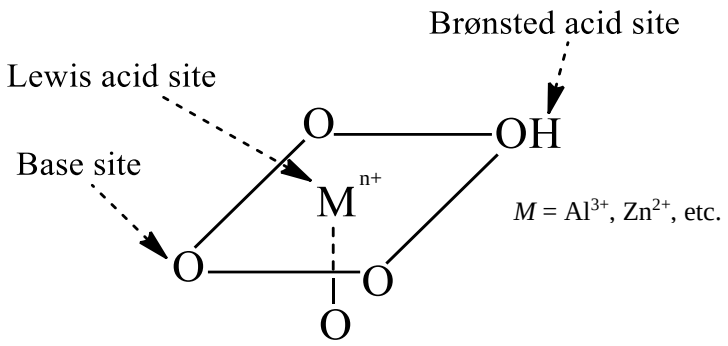

Scheme 1.1. Fragment of metal oxide surface possessing acid and base sites [12,20,27].

Catalyst acidity is commonly expressed in terms of the number of acid sites per unit surface area or weight of the catalyst and is referred to as the density of acid sites [20]. The strength of acid sites depends on their ability to donate a proton. The strength of Brønsted and Lewis acid sites varies with the coordination number of the oxygen atom of the hydroxyl groups and the coordination number of the metal cations, respectively [20]. The strength of Brønsted and Lewis acid sites is also affected by their location and types of interaction [20].

Various analytical methods have been used to investigate the acidic properties of solid acid catalysts [19,24,25]. The following methods are the most frequently used: (i) indicator method (titration with bases); (ii) methods based on adsorption/desorption of basic probe molecules, which include adsorption calorimetry, temperature-programmed desorption and spectroscopy of adsorbed molecules; (iii) direct spectroscopic observation of the solid surface; and (iv) acid-base test reactions. Since no method can identify all acid properties at the same time, it is preferable to use a combination of methods to gain more comprehensive knowledge of the acidic characteristics of solid catalysts [20,21,26]. Fundamental understanding of all parameters that affect acid sites would lead to the ideal scenario in which the acid catalysts could be rationally designed and synthesised for maximum activity, optimum selectivity and high performance stability [20].

1.3.1.2. The role of acid sites in heterogeneous acid catalysis

Heterogeneous acid catalysis is suggested to occur via a carbenium ion (stepwise) mechanism or a concerted mechanism. Several studies have proposed that Lewis acid sites serve primarily as adsorption sites, while Brønsted acid sites activate the reactant molecules through H^+ transfer [20,26,28,29].

1.3.1.2.1. Carbenium ion mechanism

This mechanism involves the generation of a carbenium ion intermediate or transition state by H^+ transfer from a Brønsted acid site of an acid catalyst to the reactant molecule [12,20,29]. As an example, Scheme 1.2 shows the hydration of an alkene through the carbenium ion mechanism. The rate of reaction is influenced by the acidity of the catalyst (i.e., the number and strength of acid sites) and the stability of the carbenium ion (primary < secondary < tertiary) [12,26,27,29].

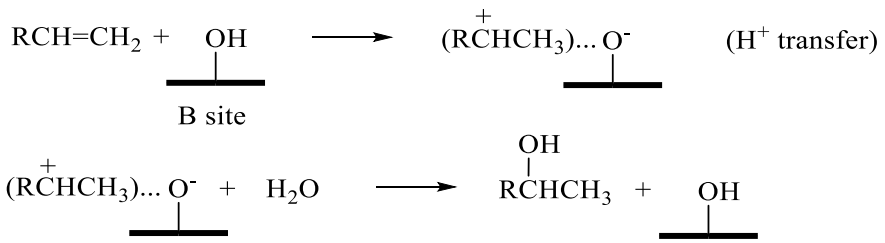

Scheme 1.2. Hydration of an alkene through the carbenium ion mechanism [27].

1.3.1.2.2. Concerted mechanism

The concerted mechanism implicates bifunctional acid-base catalysis by acid-base pairs [20,28,29]. Dehydration of an alcohol on a metal oxide, for example, can occur without carbenium-ion formation through simultaneous abstraction of H^+ by a base site and of OH^- by an adjacent Lewis acid site (Scheme 1.3) [12,20,28,29]. In this case, the rate may or may not correlate with the acidity of the catalyst [29,30].

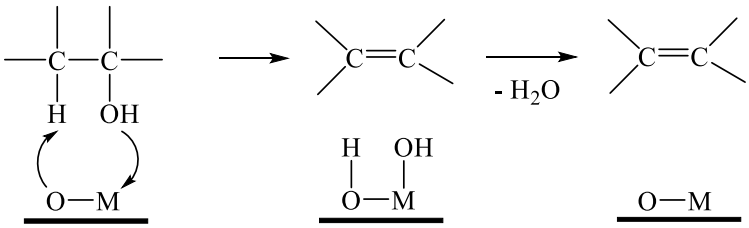

Scheme 1.3. Alcohol dehydration over metal oxide through the concerted mechanism [28].

1.4. Heteropoly acids as solid acid catalysts

1.4.1. Definition and background of heteropoly acids

HPAs consist of polyoxometalate (POM) anions and protons as counter cations [31,32]. Heteropoly anions are metal-oxygen clusters that have the chemical formula $[X_xM_mO_y]^{q-}$ ($x < m$), in which *X* represents the heteroatom and *M* the addenda atom [33]. Typical heteroatoms (central atoms) are P^{5+}, As^{5+}, Si^{4+}, Ge^{4+} and B^{3+} [20]. In most cases, the addenda atom is either molybdenum (VI) or tungsten (VI), possessing an appropriate combination of charge and ionic radius and the availability of vacant d-orbitals for the formation of metal-oxygen π bonds [31,34,35].

Heteropoly anions are synthesised through a self-assembly of oxoanions in an aqueous solution at low pH, as illustrated by Eqs. (1.1) and (1.2) [20,31,36]. Heteropoly anions can be separated as a solid with a suitable counter cation, such as H^+, NH_4^+, alkali metal cation, etc. [37].

$$24H^+ + PO_4^{3-} + 12WO_4^{2-} \rightarrow [PW_{12}O_{40}]^{3-} + 12\ H_2O \quad \textbf{(1.1)}$$

$$24H^+ + SiO_4^{4-} + 12WO_4^{2-} \rightarrow [SiW_{12}O_{40}]^{4-} + 12\ H_2O \quad \textbf{(1.2)}$$

In 1826, Berzelius discovered the first heteropoly salt [31]. After that, many heteropoly compounds were synthesised, and several hypotheses were proposed to explain their structures [31]. However, the structures of POMs remained unsolved until J.F. Keggin successfully discerned the crystal structure of 12-tungstophosphoric acid through the use of X-ray

diffraction in 1933 [38]. Many researchers have contributed to the field of POM chemistry, including Pope [39–41], Muller [42–44], and Tsigdinos [45–47].

HPAs have unique physicochemical features that include their structural mobility, strong Brønsted acidity, thermal stability, multifunctionality and appropriate redox properties. Therefore, HPAs can be considered as promising acid, redox and bifunctional catalysts [32,33,48–52]. Heteropoly compounds have been applied in numerous reactions as catalysts; they offer significant environmental and economic benefits compared with other solid acid catalysts [20,31,32,48,53–58]. Many researchers around the world have studied HPAs catalysis; these include Moffat [50,59,60], Misono [49,55,61], Kozhevnikov [31,32,57,62], Hill [63–65], and Neumann [66–69].

1.4.2. Structures of solid heteropoly acids

Misono et al. [36,54] proposed a novel hierarchical structural classification of solid heteropoly compounds, which reflected the importance of HPA structural flexibility. This classification can be used to explain heterogeneous catalysis by POM compounds [49]. This classification is illustrated in Figure 1.3. Three distinct structural levels - primary, secondary and tertiary - have been identified [54]. Generally, HPAs and their salts are composed of ionic crystals in the solid state [31,32,48]. The heteropoly anion is a primary structure that can be identified in solution [48]. In the solid material, the structure is composed of POMs, counter cations, water of crystallisation and other molecules organised in three–dimensional arrangements known as secondary structures [48,54,55]. The tertiary structure (solid texture) refers to the assembly of solid HPA [54]. The tertiary structure includes the particle size, pore structure, proton distribution in the particles, etc., which play a vital role in heterogeneous catalysis [31,48,49].

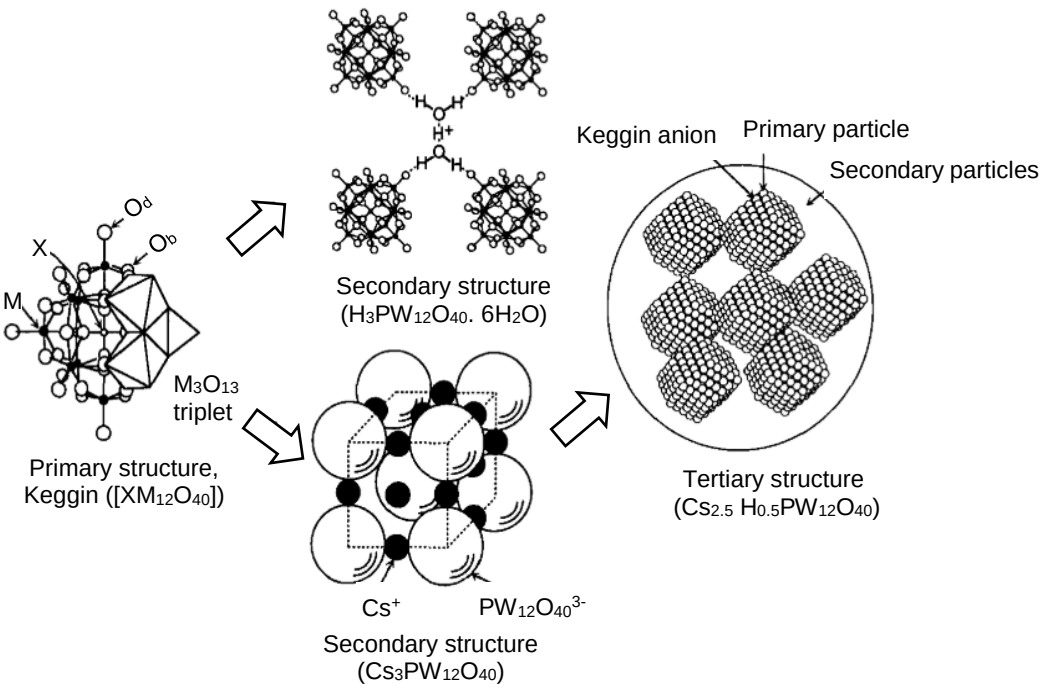

Figure 1.3. Hierarchical structures of heteropoly compounds (primary, secondary and tertiary) [48].

The primary structure (the heteropoly anion) can be divided into different classes based on the atomic ratio of the heteroatom (*X*) to the addendum atom (*M*) [36,70]. Table 1.3 illustrates the most common classes of heteropoly anions.

Table 1.3. Most common classes of heteropoly anions [31,56,70].

X/*M* ratio	Chemical formula (*M* = Mo or W)	*X*	Structure name
1:12	$[X^{n+}M_{12}O_{40}]^{(8-n)-}$	P^{5+}, Si^{4+}, Ge^{4+}	Keggin
1:11	$[X^{n+}M_{11}O_{39}]^{(12-n)-}$	P^{5+}, Si^{4+}, Ge^{4+}	Lacunary Keggin
2:18	$[X_2^{n+}M_{18}O_{62}]^{(16-2n)-}$	P^{5+}, As^{5+}	Dawson
1:6	$[X^{n+}M_6O_{24}]^{n-}$	Te^{6+}, I^{7+}	Anderson

Among the structures of heteropoly anions, the Keggin structure is the most commonly investigated type due to its high thermal stability, strong acidity, tunable redox properties, and the ease of preparation [31,48,71,72].

The catalysts that were investigated in this thesis were based on the Keggin structure. This structure is discussed in a more detail in the next section. Additional information about other types of heteropoly anions can be found in reviews [31,48,50,73].

1.4.3. The Keggin structure

The Keggin was the first characterised structure of POMs [31]. Over the past 50 years, Keggin HPAs have been applied in a variety of catalysis processes due to their availability, structural mobility and thermal stability [31,48,71,72]. The Keggin heteropoly anions have the composition $[XM_{12}O_{40}]^{x-8}$, where *X* is the heteroatom (P^{5+}, Si^{4+}, etc.), *x* is the oxidation state of the heteroatom, and *M* is the addenda atom (Mo^{6+}, W^{6+}, etc.) [48,53,70].

As shown in Figure 1.4, the Keggin anion comprises a central XO_4 tetrahedron that is surrounded by 12 edge- and corner-sharing MO_6 octahedra. The metal-oxygen octahedra are organised into four groups (M_3O_{13}) of three edge-sharing MO_6 octahedra associated with the central XO_4 tetrahedron [31,32].

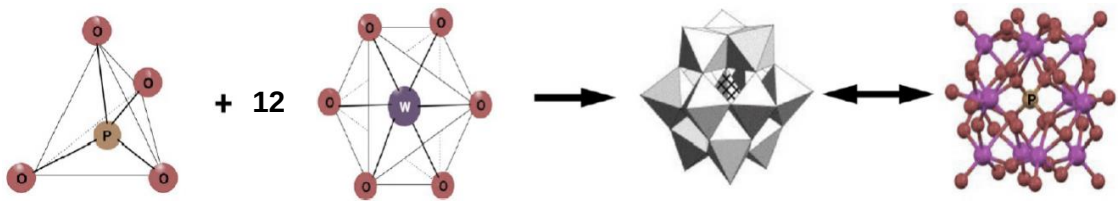

Figure 1.4. Keggin structure of heteropoly anions $PM_{12}O_{40}^{3-}$ [74].

The Keggin structure contains four distinct forms of oxygen atom [31,32,73,75] (Figure 1.5). These are present as:

- 12 terminal $M{=}O_t$;
- 12 corner-bridging quasi-linear $M–O_{b2}–M$ linking two M_3O_{13} groups;
- 12 edge-bridging angular $M–O_{b1}–M$ shared by the octahedra within a M_3O_{13} group and
- 4 internal $X–O_c–M$.

These oxygen species can be identified through application of ^{17}O nuclear magnetic resonance spectroscopy (^{17}O NMR) or through use of Fourier transform infrared spectroscopy (FTIR) [31,36,50].

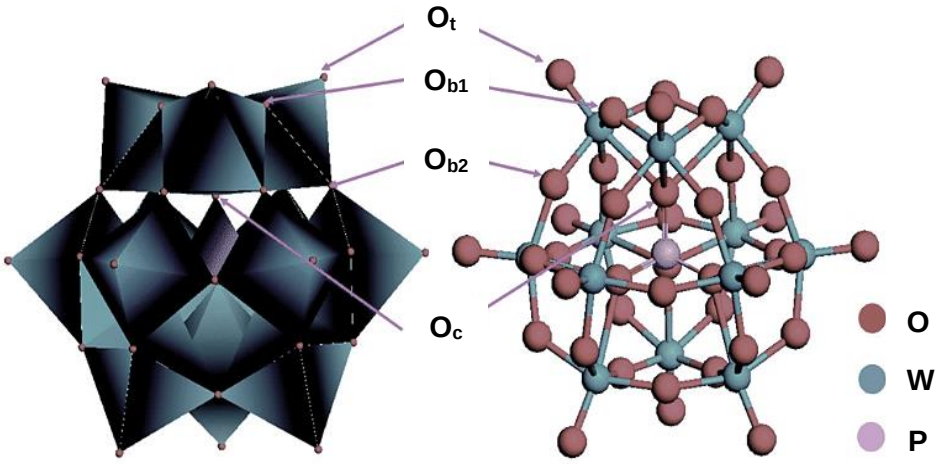

Figure 1.5. Location of oxygen atoms in the $PW_{12}O_{40}^{3-}$ anion (Keggin structure) [76].

The most common Keggin-type HPAs that are commercially available as crystalline hydrates are 12-phosphotungstic acid ($H_3PW_{12}O_{40}$, HPW), 12-silicotungstic acid ($H_4SiW_{12}O_{40}$, HSiW), 12-silicomolybdic acid ($H_4SiMo_{12}O_{40}$, HSiMo), and 12-phosphomolybdic acid ($H_3PMo_{12}O_{40}$, HPMo) [57,77].

1.4.4. Proton structures of heteropoly acids

The identification of structure and location of proton sites in solid HPAs is essential for their use as acid catalysts. Solid HPAs and their salts are composed of a polyanion and hydrated or non-hydrated protons as counter cations (H^+, H_3O^+, $H_5O_2^+$) [48,54,55]. The HPA crystal structure is strongly dependent on the hydration state, which can be controlled easily by thermal treatment [32,49,54,78]. In solid HPAs, the hydrated and non-hydrated protons, which can be represented as $[H(H_2O)_n]^+$, have been identified by the solid-state ^1H NMR [31]. In the stable solid $H_3PW_{12}O_{40}$ hexahydrate, which involves six crystallisation water molecules per Keggin

unit, the bulk protons are present as hydronium ion dimers ($H_5O_2^+$) [32]. The $H_5O_2^+$ ion binds to the terminal oxygen atoms in the Keggin unit and joins four neighbouring heteropoly anions. The acidic protons are found in the $H_5O_2^+$ bridges between lattice points, as illustrated in Figure 1.6 A [32,54]. The crystalline structure of hexahydrate $(H_5O_2^+)_3[PW_{12}O_{40}]^{3-}$ has been determined via neutron and single-crystal X-ray diffraction [20,54,78,79]. When the number of crystallisation water molecules is less than six, the acidic protons might be linked directly to the polyanion's peripheral oxygen atoms as H^+ or H_3O^+ (hydronium ion monomer) or could remain as $H_5O_2^+$ bridges (Figure 1.6 B, C and C`) [54,78,80].

Hydrated and non-hydrated protons form the crystal structures of solid HPAs by linking the neighbouring heteropoly anions [31]. Hydrated protons possess high mobility, which induces high proton conductivity in crystalline HPA hydrates [20,31]. It has been proposed that, in HPA solids, the protons can be transferred across the hydrogen-bonded network in the same way that they move in an aqueous solution [20,72]. Non-hydrated protons, in contrast, are less mobile and probably hop between surface oxygen atoms in the Keggin unit or between neighbouring Keggin anions [31,72,81].

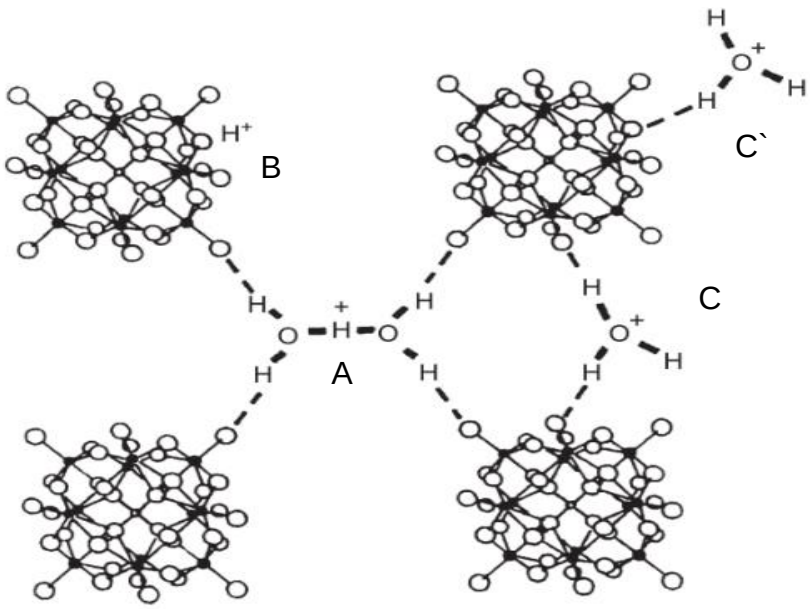

Figure 1.6. Schematic structure of bulk proton sites in solid $H_3PW_{12}O_{40}.nH_2O$ (n = 0–6) [54].

The location of the bulk protons in heteropoly anions has been the topic of several studies [72,82–84]. There are two potential protonation centres in Keggin anions: terminal oxygens ($M=O_t$) and bridging oxygens ($M–O_b–M$; edge-sharing) [72,85]. In solid HPW and HSiW hydrates, application of the ^{17}O NMR technique and comparison of the solid state and solution spectra of the HPAs have indicated the predominant protonation of the terminal oxygens in the solid state [82–84]. In anhydrous HPW, on the other hand, the acidic protons are located on terminal and bridging oxygens of the Keggin unit [80,85]. The protons, both hydrated and non-hydrated, can participate in heterogeneous catalysis.

In solid HPAs, the surface protons seem to be stronger than the bulk protons [31]. It has been suggested that the proton sites on the surface of Keggin HPAs are located at the bridging oxygen atoms [31,32].

1.4.5. Properties of heteropoly acids

1.4.5.1. Thermal stability of heteropoly acids

The thermal stability of HPAs is important for their application in heterogeneous catalysis [48,50]. Some solid HPAs are thermally stable and can be utilised in reactions that occur at temperatures of up to 300–350 °C [31]. Nevertheless, this may not be sufficient for reactions that require higher temperatures or for catalyst regeneration [20,31,57], which is usually achieved through combustion of coke at 450–550 °C in an oxygen atmosphere [31,57].

Several analytical methods can be used for the evaluation of HPAs thermal stability. These include thermogravimetric analysis (TGA), differential scanning calorimetry (DSC), differential thermal analysis (DTA), infrared spectroscopy (IR), solid-state NMR and X-ray diffraction (XRD) [31].

Keggin HPAs decompose thermally through a multistage process that produces an oxide mixture [33]. Scheme 1.4 illustrates the course of the thermal decomposition of HPW.

The thermal stability of HPAs can be determined via assessment of the decomposition temperature that results in the loss of all acidic protons [31,32,57,86].

$$H_3PW_{12}O_{40}.nH_2O \underset{-(n-6)H_2O}{\overset{<100\ ^oC}{\rightleftharpoons}} H_3PW_{12}O_{40}.6H_2O \underset{-6H_2O}{\overset{200\ ^oC}{\rightleftharpoons}} H_3PW_{12}O_{40} \underset{-1.5H_2O}{\overset{450\text{-}470\ ^oC}{\rightleftharpoons}} PW_{12}O_{38.5} \overset{600\ ^oC}{\rightleftharpoons} 1/2P_2O_5 + 12WO_3$$

Scheme 1.4. Thermal decomposition of Keggin HPW hydrate [31,33].

From TGA the decomposition temperature of Keggin HPAs reduces in the order: HPW (465 °C) > HSiW (445 °C) > HPMo (375 °C) > HSiMo (350 °C). It can be seen that HPW is the most stable compound in this series [31]. At higher temperatures, the Keggin structure decomposes completely into its constituent oxides in the same order as above and at temperatures of 610 °C, 540 °C, 495 °C, and 375 °C, respectively [51].

Heteropoly salts have a higher thermal stability compared with their parent acids. For example, the acidic salt CsPW ($Cs_{2.5}H_{0.5}PW_{12}O_{40}$) begins to lose protons at 500 °C, and hence is more thermally stable than the parent HPW [48,49,87].

1.4.5.2. Acidity of heteropoly acids

The acid properties of HPAs are influenced by the following factors: the composition of the heteropoly anion, the counter cation (if present), the type of support (for supported HPAs) and the way in which the HPAs is dispersed on the surface of support [20,48,88].

1.4.5.2.1. Bulk heteropoly acids

The acidity of HPAs in solutions has been characterised in terms of Hammett acidity functions and dissociation constants [48,62]. The acidity of bulk HPW and HSiW has been well documented regarding the nature, the number, the strength and the distribution of acid sites [32,48,49,88–92]. The nature of acidic sites (Brønsted or Lewis) has been characterised via

FTIR spectroscopy of adsorbed pyridine [48,93]. Solid HPAs are purely Brønsted acids and are stronger than other traditional solid acids such as aluminosilicates (SiO_2-Al_2O_3) [31,49,62]. The acid properties of HPAs have also been revealed through thermal desorption of basic probe molecules. Okuhara et al. [48] utilised this method to compare the acid strength of HPW and SiO_2-Al_2O_3. They reported that, pyridine molecules that had been adsorbed to the surface of SiO_2-Al_2O_3 were totally desorbed at 300 °C, whereas in HPW, the pyridine molecules remained adsorbed at much higher temperature. These results confirmed that HPW was much stronger than SiO_2-Al_2O_3 [31].

The strong acidity of HPAs can be explained based on the electrostatic theory. The electrostatic interaction between large heteropoly anions and protons is significantly weaker than that found in mineral acids. This is because the negative charge of the heteropoly anion is dispersed over 36 outer oxygen atoms. Besides, the π-backdonation in the M=O terminal groups reduces the negative charge on the outer surface of polyanion [31,36,48].

The acid strength of HPAs can be precisely assessed through use of NH_3 adsorption microcalorimetry (NH_3-MC) [49,94–96]. Jozefowicz et al. investigated the acidity of various solid bulk HPAs at 150 °C [96]. They observed that the acid strength of bulk HPAs declined in the following order:

$$\text{HPW} > \text{HSiW} \geq \text{HPMo} \geq \text{HSiMo}.$$

The HPA acid strength reduces when the addenda atom W(VI) is replaced by Mo(VI) and the heteroatom P(V) is exchanged with Si(IV). This order is consistent with the electrostatic theory since the strength of acid sites decreases as the negative charge of the heteropoly anion increases [62].

1.4.5.2.2. Salts of heteropoly acids

HPA salts can be formed by the ion exchange method. The protons in the parent acids exchange with metal ions without altering the Keggin structure [32,49,97]. The nature of the counter cations controls the features of HPA salts such as the thermal stability, porosity, solubility and acidity [49,56]. The HPA salts can be categorised into two main groups according to the size of the counter cation [98].

- **Group A**: HPA salts with small metal cations such as Li^+ or Na^+. These salts have small surface areas (1–15 m^2g^{-1}), some ability to absorb polar molecules in the solid bulk and are highly soluble in water (hydrophilic salts) [32,98].
- **Group B**: HPA salts with large metal cations such as Cs^+ or K^+. Group B salts have large surface areas (50–200 m^2g^{-1}), do not absorb polar molecules in the solid bulk, are water-insoluble (hydrophobic salts) and are more thermally stable than Group A salts [20,31,32,56].

Considerable research has been performed to define the acid properties of the HPA salts. It has involved the application of several methods including adsorption and thermal desorption of basic molecules and solid-state ^{31}P-NMR spectroscopy [99–102]. Okuhara et al. [48] examined the acid characteristics of the heteropoly salts $Cs_xH_{3-x}PW_{12}O_{40}$ and concluded that CsPW had a useful combination of high surface area (100–180 m^2g^{-1}) and strong surface acidity (Figure 1.7). It has been reported that the catalytic activity of Cs salt in many reactions correlates with their surface acidity [20,54,101].

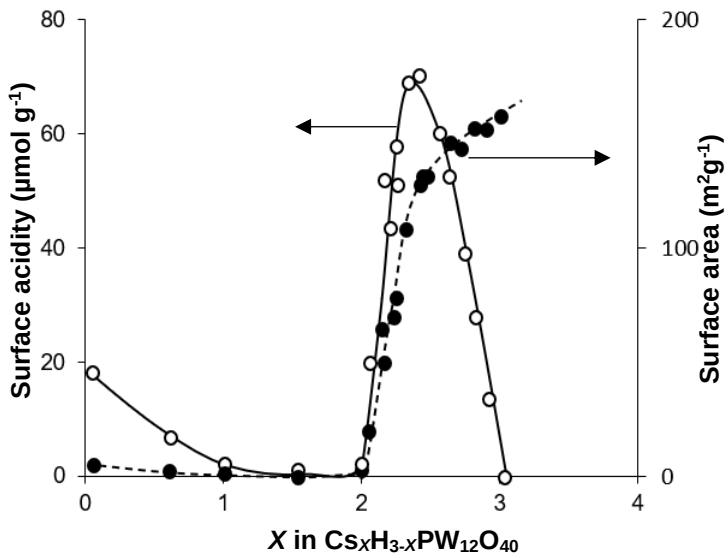

Figure 1.7. Surface acidity and surface area of $Cs_xH_{3-x}PW_{12}O_{40}$ as a function of Cs content (adapted from [56]).

CsPW and HPW have comparable acid strengths according to the temperature programmed desorption (NH_3-TPD) studies and indicator tests [49,103]. Regarding the NH_3-TPD, CsPW produced a significantly wider peak than HPW, indicating a heterogeneity of acid sites.

NH_3-MC, which is considered a more accurate technique, has confirmed that CsPW is a strong acid that is only slightly weaker than the parent HPW (Figure 1.8) [54].

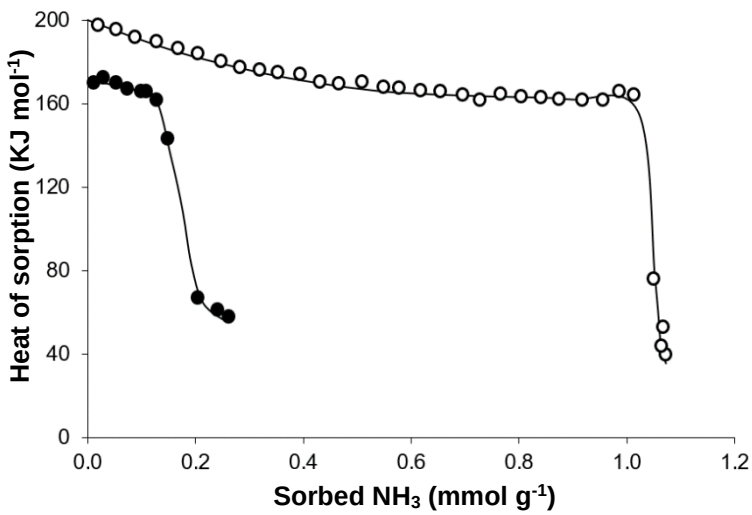

Figure 1.8. Differential heat of NH_3 sorption measured at 150 °C: bulk HPW(○), CsPW(●) (adapted from [54]).

1.4.5.2.3. Supported heteropoly acids

Bulk HPAs have a low surface area (1–10 m^2g^{-1}), resulting in a low density of acid sites on the surface [31,32,48,50,91]. Supporting the HPAs on inert porous materials can enhance the catalyst surface area and the number of surface proton sites [32,104]. Therefore, supported HPAs catalysts are mostly applied in heterogeneous acid catalysis (Section 1.4.7).

HPAs have been supported on acidic or neutral solids, which have a weak interaction with HPAs such as SiO_2 [93,105–108], acid ion-exchange resin [109,110], ZrO_2 [107,111,112], Nb_2O_5 [95,112], TiO_2 [107,113], mesoporous silicas MCM-41 [108,114] and SBA-15 [115], zeolites [105]. It has also been reported that boron nitride (BN) has the potential to be an inert support for HPAs, albeit with the downside that it has a low surface area [116].

In contrast, amphoteric and basic solid supports such as Al_2O_3 and MgO are rarely applied because these supports often decrease the HPA acidity and decompose the HPA structure [31,32,48,50,91].

Silica is the most frequently applied support because of its inertness towards HPAs and its availability in a wide variety of textures [11,58,117,118]. An X-ray spectroscopy study [119] showed that the structural distortion of the Keggin unit in supported HPW catalysts increased for the following supports in the order shown: $SiO_2 < TiO_2 < ZrO_2$.

SiO_2 is relatively inert towards HPAs above a certain level of loading [11,32,120]. The Keggin structure of HPW and HSiW is preserved when these acids are supported on silica at a loading above 10%. However, the HPAs may partially degrade at lower loadings due to interaction with surface silanol groups [49,117].

The acid properties of bulk and supported HPW catalysts were examined by NH_3-MC. HPW was supported on SiO_2, active carbon, ZrO_2 and Nb_2O_5 supports and pre-treated at 200 °C for 1 h. The average heat of NH_3 adsorption, at half NH_3 coverage, was found to decrease in the following order: HPW > HPW/SiO_2 > HPW/C > HPW/Nb_2O_5 > HPW/ZrO_2. This

ranking also confirmed that the strong interaction of solid HPAs with the supports affected the acid strength of the HPA catalysts [120].

Alharbi et al. [88] evaluated the acidity of 15% HPW that was impregnated on different oxide supports using NH_3-MC. Table 1.4 presents the effect of support on the acid strengths of the HPW catalysts in terms of the initial enthalpy of NH_3 adsorption. As can be seen, the strength of the acid catalysts, measured by NH_3-MC at 150 °C, decreased with the following order of supports: SiO_2 > TiO_2 > Nb_2O_5 > ZrO_2 [95].

Table 1.4. Acid strengths of bulk and supported HPW catalysts [88,95].

Catalyst	ΔH_o (kJ mol^{-1})
HPW	-195
15%HPW/SiO_2	-154
15%HPW/TiO_2	-143
15% HPW/Nb_2O_5	-132
15% HPW/ZrO_2	-121

Newman et al. investigated the acidity of SiO_2-supported HPW prepared by impregnation from MeOH at 3.6–62.5% HPA loading using DSC of ammonia adsorption. They demonstrated that the Keggin unit of HPW remained intact over the whole range of HPA loadings. Furthermore, they found that the acid strength of the HPW/SiO_2 catalysts did not depend on the HPA loading above 6.2% (ΔH = -164 kJ mol^{-1}). However, the catalysts exhibited weaker acidity at a lower loading (3.6%) (ΔH = -140 kJ mol^{-1}). They assumed that the inability of highly dispersed clusters of HPW to hydration led to a reduction in the acidity of proton sites [93].

Bardin and Davis [121] evaluated the acidity of silica-supported phosphotungstic acid by NH_3-MC at a loading range of 5–25% after pre-treatment at 300 °C. Figure 1.9 shows that the acid strength of HPW catalysts decreased as the HPA loading on the SiO_2 decreased from 25% to 5%. They observed that at an HPA loading of 25%, the initial heat of NH_3 adsorption

was near to that for the bulk HPW (150 kJ mol^{-1}). Besides, it was found that the acid strength of 5% HPW/SiO_2 increased as the pre-treatment temperature was decreased. The heats of NH_3 adsorption were approximately 100 and 140 kJ mol^{-1} for the pre-treatment temperatures of 300 °C and 200 °C, respectively.

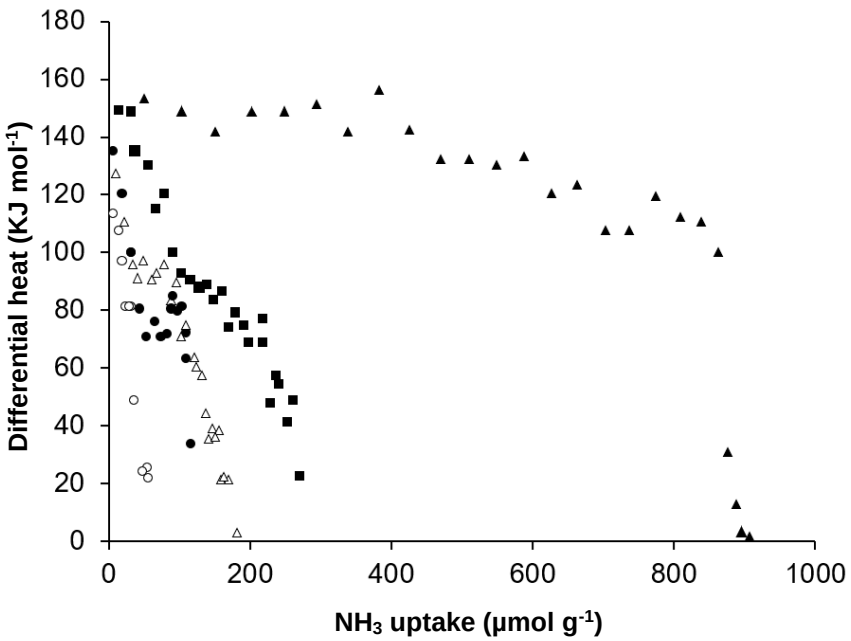

Figure 1.9. NH_3-MC for SiO_2 support (○), bulk HPW (▲), 5%HPW/SiO_2 (●), 10%HPW/SiO_2 (△) and 25%HPW/SiO_2 (■) catalysts after pre-treatment at 300 °C for 2 h (adapted from [121]).

Hence, the acid strength of supported HPAs depends on the nature of support, pre-treatment temperature and HPA loading. Therefore, modification of these factors can profoundly affect the activity and stability of HPA catalysts in heterogeneous catalysis.

1.4.6. HPAs in heterogeneous catalysis

Solid HPAs have a broad range of catalytic applications in gas-solid and liquid-solid heterogeneous systems [122]. According to Misono et al. [48,49,54], there are three main catalysis processes that occur with solid HPAs: (a) surface-type, (b) bulk type I (pseudo-liquid) and (c) bulk type II. These are displayed in Table 1.5.

Table 1.5. Types of heterogeneous catalysis over solid HPAs [31,49].

Types	Comment	Examples
Conventional surface catalysis	Reactions occur on HPA surface	Alkane isomerisation
Bulk catalysis I (pseudo-liquid phase)	Reactants absorbed in HPA bulk and react pseudo-homogeneously	Alcohol dehydration at low temperatures
Bulk catalysis II (redox catalysis)	Reactions take place on HPA surface, redox carriers diffuse through HPA bulk	Oxidative dehydrogenation

Acid catalysis by solid heteropoly compounds is classified as surface type or bulk type I catalysis [20,49]. Surface-type catalysis is the conventional type of heterogeneous catalysis. It occurs on the acid sites that are localised on the outer surface and pore walls of solid acid catalysts [48,49,58,123]. In this case, the rate of reaction is correlated with the number of surface acid sites [3,8]. For instance, the rate of acid-catalysed reactions over $Cs_xH_{3-x}PW_{12}O_{40}$ ($2 < x < 3$) has been found to scale with the surface acidity [20,54,98,101].

On the other hand, bulk type I catalysis occurs in reactions of polar molecules (e.g., alcohols and amines) on bulk HPAs and HPA salts of group A [32,49]. Polar substrates such as water, primary alcohols and ethers are readily absorbed in the interstitial spaces between heteropoly anions as they replace crystallisation water or expand the crystal lattice [48,49]. In this instance, solid HPA catalysts behave similarly to a concentrated solution (pseudo-liquid phase), and all acid sites, both the surface and the bulk ones, participate in the reaction [58,124]. The rate of such reactions scales with the total number of acid sites or the weight of the catalyst [31]. This type of catalysis has been suggested for the dehydration of alcohols at low temperatures and the synthesis of methyl tert-butyl ether (MTBE) [36,49,124]. Misono et al. [31,48] investigated the dehydration of isopropanol over bulk HPA at a low temperature of 80 °C. They found that bulk HPW showed high efficiency in isopropanol dehydration despite the low surface area. Therefore, they attributed this behaviour to the bulk type I mechanism.

1.4.7. Application of heteropoly acids in heterogeneous acid catalysis

The unique properties of HPAs, such as strong Brønsted acidity, high thermal stability, hierarchical structures and pseudo-liquid phase behaviour, make them promising acid catalysts. HPA catalysts have been utilised in a wide range of applications [31,49–51,54]. The strongest Keggin HPAs, namely HPW and HSiW, are the most frequently used HPAs in heterogeneous acid catalysis [125]. In general, due to their strong acidity, solid HPA catalysts display superior activity compared with traditional solid acid catalysts (e.g., zeolites and mixed oxides) [32,88].

Misono et al. studied isopropanol dehydration over various types of bulk solid HPAs, they found the activity of the HPAs decreased in line with their acid strengths: HPW > HSiW > HPMo > HSiMo [31,48].

The catalytic activity of bulk and supported HPW at 15% loading in the dehydration of isopropanol was studied by Alsalme et al. [112]. The reaction was performed at 120 °C, and the catalytic activity decreased in the order: HPW/SiO_2 (99%) > HPW (81%) > HPW/TiO_2 (67%) > HPW/Nb_2O_5 (9%) > HPW/ZrO_2 (5%). This follows the order of the acid strength of these catalysts as measured by NH_3-MC (Table 1.4).

It has been found that HSiW/SiO_2 was a superior catalyst for the direct addition of acetic acid to ethene to form ethyl acetate [126]. With HSiW/SiO_2 catalyst, the conversion was higher than with other acids such as bulk HSiW, WO_3-ZrO_2 and H_3PO_4/SiO_2. However, the selectivity for ethyl acetate was over 98% regardless of the catalyst. It has been demonstrated that the impregnation of HSiW on SiO_2 support with a high surface area and moderate pore size (ca. 6 nm) produced the highest catalyst activity.

The skeletal isomerisation of linear alkanes over HPAs has been investigated by Bardin and Davis [48]. The activity of bulk and silica-supported HPW catalysts in n-butane and n-pentane isomerisation at 200 °C declined as the temperature of the catalyst pre-treatment was

increased [121]. This indicates that the hydration level of HPA has an impact on its catalytic activity.

HPAs and their salts have also been applied as catalysts for MeOH conversion to hydrocarbons [50,127]. For example, Meng et al. [128] applied phosphotungstic and silicotungstic acid metal salts (CuPW, CuSiW, FePW and FeSiW) as the catalysts at 100–400°C. They found that dimethyl ether (DME) was the main product at low temperatures. However, at higher temperatures (250–350 °C), the copper-containing catalyst CuSiW displayed the highest selectivity for propene and ethene (44%). The high activity of the copper salt in this reaction can be explained by its optimal acidity.

The synthesis of MTBE from isobutene and MeOH has been examined over various supported HPMo catalysts in the vapour phase. The catalytic activity was found to decline in the following order of supports: SiO_2 > SiO_2-Al_2O_3 (13% Al_2O_3) > SiO_2-Al_2O_3 (26% Al_2O_3) > Al_2O_3 > MgO. Furthermore, when Al_2O_3 and MgO were used, most of the supported HPA was decomposed, apparently due to the basic nature of these supports [20,129].

Esterification of acetic acid with butanol was conducted over clay-supported HPAs. HPW, HSiW and HPMo were supported on the surface of acid-activated bentonite (HPA/B) at 10–30% loading. The highest catalytic activity and selectivity was observed for 20% HPW/B catalyst [130].

HPA supported over mesoporous silica MCM-41 was utilised to catalyse glycerol dehydration in the gas phase [131]. The catalysts were prepared at various HPW loadings (10–50%). It was found that the conversion of glycerol and acrolein selectivity increased with HPW loading. The optimum loading was found to be 40% HPW, which exhibited 85% glycerol conversion and 80% acrolein selectivity at 320 °C. This result indicates that supporting HPW on MCM-41 generates an appropriate Brønsted acidity [117].

HPA catalysts have been utilised in polymerisation processes. Bulk HPW, HSiW, HPMo and silica-supported HPW catalysts were used for cationic polymerisation of β-pinene. Of the three HPAs, the silica-supported HPW catalyst showed the best performance; it exhibited the highest activity and stability, and polymer yield reached 90% [132].

1.5. Alcohols and ethers as alternative transportation fuels

In recent years, there has been a significant rise in oil consumption as an energy source [133]. The combustion of petroleum-based fuels (gasoline, diesel and liquefied petroleum gas (LPG)) causes emissions of greenhouse gases, particularly CO_2, which contribute to the environmental issues such as global warming [134,135]. Most vehicles that operate on gasoline and diesel are considered to be primary sources of greenhouse gases [134,136]. Biofuels, such as biodiesel and bio-alcohols, are considered as replacement fuels for internal combustion engines in vehicles [137–139].

It has been shown that use of biodiesel as fuel in diesel engines can provide economic and environmental benefits [140]. For instance, use of biodiesel can reduce air pollution as it lowers emissions of CO_2, hydrocarbons and particulate matter [140]. However, biodiesel also has several drawbacks, which include high operating costs, high viscosity and low volatility [137]. Biofuels can provide solutions to the energy and environmental problems that are associated with conventional fuels, but further research is required to improve biofuel properties [137].

Alcohols and ethers have been considered as the possible alternative transportation fuels [137]. Compared with gasoline, alcohol production is more economical, simpler, and more environmentally friendly [136]. Primary alcohols such as MeOH and EtOH have higher octane numbers than petroleum fuels, and this enables the engine to produce power more efficiently and economically [136]. Besides, alcohol combustion produces less unburned

hydrocarbons and CO_2 than combustion of conventional gasoline [139,141]. In addition, alcohols have a higher vaporisation heat which lowers the peak temperature within the combustion chamber and, in turn, results in lower NO_x emissions and increased engine efficiency [139]. Although the high vaporisation heat of primary alcohols is beneficial in fuel performance, it also causes some difficulties during the ignition of engines in cold weather [136,137,141].

EtOH and MeOH are recognised to be renewable energy sources and feedstock for a variety of chemicals [142]. Dehydration of EtOH over solid acid catalysts produces ethene, a critical feedstock in the petrochemical industry, and diethyl ether (DEE), a transportation fuel with remarkable features (cetane number > 125) [142]. DEE has excellent burning properties, which make it a prospective alternative fuel or diesel fuel additive. The blending of DEE with EtOH has been reported to improve the cold start of EtOH-fuelled vehicles [141–143].

MeOH dehydration produces DME, which is another environmentally clean diesel fuel alternative [142]. DME has a higher cetane number (55–60) and emits significantly less NOx than does the traditional diesel fuel. Additionally, near-zero smoke generation has been reported from vehicles that utilise DME as fuel [133,141,144,145].

Therefore, the production of DEE and DME has received significant attention due to the rising cost of crude oil and the need to improve the environment [146].

1.6. Dehydration of methanol and ethanol using heterogeneous catalysis

Heterogeneously-catalysed dehydration of alcohols can be carried out in liquid or gas phase over solid acid catalysts. Zeolites (Si/Al) such as HZSM-5 (30), H-Y(80) and H-Mordenite (90), as well as γ-alumina and silica-alumina, have investigated as the solid acid catalysts for the liquid-phase dehydration of MeOH to DME [147]. H-Mordenite exhibited the highest activity in this process. However, it suffered from deactivation during the reaction due to coke

formation. Vanoye et al. [148] reported a strong effect of solvents on EtOH dehydration over various sulfonic acid catalysts in liquid phase. The solvents affected the reaction rate and the accessibility of catalyst active sites as well as the rate of catalyst deactivation, which is a serious limitation of the liquid-phase process.

1.6.1. Dehydration of methanol to dimethyl ether in the gas phase

DME is a simple oxygenated compound that is applied as an environmentally friendly aerosol propellant and as a refrigerant; it is also an intermediate in the production of chemicals such as dimethyl sulfate [88,149–151]. In recent decades, DME has received significant attention as a cleaner fuel alternative to LPG and as a non-polluting substitute for diesel [88]. Therefore, DME is a promising alternative to conventional fuels [145,152].

DME can be produced from the synthesis gas (H_2 + CO) through use of a hybrid (bifunctional) catalyst or via MeOH dehydration over a solid acid catalyst [153,154]. Typically, the dehydration of MeOH to DME is carried out over solid acid catalysts such as zeolites and γ-Al_2O_3 in the gas phase at 240–250 °C [150,155].

Thermodynamically, the dehydration of MeOH to DME is favoured at lower temperatures owing to the exothermic nature of this reaction. Under such conditions, production of undesirable by-products such as olefins and/or coke can be avoided, as these are formed at higher temperatures [156,157].

MeOH dehydration is suggested to be catalysed by Brønsted and Lewis acid sites of weak to medium acid strength. Both these sites may be involved in the catalytic reaction, although it is believed that Brønsted acid sites of appropriate acid strengths are mainly accountable for DME formation [147,150,152].

DME formation on Brønsted acid sites is suggested to occur by associative or dissociative pathways (Scheme 1.5) [88]. The associative pathway involves adsorption of two

MeOH molecules to the catalyst surface, where they react directly to form DME. The dissociative pathway begins with the adsorption of MeOH and the elimination of water, which leads to the formation of an adsorbed methyl group. Then the methyl group interacts with a gas-phase MeOH molecule to produce DME [88,158,159].

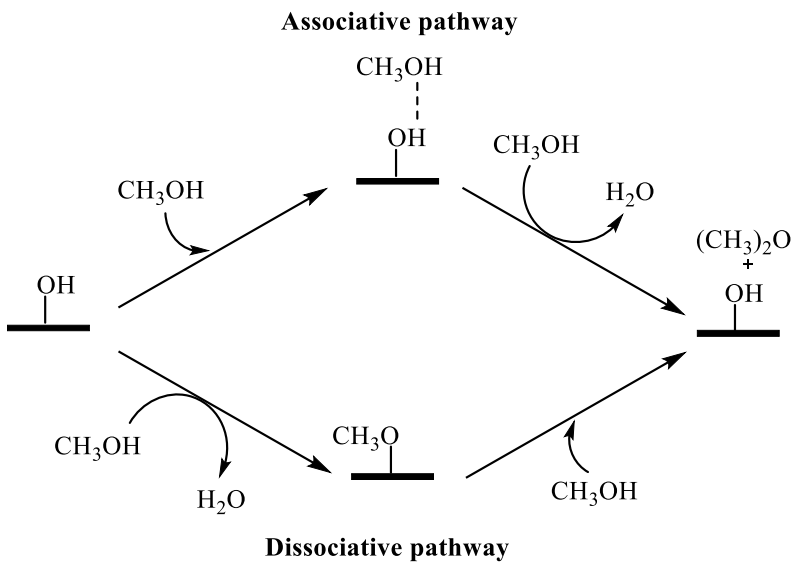

Scheme 1.5. Associative and dissociative pathways for dehydration of MeOH to form DME [88].

The MeOH dehydration reaction can occur on various solid acid catalysts such as γ-alumina, silica-alumina [155,160,161], zeotypes [159,162,163], HPAs [88] and Nafion [164]. However, much of the recent research has concentrated on the optimisation of the conversion of MeOH to DME in the gas phase over acidic zeolites, particularly MFI (HZSM-5), γ-alumina and HPAs, namely HPW and HSiW, since these catalysts exhibit high activity in ether production [88,155,157,165–167].

Xu et al. examined the efficiency of γ-Al_2O_3 as a catalyst to produce DME. They found that γ-Al_2O_3 exhibited high MeOH conversion (90%) at 250 °C. However, they pointed out that the catalyst was poisoned during the reaction, which reduced its activity and stability.

This result was explained as being due to the competitive water adsorption on the Lewis acid sites of the catalyst [168].

To improve the activity and stability of γ-Al_2O_3, Yaripour et al. modified the catalyst with silica at different loadings and compared the MeOH conversion with these catalysts against pure γ-Al_2O_3 at 300 °C. They observed that the modified γ-Al_2O_3 showed improved performance compared with the unmodified γ-Al_2O_3. In addition, the conversion of MeOH increased as the amount of silica was increased. The catalyst with 6% silica exhibited high activity and stability without formation of any by-products. These results could be attributable to the increased strength and number of Brønsted acid sites on the catalyst surface after modification with silica [155].

Zeolites have also been investigated in MeOH-to-DME dehydration. Fua et al. studied the activity of HZSM-5 (25) at 150–330 °C. They found that this catalyst exhibited high activity in MeOH dehydration even at low temperatures because it possessed strong Brønsted acid sites. However, at higher temperatures (> 280 °C), the DME selectivity decreased due to formation of hydrocarbons and coke [169]. It is well-known that catalysts with very strong Brønsted acidity are prone to deactivation and produce undesired hydrocarbons, which are responsible for coke formation [167,169].

Vishwanathan et al. enhanced the coke resistance and stability of HZSM-5 (20) in a wide temperature range of 190–370 °C by partial substitution of Na in HZSM-5. The Na-modified HZSM-5 significantly improved MeOH dehydration, reaching > 90% conversion and 100% selectivity for DME at 340 °C. These findings were mainly attributed to the reduction of strong Brønsted acid sites at the surface [162]. Further, the modified zeolite catalysts were observed to enhance resistance to the production of coke in the dehydration of MeOH to DME [146,169–172].

In the last three decades, HPAs have attracted great attention as catalysts for use in alcohol dehydration reactions due to their unique catalytic properties. Solid Keggin-type HPAs have stronger Brønsted acid sites than those in zeolites and metal oxides [95]. Hence, some HPAs have exhibited higher catalytic activity than traditional solid acid catalysts in MeOH dehydration to DME at low temperatures [88,173]. Besides, the presence of heteropoly anions as conjugated bases is thought to accelerate the reactions. This is in contrast with conventional proton acids, in which the counter anion is not involved in the activation of the reactants [31,51,174]. HPW and HSiW are among the most used HPAs for dehydration of alcohols [86,157,175].

Many researchers have demonstrated high conversion and selectivity of MeOH dehydration over HPA catalysts, particularly at low temperatures of 140–180 °C [86,88,173]. However, since bulk Keggin HPAs have low specific surface areas, most protons present in the bulk of the HPA are inaccessible [31]. This drawback can be overcome by supporting HPAs on suitable porous supports [176]. Only a few articles have been published on catalysis by supported HPAs for the dehydration of MeOH.

Ciftci et al. also demonstrated the high activity of HPW during MeOH dehydration when the catalyst was supported on mesoporous silica (MCM-41) [142]. Supported HPW catalysts were synthesised by a one-pot hydrothermal method and the conventional impregnation method. The impregnated catalyst showed higher Brønsted acidity and higher activity in MeOH dehydration at 200 °C than that prepared by the hydrothermal method. However, at temperatures above 200 °C, coke was formed, which deactivated the catalyst. The catalysts prepared by the one-pot hydrothermal method showed stable performance without any coke formation and 100% DME selectivity at temperatures below 300 °C [142].

In addition, Ciftci et al. reported that MeOH conversion and DME selectivity over supported HPA catalysts increased at temperatures up to 200–250 °C but decreased at higher

temperatures. Schnee et al. found similar results and reported that MeOH conversion over bulk HPW at 200 °C decreased with the time on stream [157,177].

Alharbi et al. investigated MeOH dehydration over zeolites and supported HPA catalysts with 15% HPA loading at a MeOH partial pressure of 3.83 kPa and 120 °C [88]. The results showed that the activity of HPA catalysts was higher than that of HZSM-5 zeolites (10–120). It was observed that the conversion of MeOH to DME over supported HPA catalysts declined in the following order: 15%HPW/SiO_2 (16%) > $Cs_{2.25}H_{0.75}PW$ (13%) ≥ 15%HSiW/SiO_2 (13%) > $Cs_{2.5}H_{0.5}PW$ (8.6%) ≈ 15%HPW/TiO_2 (8.7%) > 15%HPW/Nb_2O_5 (1.3%) ≈ 15%HPW/ZrO_2 (1.7%). This was explained by decreasing the acid strength of the HPA catalysts the order of supports SiO_2 > TiO_2 > Nb_2O_5 ≈ ZrO_2 in line with increasing interaction between the support and the HPA.

The catalytic performance of HSiW supported on ZrO_2, TiO_2 and SiO_2 for DME production was studied by Peinado et al. [157]. The catalysts were prepared by wet impregnation of HSiW on supports at a variety of HPA loadings. Most of the catalysts exhibited high catalytic activity during MeOH dehydration at 180°C, and MeOH conversion varied between 40% and 90%. The MeOH conversion decreased in the following order: 73%HSiW/SiO_2 (90%) > 52%HSiW/TiO_2 (80%) > 46%HSiW/ZrO_2 (60%) > bulk HSiW (40%). They indicated that the activity of the catalysts decreased in line with their acidity (amount of NH_3 chemisorbed per gram of catalyst) as follows: 73%HSiW/SiO_2 (0.382 $mmol_{NH3}$ g_{cat}^{-1}) > 52%HSiW/TiO_2 (0.274 $mmol_{NH3}$ g_{cat}^{-1}) > 46%HSiW/ZrO_2 (0.209 $mmol_{NH3}$ g_{cat}^{-1}), except for bulk HSiW (0.512 $mmol_{NH3}$ g_{cat}^{-1}).

Ladera et al. [173] studied the dehydration of MeOH over TiO_2-supported HPW and HSiW at a loading that varied from 27% to 70%. The catalysts exhibited high activity during MeOH dehydration at 140 °C. The catalytic activity of the TiO_2-supported HPA was strongly affected by the loading of HPA on the surface of TiO_2. The optimum loading for HPW and

HSiW catalysts was 37% due to the high HPA dispersion on the TiO_2 surface. At higher HPA loadings, the dispersion of HPA decreased due to the formation of larger HPA particles on the surface, which may have prevented the access of MeOH to the inner acid sites. Although the catalysts were well dispersed at HPA loadings lower than 37%, the catalytic activity was reduced at these loadings owing to strong interaction between the HPA and the TiO_2 support. The effect of HPA loading on MeOH dehydration was attributed to the catalyst structure [173].

1.6.2. Dehydration of ethanol to diethyl ether and ethene in the gas phase

Ethene is an essential building block in the chemical industry [178]. Ethene is used to produce many chemicals such as acetaldehyde, acetic acid and styrene, etc. [179,180]. It is also used in the production of plastics such as polyethylene, polystyrene and polyvinyl chloride, which are widely utilised in the packaging and construction industries [180,181]. As stated in section 1.5, DEE is a prospective alternative fuel and fuel additive because of its high transportation fuel characteristics **(**cetane number > 125) [133,141,142]. Moreover, DEE can be used as a solvent in various fine chemical and pharmaceutical processes [182].

EtOH dehydration is carried out with the use of solid acid catalysts [48,95,142,179,183]. There are two competitive pathways via which catalytic EtOH dehydration occurs: the intramolecular dehydration of EtOH to ethene, and the intermolecular dehydration of EtOH to DEE [95]. These two pathways can occur in parallel during catalytic EtOH dehydration. At relatively low temperatures, the formation of DEE is favoured (exothermic), whereas the more demanding EtOH-to-ethene conversion occurs at higher temperatures (endothermic) [95]. Similar to DME formation from MeOH, the EtOH-to-DEE dehydration may be represented by associative and dissociative mechanisms (Scheme 1.6). [88,95].

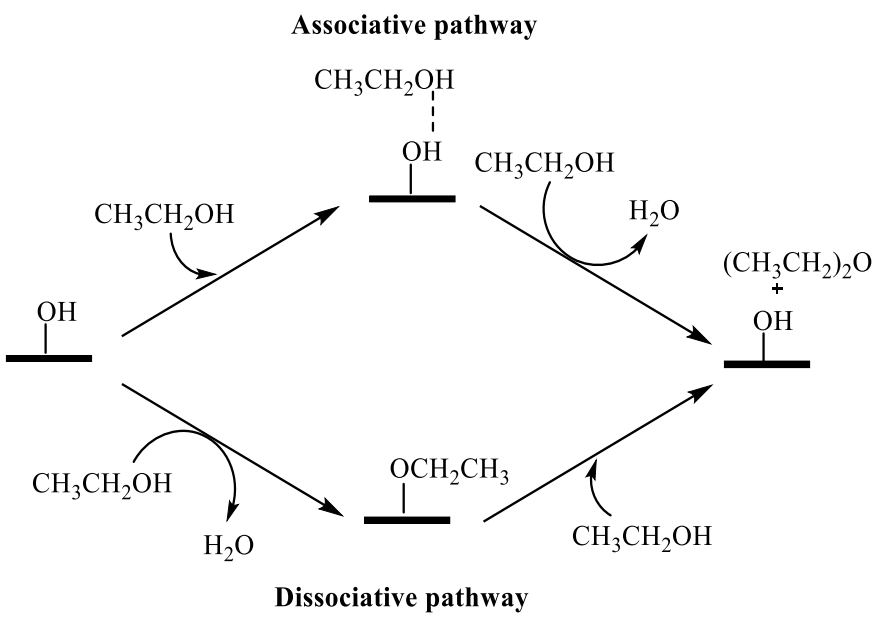

Scheme 1.6. Associative and dissociative pathways for dehydration of EtOH to produce DEE [95].

The EtOH-to-ethene dehydration is proposed to occur via the E2 elimination route (bimolecular elimination). This mechanism involves a concerted cleavage of the C–H and C–O bonds in the alcohol through use of a pair of acidic (H^+) and basic (B^-) catalytic sites (Scheme 1.7).

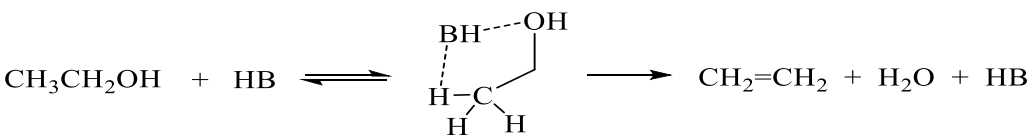

Scheme 1.7. E2 elimination of EtOH to form ethene through use of a pair of acidic (H^+) and basic (B^-) catalytic sites [95].

Numerous acid catalysts have been used in EtOH dehydration to DEE and ethene, such as alumina, silica-alumina, zeolites, HPAs and phosphoric acid [185–189]. Takahara et al. [190] examined the catalytic activity of zeolites (H-Mordenite, HZSM-5) and silica-alumina in EtOH dehydration to ethene at temperatures ranging from 180°C to 300 °C. They reported that

H-Mordenite was the most active catalyst for this reaction due to the existence of strong Brønsted acid sites.

Phung et al. [191] investigated EtOH dehydration through use of commercial H-Ferrierite (20), H-Mordenite (20), H-MFI (50), H-BEA (25) and H-USY(30) zeolite catalysts, as well as alumina and silica-alumina (11). They found that at 200 °C, all zeolites showed EtOH conversion > 45%, which was much higher than the figures for silica-alumina and alumina (both 20%). The high activity of zeolites was attributed to the presence of Brønsted acidic bridging hydroxyl groups in the zeolite cavities. The activity trend of the zeolite samples at 140 °C was H-Mordenite (16.3%) > H-MFI (11.5%) > H-BEA (7.7%) ≈ H-Ferrierite (7.0%) > H-USY (2.5%). A similar finding was reported by Phung and Busca, who stated that protonic zeolites (MFI and USY) were significantly more active than alumina or silica-alumina for EtOH dehydration at temperatures from 200 °C to 300 °C [182].

HPA catalysts were also utilised in EtOH dehydration. Varisli et al. investigated EtOH dehydration over bulk HPAs (namely HPW, HSiW and HPMo) at 140–250 °C in the gas phase. The catalytic activity of these HPA catalysts was found to decline in the following order: HSiW > HPW > HPMo. This result was explained by the fact that HSiW had more protons than the other HPAs per Keggin unit. In addition, the researchers detected that DEE was the main product at lower temperatures, whereas increasing the temperature of reaction from 140 °C to 250 °C led to a significant increase in ethene yield. They obtained 75% ethene selectivity over HPW at 250 °C [192].

Alharbi et al. [95] examined the dehydration of EtOH to DEE over different solid Brønsted acid catalysts based on Keggin-type HPAs in the gas phase. They used HPW and HSiW supported on SiO_2, TiO_2, ZrO_2 and Nb_2O_5, with a sub-monolayer loading of HPA (15%). At 120 °C and at an EtOH partial pressure of 1.48 kPa, the EtOH conversion declined in the following order: HPW/SiO_2 (52%) ≥ HSiW/SiO_2 (51%) > HPW/TiO_2 (19%) > HPW/ZrO_2

(7.6%) > HPW/Nb_2O_5 (6.9%). This order corresponds to the acid strength of these catalysts, which exhibit initial heats of NH_3 adsorption of -154, 154, 143, 121 and 132 kJ mol^{-1}, respectively. Under the same conditions, EtOH dehydration was also tested over bulk acidic Cs salts of HPW ($Cs_xH_{3-x}PW_{12}O_{40}$). EtOH conversion efficiencies were reduced as the density of surface proton sites decreased in the Cs salts: $Cs_{2.25}H_{0.75}PW_{12}O_{40}$ (49%) > $Cs_{2.5}H_{0.5}PW_{12}O_{40}$ (33%) > $Cs_3PW_{12}O_{40}$. This result indicated that the Brønsted acid sites played a vital role in the dehydration of EtOH to DEE over solid HPA catalysts. Similar results were obtained in the dehydration of EtOH over potassium salts of HPW [193].

Popa et al. [194] investigated the dehydration of EtOH in the gas phase over cobalt salts of tungstophosphoric acid (CoHPW) supported on mesoporous silica at different loadings (20–40%). The activity of CoHPW/SiO_2 catalysts was higher than that of bulk CoHPW. This result may be due to the high dispersion of CoHPW on the silica surface.

Several studies have found that DEE can act as an intermediate in ethene production from EtOH [142,182,190,195]. Garbarino et al. [196] investigated the elimination of DEE over commercial large-pore γ-Al_2O_3 and commercial La-doped γ-Al_2O_3 catalysts at 100–500 °C. It was observed that the DEE conversion and ethene selectivity were slightly higher on pure alumina than on La-containing catalysts. All these catalysts reached nearly total DEE conversion at 350 °C. Generally, doping La^{3+} on γ-Al_2O_3 slightly decreased the catalytic activity but improved catalyst stability towards coking.

Moreover, the DEE conversion to ethene at 150–450 °C over solid acid catalysts that included alumina, zeolites (MFI and USY), silica-alumina and calcined hydrotalcite was examined by Phung and Busca [182]. They observed that DEE conversion at 300°C decreased in the following order: MFI (98.3%) > USY (83.8%) > alumina (55.9%) > silica-alumina (52.1%) > calcined hydrotalcite (0.1%). They demonstrated that the protonic zeolites (Brønsted acid catalysts) exhibited a higher DEE conversion rate than alumina (a Lewis acid catalyst) and

calcined hydrotalcite (a basic catalyst). These findings imply that the Brønsted acid sites are active in the conversion of DEE to ethene.

1.7. Research aims and objectives

In recent years, HPAs have received significant attention as catalysts for alcohol dehydration. HPAs exhibit higher catalytic activities than the conventional acid catalysts and therefore provide potential environmental and economic benefits. Silica has been demonstrated to be an effective support for HPAs due to its neutral nature, large surface area, porosity and availability in a wide range of textures [197]. Silica is also a relatively inert material that interacts weakly with HPAs. However, there is limited knowledge regarding silica-supported HPA catalysts. This knowledge gap concerns the effect of HPA loading on the strength of proton sites and their density in SiO_2-supported HPA catalysts. Likewise, there is limited data concerning the impact of HPA loading on the catalytic performance of HPA/SiO_2 catalysts used in alcohol dehydration and related reactions. Such information is essential for catalyst development and process optimisation and to gain mechanistic insights, for example, regarding the role of bulk versus surface catalysis in alcohol dehydration over HPA catalysts.

The first aim of this study was to gain detailed knowledge of the acidic properties of silica-supported HPA catalysts, including the Keggin-type HPAs that are most important for heterogeneous acid catalysis, namely HPW and HSiW. These catalysts were studied at a wide range of HPA loadings that are relevant to commercial practice, from 5% to 100%. Secondly, the knowledge obtained was used to investigate the dehydration of MeOH and EtOH over HPA/SiO_2 catalysts to optimise catalyst performance and to gain new mechanistic insights. In addition, DEE elimination to EtOH and ethene, which is a step in the process of dehydration EtOH, was investigated in the presence of HPA/SiO_2 catalysts. Therefore, the work included the following objectives:

- to examine the impact of the loading of HPA on the acid strength of HPA/SiO_2 catalysts via systematic, quantitative evaluation of the acidity of bulk and silica-supported HPW and HSiW at a gas-solid interface using ammonia adsorption microcalorimetry (NH_3-MC) and simultaneous thermogravimetric analysis and differential scanning calorimetry (TGA–DSC).
- to explore the effect of HPA loading and acid strength on the MeOH and EtOH dehydration reactions at conditions relevant to practice (5–100% HPA loading);
- to gain new mechanistic insights into the role of the bulk-type and surface-type HPA catalysis in the dehydration of MeOH and EtOH in the gas phase over silica-supported HPA catalysts; and
- to investigate the elimination of DEE to form ethene and EtOH in the presence of bulk and supported Brønsted solid-acid catalysts based on tungsten Keggin HPAs (HPW and HSiW) at a gas-solid interface and to compare the activity and selectivity of HPA catalysts with those of conventional catalysts such as zeolites and metal oxides.

1.8. Outline of the thesis

The thesis is structured as six chapters and one appendix. Their contents are as follows:

Chapter 1: provides an overview of heterogeneous catalysis and the concepts of heterogeneous acid catalysis. Additionally, this Chapter contains an overview of HPAs as solid acid catalysts. Recent research on alcohol dehydration and DEE elimination over solid acid catalysts is also reviewed.

Chapter 2: contains a description of the synthesis of the HPA catalysts and the techniques that were applied to characterise these catalysts. It also describes the set-up of a fixed-bed reactor with on-line gas chromatographic (GC) analysis, reaction conditions and catalyst testing methodology.

Chapter 3: describes the acid properties of bulk and SiO_2-supported HPA catalysts, which were studied via NH_3-MC, and presents information regarding the structure and physicochemical properties of the HPA/SiO_2 catalysts.

Chapter 4: contains details of the dehydration of MeOH and EtOH in the gas phase over bulk and SiO_2-supported Brønsted acid catalysts based on tungsten Keggin HPAs.

Chapter 5: describes the elimination of DEE to form ethene and EtOH over HPW and HSiW supported on TiO_2, ZrO_2 and SiO_2, as well as bulk acidic CsPW salt.

Chapter 6: gives a summary of the major conclusions that were derived from the results of this work and outlines the proposed directions of future studies.

Reference

[1] G.C. Bond, Heterogeneous Catalysis: Principles and Applications, Oxford University Press, New York, 1987.

[2] J. Wisniak, The history of catalysis. from the beginning to nobel prizes, Educ. Quim. 21 (2010) 60–69.

[3] M. Bowker, The Basis and Applications of Heterogeneous Catalysis, Oxford University Press Inc, New York, 1998.

[4] O. Deutschmann, H. Knozinger, K. Kochloefl, T. Turek, Heterogeneous Catalysis and Solid Catalysts, Wiley–VCH Verlag GmbH & Co. KGaA, Weinheim, 2009.

[5] G. Rothenberg, Catalysis Concepts and Green Applications, Wiley–VCH Verlag GmbH & Co.KGaA, Weinheim, 2008.

[6] M. Misono, Chapter 1-Basis of heterogeneous catalysis, in: M. Misono (Eds.), Studies in Surface Science and Catalysis, Elsevier B.V., Oxford, 2013: pp. 1–173.

[7] R.A. Sheldon, I. Arends, U. Hanefeld, Green Chemistry and Catalysis, Wiley–VCH Verlag GmbH & Co, Weinheim, 2007.

[8] P. Unnikrishnan, D. Srinivas, Chapter 3-Heterogeneous catalysis, in: S.S. Joshi, V.V. Ranade (Eds.), Industrial Catalytic Processes for Fine and Specialty Chemicals, Elsevier, Cambridge, 2016: pp. 41–111.

[9] J.M. Thomas, W.J. Thomas, Principles and Practice of Heterogeneous Catalysis, VCH Verlagsgesllscharft mbH, Weinheim, 1997.

[10] M. Schmal, Heterogeneous Catalysis and its Industrial Applications, Springer International Publishing AG, Switzerland, 2016.

[11] P. Gupta, S. Paul, Solid acids: Green alternatives for acid catalysis, Catal. Today 236 (2014) 153–170.

[12] X. Li, A. Wang, R. Prins, Introduction to Heterogeneous Catalysis, Imperial College Press, United Kingdom, 2016.

[13] R.A. Sheldon, H.V. Bekkum, Fine Chemicals through Heterogeneous Catalysis, Wiley-VCH, Weinheim, 2001.

[14] W. Keim, Multiphase catalysis and its potential in catalytic processes: The story of biphasic homogeneous catalysis, Green Chem. 5 (2003) 105–111.

[15] J. Li, M.F. Stephanopoulos, Y. Xia, Introduction: Heterogeneous single-atom catalysis, Chem. Rev. 120 (2020) 11699–11702.

[16] I. Chorkendorff, J.W. Niemantsverdriet, Concepts of Modern Catalysis and Kinetics, second ed., Wiley–VCH Verlag GmbH & Co. KGaA, Weinheim, 2007.

[17] Y. Pan, X. Shen, L. Yao, A. Bentalib, Z. Peng, Active sites in heterogeneous catalytic reaction on metal and metal oxide: Theory and practice, Catalysts 8 (2018) 478.

[18] G. Leofanti, M. Padovan, G. Tozzola, B. Venturelli, Surface area and pore texture of catalysts, Catal. Today 41 (1998) 207–219.

[19] S.A. Kondrat, J.A. van Bokhoven, A Perspective on counting catalytic active sites and rates of reaction using X-Ray spectroscopy, Top. Catal. 62 (2019) 1218–1227.

[20] H. Hattori, Y. Ono, Solid Acid Catalysis from Fundamentals to Applications, Pan Stanford Publishing, Singapore, 2015.

[21] H. Hattori, Solid acid catalysts: Roles in chemical industries and new concepts, Top. Catal. 53 (2010) 432–438.

[22] J.M. Fernández-Morales, E. Castillejos, E. Asedegbega-Nieto, A.B. Dongil, I. Rodríguez-Ramos, A. Guerrero-Ruiz, Comparative study of different acidic surface structures in solid catalysts applied for the isobutene dimerization reaction, Nanomaterials 10 (2020) 1235.

[23] O. Muraza, A. Galadima, Isomerization and alkylation of biomass-derived compounds in aqueous media over hydrophobic solid acid catalysts: A mini review, Ind. Eng. Chem. Res. 53 (2014) 17869–17877.

[24] A. Zheng, S. Li, S. Liu, F. Deng, Acidic properties and structure-activity correlations of solid acid catalysts revealed by solid-state NMR spectroscopy, Acc. Chem. Res. 49 (2016) 655–663.

[25] A. Zheng, S.J. Huang, S. Bin Liu, F. Deng, Acid properties of solid acid catalysts characterized by solid-state ^{31}P NMR of adsorbed phosphorous probe molecules, Phys. Chem. Chem. Phys. 13 (2011) 14889–14901.

[26] J.C. Védrine, Acid-base characterization of heterogeneous catalysts: An up-to-date overview, Res. Chem. Intermed. 41 (2015) 9387–9423.

[27] R.A. Van Santen, Modern Heterogeneous Catalysis, Wiley–VCH Verlag GmbH & Co. KGaA, Weinheim, 2017.

[28] P. Kostestkyy, J. Yu, R.J. Gorte, G. Mpourmpakis, Structure-activity relationships on metal-oxides: Alcohol dehydration, Catal. Sci. Technol. 4 (2014) 3861–3869.

[29] B.C. Gates, Catalytic Chemistry, John Wiley & Sons, Inc, Singapore, 1992.

[30] M. Abdelgaid, J. Dean, G. Mpourmpakis, Improving alkane dehydrogenation activity on γ-Al_2O_3 through Ga doping, Catal. Sci. Technol. 10 (2020) 7194–7202.

[31] I.V. Kozhevnikov, Catalysts for Fine Chemical Synthesis Catalysis by Polyoxometalates, Vol. 2, John Wiley, Chichester, England, 2002.

[32] I.V. Kozhevnikov, Catalysis by heteropoly acids and multicomponent polyoxometalates in liquid-phase reactions, Chem. Rev. 98 (1998) 171–198.

[33] I.V. Kozhevnikov, Heterogeneous acid catalysis by heteropoly acids: Approaches to catalyst deactivation, J. Mol. Catal. A: Chem. 305 (2009) 104–111.

[34] S. Passadis, T.A. Kabanos, Y.F. Song, H.N. Miras, Self-assembly in polyoxometalate and metal coordination-based systems: Synthetic approaches and developments, Inorganics 6 (2018) 71.

[35] M.T. Pope, Heteropoly and Isopoly Oxometalates; Inorganic Chemistry Concepts, Vol. 8, Springer-Verlag, Berlin, 1983.

[36] M. Misono, Chapter 4-Catalysis of Heteropoly Compounds (Polyoxometalates), in: M. Misono (Eds.), Studies in Surface Science and Catalysis, Elsevier B.V., Oxford, 2013: pp. 97–155.

[37] M.J. Craven, Development of Phosphazene-Polyoxometalate Catalyst Systems for Multiphase Oxidations with Hydrogen Peroxide, Doctoral dissertation, University of Liverpool, Liverpool, 2017.

[38] J.F. Keggin, Structure of the molecule of 12-Phosphotungstic acid, Nature 131 (1933) 908.

[39] H. So, M.T. Pope, Origin of some charge-transfer spectra. Oxo compounds of vanadium, molybdenum, tungsten, and niobium including heteropoly anions and heteropoly blues, Inorg. Chem. 11 (1972) 6.

[40] M.A. Leparulo-Loftus, M.T. Pope, Vanadium-51 NMR spectroscopy of tungstovanadate polyanions. Chemical shift and line-width patterns for the identification of stereoisomers, Inorg. Chem. 26 (1987) 2112–2120.

[41] M.T. Pope, G.M. Varga, Proton magnetic resonance of aqueous metatungstate ion: Evidence for two central hydrogen atoms, Chem. Commun. 583 (1966) 18.

[42] A. Müller, S. Roy, En route from the mystery of molybdenum blue via related manipulatable building blocks to aspects of materials science, Coord. Chem. Rev. 245 (2003) 153–166.

[43] M.T. Pope, A. Müller, Polyoxometalate Chemistry from Topology via Self-Assembly to Applications, Kluwer Academic Publishers, New York, 2002.

[44] M.T. Pope, A. Müller, Polyoxometalate chemistry: An old field with new dimensions in several disciplines, Angew Chem. Int. Ed. Engl. 30 (1991) 34–48.

[45] G.A. Tsigdinos, C.J. Hallada, Molybdovanadophosphoric acids and their salts. I. investigation of methods of preparation and characterization, Inorg. Chem. 7 (1968) 3.

[46] G.A. Tsicdinos, C.J. Hallada, Synthesis and electrochemical properties of heteropoly molybdates, J. Less-common Met. 36 (1974) 79–93.

[47] G.A. Tsigdinos, C.J. Hallada, Solution properties of 12-heteropoly acids of molybdenum, Inorg. Chem. 9 (1970) 11.

[48] T. Okuhara, N. Mizuno, M. Misono, Catalytic Chemistry of Heteropoly Compounds, in: D.D. Eley, Werner O. Haag, Bruce Gates (Eds.), Advances in Catalysis, Vol. 41, Academic Press, 1996: pp. 113–252.

[49] N. Mizuno, M. Misono, Heterogeneous catalysis, Chem. Rev. 98 (1998) 199–217.

[50] J.B. Moffat, Metal-Oxygen Clusters the Surface and Catalytic Properties of Heteropoly Oxometalates, Kluwer Academic Publishers, New York, 2002.

[51] Y. Izumi, K. Urabe, M. Onaka, Zeolite, Clay and Heteropoly Acid in Organic Reactions, Kodansha/VCH, Tokyo, 1992.

[52] J.G. Hernández-Cortez, M. Manríquez, L. Lartundo-Rojas, E. López-Salinas, Study of acid-base properties of supported heteropoly acids in the reactions of secondary alcohols dehydration, Catal. Today 220–222 (2014) 32–38.

[53] M.N. Timofeeva, Acid catalysis by heteropoly acids, Appl. Catal. A: Gen. 256 (2003) 19–35.

[54] M. Misono, Unique acid catalysis of heteropoly compounds (heteropolyoxometalates) in the solid state, Chem. Commun. 1 (2001) 1141–1153.

[55] Y. Kamiya, T. Okuhara, M. Misono, A. Miyaji, K. Tsuji, T. Nakajo, Catalytic chemistry of supported heteropolyacids and their applications as solid acids to industrial processes, Catal. Surv. Asia12 (2008) 101–113.

[56] A. Enferadi-Kerenkan, T-O. Do, S. Kaliaguine, Heterogeneous catalysis by tungsten-based heteropoly compounds, Catal. Sci. Technol. 8 (2018) 2257–2284.

[57] I.V. Kozhevnikov, Sustainable heterogeneous acid catalysis by heteropoly acids, J. Mol. Catal. A: Chem. 262 (2007) 86–92.

[58] T. Kella, A.A. Vennathan, S. Dutta, S.S. Mal, D. Shee, Selective dehydration of 1-butanol to butenes over silica supported heteropolyacid catalysts: Mechanistic aspect, Mol. Catal. 516 (2021) 111975.

[59] D.B. Taylor, J.B. McMonagle, J.B. Moffat, Cation effects on the surface and bulk structure of the salts of 12-tungstosilicic acid, J. Colloid Interface Sci.108 (1985) 1.

[60] J.G. Highfield, J.B. Moffat, Elucidation of the mechanism of dehydration of methanol over acid using infrared photoacoustic spectroscopy, J. Catal. 95 (1985) 108–119.

[61] M. Misono, A view on the future of mixed oxide catalysts The case of heteropoly acids (polyoxometalates) and perovskites, Catal. Today 100 (2005) 95–100.

[62] I.V. Kozhevnikov, Advances in catalysis by heteropolyacids, Russ. Chem. Rev. 56 (1987) 811–825.

[63] C.L. Hill, Progress and challenges in polyoxometalate-based catalysis and catalytic materials chemistry, J. Mol. Catal. A: Chem. 262 (2007) 2–6.

[64] V.A. Grigoriev, C.L. Hill, I.A. Weinstock, Role of cation size in the energy of electron transfer to 1:1 polyoxometalate ion pairs $\{(M^{+})\ (Xn^{+}VW_{11}O_{40})\}^{(8-n)-}$ (M=Li,Na,K), J. Am. Chem. Soc.122 (2000) 3544–3545.

[65] C. Hill, Introduction: Polyoxometalates-multicomponent molecular vehicles to probe fundamental issues and practical problems, Chem. Rev. 98 (1998) 1.

[66] A.M. Khenkin, G. Leitus, R. Neumann, Electron transfer-oxygen transfer oxygenation of sulfides catalyzed by the $H_5PV_2Mo_{10}O_{40}$ polyoxometalate, J. Am. Chem. Soc. 132 (2010) 11446–11448.

[67] A.M. Khenkin, L. Weiner, Y. Wang, R. Neumann, Electron and oxygen transfer in polyoxometalate, $H_5PV_2Mo_{10}O_{40}$, catalysed oxidation of aromatic and alkyl aromatic compounds: Evidence for aerobic Mars-van Krevelen-type reactions in the liquid homogeneous phase, J. Am. Chem. Soc. 123 (2001) 8531–8542.

[68] I. Efremenko, R. Neumann, Computational insight into the initial steps of the mars-van krevelen mechanism: Electron transfer and surface defects in the reduction of polyoxometalates, J. Am. Chem. Soc. 134 (2012) 20669–20680.

[69] I. Efremenko, R. Neumann, Protonation of phosphovanadomolybdates $H_{3+x}PV_xMo_{12x}O_{40}$: Computational insight into reactivity, J. Phys. Chem. A. 115 (2011) 4811–4826.

[70] G.S. Armatas, Chapter 13-Heterogeneous polyoxometalate-containing mesoporous catalysts, in: S.L. Suib (Eds.), New and Future Developments in Catalysis, Elsevier Inc., Netherlands, 2013: pp. 311–342.

[71] M.R. Horn, A. Singh, S. Alomari, S. Goberna-Ferrón, R. Benages-Vilau, N. Chodankar, N. Motta, K. Ostrikov, J. MacLeod, P. Sonar, P. Gomez-Romero, D. Dubal, Polyoxometalates (POMs): from electroactive clusters to energy materials, Energy Environ. Sci. 14 (2021) 1652–1700.

[72] L. Zhai, H. Li, Polyoxometalate-polymer hybrid materials as proton exchange membranes for fuel cell applications, Molecules 24 (2019) 3425.

[73] J.J. Borrás-Almenar, E. Coronado, A. Müller, M.T. Pope, Polyoxometalate Molecular Science, Kluwer Academic Publishers, Netherlands, 2003.

[74] C. Baroi, A.K. Dalai, Review on biodiesel production from various feedstocks using

12-Tungstophosphoric acid (TPA) as a solid acid catalyst precursor, Ind. Eng. Chem. Res. 53 (2014) 18611–18624.

[75] B.B. Bardin, R.J. Davis, M. Neurock, Ammonia adsorption on Keggin-type heteropoly acid catalysts explored by density functional quantum chemistry calculations, J. Phys. Chem. B 104 (2000) 3556–3562.

[76] S.P. Jiang, Functionalized mesoporous structured inorganic materials as high temperature proton exchange membranes for fuel cells, J. Mater. Chem. A 2 (2014) 7637–7655.

[77] J. Zhong, J. Pérez-Ramírez, N. Yan, Biomass valorisation over polyoxometalate-based catalysts, Green Chem. 23 (2021) 18–36.

[78] G.D. Yadav, Synergism of clay and heteropoly acids as nano-catalysts for the development of green processes with potential industrial applications, Catal. Surv. Asia 9 (2005) 117–137.

[79] G.M. Brown, M.R. Noe-Spirlet, W.R. Bushing, H.A. Levy, Dodecatungstophosphoric acid hexahydrate, $(H_5O_2^+)^3(PW_{12}O_{40}^{3-})$. The true structure of Keggin's `pentahydrate' from single-crystal X-ray and neutron diffraction data, Acta Crystallogr. 33 (1977) 1038–1046.

[80] M.J. Janik, K.A. Campbell, B.B. Bardin, R.J. Davis, M. Neurock, A computational and experimental study of anhydrous phosphotungstic acid and its interaction with water molecules, Appl. Catal. A: Gen. 256 (2003) 51–68.

[81] D.I. Kolokolov, M.S. Kazantsev, M.V. Luzgin, H. Jobic, A.G. Stepanov, Direct ^2H NMR observation of the proton mobility of the acidic sites of anhydrous 12-tungstophosphoric acid, ChemPhysChem 14 (2013) 1783–1786.

[82] I.V. Kozhevnikov, A. Sinnema, R.J.J. Jansen, H. Van Bekkum, ^{17}O NMR determination of proton sites in solid heteropoly acid $H_3PW_{12}O_{40}$.^{31}P,^{29}Si and^{17}O NMR, FT-IR and

XRD study of $H_3PW_{12}O_{40}$ and $H_4SiW_{12}O_{40}$ supported on carbon, Catal. Lett. 27 (1994) 187–197.

[83] I.V. Kozhevnikov, A. Sinnema, H. Van Bekkum, Proton sites in Keggin heteropoly acids from ^{17}O NMR, Catal. Lett. 34 (1995) 213–221.

[84] I.V. Kozhevnikov, A. Sinnema, H. Van Bekkum, M. Fournier, ^{17}O MAS NMR study of 12-molybdophosphoric acid, Catal. Lett. 41 (1996) 153–157.

[85] S. Ganapathy, M. Fournier, J.F. Paul, L. Delevoye, M. Guelton, J.P. Amoureux, Location of protons in anhydrous Keggin heteropolyacids $H_3PMo_{12}O_{40}$ and $H_3PW_{12}O_{40}$ by $^{1}H\{^{31}P\}/^{31}P\{^{1}H\}$ REDOR NMR and DFT quantum chemical calculations, J. Am. Chem. Soc. 124 (2002) 7821–7828.

[86] R.M. Ladera, J.L.G. Fierro, M. Ojeda, S. Rojas, TiO_2-supported heteropoly acids for low-temperature synthesis of dimethyl ether from methanol, J. Catal. 312 (2014) 195–203.

[87] K. Na, T. Okuhara, M. Misono, Skeletal isomerization of n-butane over caesium hydrogen salts of 12-tungstophosphoric acid, J. Chem. Soc. Faraday Trans. 91 (1995) 367–373.

[88] W. Alharbi, E.F. Kozhevnikova, I.V. Kozhevnikov, Dehydration of methanol to dimethyl ether over heteropoly acid catalysts: The relationship between reaction rate and catalyst acid strength, ACS Catal. 5 (2015) 7186–7193.

[89] F.J. Berry, G.R. Derrick, M. Mortimer, Identification and characterisation of stable phases of silicotungstic acid, $H_4SiW_{12}O_{40}{\cdot}nH_2O$, Polyhedron 68 (2014) 17–22.

[90] J. Zhang, M. Kanno, Y. Wang, H. Nishii, Y.K. Miura, Y. Kamiya, Changes in surface acidity of silica-supported dodecatungstosilicic acid in relation to the loading amount, J. Phys. Chem. C 115 (2011) 14762–14769.

[91] E.F. Kozhevnikova, I.V. Kozhevnikov, A calorimetric study of the acidity of bulk and silica-supported heteropoly acid $H_3PW_{12}O_{40}$, J. Catal. 224 (2004) 164–169.

[92] A. Ghanbari-Siahkali, A. Philippou, J. Dwyer, M.W. Anderson, The acidity and catalytic activity of heteropoly acid on MCM-41 investigated by MAS NMR, FTIR and catalytic tests, Appl. Catal. A: Gen. 192 (2000) 57–69.

[93] A.D. Newman, D.R. Brown, P. Siril, A.F. Lee, K. Wilson, Structural studies of high dispersion $H_3PW_{12}O_{40}/SiO_2$ solid acid catalysts, Phys. Chem. Chem. Phys. 8 (2006) 2893–2902.

[94] F. Lefebvre, F.X. Liu-Cai, A. Auroux, Microcalorimetric study of the acidity of tungstic heteropolyanions, J. Mater. Chem. 4 (1994) 125–131.

[95] W. Alharbi, E. Brown, E.F. Kozhevnikova, I.V. Kozhevnikov, Dehydration of ethanol over heteropoly acid catalysts in the gas phase, J. Catal. 319 (2014) 174–181.

[96] L.C. Jozefowicz, H.G. Karge, E. Vasilyeva, J.B. Moffat, A microcalorimetric investigation of heteropolyacids, Microporous Mater. 1 (1993) 313–322.

[97] T. Okuhara, Microporous heteropoly compounds and their shape selective catalysis, Appl. Catal. A: Gen. 256 (2003) 213–224.

[98] G. Koyano, K. Ueno, M. Misono, Three types of acid catalysis in liquid phase of metal salts of 12-Tungstophosphoric acid, $M_{xn+}H_{3-nx}PW_{12}O_{40}$, Appl. Catal. A: Gen. 181 (1999) 267–275.

[99] T. Okuhara, H. Watanabe, T. Nishimura, K. Inumaru, M. Misono, Microstructure of cesium hydrogen salts of 12-tungstophosphoric acid relevant to novel acid catalysis, Chem. Mater. 12 (2000) 2230–2238.

[100] N. Essayem, R. Frety, G. Coudurier, J.C. Vedrine, Ammonia adsorption-desorption over the strong solid acid catalyst $H_3PW_{12}O_{40}$ and its Cs^+ and $NH4^+$ salts Comparison with sulfated zirconia, J. Chem. Soc. Faraday Trans. 93 (1997) 3243–3248.

[101] N. Essayem, G. Coudurier, M. Fournier, J.C. Védrine, Acidic and catalytic properties of $Cs_xH_{3-x}PW_{12}O_{40}$ heteropolyacid compounds, Catal. Lett. 34 (1995) 223–235.

[102] N. Essayem, Y.Y. Tong, H. Jobic, J.C. Vedrine, Characterization of protonic sites in $H_3PW_{12}O_{40}$ and $Cs_{1.9}H_{1.1}PW_{12}O_{40}$: a solid-state ^{1}H, ^{2}H, ^{31}P MAS-NMR and inelastic neutron scattering study on samples prepared under standard reaction conditions, Appl. Catal. A: Gen. 194 (2000) 109–122.

[103] T. Okuhara, T. Nishimura, H. Watanabe, M. Misono, Insoluble heteropoly compounds as highly active catalysts for liquid-phase reactions, J. Mol. Catal. 74 (1992) 247–256.

[104] M.A. Hanif, S. Nisar, U. Rashid, Supported solid and heteropoly acid catalysts for production of biodiesel, Catal. Rev. -Sci. Eng. 59 (2017) 165–188.

[105] J. Haber, K. Pamin, L. Matachowski, D. Mucha, Catalytic performance of the dodecatungstophosphoric acid on different supports, Appl. Catal. A: Gen. 256 (2003) 141–152.

[106] K.M. Rao, R. Gobetto, A. Iannibello, A. Zecchina, Solid state NMR and IR studies of phosphomolybdenum and phosphotungsten heteropoly acids supported on SiO_2, γ-Al_2O_3, and SiO_2-Al_2O_3, J. Catal. 119 (1989) 512–516.

[107] P. Sun, D.H. Yu, Y. Hu, Z.C. Tang, J.J. Xia, H. Li, H. Huang, $H_3PW_{12}O_{40}/SiO_2$ for sorbitol dehydration to isosorbide: High efficient and reusable solid acid catalyst, Korean J. Chem. Eng. 28 (2011) 99–105.

[108] I.V. Kozhevnikov, K.R. Kloetstra, A. Sinnema, H.W. Zandbergen, H.V. Bekkum, Study of catalysts comprising heteropoly acid $H_3PW_{12}O_{40}$ supported on MCM-41 molecular sieve and amorphous silica, J. Mol. Catal. A: Chem. 114 (1996) 287–298.

[109] T. Baba, Y. Ono, Heteropolyacids and their salts supported on acidic ion-exchange resin as highly active solid-acid catalysts, Appl. Catal. 22 (1986) 321–324.

[110] T. Baba, Y. Ono, T. Ishimoto, S. Moritaka, S. Tanooka, Heteropoly acids supported on acidic ion-exchange resin as highly active solid acid catalysts, Bull. Chem. Soc. Jpn. 58 (1985) 2155–2156.

[111] B.M. Devassy, F. Lefebvre, S.B. Halligudi, Zirconia-supported 12-tungstophosphoric acid as a solid catalyst for the synthesis of linear alkyl benzenes, J. Catal. 231 (2005) 1–10.

[112] A.M. Alsalme, P.V. Wiper, Y.Z. Khimyak, E.F. Kozhevnikova, I.V. Kozhevnikov, Solid acid catalysts based on $H_3PW_{12}O_{40}$ heteropoly acid: Acid and catalytic properties at a gas-solid interface, J. Catal. 276 (2010) 181–189.

[113] A. Micek-Ilnicka, E. Bielańska, L. Lityńska-Dobrzyńska, A. Bielański, Carbon nanotubes, silica and titania supported heteropolyacid $H_3PW_{12}O_{40}$ as the catalyst for ethanol conversion, Appl. Catal. A: Gen. 421–422 (2012) 91–98.

[114] T. Blasco, A. Corma, A. Martínez, P. Martínez-Escolano, Supported heteropolyacid (HPW) catalysts for the continuous alkylation of isobutane with 2-butene: The benefit of using MCM-41 with larger pore diameters, J. Catal. 177 (1998) 306–313.

[115] A. Lapkin, C. Savill-Jowitt, K. Edler, R. Brown, Microcalorimetric study of ammonia chemisorption on $H_3PW_{12}O_{40}$ supported onto mesoporous synthetic carbons and SBA-15, Langmuir 22 (2006) 7664–7671.

[116] J. Schnee, A. Eggermont, E.M. Gaigneaux, Boron nitride: A support for highly active heteropolyacids in the methanol-to-DME reaction, ACS Catal. 7 (2017) 4011–4017.

[117] Z. Wang, L. Liu, Mesoporous silica supported phosphotungstic acid catalyst for glycerol dehydration to acrolein, Catal. Today 376 (2021) 55–64.

[118] E. Tsukuda, S. Sato, R. Takahashi, T. Sodesawa, Production of acrolein from glycerol over silica-supported heteropoly acids, Catal. Commun. 8 (2007) 1349–1353.

[119] E.I. García-López, G. Marcì, I. Krivtsov, J.C. Espina, L.F. Liotta, A. Serrano, Local structure of supported Keggin and Wells-Dawson heteropolyacids and its influence on the catalytic activity, J. Phys. Chem. C 123 (2019) 19513–19527.

[120] A. Patel, Environmentally Benign Catalysts for Clean Organic Reactions, Panch Tattva Publishers, Pune, India, 2013.

[121] B.B. Bardin, R.J. Davis, Effect of water on silica-supported phosphotungstic acid catalysts for 1-butene double bond shift and alkane skeletal isomerization, Appl. Catal. A: Gen. 200 (2000) 219–231.

[122] A. Micek-Ilnicka, The role of water in the catalysis on solid heteropolyacids, J. Mol. Catal. A: Chem. 308 (2009) 1–14.

[123] E. Rafie, S. Eavani, Heterogenization of heteropoly compounds: A review of their structure and synthesis, RSC Adv. 6 (2016) 46433–46466.

[124] K.Y. Lee, T. Arai, S-I. Nakata, S. Asaoka, T. Okuhara, M. Misono, Catalysis by Heteropoly Compounds. 20. An NMR study of ethanol dehydration in the pseudoliquid phase of 12-tungstophosphoric acid, J. Am. Chem. Soc. 114 (1992) 2836–2842.

[125] P.S. Kong, M.K. Aroua, W.M.A.W. Daud, H.V. Lee, P. Cognet, Y. Pérès, Catalytic role of solid acid catalysts in glycerol acetylation for the production of bio-additives: A review, RSC Adv. 6 (2016) 68885–68905.

[126] Y. Yamamoto, S. Hatanaka, K. Tsuji, K. Tsuneyama, R. Ohnishi, H. Imai, Y. Kamiya, T. Okuhara, Direct addition of acetic acid to ethylene to form ethyl acetate in the presence of $H_4SiW_{12}O_{40}/SiO_2$, Appl. Catal. A: Gen. 344 (2008) 55–60.

[127] T. Baba, Y. Ono, The conversion of methanol into hydrocarbons over copper (II) dodecatungtophosphate, Appl. Catal. 8 (1983) 321–324.

[128] Y. Yu, D. Sun, S. Wang, M. Xiao, L. Sun, Y. Meng, Heteropolyacid salt catalysts for methanol conversion to hydrocarbons and dimethyl ether: Effect of reaction temperature, Catalysts 9 (2019) 230.

[129] T. Matsuda, A. Igarashi, Y. Ogino, Catalyst for synthesis of methyl tertiary butyl ether the effect of catalyst support on the property of 12-Molybdosilicic acid catalyst, J. Japan Pet. Inst. 23 (1980) 30–34.

[130] S.K. Bhorodwaj, D.K. Dutta, Activated clay supported heteropoly acid catalysts for esterification of acetic acid with butanol, Appl. Clay Sci. 53 (2011) 347–352.

[131] D. Jianfei, M.A. Tianlin, Y.U.N. Zhi, S. Rong, Heteropolyacid ($H_3PW_{12}O_{40}$) supported MCM-41: An effective solid acid catalyst for the dehydration of glycerol to acrolein, J. Wuhan Univ. Technol. Mater. Sci. 32 (2017) 6.

[132] Z. Liu, S. Cao, S. Wang, W. Zeng, T. Zhang, Silica-supported phosphotungstic acid as a novel heterogeneous catalyst for β-pinene polymerization, React. Kinet. Mech. Catal. 111 (2014) 577–590.

[133] A. Ciftci, D. Varisli, T. Dogu, Dimethyl ether synthesis over novel silicotungstic acid incorporated nanostructured catalysts, Int. J. Chem. React. Eng. 8 (2010) A45.

[134] W. Choi, E. Yoo, E. Seol, M. Kim, H.H. Song, Greenhouse gas emissions of conventional and alternative vehicles: Predictions based on energy policy analysis in South Korea, Appl. Energy. 265 (2020) 114754.

[135] X. Cao, Climate change and energy development: Implications for developing countries, Resour. Policy. 29 (2003) 61–67.

[136] A.K. Agarwal, Biofuels (alcohols and biodiesel) applications as fuels for internal combustion engines, Prog. Energy Combust. Sci. 33 (2007) 233–271.

[137] Erdiwansyah, R. Mamat, M.S.M. Sani, K. Sudhakar, A. Kadarohman, R.E. Sardjono, An overview of higher alcohol and biodiesel as alternative fuels in engines, Energy Rep. 5 (2019) 467–479.

[138] M.S.M. Zaharin, N.R. Abdullah, G. Najafi, H. Sharudin, T. Yusaf, Effects of physicochemical properties of biodiesel fuel blends with alcohol on diesel engine performance and exhaust emissions: A review, Renew. Sustain. Energy Rev. 79 (2017) 475–493.

[139] I.M. Yusri, R. Mamat, G. Najafi, A. Razman, O.I. Awad, W.H. Azmi, W.F.W. Ishak, A.I.M. Shaiful, Alcohol based automotive fuels from first four alcohol family in compression and spark ignition engine: A review on engine performance and exhaust emissions, Renew. Sustain. Energy Rev. 77 (2017) 169–181.

[140] M. Zheng, M.C. Mulenga, G.T. Reader, M. Wang, D.S-K. Ting, J. Tjong, Biodiesel engine performance and emissions in low temperature combustion, Fuel 87 (2008) 714–722.

[141] T. Doğu, D. Varişli, Alcohols as alternatives to petroleum for environmentally clean fuels and petrochemicals, Turkish J. Chem. 31 (2007) 551–567.

[142] A. Ciftci, D. Varisli, K. Cem, N.A. Sezgi, T. Dogu, Dimethyl ether, diethyl ether & ethylene from alcohols over tungstophosphoric acid based mesoporous catalysts, Chem. Eng. J. 207–208 (2012) 85–93.

[143] L. Chmielarz, A. Kowalczyk, M. Skoczek, M. Rutkowska, B. Gil, P. Natkański, M. Radko, M. Motak, R. Dębek, J. Ryczkowski, Porous clay heterostructures intercalated with multicomponent pillars as catalysts for dehydration of alcohols, Appl. Clay Sci. 160 (2018) 116–125.

[144] M. Migliori, A. Aloise, E. Catizzone, G. Giordano, Kinetic analysis of methanol to dimethyl ether reaction over H-MFI catalyst, Ind. Eng. Chem. Res. 53 (2014) 14885–14891.

[145] C. Arcoumanis, C. Bae, R. Crookes, E. Kinoshita, The potential of di-methyl ether (DME) as an alternative fuel for compression ignition engines: A review, Fuel 87 (2008) 1014–1030.

[146] D. Jin, B. Zhu, Z. Hou, J. Fei, H. Lou, X. Zheng, Dimethyl ether synthesis via methanol and syngas over rare earth metals modified zeolite Y and dual Cu-Mn-Zn catalysts, Fuel 86 (2007) 2707–2713.

[147] N. Khandan, M. Kazemeini, M. Aghaziarati, Determining an optimum catalyst for liquid-phase dehydration of methanol to dimethyl ether, Appl. Catal. A: Gen. 349 (2008) 6–12.

[148] L. Vanoye, M-L. Zanota, A. Desgranges, A. Favre-Reguillon, C. De Bellefon, Solvent effects in liquid-phase dehydration reaction of ethanol to diethylether catalysed by sulfonic-acid catalyst, Appl. Catal. A: Gen. 394 (2011) 276–280.

[149] E.A. Volnina, M.A. Kipnis, S.N. Khadzhiev, Catalytic chemistry of dimethyl ether (review), Pet. Chem. 57 (2017) 353–373.

[150] J. Sun, G. Yang, Y. Yoneyama, N. Tsubaki, Catalysis chemistry of dimethyl ether synthesis, ACS Catal. 4 (2014) 3346–3356.

[151] T.H. Fleisch, A. Basu, R.A. Sills, Introduction and advancement of a new clean global fuel: The status of DME developments in China and beyond, J. Nat. Gas Sci. Eng. 9 (2012) 94–107.

[152] A. Bakhtyari, M.R. Rahimpour, Chapter 10-Methanol to Dimethyl Ether, in: A. Basile, F. Dalena (Eds.), Methanol, Elsevier B.V., 2018: pp. 281–311.

[153] K.C. Tokay, T. Dogu, G. Dogu, Dimethyl ether synthesis over alumina-based catalysts, Chem. Eng. J. 184 (2012) 278–285.

[154] F. Dadgar, R. Myrstad, P. Pfeifer, A. Holmen, H.J. Venvik, Catalyst deactivation during one-step dimethyl ether synthesis from synthesis gas, Catal. Lett. 147 (2017) 865–879.

[155] F. Yaripour, F. Baghaei, I. Schmidt, J. Perregaard, Catalytic dehydration of methanol to dimethyl ether (DME) over solid-acid catalysts, Catal. Commun. 6 (2005) 147–152.

[156] Z. Azizi, M. Rezaeimanesh, T. Tohidian, M.R. Rahimpour, Dimethyl ether: A review

of technologies and production challenges, Chem. Eng.: Process. Process Intensif. 82 (2014) 150–172.

[157] C. Peinado, D. Liuzzi, R.M. Ladera-Gallardo, M. Retuerto, M. Ojeda, M.A. Peña, S. Rojas, Effects of support and reaction pressure for the synthesis of dimethyl ether over heteropolyacid catalysts, Sci. Rep. 10 (2020) 8551.

[158] R.T. Carr, M. Neurock, E. Iglesia, Catalytic consequences of acid strength in the conversion of methanol to dimethyl ether, J. Catal. 278 (2011) 78–93.

[159] P.G. Moses, J.K. Nørskov, Methanol to dimethyl ether over ZSM-22: A periodic density functional theory study, ACS Catal. 3 (2013) 735–745.

[160] K.W. Jun, H-S. Lee, H-S. Roh, S-E. Park, Catalytic dehydration of methanol to dimethyl ether (DME) over solid-acid catalysts, Bull. Korean Chem. Soc. 23 (2002) 803–806.

[161] S.S. Akarmazyan, P. Panagiotopoulou, A. Kambolis, C. Papadopoulou, D.I. Kondarides, Methanol dehydration to dimethylether over Al_2O_3 catalysts, Appl. Catal. B: Environ. 145 (2014) 136–148.

[162] V. Vishwanathan, K.W. Jun, J.W. Kim, H.S. Roh, Vapour phase dehydration of crude methanol to dimethyl ether over Na-modified H-ZSM-5 catalysts, Appl. Catal. A: Gen. 276 (2004) 251–255.

[163] W. Dai, W. Kong, G. Wu, N. Li, L. Li, N. Guan, Catalytic dehydration of methanol to dimethyl ether over aluminophosphate and silico-aluminophosphate molecular sieves, Catal. Commun. 12 (2011) 535–538.

[164] D. Varişli, T. Doğu, Production of clean transportation fuel dimethylether by dehydration of methanol over nafion catalyst, Gazi Univ. J. Sci. 21 (2010) 37–41.

[165] M. Mollavali, F. Yaripour, S. Mohammadi-Jam, H. Atashi, Relationship between surface acidity and activity of solid-acid catalysts in vapour phase dehydration of methanol, Fuel Process. Technol. 90 (2009) 1093–1098.

[166] D. Varişli, K.C. Tokay, A. Çiftçi, T. Doğu, G. Doğu, Methanol dehydration reaction to produce clean diesel alternative dimethylether over mesoporous aluminosilicate-based catalysts, Turkish J. Chem. 33 (2009) 355–366.

[167] D. Masih, S. Rohani, J.N. Kondo, T. Tatsumi, Low-temperature methanol dehydration to dimethyl ether over various small-pore zeolites, Appl. Catal. B: Environ. 217 (2017) 247–255.

[168] M. Xu, J.H. Lunsford, D.W. Goodman, A. Bhattacharyya, Synthesis of dimethyl ether (DME) from methanol over solid-acid catalysts, Appl. Catal. A: Gen. 149 (1997) 289–301.

[169] Y. Fu, T. Hong, J. Chen, A. Auroux, J. Shen, Surface acidity and the dehydration of methanol to dimethyl ether, Thermochim. Acta 434 (2005) 22–26.

[170] H. Li, S. He, K. Ma, Q. Wu, Q. Jiao, K. Sun, Micro-mesoporous composite molecular sieves H-ZSM-5/MCM-41 for methanol dehydration to dimethyl ether: Effect of SiO_2/Al_2O_3 ratio in H-ZSM-5, Appl. Catal. A: Gen. 450 (2013) 152–159.

[171] S. Kim, Y.T. Kim, C. Zhang, G. Kwak, K-W. Jun, Effect of reaction conditions on the catalytic dehydration of Methanol to dimethyl ether over a K-modified HZSM-5 catalyst, Catal. Lett. 147 (2017) 792–801.

[172] E. Catizzone, A. Aloise, E. Giglio, G. Ferrarelli, M. Bianco, M. Migliori, G. Giordano, MFI vs. FER zeolite during methanol dehydration to dimethyl ether: The crystal size plays a key role, Catal. Commun. 149 (2021) 106214.

[173] R.M. Ladera, M. Ojeda, J.L.G. Fierro, S. Rojas, TiO_2-supported heteropoly acid catalysts for dehydration of methanol to dimethyl ether: Relevance of dispersion and support interaction, Catal. Sci. Technol. 5 (2015) 484–491.

[174] P. Vázquez, L. Pizzio, C. Cáceres, M. Blanco, H. Thomas, E. Alesso, L. Finkielsztein, B. Lantaño, G. Moltrasio, J. Aguirre, Silica-supported heteropolyacids as catalysts in alcohol dehydration reactions, J. Mol. Catal. A: Chem.161 (2000) 223–232.

[175] J.G. Hernández-cortez, M. Manríquez, L. Lartundo-rojas, E. López-salinas, Study of acid-base properties of supported heteropoly acids in the reactions of secondary alcohols dehydration, Catal. Today 220–222 (2014) 32–38.

[176] M.J.D. Silva, N.A. Liberto, Soluble and solid supported Keggin heteropolyacids as catalysts in reactions for biodiesel production: challenges and recent advances, Curr. Org. Chem. 20 (2015) 1263–1283.

[177] J. Schnee, E.M. Gaigneaux, Lifetime of the $H_3PW_{12}O_{40}$ heteropolyacid in the methanol-to-DME process: A question of pre-treatment, Appl. Catal. A: Gen. 538 (2017) 174–180.

[178] K. Weissermel, H-J. Arpe, Industrial Organic Chemistry, fourth ed., Wiley-VCH, Weinheim, 2003.

[179] M.C.H. Clemente, G.A. V. Martins, E.F. de Freitas, J.A. Dias, S.C.L. Dias, Ethylene production via catalytic ethanol dehydration by 12-tungstophosphoric acid@ceria-zirconia, Fuel 239 (2019) 491–501.

[180] P. Haro, P. Ollero, F. Trippe, Technoeconomic assessment of potential processes for bio-ethylene production, Fuel Process. Technol. 114 (2013) 35–48.

[181] H.M. Torres Galvis, K.P. De Jong, Catalysts for production of lower olefins from synthesis gas: A review, ACS Catal. 3 (2013) 2130–2149.

[182] T.K. Phung, G. Busca, Diethyl ether cracking and ethanol dehydration: Acid catalysis and reaction paths, Chem. Eng. J. 272 (2015) 92–101.

[183] W. Knaeble, E. Iglesia, Kinetic and theoretical insights into the mechanism of alkanol dehydration on solid Brønsted acid catalysts, J. Phys. Chem. C 120 (2016) 3371–3389.

[184] H. Noller, P. Andréu, M. Hunger, The mechanism of contact elimination, A contribution to understanding the function of polar catalysts, Angew. Chemie Int. Ed. 10 (1971) 172–181.

[185] D. Fan, D-J. Dai, H-S. Wu, Ethylene formation by catalytic dehydration of ethanol with industrial considerations, Materials 6 (2013) 101–115.

[186] A. Mohsenzadeh, A. Zamani, M.J. Taherzadeh, Bioethylene production from ethanol: A review and techno-economical evaluation, ChemBioEng Rev. 4 (2017) 75–91.

[187] R. Batchu, V. V. Galvita, K. Alexopoulos, T.S. Glazneva, H. Poelman, M.F. Reyniers, G.B. Marin, Ethanol dehydration pathways in H-ZSM-5: Insights from temporal analysis of products, Catal. Today 355 (2020) 822–831.

[188] M. Zhang, Y. Yu, Dehydration of ethanol to ethylene, Ind. Eng. Chem. Res. 52 (2013) 9505–9514.

[189] J.F. DeWilde, C.J. Czopinski, A. Bhan, Ethanol dehydration and dehydrogenation on γ-Al_2O_3: Mechanism of acetaldehyde formation, ACS Catal. 4 (2014) 4425–4433.

[190] I. Takahara, M. Saito, M. Inaba, K. Murata, Dehydration of ethanol into ethylene over solid acid catalysts, Catal. Lett.105 (2005) 249–252.

[191] T.K. Phung, L. Proietti Hernández, A. Lagazzo, G. Busca, Dehydration of ethanol over zeolites, silica alumina and alumina: Lewis acidity, Brønsted acidity and confinement effects, Appl. Catal. A: Gen. 493 (2015) 77–89.

[192] D. Varisli, T. Dogu, G. Dogu, Ethylene and diethyl-ether production by dehydration reaction of ethanol over different heteropolyacid catalysts, Chem. Eng. Sci. 62 (2007) 5349–5352.

[193] I. Holclajtner-Antunović, S. Uskoković-Marković, A. Popa, A. Jevremović, B. Nedić Vasiljević, M. Milojević-Rakić, D. Bajuk-Bogdanović, Ethanol dehydration over Keggin type tungstophosphoric acid and its potassium salts supported on carbon, React. Kinet. Mech. Catal. 128 (2019) 121–137.

[194] A. Popa, V. Sasca, O. Verdes, A. Oszko, Preparation and catalytic properties of cobalt salts of Keggin type heteropolyacids supported on mesoporous silica, Catal. Today 306 (2018) 233–242.

[195] M.A. Christiansen, G. Mpourmpakis, D.G. Vlachos, Density functional theory-computed mechanisms of ethylene and diethyl ether formation from ethanol on γ-Al_2O_3(100), ACS Catal. 3 (2013) 1965–1975.

[196] G. Garbarino, R. Prasath, P. Vijayakumar, P. Riani, E. Finocchio, G. Busca, R. Prasath Parameswari Vijayakumar, P. Riani, E. Finocchio, G. Busca, Ethanol and diethyl ether catalytic conversion over commercial alumina and lanthanum-doped alumina: Reaction paths, catalyst structure and coking, Appl. Catal. B: Environ. 236 (2018) 490–500.

[197] M. Kaur, S. Sharma, P.M.S. Bedi, Silica supported Brönsted acids as catalyst in organic transformations: A comprehensive review, Chin. J. Catal. 36 (2015) 520–549.

Chapter 2: Experimental

Chapter 2 : Experimental

In this Chapter, the experimental techniques that were applied in the gas-phase dehydration of alcohols and the elimination of DEE over bulk and supported HPA catalysts are described in detail, beginning with catalyst preparation. The catalysts were investigated using various techniques such as TGA, BET, XRD and DRIFT spectroscopy to characterise the catalyst texture and the structural integrity of the HPAs. Additionally, NH_3-MC and TGA–DSC were applied to characterise the strength and number of acid sites on the bulk and silica-supported HPA catalysts at the gas-solid interfaces. Finally, the catalytic processes were examined using a fixed-bed microreactor fitted with on-line GC analysis. This is discussed in detail in this Chapter, along with conversion calculations and product selectivity.

2.1. Chemicals

$H_3PW_{12}O_{40}$ hydrate (99%) was purchased from Sigma–Aldrich and $H_4SiW_{12}O_{40}$ hydrate (99.9%) was purchased from Fluka; these contained 20 and 28 H_2O molecules per Keggin unit, respectively, according to TGA. The quantity of crystallisation water in the HPAs hydrates was considered in catalyst preparation. Zeolites NH_4^+-ZSM-5 (Si/Al = 47 and 12) were provided by Zeolyst International. These zeolites were transformed into the H^+ form via air calcination at 500 °C for 2 h [1].

Anhydrous MeOH (99.8%), EtOH (99.8%), 2,6-di-tert-butylpyridine (>97%), Cs_2CO_3 (99.9%) and $ZrOCl_2.8H_2O$ (98.0%) were purchased from Sigma–Aldrich. DEE (>97%) was purchased from Fisher Scientific. Commercial Aerosil 300 silica support (surface area $S_{BET} \approx 300\ m^2g^{-1}$) and P25 titania (anatase/rutile = 3:1; $S_{BET} = 44\ m^2g^{-1}$) were obtained from Degussa and used without further purification. ZrO_2 oxide was synthesised in-house as described in the literature [2,3] in order to acquire a catalyst support with a high surface area. NH_3 (99.99% pure) was supplied by the British Oxygen Company.

2.2. Catalyst preparation

2.2.1. Preparation of SiO_2-supported HPA catalysts

Silica-supported HPA catalysts, 5–70% HPA/SiO_2 (HPW and HSiW), were prepared by the wet impregnation method as described elsewhere [4,5]. A suspension of 5–6 g SiO_2 in 60–80 mL of water was stirred with certain quantities of HPA dissolved in a minimum amount of water. The mixtures were stirred for 3 h and aged overnight at room temperature. Once aged, the mixtures were dried using a rotary evaporator at 65 °C under a vacuum (3 kPa). Then the catalysts were ground in a mortar and sieved to 45–180 μm particle size. Finally, the catalysts were pre-treated under a vacuum (10^{-3} kPa) at 150 °C for 1.5 h. For comparison, silica-supported HPA catalysts were also prepared by wet impregnation of SiO_2 from a solution of HPA in MeOH. To preserve the catalysts, they were stored in a desiccator over calcined silica gel. The loading of HPA in the supported catalysts was quantified from W analysis using inductively coupled plasma optical emission spectroscopy (ICP-OES). Tables 3.1 and 3.2 in the next Chapter provide all the obtained data regarding the prepared catalysts.

2.2.2. Preparation of ZrO_2- and TiO_2-supported HPW catalysts

ZrO_2- and TiO_2-supported 15% HPW were prepared using the wet impregnation method [2,3]. The HPW was dissolved in a small amount of H_2O and mixed with 5.1 g of oxide supports to make a slurry with a small amount of aqueous phase (~5 mL). Then, the slurries were stirred for 3 h and aged overnight at room temperature. The catalyst samples were dried in an oven at 100 °C for 24 h. Finally, the catalysts were pre-treated under vacuum (10^{-3} kPa) at 150 °C for 1.5 h. Information regarding the prepared catalysts is presented in Table 5.1 in Chapter 5.

2.2.3. Preparation of silica

Compacted silica support was prepared using finely dispersed Aerosil 300 by stirring the SiO_2 with water or MeOH for 3 h and ageing overnight at room temperature. Then, the material was

dried under vacuum (3 kPa) in a rotary evaporator at 65 °C and pre-treated under vacuum (10^{-3} kPa) at 150 °C for 1.5 h.

2.2.4 Preparation of ZrO_2 support

The catalyst support ZrO_2 oxide was prepared in the lab using the following method (Eq. (2.1)) [2,3].

$$ZrOCl_2 + 2NH_3 + H_2O \rightarrow ZrO_2 + 2NH_4Cl \quad \textbf{(2.1)}$$

10 mL of 30% aqueous NH_3 (from BDH) was added dropwise at room temperature using a burette to a solution of 15 g (0.046 mol) of $ZrOCl_2.8H_2O$ in 200 mL of H_2O. This solution was stirred continuously until it reached a pH of 10 (pH paper) and hydrous zirconium oxide was formed as a white precipitate. The formed hydrogel was aged with stirring overnight at room temperature. Then the hydrogel was filtered and washed with distilled water until chloride-free (as determined by use of 0.02 M $AgNO_3$) [6]. After this, the oxide was dried at 100 °C for 24 h in an oven and then calcined in air at 400 °C for 3 h.

2.2.5. Preparation of $Cs_{2.5}H_{0.5}PW_{12}O_{40}$

Caesium tungstophosphate (CsPW) was prepared according to the method described in the literature [7,8]. Dropwise addition of the required amount of aqueous Cs_2CO_3 solution (0.47 M) to the aqueous HPW solution (0.75 M) with continuous stirring at 40 °C resulted in the formation of CsPW salt (white precipitate). The precipitate was then aged in the aqueous mixture for 48 h at room temperature. Then, it was dried using a rotary evaporator under vacuum (3 kPa) at 45 °C and pre-treated at 150° C/10^{-3} kPa for 1.5 h.

2.3. Catalyst characterisation techniques

2.3.1. Thermogravimetric analysis (TGA)

TGA is a quantitative analytical method that can be used to evaluate sample mass variations against temperature or time under a controlled gas atmosphere [9,10]. The variations of sample weight may occur in solid-gas systems owing to chemical interactions or physical changes. For instance, mass can be gained due to oxidation or adsorption reactions or it can be lost due to loss of water or volatile substances [9]. TGA can be applied to determine the thermal stability of a material, the moisture or coke content in a sample and its oxidation temperature [11].

A thermogravimetric analyser consists of a precise balance that is connected to a pan in which a sample is placed. The pan is inside a programmable furnace and connected to a thermo-balance [10]. Figure 2.1 displays a schematic diagram of a TGA instrument. The results of TGA are recorded as the thermogravimetric curve, which displays the weight change in a sample versus temperature [9].

In this research, a Perkin Elmer TGA 7 instrument was applied to evaluate the water content of the precursors that were used to synthesise the catalysts and of the synthesised HPAs catalysts under investigation. The samples were analysed at temperatures that ranged from 25 °C to 600 °C and at a heating rate of 20 °C min^{-1} under N_2 atmosphere [12].

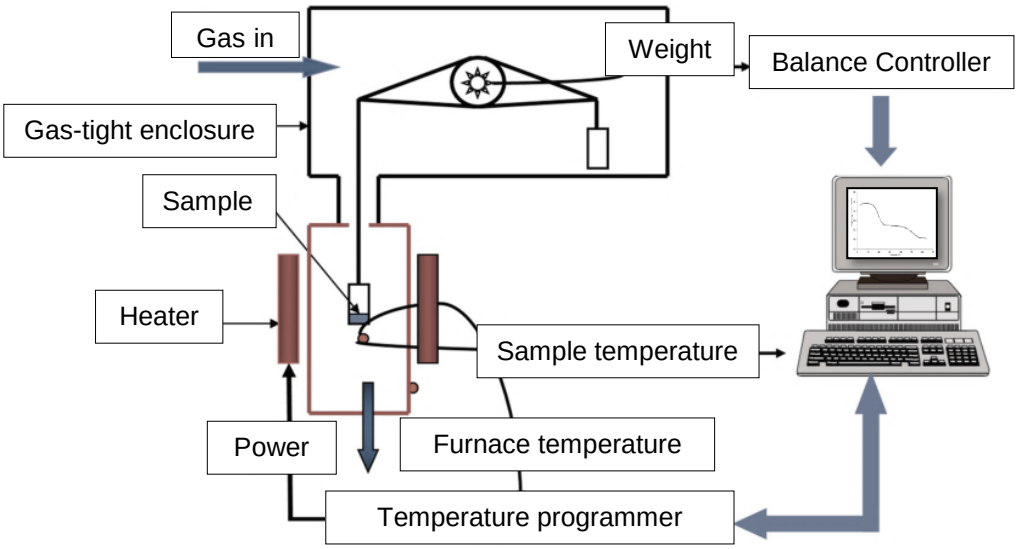

Figure 2.1. Schematic diagram of a TGA instrument [13].

2.3.2. Surface area and porosity analysis

The majority of heterogeneous catalysts are composed of porous solids [14]. The surface area and pore texture have a major influence on catalyst activity, stability and selectivity [15]. Nitrogen adsorption at boiling temperature of liquid nitrogen (-196 ^{o}C, 77K) is the most common method that is used to assess the surface area and porosity of catalysts [16–19].

Catalysts may contain one or more types of pores, and the texture (size and volume) of these pores depends on the preparation method [17]. Generally, pore sizes are categorised into three classes in accordance with the International Union of Pure and Applied Chemistry (IUPAC) classification [17,20]:

- Micropores - size < 20 Å, ultramicropores size < 7 Å;
- Mesopores - 20 Å < size < 500 Å; and
- Macropores - size > 500 Å.

In addition, pore walls contribute to the surface area of porous solid catalysts, making the total surface area of such catalysts much higher than the external surface [17]. Porous solid catalysts have specific surface areas that range from 1 to 1000 m^2g^{-1}, whereas their external surface areas range from 0.01 to 10 m^2g^{-1} [17]. The type of the pores determines the contribution of pore walls to the total surface area (Figure 2.2). The catalyst granules typically contain pores with various sizes; therefore, it is essential to identify the distribution of pore size (pore volume versus pore size) [17].

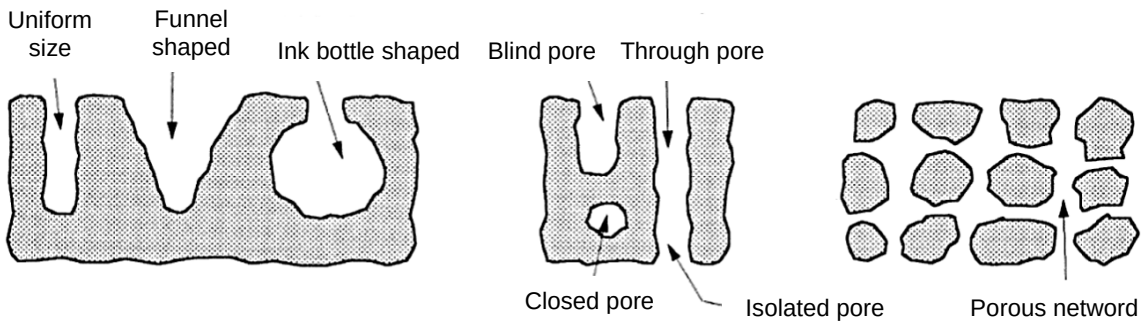

Figure 2.2. Types of pores [17].

An adsorption isotherm may be obtained by plotting the adsorbed volume of N_2 (V) against its relative pressure (P/P_o), and the shape of this isotherm is influenced by the porous texture of the catalyst [17,18]. Figure 2.3 illustrates the most frequent adsorption isotherm types that are obtained from N_2 adsorption on the surface of catalysts according to IUPAC classifications [19–21]. These adsorption isotherms are classified as I, II, IV and VI, and they represent microporous, macroporous, mesoporous and uniform ultramicroporous solids, respectively [17]. The isotherms of type IV (mesoporous solids) are explained in more detail here because HPA solid catalysts that were the subject of this research belong to this class of solids (see Chapter 3).

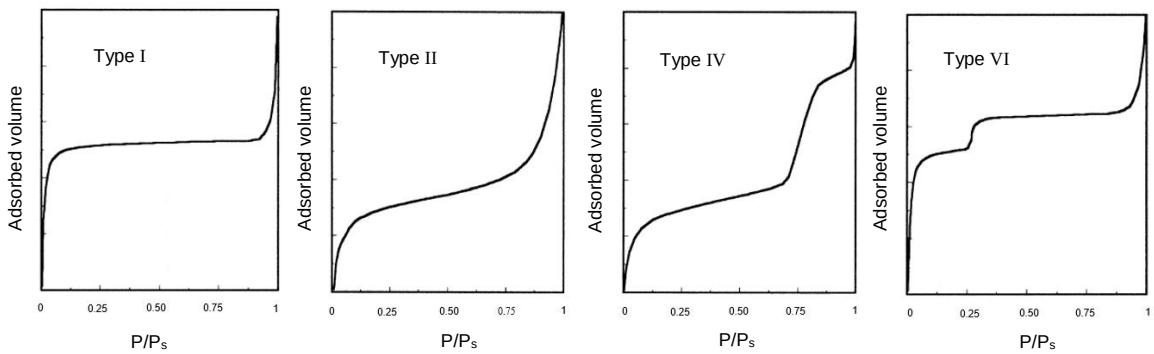

Figure 2.3. The most common types of N_2 adsorption isotherms [17].

On a type IV mesoporous solid material [22], a monolayer of adsorbed N_2 is formed at low pressure. At high relative pressures, multilayer adsorption ensues until capillary condensation occurs, which results in a sharp rise in adsorption volume. Adsorption to the catalyst exterior surface proceeds until the mesopores are saturated (Figure 2.3) [17,21]. After saturation is achieved, desorption of N_2 occurs through its liberation from the surface and pores in the reverse direction of the adsorption. This occurs at a lower pressure than N_2 adsorption in mesoporous solids, leading to a hysteresis loop. According to the IUPAC categorisation, solid catalysts exhibit four distinct types of hysteresis, as shown in Figure 2.4 [17].

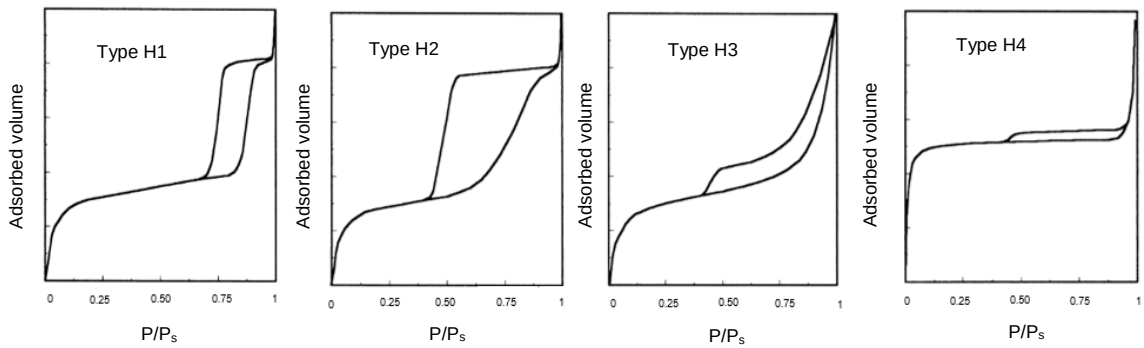

Figure 2.4. The four hysteresis shapes that frequently obtained in N_2 adsorption [17].

Hysteresis is typically caused because the material is composed of pores of different sizes and different mouth shapes, as in the ink-bottle pore shape, or shows different behaviours of adsorption and desorption through cylindrical pores [17,23]. The H1 and H2 types of hysteresis are correlated with solid compounds that comprise particles that are crossed by spheroidal aggregates or agglomerates or contain almost cylindrical channels shape [17]. H1 hysteresis occurs in pores of uniform shape and size, whereas H2 hysteresis takes place in pores of non-uniform shape [17]. The typical mesoporous solid materials, such as supported HPAs, exhibit hysteresis of types H1 or H2 (see Chapter 3).

In addition, H3 and H4 hysteresis isotherms are commonly observed in solids composed of agglomerates or aggregates of particles forming nonuniform (type H3) size and/or shape or slit-shaped uniform pores (type H4). Zeolites and active carbon are considered as typical examples of this hysteresis type [17,23]. No hysteresis loop has been observed in solid materials that contain cone- and wedge-shaped pores, or in those with blind cylindrical pores [17].

The Brunauer-Emmett-Teller (BET) method, developed in 1938, is widely used for estimating the total surface area of porous solid catalysts [9,17,24]. The BET isotherm can be used to calculate the volume of adsorbed N_2 gas in the monolayer (V_m) and in the solid surface area (S), as determined by Eqs. (2.2) and (2.3) [14], respectively.

$$\frac{P}{V(P_o - P)} = \frac{1}{V_m C} + \frac{C-1}{V_m C}\frac{P}{P_o} \qquad \textbf{(2.2)}$$

Here P is the adsorbate gas pressure at the equilibrium with the surface solid, P_o is the saturation pressure, V is the adsorbed gas volume and C is the constant of BET.

A plot of P/V (P_o-P) versus the relative pressure (P/P_o) in the range $0.05 < P/P_o < 0.35$ gives a linear correlation where the system complies with the BET equation with the intercept $1/V_mC$ and the slope $(C-1)/V_mC$. Consequently, the value of V_m can be obtained [14]. The surface area (SA) can be calculated from the V_m value (Eq. (2.3)) [14]:

$$SA = (V_m/V_A)\, N_a\, A \qquad \textbf{(2.3)}$$

Here, V_A is the molar volume of N_2, N_a is the constant of Avogadro and A is the area covered by one N_2 molecule (0.162 nm^2) [18].

The BET surface area and porosity of the catalysts were determined by use of a Micromeritics ASAP 2010 instrument at -196 °C. Prior to measurement, the test samples (typically 100–300 mg) were placed in a tube furnace (heating mantle) at 250 °C for 2 h and the air evacuated until the vacuum approached 10 µmHg, which would remove all adsorbed gases. Then, the sample was left to cool to room temperature before it was weighed. Following that, the sample tube was immersed in a dewar flask that contained liquid nitrogen. Finally, after the pressure of the gas had achieved equilibrium, a sequence of 55 successive nitrogen doses was applied to produce the isotherm of adsorption. The surface analyser that was applied in the research is displayed in Figure 2.5.

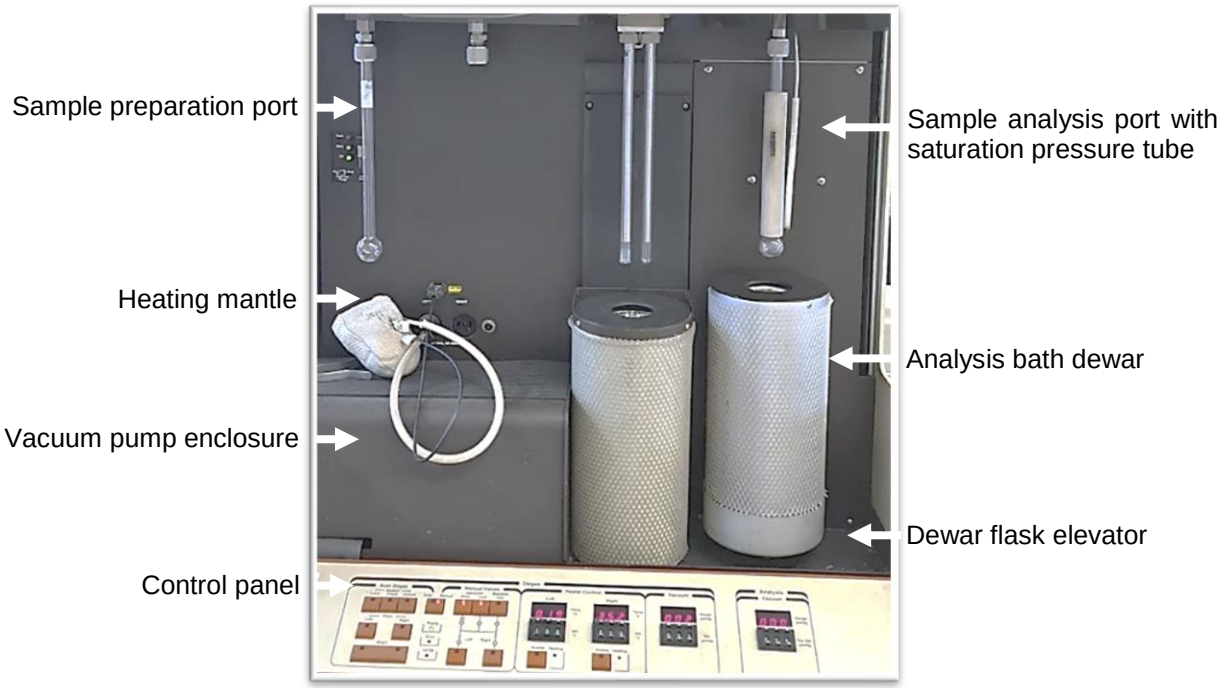

Figure 2.5. Micromeritics ASAP 2010 analyser applied to identify the surface area and porosity of catalysts.

2.3.3. Inductively coupled plasma optical emission spectroscopy (ICP-OES)

ICP-OES is a spectroscopic method that can be used to elucidate the quantity of elements in a solution. This extremely precise method can be used to detect traces of elements as low as parts per billion (ppb) [25]. The instrument contains an optical spectrometer and inductively coupled plasma. The plasma is generated through the ignition of gaseous argon (Ar) in a radio frequency (RF) coil that maintains a temperature of around 7000 K. The analysis method is dependent on the spontaneous emission of photons from excited atoms and ions in an RF discharge [25]. The solution of the sample is transformed into an aerosol and introduced to the central plasma channel via an analytical nebuliser [26]. The elements in the sample interact with the plasma electrons and ions, which excite the electrons to be in higher electronic states. When electrons relax, they release energy photons at specific wavelengths that are distinctive for each element that is present [25,27]. The spectrometer records the wavelengths of the energies as emission

lines, and the intensities of these lines are proportional to the concentration of the element in the sample solution. The element quantity can be estimated by comparing the intensities of the emission line with those for standard calibration solutions of the corresponding element [26].

During this research, ICP-OES spectroscopy was applied to measure the W content of supported HPA catalysts and to evaluate the Si and Al content of NH_4^+-ZSM-5 zeolites. For the ICP analysis, 20–30 mg of a catalyst sample was refluxed in a 15% KOH aqueous solution for 3 h. The solution was diluted with distilled water to 50 mL in a standard measure flask. Mr. Stephen in the Chemistry Department at the University of Liverpool conducted the ICP-OES analysis of our catalysts.

2.3.4. CHN analysis

Combustion analysis is an effective technique to measure the carbon, hydrogen and nitrogen (CHN) content of solid catalysts. Generally, the CHN analysis of solid materials is performed by placing a small amount of the material under study (~1 mg) in the combustion reactor, where it is heated to 1000 °C under flowing helium gas, and then exposed to pure oxygen to convert the carbon and hydrogen to carbon dioxide and water. Then, the gas mixtures pass into a chromatographic column and are detected by use of GC [28]. This technique was applied in this study to quantify the content of carbon in the spent catalysts. This figure could be used to determine the impact of coke on the deactivation of catalysts. The spent catalysts were examined using a Thermo Flash EA 1112 series analyser in the Chemistry Department at the University of Liverpool.

2.3.5. Powder X-ray diffraction (XRD)

Powder XRD is one of the most common characterisation techniques that is applied to analyse the crystalline phase structure of solid materials [29]. The wavelength of X-rays corresponds to the spacing between the ions or atoms in crystalline lattice planes, resulting in the diffraction

of X-rays that penetrate the crystal [30]. The method is based on the interaction of incident monochromatic X-rays (such as those produced by a CuKα source) with the periodic lattice atoms [29]. The scattering angle of the X-rays is influenced by diverse aspects that follow Bragg's law (Eq. (2.4)) [31].

$$n\lambda = 2d\mathrm{Sin}\theta \quad \textbf{(2.4)}$$

In this equation n, λ, d and θ are the reflection order (an integer value), the wavelength of the X-ray, the lattice planar spacing and the angle of diffraction, respectively.

The Bragg peaks are determined by plotting the intensity of the reflected X-rays against the diffraction angle 2θ [30]. The X-ray diffractogram offers valuable information about the crystal structure of a solid material and the average particle size. The Scherrer equation (2.5) can be applied to obtain the crystal particle size of the solid material [30,32]:

$$\mathrm{t} = 0.9\lambda/B\cos\theta \quad \textbf{(2.5)}$$

Here t, λ, θ and B are the particle thickness, the incident X-ray wavelength, the diffraction angle and the full width at half maximum (FWHM) of the peak of X-ray diffraction, respectively.

In this work, powder XRD patterns of bulk and SiO_2-supported HPA catalysts (fresh and spent) were recorded on a PANalytical Xpert diffractometer with CuKα radiation (λ = 1.542 Å) and attributed to the JCPDS database. Zeolite and HPA/SiO_2(m) catalysts were measured by use of a Bruker D8 discover diffractometer with CuKα1 radiation (λ = 1.541 Å). Crystal particle size was determined using the Origin software. The powdered sample was typically placed at room temperature on the sample holder and exposed to the X-ray radiation. The pattern was recorded of 2θ at angles that ranged from 4° to 100°. XRD analysis was carried out in the Chemistry Department at the University of Liverpool.

2.3.6. Diffuse reflectance infrared Fourier transform spectroscopy (DRIFTS)

Infrared spectroscopy is an efficient technique for the determination of the structural framework of materials [9,30,33]. This technique depends on the vibrations of chemical bonds of a compound, which occur in the infrared (IR) region of the electromagnetic spectrum [9,29]. A beam of IR radiation, which is provided by a laser source, passes through a sample, causing vibration, bending or rotation of the chemical bond [30]. The resulting IR spectrum is plotted as the intensity of the signal versus the wavenumber (cm^{-1}), which can be shown in transmission or absorption mode [30]. The analysis of the shape, position and intensity of the absorption peaks in the recorded spectrum reveals details of the sample molecular structure [30].

In our investigation, DRIFT spectroscopy was utilised to record the spectra of HPA catalysts. In this method, flat reflectors and an alignment mirror collect diffusely scattered light directly from the catalyst powder surface and pass it to a detector (Figure 2.6) [9]. A sample with a high absorption coefficient can be diluted with a diffusely scattering background, such as KBr, to minimise the amount of absorption. The DRIFTS technique is appropriate for powder samples [9,34].

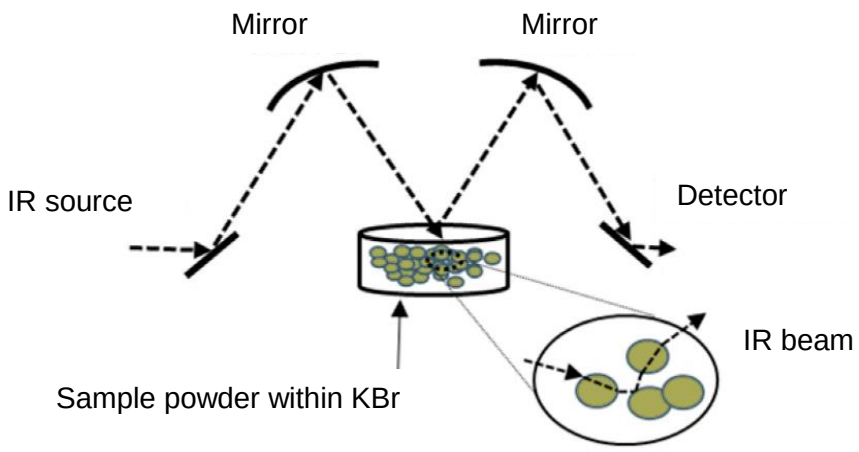

Figure 2.6. Diagram of DRIFT spectroscopic method [34].

This research examined the structural framework of bulk and SiO_2-supported HPA (fresh and spent) catalysts, and the IR spectra were collected via a Nicolet model NEXUS Fourier transform IR (FTIR)–Raman spectrometer. For DRIFT spectroscopy analysis, a small amount of catalyst (16 mg) was diluted with 384 mg of dried powdered KBr (4 wt%) and ground completely to generate a diffusely scattering matrix that reduced the sample absorption and thus improved the beam throughput and the resolution of the spectra. At room temperature, the spectra were recorded by averaging 254 scans with 4 cm^{-1} resolutions ranging from 4000 to 400 cm^{-1}. The range of 1200–500 cm^{-1} provided details of the primary structure of the Keggin HPAs (see Chapter 3).

2.3.7. Calorimetric methods of analysis

2.3.7.1. Microcalorimetry (MC)

The calorimeter is the most reliable and accurate method to assess the adsorption strength (either physical or chemical) [35,36]. Tian-Calvet heat-flow microcalorimeters attached to precise volumetric systems are highly sensitive instruments that can be used to analyse the gas-solid interactions [36–39].

The apparatus set-up of Tian-Calvet heat-flow microcalorimeter (Figure 2.7) involves two vessels, one of them for the reference and the other for the sample. These vessels are surrounded by thermocouples and are placed in the calorimetric block, which operates as a heat sink [40]. Twin heat-flux detectors thermally connect the vessels to the block to maintain them at the same temperature. The differential coupling of the reference and sample detectors eliminates external thermal interference resulting in a highly precise signal from the heat exchange with the solid surface [36,40].

The differential heats of NH_3 adsorption on bulk and supported HPA/SiO_2 catalysts were evaluated in a gas flow system (N_2 flow) by a pulse method at 150 °C and ambient

pressure using a Setaram C80 Calvet calorimeter fitted with a Metrohm DMS Titrino 716 titrator as reported previously [2,3,8].

In this experiment, catalyst samples (0.2–1 g) were pre-treated in situ for 3 h at 150 °C under dry nitrogen flow (20 mL min^{-1}). After the temperature and heat flux had stabilised, the adsorption heat was measured through application of consecutive pulses of gaseous NH_3 (0.25–0.50 mL, 0.01–0.02 mmol) into the N_2 flow using a stainless-steel loop fitted in a Valco valve. Sufficient time (~40 min) was permitted after each pulse to achieve adsorption equilibrium. The amount of NH_3 adsorbed was determined as the difference between the amount of NH_3 that was supplied in the pulse and the NH_3 broken amount through the sample cell. The latter was determined via titration with 0.01 M sulfamic acid in an aqueous buffer solution made of 1 M NH_4Cl (30 mL) and saturated boric acid (2 mL) using a Metrohm combined pH glass electrode with an end point set at pH 5.0. The results then allowed the differential enthalpies of NH_3 adsorption per mole of NH_3 adsorbed to be obtained (Figure 2.8). Extrapolation of these values to zero NH_3 uptake gave the initial enthalpy of NH_3 adsorption, ΔH_o. Typically, in the first 4–5 pulses, the total NH_3 provided was adsorbed on the sample of catalyst, without any NH_3 break through the cell observed. This enabled precise identification of the ΔH_o values without the necessity for NH_3 titration. The mean absolute error in ΔH_o was usually within ±6 kJ mol^{-1}. Our ΔH_o values for the bulk HPW and HSiW were consistent with those previously described in the literature [41–43].

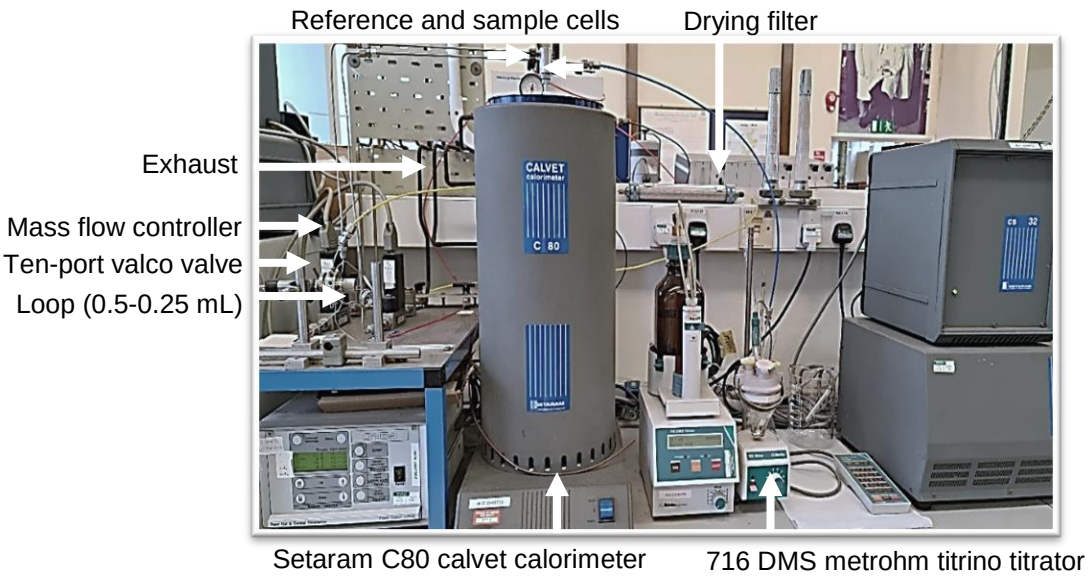

Figure 2.7. C80 Calvet calorimeter fitted with Metrohm DMS Titrino 716 titrator.

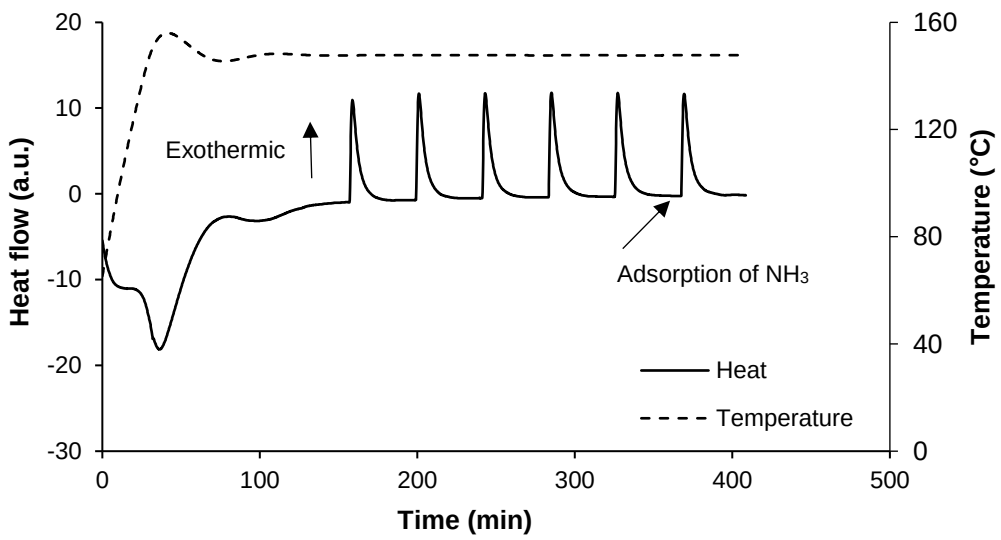

Figure 2.8. Heat flow traces for NH_3 adsorption onto bulk HPW catalyst at 150 °C.

2.3.7.2. Differential scanning calorimetry (DSC)

Differential scanning calorimetry (DSC) in combination with TGA can be used to determine the changes in heat flow and mass of a sample during a physical or chemical reaction [10,45]. It can be used to characterise the physical and chemical transitions of catalysts such as melting,

glass transition, adsorption, crystallisation, surface reactivity and transformations with mass change [10,46]. This technique is valuable for determining the acidity of materials [42,47,48]. The acid sites number and their strength distribution can be determined by the NH_3 pulse chemical adsorption method using DSC [41].

A Setaram TG–DSC 111 differential scanning calorimeter (Figure 2.9) was used in this research. The DSC is built around two refractory material tubes that cross the heating furnace chamber [48]. The detection unit, which operates on the Calvet principle, is in the centre section of the tubes. The detector surrounds the cylindrical sample crucible, so that accurate measurement of all heat exchange can be achieved. A symmetrical microbalance is seated above the calorimetric block, which is placed on a vertical stand. The suspension components of the microbalance are aligned with the tube axis. The crucibles are brought into the DSC detection zone by sliding the balance [47].

NH_3 adsorption on HPA catalysts was determined through use of the Setaram TG–DSC 111 via a pulse process in a flow system (N_2 carrier gas) as previously described [3,49]. The gases N_2 and NH_3 were passed across molecular sieve traps before they were passed into the system. Catalyst samples (20–80 mg) were placed in the calorimeter and pre-treated under N_2 flow (30 mL min^{-1}) at 150 or 300 °C for 1 h. Then, the temperature was reduced to 150 °C and, after the sample weight reached stabilization (about 1 h), the measurement was conducted at 150 °C through consecutive 2–5 mL pulses of pure NH_3 into the N_2 flow using a loop fitted in a 6–port valve. Sufficient time was permitted after each pulse to achieve the adsorption equilibrium (about 30 min). Weight gains owing to NH_3 adsorption, and the corresponding adsorption heat were recorded. These data enabled the determination of the total amount of NH_3 adsorbed and the average enthalpy of NH_3 adsorption (ΔH) (Figure 2.10). The NH_3 pulses applied (2–5 mL) were large enough to ensure accurate measurement of the NH_3 adsorbed

amount. Such pulses contained the amount of NH_3 that corresponded to 20–50% of the total number of protons in HPA catalysts.

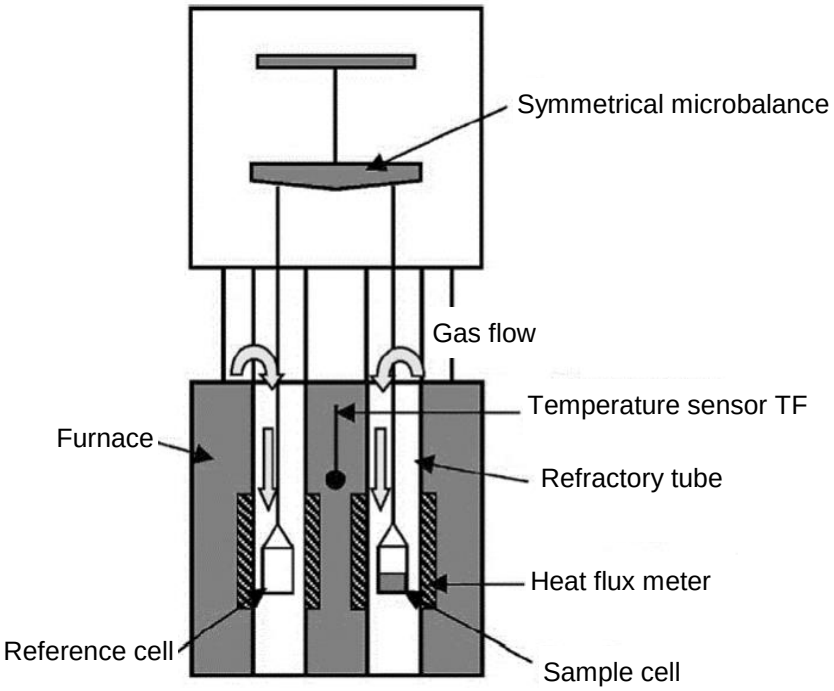

Figure 2.9. Schematic view of TG–DSC 111 Setaram set-up [49].

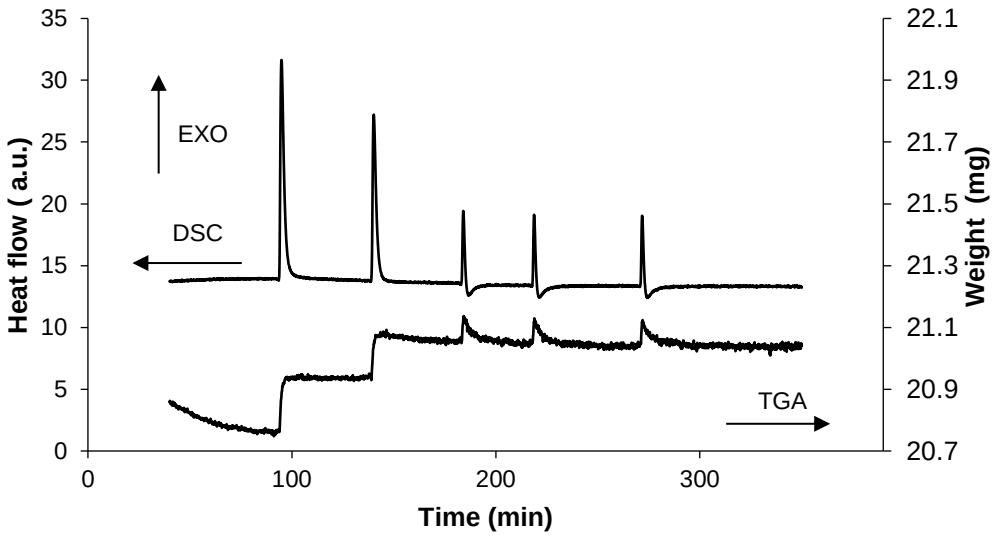

Figure 2.10. TGA–DSC traces showing NH_3 adsorption onto 71%HSiW/SiO_2 at 150 °C: TGA (bottom) and DSC (top) traces.

2.4. Catalyst testing

2.4.1. Product analysis

2.4.1.1. Gas chromatography (GC)

GC is the most widely applied technique for qualitative and quantitative detection of chemical compounds [51]. This method can be functional for separation, identification and quantitative analysis of catalytic reactions [28,51].

A gas chromatograph is composed of three major components: (i) an injector; (ii) a column with stationary phase that comprises polymeric material; and (iii) a detector, which is used to determine the analyte composition and concentration [51,52]. Figure 2.11 shows a schematic diagram of a gas chromatograph.

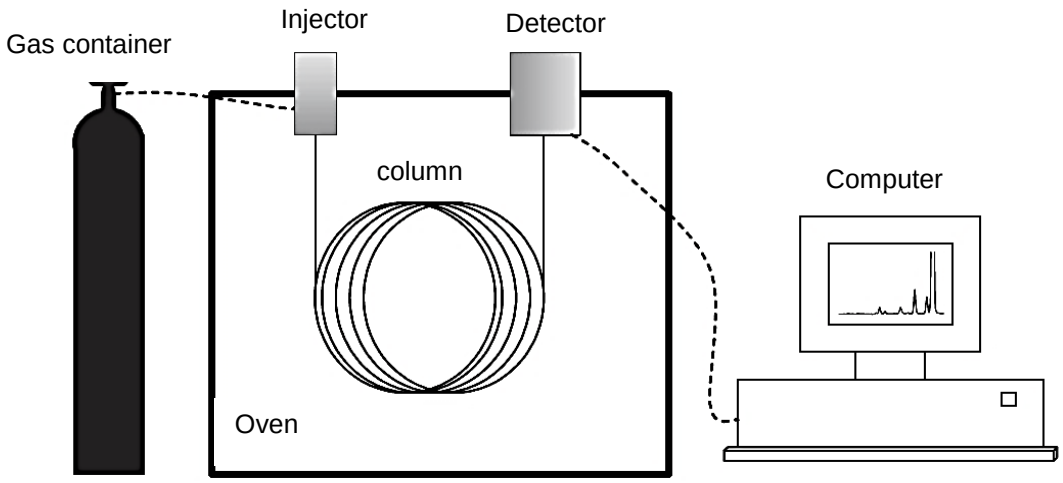

Figure 2.11. A diagrammatical representation of a gas chromatograph set-up [51].

During the analysis process, the volatilised sample is injected and swept through a heated column via an inert carrier gas stream, such as Ar, He, H_2 or N_2. A split/splitless injector (Figure 2.12) is the most common inlet that is used to inject the samples into the GC column [52]. The analyte molecules are dispersed between the column stationary and mobile phases

based on their polarity and boiling points [52,53]. Therefore, the gas components are eluted to the detector by the mobile phase at different times. These are called the retention times, which are identified for each component. However, these retention times vary according to the conditions of the experiment such as specific pressure, temperature condition, gas flows, etc. [53].

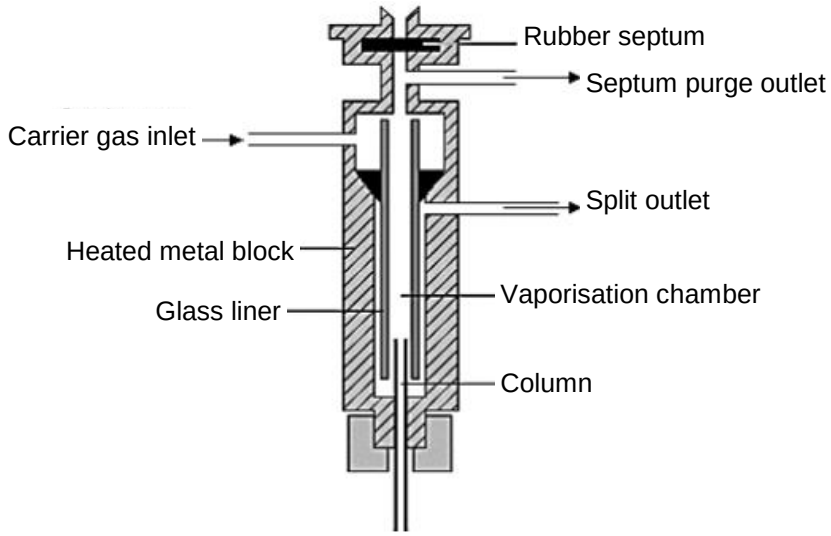

Figure 2.12. A split-splitless vaporising injector [53].

A flame ionisation detector (FID) (Figure 2.13), which is the most common type of detector, was used in this research to analyse the samples [52]. In this detector, the analyte becomes ionised in a flame that is produced by combustion of H_2 in air [53]. An electrical potential then drives these ions to a collecting electrode, which creates a small current measured by the detector in picoampers. The charge quantity formed is relative to the concentration of the compound present. This current, the response of the detector, is amplified and displayed on the computer as a chromatogram (electron volts (V) against time (min)) [28,50,51].

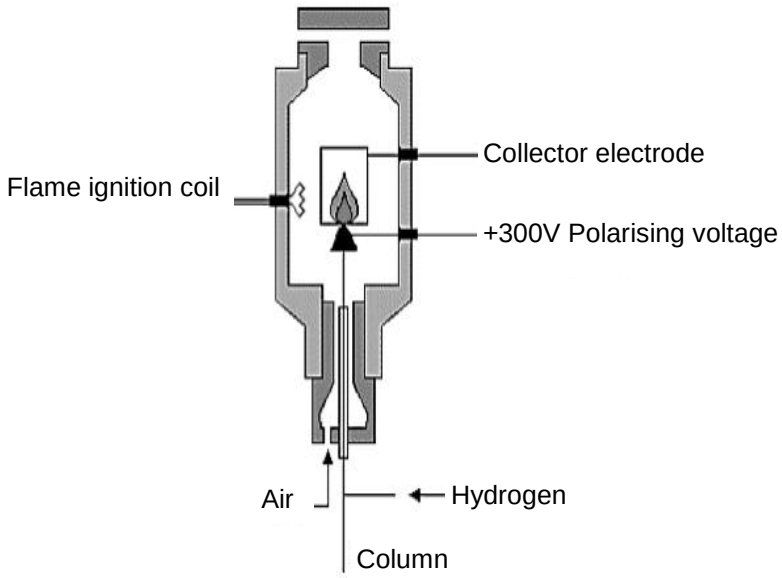

Figure 2.13. A flame ionisation detector [53].

In this research, the reaction products were analysed on a Varian Star 3400 CX on-line GC instrument that was fitted with a flame ionisation detector and i) a 30 m×0.32 mm×0.5 µm, 10 psi SUPELCOWAX 10, ii) CP-WAX 52CB 30 m×0.32 mm×0.5 µm, 15 psi capillary column (polyethylene glycol, stationary phases). The temperatures of the detector and injector were selected to be 250 °C and 210 °C, respectively. The flow rate of N_2 in the column was 2 mL min^{-1}. The column oven temperature was programmed as displayed in Figures 2.14 and 2.15.

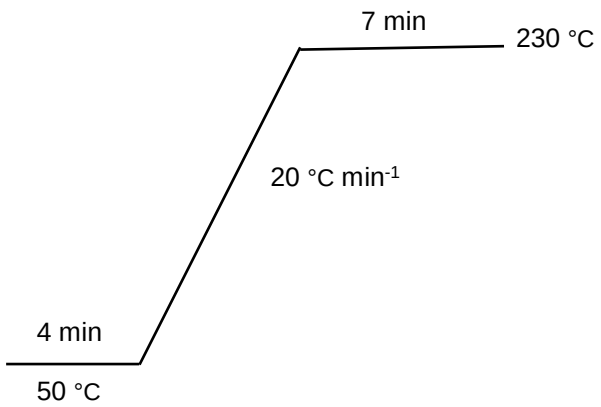

Figure 2.14. Temperature program of the column oven COWAX 10 capillary column.

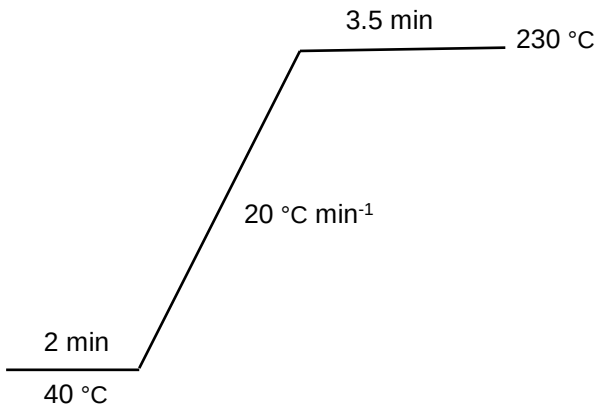

Figure 2.15. Temperature program of the column oven CP-WAX 52CB capillary column.

2.4.1.2. Quantitative analysis of products by gas chromatography

Typically, the quantitative chromatographic analysis requires calibration of the response of the detector to each analyte. This can be applied by the utilisation of an internal standards method [55]. The standard calibrations enable the recognition of the response factor for each analyte, and this helps to quantify each target sample (Eq. (2.6)) [55].

$$M = 1/R_f \times \frac{S}{S_o} \times M_o \quad \textbf{(2.6)}$$

In this equation, M and M_o are the molar concentrations of the analyte compound and internal standard, S/S_o is the ratio of the peak areas (detector response), and R_f is the response factor of the product or the reactant relative to the internal standard.

However, this approach cannot be applied for complex mixtures and very volatile organic compounds. To overcome this situation, the effective carbon number (ECN) calculation can be used. This method enables theoretical estimates of relative molar response factors without the need for individual analyte calibrations [55,56]. The ECN of a molecule is calculated based on the sum of the carbon number and type of existing functional groups [55]. The FID is a mass-sensitive detector that responds to the number of carbon atoms that enter the detector per unit of time [57].

Thus, in this research, the ECN was used to examine the response factors of the GC instrument with the FID as well as to calculate the relative molar response factor through use of Eq. (2.7) [58]. Table 2.1 below illustrates the ECNs and relative molar response factors for organic compounds that were studied in this research.

$$F_{\text{molar}} = (\text{ECN of reference})/(\text{ECN of compound}) \quad \textbf{(2.7)}$$

Table 2.1. The molecular weights, boiling points, ECNs and relative molar response factors (F_{molar}) for the organic compounds.

Compound	Molecular weight (g/mol)	Boiling point (°C)	Effective carbon number [57]	Relative molar response factor (F)
MeOH	32	65	0.5	1.0
DME	46	-24	1.0	0.5[a]
EtOH	46	78	1.5	1.0
DEE	74	35	3.0	0.5[b]
Ethene	28	-104	1.9	0.79[b]

[a] relative to MeOH. [b] relative to EtOH.

The conversion of the reactant, the selectivity of the product, the rate of reaction and the activation energy were determined using Eqs. (2.8) to (2.14).

The yield of product (*Yp*), total conversion (*X*) and the selectivity of a particular product (*S*) were evaluated by using Eqs. (2.8), (2.9) and (2.10), respectively.

$$\text{Product yield } (YP) = \frac{\text{moles of product formed}}{\text{moles of substrate supplied}} \times 100 = \frac{(Sp \times Fp \times B)}{(S_R + (\sum Sp \times Fp \times B)} \times 100 \quad \textbf{(2.8)}$$

$$\text{Conversion } (X) = \frac{\text{moles of substrate reacted}}{\text{moles of substrrate supplied}} \times 100 = \sum Y_p \quad \textbf{(2.9)}$$

$$\text{Selectivity } (S) = \frac{\text{moles of product formed}}{\text{moles of substrate reacted}} \times 100 = \frac{Y_p}{X} \times 100 \quad \textbf{(2.10)}$$

Where S_R and S_P are the peak areas of the unreacted substrate and product, respectively, F_P is the relative response factor, *B* is the stoichiometry factor of the product relative to the substrate.

In addition, the rate of reaction (*R*, mol g^{-1} h^{-1}) was determined as:

$$R = X \frac{F}{W} \quad \textbf{(2.11)}$$

Here, *X* is the fractional alcohol conversion, *W* is the weight of HPAs catalyst and *F* is the inlet alcohol molar flow rate.

Turnover rates (per accessible Brønsted site, h^{-1}) were calculated as [59,60]:

$$\text{TOF} = \frac{\text{molecules product}}{\text{time} \times \text{active site}} \quad \textbf{(2.12)}$$

Furthermore, the activation energy (E_a) for alcohol dehydration and ether elimination was quantified under low conversion conditions (conversion ≤ 15%). In this case, the rate of reaction became almost linearly proportional to the conversion of the substrate. Thus, the activation energy could be determined using the conversion instead of reaction rate at different temperatures [61]. The Arrhenius equation was applied to calculate the activation energy (Eqs.

(2.13) and (2.14)) [31]. A plot of ln *k* versus *1/T* created a straight line, which could be applied to calculate the activation energy [18].

$$k = A\exp(\frac{-Ea}{RT}) \quad \textbf{(2.13)}$$

$$\ln k = \ln A - E_a/RT \quad \textbf{(2.14)}$$

Here *k* is the reaction rate constant, *A* is the pre-exponential factor, E_a is the apparent activation energy, *R* is the gas constant and *T* is the absolute temperature.

2.5. Catalyst testing in fixed-bed microreactor

2.5.1. Dehydration of methanol and ethanol

The dehydration of MeOH and EtOH was conducted under atmospheric pressure at 100–160 °C in a Pyrex fixed-bed downflow reactor (9 mm internal diameter) fitted with an on-line GC analysis (Varian Star 3400 CX instrument with a flame ionization detector and a 30 m×0.32 mm×0.5 µm SUPELCOWAX 10 capillary column for MeOH dehydration and CP-WAX 52CB 30 m×0.32 mm×0.5 µm capillary column for EtOH dehydration). The temperature in the reactor was controlled by a Eurotherm controller using a thermocouple placed at the top of the catalyst bed. The alcohols were supplied by passing N_2 carrier gas (10–20 mL min^{-1}) controlled by a Brooks mass flow controller through a saturator, which held liquid anhydrous alcohol at a controlled temperature (±1°C) to maintain the chosen alcohol partial pressure (Table 2.2) [61]. The downstream gas lines and valves were heated at 120 °C to prevent the condensation of substrate and product. The set-up of the continuous flow fixed-bed reactor is shown in Figure 2.16.

Before reaction, the catalysts (0.20 g, 45–180 µm particle size) were pre-treated in situ in N_2 flow at the reaction temperature for 1 h. Bulk HPW and HSiW catalysts, having high densities, were diluted with 0.1 g silica to achieve a plug-flow regime [60]. At regular time

intervals (ca. 15 min), the downstream gas flow was evaluated via the on-line GC to estimate the conversion of alcohol and the selectivity of product. The product selectivity was defined as the percentage of MeOH converted into DME and of EtOH to DEE and ethene considering reaction stoichiometry; for example, 100% selectivity of DME would mean that 1 mole of MeOH converted to form 0.5 mole of DME. Typically, the carbon balance was retained within 95%, with a mean absolute percentage error of ≤ 5%. Typical traces of GC for the MeOH and EtOH dehydration are presented in Figures 2.17 and 2.18.

Table 2.2. Partial vapour pressure of MeOH, EtOH and DEE at different temperatures (calculated from [61]).

Reactant	Temperature (°C)	Partial vapour pressure (kPa)
	0	3.83
MeOH	25	16.7
	30	21.5
	0	1.48
EtOH	25	7.66
	35	13.6
DEE	0	24
MeOH-H_2O (0.18:0.82 mol)	30	3.84 (MeOH), 3.5 (H_2O) [62]
EtOH-H_2O (2.08:0.25 mol)	35	≈13.6

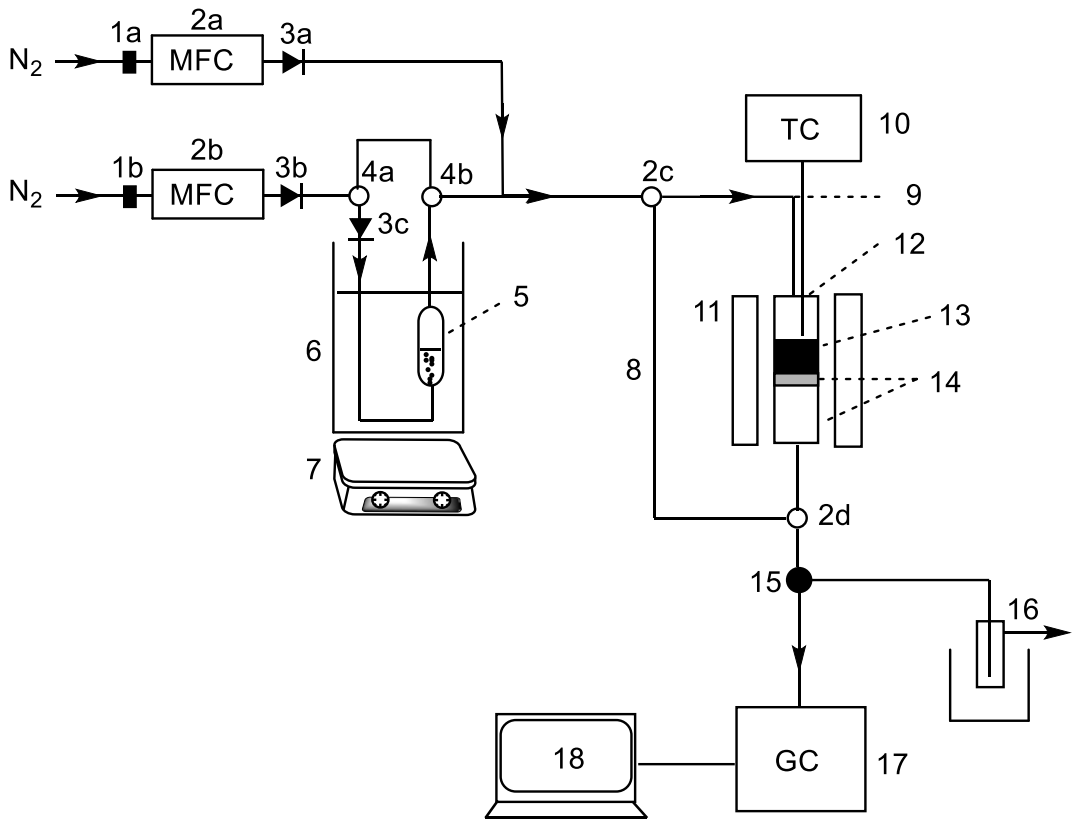

Figure 2.16. Continuous flow fixed-bed reactor set-up for dehydration of alcohols and DEE elimination.

Where the Key is: (1) particulate filter, (2) Brooks mass flow controller [2a MFC is used to vary substrate pressure at constant N_2 flow rate], (3) check valve (non-return valve), (4) 3-way valve, (5) saturator containing liquid substrate, (6) temperature-controlled water bath, (7) stirring hotplate, (8) bypass, (9) thermocouple, (10) Eurotherm temperature controller, (11) furnace, (12) Pyrex tubular reactor, (13) catalyst bed, (14) glass wool support, (15) Valco multiposition sampling valve with air actuator, (16) product trap, (17) Varian gas chromatograph, (18) computer.

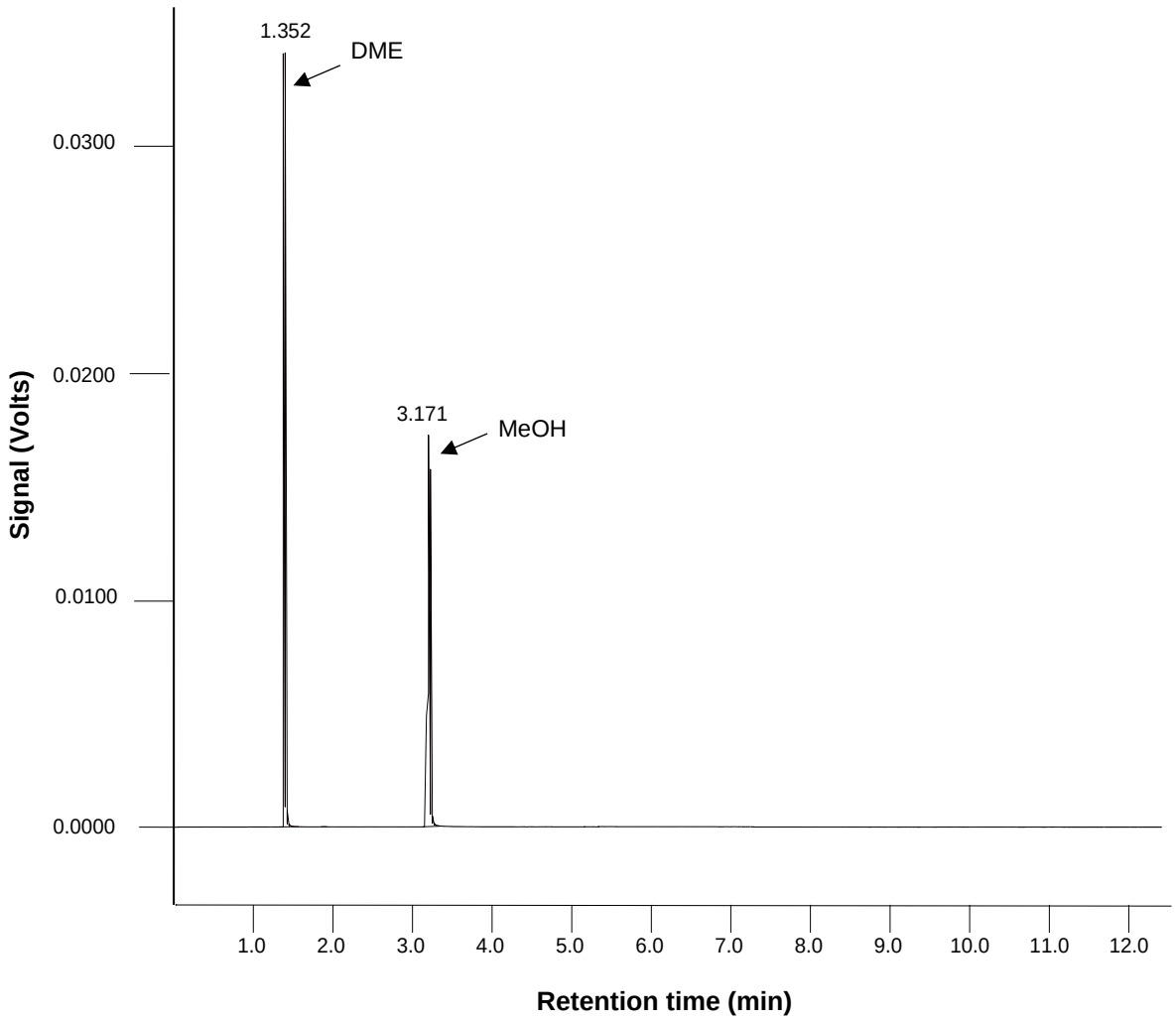

Figure 2.17. GC trace for MeOH dehydration to DME.

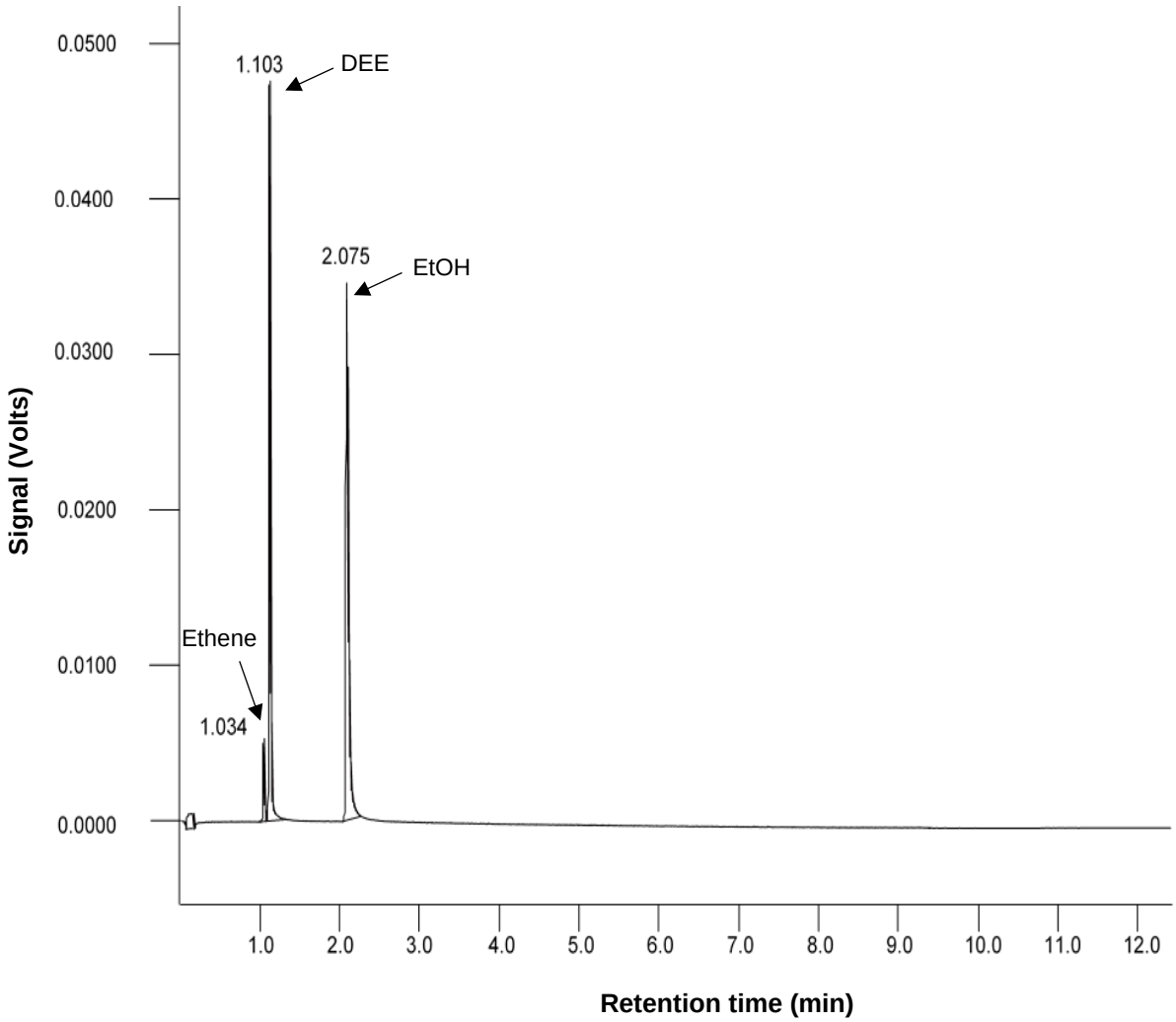

Figure 2.18. GC trace for EtOH dehydration to DEE and ethene.

2.5.1.1. Proton titration by 2,6-di-tert-butylpyridine during alcohol dehydration

The number of accessible proton sites in HPA catalysts was determined by in-situ titration with 2,6-di-tert-butylpyridine (DTBP) during alcohol dehydration [63,64]. DTBP pulses (6.5–13 μmol, 25–50 μL of 0.26 M DTBP solution in MeOH or EtOH) were injected using a microsyringe into the gas feed before the reactor at regular time intervals until the reaction was terminated. The DTBP pulses were injected ~15 min prior to sampling the gas flow for on-line GC analysis to allow sufficient time for DTBP adsorption onto the catalyst. The DTBP that passed through the catalyst was absorbed in a trap and analysed by GC. Dehydration rates were extrapolated to zero linearly to determine the amount of DTBP required to suppress the reaction. The number of accessible H^+ sites in the HPA catalysts was assumed to be equal to the amount of DTBP (per mole basis) required to terminate the alcohol dehydration (using a 1:1 H^+:DTBP adsorption stoichiometry) [64,65].

2.5.2. Diethyl ether elimination to ethanol and ethene

Elimination of DEE was performed in the gas phase. The catalytic activities were investigated under atmospheric pressure in the same fixed-bed microreactor that was used in the dehydration of EtOH. The substrate was fed by passing the carrier gas (N_2) flow controlled by a Brooks mass flow controller through a saturator, which held liquid DEE at 0 °C (ice bath) to maitain the DEE partial pressure at 24 kPa [61]. The DEE pressure was varied from 6–24 kPa by diluting the downstream flow with N_2 (Figure 2.16).

The reactor was packed with catalyst powder (0.20 g, 45–180 μm particle size). Bulk HPW and HSiW catalysts were diluted with 0.1 g silica to achieve plug-flow. Before the reaction, the catalysts were pre-treated in situ in N_2 flow at the reaction temperature for 1 h. At regular time intervals (ca. 15 min), the downstream gas flow was analysed through the on-line

GC to gain the conversion of alcohol and the selectivity of the product. The selectivity was defined on a carbon basis as the molar percentage of DEE converted to EtOH and ethene, taking into account reaction stoichiometry. The carbon balance was retained within 95%, with a mean absolute percentage error of ≤ 5%. A typical GC trace for the DEE elimination is shown in Figure 2.19.

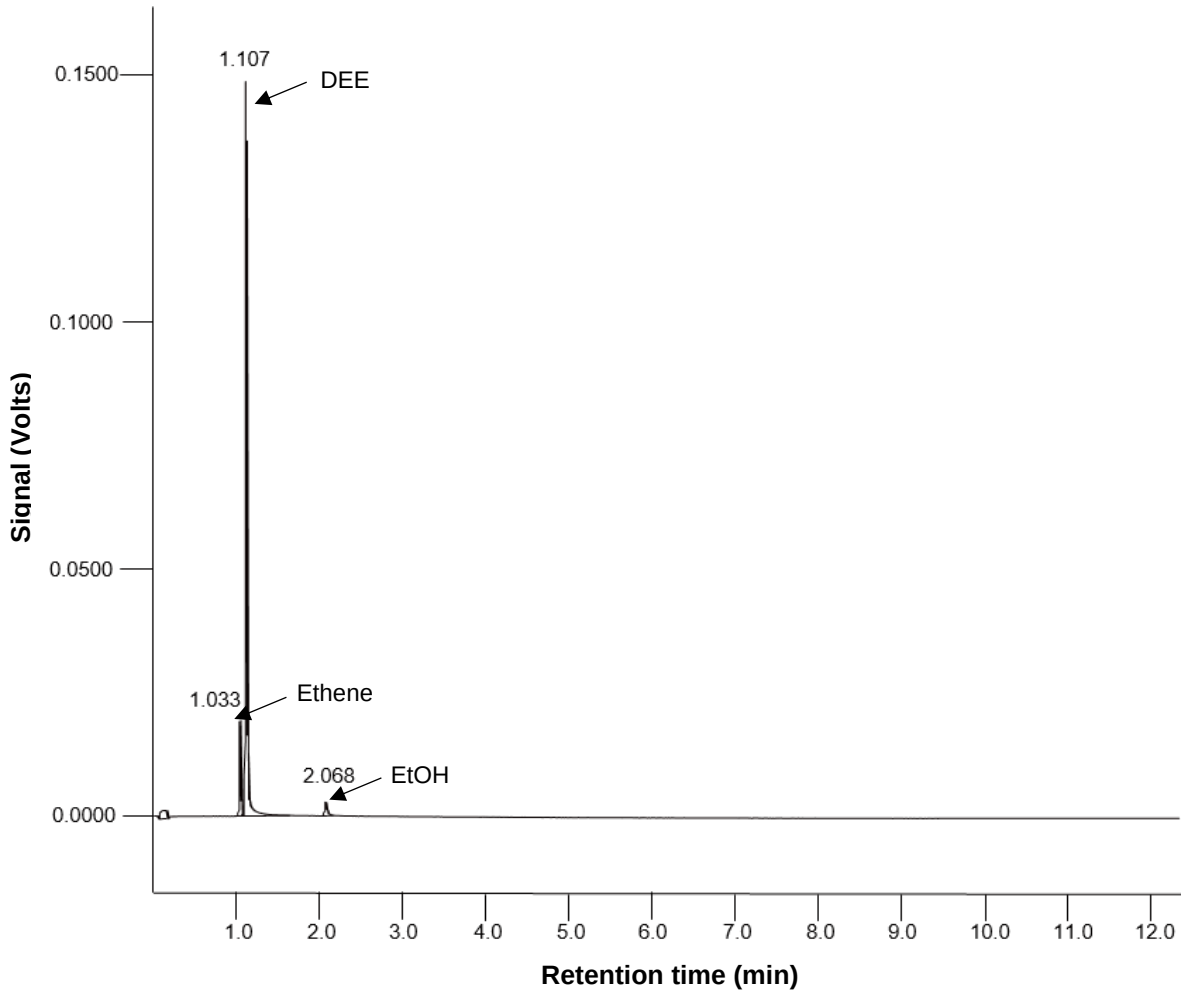

Figure 2.19. GC trace for DEE elimination to EtOH and ethene.

References

[1] N. Khandan, M. Kazemeini, M. Aghaziarati, Determining an optimum catalyst for liquid-phase dehydration of methanol to dimethyl ether, Appl. Catal. A: Gen. 349 (2008) 6–12.

[2] W. Alharbi, E. Brown, E.F. Kozhevnikova, I.V. Kozhevnikov, Dehydration of ethanol over heteropoly acid catalysts in the gas phase, J. Catal. 319 (2014) 174–181.

[3] A.M. Alsalme, P.V. Wiper, Y.Z. Khimyak, E.F. Kozhevnikova, I.V. Kozhevnikov, Solid acid catalysts based on $H_3PW_{12}O_{40}$ heteropoly acid: Acid and catalytic properties at a gas-solid interface, J. Catal. 276 (2010) 181–189.

[4] E.F. Kozhevnikova, I.V. Kozhevnikov, A calorimetric study of the acidity of bulk and silica-supported heteropoly acid $H_3PW_{12}O_{40}$, J. Catal. 224 (2004) 164–169.

[5] I.V. Kozhevnikov, K.R. Kloetstra, A. Sinnema, H.W. Zandbergen, H.V. Bekkum, Study of catalysts comprising heteropoly acid $H_3PW_{12}O_{40}$ supported on MCM-41 molecular sieve and amorphous silica, J. Mol. Catal. A: Chem. 114 (1996) 287–298.

[6] T.L. Stuchinskaya, M. Musawir, E.F. Kozhevnikova, I.V. Kozhevnikov, Liquid-phase oxidation of alcohols by oxygen and nitrous oxide catalysed by Ru-Co oxide, J. Catal. 231 (2005) 41–47.

[7] Y. Izumi, M. Ono, M. Kitagawa, M. Yoshida, K. Urabe, Silica-included heteropoly compounds as solid acid catalysts, Microporous Mater. 5 (1995) 255–262.

[8] W. Alharbi, E.F. Kozhevnikova, I.V. Kozhevnikov, Dehydration of methanol to dimethyl ether over heteropoly acid catalysts: The relationship between reaction rate and catalyst acid strength, ACS Catal. 5 (2015) 7186–7193.

[9] M. Che, J.C. Védrine, Characterization of Solid Materials and Heterogeneous Catalysts, second ed., Wiley–VCH Verlag & Co. KGaA, Weinheim, 2012.

[10] N. Saadatkhah, A.C. Garcia, S. Ackermann, P. Leclerc, M. Latifi, S. Samih, G.S. Patience, J. Chaouki, Experimental methods in chemical engineering: Thermogravimetric analysis-TGA, Can. J. Chem. Eng. 98 (2020) 34–43.

[11] P. Patnaik, Chapter 15-Thermal analysis, in: P. Patnaik (Ed.), Dean's Analytical Chemistry Handbook, second ed., McGraw–Hill Education, New York, 2004.

[12] F.J. Berry, G.R. Derrick, M. Mortimer, Identification and characterisation of stable phases of silicotungstic acid, $H_4SiW_{12}O_{40}{\cdot}nH_2O$, Polyhedron 68 (2014) 17–22.

[13] M.S.H. Akash, K. Rehman, Chapter 19-Thermo gravimetric analysis, in: M.S.H. Akash, K. Rehman (Eds.), Essentials of Pharmaceutical Analysis, Springer Nature Singapore Pte Ltd, Singapore, 2020: pp. 2115–222.

[14] M. Bowker, The Basis and Applications of Heterogeneous Catalysis, Oxford University Press Inc, New York, 1998.

[15] J.R.H. Ross, Chapter 4-Catalyst preparation, in: J.R.H. Ross (Ed.), Heterogeneous Catalysis, Elsevier, Amsterdam, 2012: pp. 65–96.

[16] R.A. Santen, J.A. Moulijn, P.W.N. Van Leeuwen, B.A. Averill, Catalysis: An Integrated Approach, second ed., Elsevier Science & Technology, 1999.

[17] G. Leofanti, M. Padovan, G. Tozzola, B. Venturelli, Surface area and pore texture of catalysts, Catal. Today 41 (1998) 207–219.

[18] G. Attard, C. Barnes, Surfaces, Oxford University Press Inc., New York, 1998.

[19] Y. Nishi, M. Inagaki, Chapter 11- Gas adsorption/desorption isotherm for pore structure characterization, in: M. Inagaki, F. Kang (Ed.), Materials Science and Engineering of Carbon, Elsevier Inc., 2016: pp. 227–247.

[20] S.J. Gregg, K.S.W. Sing, Adsorption, Surface Area and Porosity, second ed., Academic Press, London, 1982.

[21] G. Rothenberg, Catalysis Concepts and Green Applications, Wiley–VCH Verlag GmbH & Co.KGaA, Weinheim, 2008.

[22] E.F. Vansant, P.V.D. Voort, K.C. Vrancken, Characterzation and chemical modification of the silica surface, Vol. 93, Elsevier, Amsterdam, 1995.

[23] P. Unnikrishnan, D. Srinivas, Chapter 3-Heterogeneous catalysis, in: S.S. Joshi, V.V. Ranade (Eds.), Industrial Catalytic Processes for Fine and Specialty Chemicals, Elsevier, Cambridge, 2016: pp. 41–111.

[24] S. Brunauer, P.H. Emmett, E. Teller, Adsorption of gases in multimolecular Layers, J. Am. Chem. Soc. 60 (1938) 309–319.

[25] ABM. Helaluddin, R.S. Khalid, M. Alaama, S.A. Abbas, Main analytical techniques used for elemental analysis in various matrices, Trop. J. Pharm. Res. 15 (2016) 427–434.

[26] X. Hou, B.T. Jones, Inductively coupled plasma optical emission spectroscopy, in: R.A. Meyers (Ed.), Encyclopedia of Analytical Chemistry, John Wiley & Sons Ltd, Chichester, 2000: pp. 9468–9485.

[27] J.R. Dean, Practical Inductively Coupled Plasma Spectroscopy, John Wiley & Sons Ltd, Chichester, 2005.

[28] G.H. Jeffery, J. Bassett, J. Mendham, R.C. Denney, Vogel's Textbook of Quantitative Chemical Analysis, fifth ed., Longman Group UK Limited, United Kingdom, 1989.

[29] R. Kohli, K.L. Mittal, Chapter 3-Methods for Assessing Surface Cleanliness, in: R. Kohli, K.L. Mittal (Eds.), Developments in Surface Contamination and Cleaning, Vol. 12, Elsevier Inc, 2019: pp. 23–105.

[30] X. Li, A. Wang, R. Prins, Introduction to Heterogeneous Catalysis, Imperial College Press, United Kingdom, 2016.

[31] P. Atkins, J.D. Paula, Elements of Physical Chemistry, sixth ed., Oxford university press, Glasgow, 2013.

[32] L. Alexander, H.P. Klug, Determination of crystallite size with the X-ray spectrometer, J. Appl. Phys. 21 (1950) 137–142.

[33] G. Schwedt, The Essential Guide to Analytical Chemistry, John Wiley & Sons, Chichester, England, 1997.

[34] Y. Chen, C. Zou, M. Mastalerz, S. Hu, C. Gasaway, X. Tao, Applications of micro-Fourier transform infrared spectroscopy (FTIR) in the geological sciences-a review, Int. J. Mol. Sci. 16 (2015) 30223–30250.

[35] V. Solinas, I. Ferino, Microcalorimetric characterisation of acid-basic catalysts, Catal. Today 41 (1998) 179–189.

[36] A. Auroux, Calorimetry and Thermal Methods in Catalysis, Vol. 154, Springer–Verlag Berlin Heidelberg, London, 2013.

[37] G.D. Gatta, Direct determination of adsorption heats, Thermochim. Acta. 96 (1985) 349–363.

[38] A. Auroux, Acidity characterization by microcalorimetry and relationship with reactivity, Top. Catal. 4 (1997) 71–89.

[39] J.A. Dunne, M. Rao, S. Sircar, R.J. Gorte, A.L. Myers, Calorimetric heats of adsorption and adsorption isotherms. 2. O_2, N_2, Ar, CO_2, CH_4, C_2H_6, and SF_6 on NaX, H-ZSM-5, and Na-ZSM-5 zeolites, Langmuir 12 (1996) 5896–5904.

[40] X. Lu, Y. Wang, L. Estel, N. Kumar, H. Grénman, S. Leveneur, Evolution of specific heat capacity with temperature for typical supports used for heterogeneous catalysts, Processes 8 (2020) 911.

[41] F. Lefebvre, F.X. Liu-Cai, A. Auroux, Microcalorimetric study of the acidity of tungstic heteropolyanions, J. Mater. Chem. 4 (1994) 125–131.

[42] T. Okuhara, H. Watanabe, T. Nishimura, K. Inumaru, M. Misono, Microstructure of cesium hydrogen salts of 12-tungstophosphoric acid relevant to novel acid catalysis, Chem. Mater. 12 (2000) 2230–2238.

[43] B.B. Bardin, S. V. Bordawekar, M. Neurock, R.J. Davis, Acidity of Keggin-type heteropolycompounds evaluated by catalytic probe reactions, sorption microcalorimetry, and density functional quantum chemical calculations, J. Phys. Chem. B 102 (1998) 10817–10825.

[44] P. Atkins, J.D. Paula, J. Keeler, Atkins' Physical Chemistry, eleventh ed., Oxford University Press, New York, 2006.

[45] J.P. Harvey, N. Saadatkhah, G. Dumont-Vandewinkel, S.L.G. Ackermann, G.S. Patience, Experimental methods in chemical engineering: Differential scanning calorimetry-DSC, Can. J. Chem. Eng. 96 (2018) 2518–2525.

[46] V. Rakić, V. Dondur, U. Mioč, D. Jovanović, Microcalorimetry in the identification and characterization of the most reactive active sites of heterogeneous catalysts, Top. Catal. 19 (2002) 241–247.

[47] P. Leparlouer, J. Mercier, B. Jalon, Introduction to a new simultaneous TG–DSC 111, Thermochim. Acta 103 (1986) 21–26.

[48] S.T. Almutairi, E.F. Kozhevnikova, I.V. Kozhevnikov, Ketonisation of acetic acid on metal oxides: Catalyst activity, stability and mechanistic insights, Appl. Catal. A: Gen. 565 (2018) 135–145.

[49] J-H. Ferrasse, D. Lecomte, Simultaneous heat-flow differential calorimetry and thermogravimetry for fast determination of sorption isotherms and heat of sorption in environmental or food engineering, Chem. Eng. Sci. 59 (2004) 1365–1376.

[50] D. Mani, M.S. Kalpana, D.J. Patil, A.M. Dayal, Chapter 3-Organic matter in gas shales: origin, evolution, and characterization, in: A.M. Dayal, D. Mani, Shale Gas, Elsevier, 2017: pp. 25–54.

[51] A.I. Ruiz-Matute, S. Rodríguez-Sánchez, M.L. Sanz, A.C. Soria, Chapter 12-Chromatographic technique: gas chromatography (GC), in: Da-Wen Sun (Ed.), Modern Techniques for Food Authentication, Second ed., Academic Press, 2018: pp. 25–54.

[52] F.W. Fifield, D. Kealey, Principles and Practice of Analytical Chemistry, fifth ed., Blackwell Science Ltd, United Kingdom, 2000.

[53] https://teaching.shu.ac.uk/hwb/chemistry/tutorials/chrom/gaschrm.htm, (accessed 14 March 2020).

[54] C.L. Faiola, M.H. Erickson, V.L. Fricaud, B.T. Jobson, T.M. Vanreken, Quantification of biogenic volatile organic compounds with a flame ionization detector using the effective carbon number concept, Atmos. Meas. Tech. 5 (2012) 1911–1923.

[55] J.E. Szulejko, Y.H. Kim, K.H. Kim, Method to predict gas chromatographic response factors for the trace-level analysis of volatile organic compounds based on the effective carbon number concept, J. Sep. Sci. 36 (2013) 3356–3365.

[56] C. Zhang, Fundamentals of Environmental Sampling and Analysis, John Wiley & Sons, Inc., Hoboken, New Jersey, 2007.

[57] J.T. Scanlon, D.E. Willis, Calculation of flame ionization detector relative response factors using the effective carbon number concept, J. Chromatogr. Sci. 23 (1985) 333–340.

[58] M. Boudart, Turnover rates in heterogeneous catalysis, Chem. Rev. 95 (1995) 661–666.

[59] G.C. Bond, S.J. Frodsham, P. Jubb, E.F. Kozhevnikova, I.V. Kozhevnikov, Compensation effect in isopropanol dehydration over heteropoly acid catalysts at a gas-solid interface, J. Catal. 293 (2012) 158–164.

[60] C. Perego, S. Peratello, Experimental methods in catalytic kinetics, Catal. Today 52 (1999) 133–145.

[61] D.R. Lide, Handbook of Chemistry and Physics, eighty fourth ed., CRC Press, Boca Raton, 2003.

[62] W.D.T. Dale, P.A. Flavelle, P. Kruus, Concentration fluctuations in water-methanol mixtures as studied by ultrasonic absorption, Can. J. Chem. 54 (1976) 355–366.

[63] R.T. Carr, M. Neurock, E. Iglesia, Catalytic consequences of acid strength in the conversion of methanol to dimethyl ether, J. Catal. 278 (2011) 78–93.

[64] W. Knaeble, E. Iglesia, Kinetic and theoretical insights into the mechanism of alkanol dehydration on solid Brønsted acid catalysts, J. Phys. Chem. C 120 (2016) 3371–3389.

[65] C.D. Baertsch, K.T. Komala, Y.H. Chua, E. Iglesia, Genesis of Brønsted acid sites during dehydration of 2-butanol on tungsten oxide catalysts, J. Catal. 205 (2002) 44–57.

Chapter 3: Investigation of acidity of silica-supported heteropoly acids by ammonia adsorption calorimetry

Chapter 3 : Investigation of acidity of silica-supported heteropoly acids by ammonia adsorption calorimetry

3.1. Introduction

Bulk solid HPAs, despite their very strong Brønsted acidity, have limited use in heterogeneous acid catalysis because of their low surface area (1–10 m^2g^{-1}), hence a low density of surface acid sites [1–6]. For this reason, supported HPA catalysts, which have a greater number of accessible acid sites, are generally preferred. SiO_2 is the most common support since it is relatively inert to HPAs and available in a wide textural variety [6,7]. Silica-supported tungsten heteropoly acids HPW/SiO_2 and HSiW/SiO_2 have found industrial applications as solid acid catalysts. For example, HSiW/SiO_2 is used as the catalyst for synthesising ethyl acetate from ethene and acetic acid in vapour-phase processes commercialised by Showa Denko in Japan [8] and BP Chemicals in the UK [9]. The BP process, trademarked AVADA® (AdVanced Acetates by Direct Addition of acetic acid to ethene), was launched in 2001 on a scale of 220 kt/y at Hull, UK. In 2008, this plant became the property of INEOS, and its capacity was further increased to >300 kt/y in 2017 [10]. This is the largest application of heterogeneous acid catalysis by HPA. A silica-supported HPA catalyst is also used in the Hummingbird® technology for dehydrating bioethanol to polymer grade ethene in the gas phase developed by BP Chemicals and recently acquired by TechnipFMC [11]. This technology has been successfully piloted on a commercial bioethanol feedstock with a catalyst lifetime of 2 years [11].

HPA dispersion on the SiO_2 surface depends on the HPA loading: at low loadings, HPW and HSiW form finely dispersed species on the SiO_2 surface; at higher loadings, HPA crystal phase is developed [3,4,6]. Various HPA forms have been detected on the silica surface by TEM: discrete molecules, clusters 5 nm in size and large crystallites of >50 nm. Their relative

amounts depend on the HPA loading [3,12]. Dispersion of supported HPAs is routinely characterised by powder XRD [13–15]. IR spectroscopy of adsorbed pyridine has been applied to assess the dispersion of supported HPW [15,16]. From DSC, the thermal stability of HPA may be decreased when HPA is supported on silica [2]. Thus, HPW in 30%HPW/SiO_2 decomposed at 568 °C, whereas bulk HPW decomposed at 599 °C. This has been explained by the interaction of HPW with SiO_2 support [2].

^{1}H and ^{31}P MAS NMR investigations have indicated the chemical interaction of HPW with SiO_2 support [17–23]. A ^{1}H MAS NMR study [17] showed the interaction of HPW with SiO_2 and the formation of new weaker proton sites on the SiO_2 surface, probably via dehydroxylation reaction (3.1) with the surface Si–OH groups ($m \leq 3$).

$$H_3[PW_{12}O_{40}] + m(\equiv Si–OH) \rightarrow (Si)_m^{+}(H_{3-m}[PW_{12}O_{40}])^{m-} + mH_2O \qquad \textbf{(3.1)}$$

In HPW/SiO_2 catalysts synthesised by conventional wet impregnation of SiO_2 with a HPW aqueous solution, different HPA species have been observed by ^{31}P MAS NMR, including those resonating at -15 ppm with intact Keggin structure and others resonating from -13 to -14 ppm [3,19,20]. These species have been attributed to bulk surface HPW crystallites and the "interacting" species ($(\equiv Si–OH_2^{+})_m(H_{3-m}[PW_{12}O_{40}]^{m-})$, respectively [15,19]. Evidence has been presented that the "interacting" species may be dimeric heteropoly acids $H_6[P_2W_{18}O_{62}]$ or $H_6[P_2W_{21}O_{71}]$, formed from HPW in the course of catalyst preparation [20]. The relative amounts of these species depend on the HPW loading, with the Keggin species by far dominating at higher HPW loadings [20]. These dimeric HPAs are also strong acids, although weaker than the parent HPW, as shown by NH_3-MC [24,25]. In contrast, the HPW/SiO_2 catalysts prepared by impregnation from methanol solution contain exclusively Keggin-type species over the whole range of HPW loading [3,20]. The formation of "interacting" HPA

species may be avoided by immobilizing anhydrous Keggin HPAs onto dehydroxylated SiO_2 support using surface organometallic chemistry [26]. Therefore, it would be interesting to compare the strength of acid sites and the catalytic activity of the silica-supported HPA catalysts prepared from water and MeOH.

The acid properties of the silica-supported HPW and HSiW have been documented, although less systematically than those of the bulk HPAs, especially regarding the effect of HPA loading on the acid strength (([1–5,15,27–29] and references therein). This information is of great importance for the mechanistic understanding of HPA catalysis and catalyst optimisation. Most NH_3-MC and NH_3-TPD studies [2,27,30,31] point to decreasing the acid strength when HPA is supported on silica due to HPA-support interaction. However, a NH_3-DSC study [15] claims that the strength of HPW supported on silica does not depend on the HPW loading above 6 wt% and is close to the strength of bulk HPW. It should be noted that the calorimetric results from different sources are not easy to compare because the heat and the amount of NH_3 adsorption depend on HPA pre-treatment and adsorption temperature [2,24,32].

This Chapter describes our investigation of acid properties of the silica-supported HPA catalysts, containing Keggin-type heteropoly acids HPW and HSiW, with a wide range of HPA loadings from 5 to 100%. As the silica support, a broadly applied commercial Degussa Aerosil 300 is used. Our main goal is to investigate the effect of HPA loading on the catalyst acid strength. This includes systematic quantitative evaluation of acidity of bulk and silica-supported HPW and HSiW at a gas-solid interface using NH_3 adsorption MC and TGA–DSC complemented by BET, XRD and IR spectroscopic characterisation of catalyst texture and HPA structural integrity.

3.2. HPA/SiO_2 catalysts

Silica-supported HPA catalysts, 5–70%HPA/SiO_2, were synthesised by wet impregnation of silica with an aqueous and methanol HPA solution and dried at 150 °C/10^{-3} kPa for 1.5 h as described in Chapter 2. The catalysts prepared from water are hereafter designated HPA/SiO_2 and those prepared from MeOH HPA/SiO_2(m). The HPA loading in the catalysts was determined from W analysis by ICP-OES. The water content, essential for acidity and activity characterisation, was determined by TGA. The finished SiO_2-supported catalysts prepared from water exhibited a 6 ± 1% weight loss to 600 °C attributed to the loss of adsorbed water and silanol groups of silica (Figures 3.1–3.2). For comparison, pure SiO_2 compacted by wetting with water and dried at 150 °C/10^{-3} kPa for 1.5 h had a 4% weight loss to 600 °C. HPW/SiO_2(m) catalysts prepared from MeOH had a 4 ± 1% weight loss to 600 °C largely attributable to water loss, as MeOH would be partly removed and partly dehydrated during catalyst drying. Bulk HPW and HSiW dried at 150 °C/10^{-3} kPa for 1.5 h exhibited 4 ± 1% weight loss to 600 °C (see Figures 7.1–7.5 in Appendix). Further catalyst drying was not practical because alcohol dehydration yielded water as a by-product. Acidity characterisation (see below) was carried out on the catalysts with the specified water content to determine catalyst acid strength at conditions close to reaction conditions for alcohol dehydration (see Chapter 4).

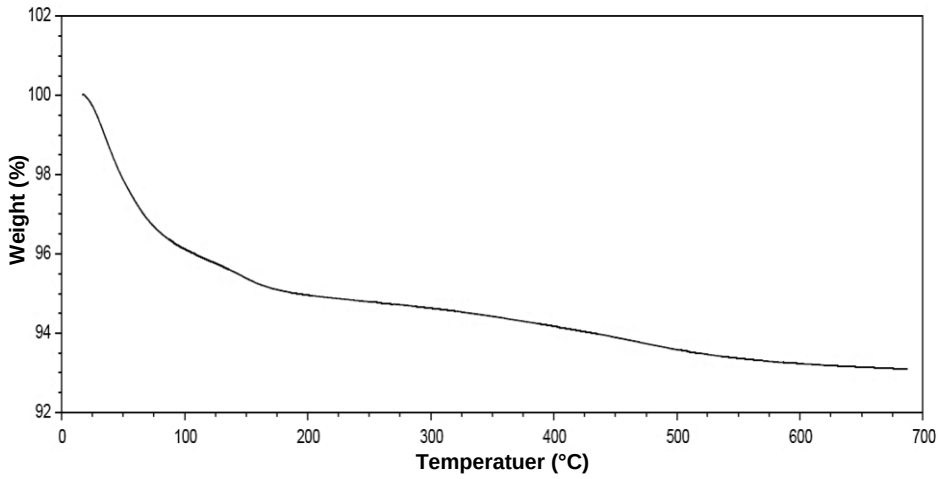

Figure 3.1. TGA of 26%HPW/SiO_2 after pre-treatment at 150 °C/10^{-3} kPa for 1.5 h (6.5% weight loss to 600 °C).

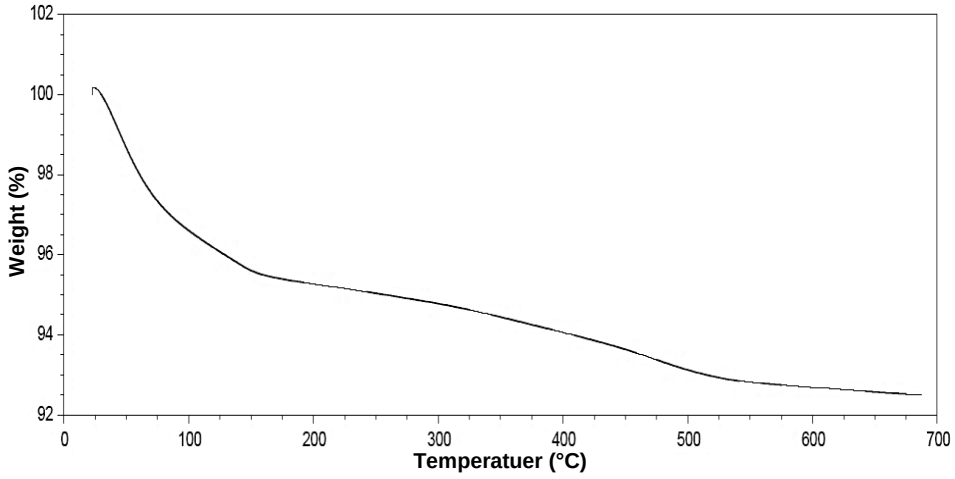

Figure 3.2. TGA of 27%HSiW/SiO_2 after pre-treatment at 150 °C/10^{-3} kPa for 1.5 h (6.9% weight loss to 600 °C).

3.3. Catalyst texture and HPA structural integrity

The texture of bulk HPAs and silica-supported HPA catalysts HPW/SiO_2, HPW/SiO_2(m), HSiW/SiO_2 and HSiW/SiO_2(m) with HPA loadings of 5–70% is represented in Tables 3.1 and 3.2, together with the texture of pure silica support. It can be seen that the catalyst surface area (per gram of catalyst) decreases monotonically with increasing the HPA loading from pure silica support at zero HPA loading down to 5.7 m^2g^{-1} for bulk HPW and 8.01 m^2g^{-1} for bulk

HSiW. Analysis shows that this is mainly the result of the addition of dense HPAs to the SiO_2 without significant change of the pore structure.

Figures 3.3–3.6 show that HPA loading had only a small effect on the surface area and the pore volume per gram of silica up to ~70%HPA loading, which corresponds to an average HPA surface coverage of ~2 monolayers (calculated assuming an HPA cross section of 144 A^2 [1,3,4] and the surface area of Aerosil 300 silica support of ~300 m^2/g). Also, the pore diameter practically did not change up to ~50%HPA loading in the catalysts prepared from water and MeOH (Figure 3.7). This suggests that in these catalysts HPAs mainly occupy the external surface and macropores in silica support without blocking meso- and micropores. At least, this is valid for the range of 0–50%HPA loading most relevant to practical use of these catalysts [33].

The HPW and HSiW catalysts prepared from water and MeOH have similar surface areas per gram of catalyst, however their porosity is different (Table 3.1 and 3.2). Those prepared from water have a pore diameter and pore volume about 2-fold greater than those prepared from MeOH. As a result, given practically the same surface area, the catalysts prepared from water are more compact, having a 2-fold greater bulk powder density (*d*) than the ones prepared from MeOH. The same applies to Aerosil 300 silica support (d = 0.054 g cm^{-3}): the support compacted with water is more dense (d = 0.38 g cm^{-3}) than that compacted with MeOH (d = 0.21 g cm^{-3}) (Table 3.1). This is the result of a predictably stronger interaction of silica with water than with MeOH.

Table 3.1. Information about HPW/SiO_2 catalysts.

Catalyst[a]	Surface area[b] (m^2g^{-1})	Pore volume[c] (cm^3g^{-1})	Pore diameter[d] (Å)	d[e] (g cm^{-3})	HPA particle size[f] (nm)	$-\Delta H_o$[g] (kJ mol^{-1})	NH_3/KU[h]
SiO_2[i]	283	1.2	164	0.38			
SiO_2(m)[j]	279	0.7	94	0.21			
5.8%HPW/SiO_2	265	1.1	161	0.34		137	
3.8%HPW/SiO_2(m)	257	0.7	107	0.16			
11%HPW/SiO_2	237	1.1	189	0.38		166	2.9
9.7%HPW/SiO_2(m)	241	0.7	113	0.17		151	
19%HPW /SiO_2	233	1.0	166	0.39		169	2.4
16%HPW/SiO_2(m)	226	0.6	100	0.19	16	167	
26%HPW/SiO_2	188	0.8	178	0.46	13	167	2.7
24%HPW/SiO_2(m)	193	0.5	98	0.23	18	175	
45%HPW/SiO_2	153	0.7	177	0.56	18	177	2.5
48%HPW/SiO_2(m)	152	0.4	99	0.32	20	175	
68%HPW/SiO_2	104	0.4	140	0.87	24	192	2.1
66%HPW/SiO_2(m)	101	0.2	88	0.53	22	184	
HPW	5.7	0.01	74	3.25	56	203	2.4
HPW (300 °C)						(144)[k]	2.7

[a] HPW/SiO_2 catalysts prepared by impregnation from water and HPW/SiO_2(m) from MeOH, both calcined at 150°C/10^{-3} kPa for 1.5 h; HPA loading from ICP analysis (nominal HPA loading in HPW/SiO_2 catalysts: 5, 10, 15, 25, 40 and 60%); water content in the catalysts 5–7%; prior to BET analysis, the catalysts pre-treated at 250 °C in a vacuum. [b] BET surface area per gram of catalyst. [c] Single point total pore volume at p/p_o = 0.97 per gram of catalyst. [d] Average BET pore diameter. [e] Bulk density of catalyst powder. [f] From XRD, calculated from the Scherrer equation. [g] Initial enthalpy of NH_3 adsorption from NH_3-MC at 150 °C, average values from 2–3 measurements (±6 kJ mol^{-1}); the catalysts pre-treated at 150 °C. [h] Molecules of NH_3 adsorbed per Keggin unit from TGA–DSC; the catalysts pre-treated at 150 °C. [i] Aerosil 300 silica compacted by wetting with water and dried at 150°C/10^{-3} kPa for 1.5 h. [j] Aerosil 300 silica compacted by wetting with MeOH and dried at 150°C/10^{-3} kPa for 1.5 h. [k] ΔH_o from TGA–DSC at 150 °C; prior to TGA–DSC, HPW pre-treated at 300 °C.

Table 3.2. Information about HSiW/SiO_2 catalysts.

Catalyst[a]	Surface area[b] (m^2g^{-1})	Pore volume[c] (cm^3g^{-1})	Pore diameter[d] (Å)	d[e] (g cm^{-3})	HPA particle size[f] (nm)	$-\Delta H_o$[g] (kJ mol^{-1})	NH_3/KU[h]
SiO_2[i]	283	1.2	164	0.38			
SiO_2(m)[j]	279	0.7	94	0.21			
5.8%HSiW/SiO_2	259	1.0	150	0.32		138	
4.4%HSiW/SiO_2(m)	255	0.7	103	0.19			
11%HSiW/SiO_2	242	1.0	170	0.36		152	3.5
8.3%HSiW/SiO_2(m)	245	0.6	101	0.18		152	
17%HSiW/SiO_2	225	0.9	160	0.36	8.3	156	3.7
13%HSiW/SiO_2(m)	229	0.6	102	0.22	5.1	158	
27%HSiW/SiO_2	184	0.8	163	0.44	11	153	3.9
27%HSiW/SiO_2(m)	192	0.5	104	0.27	11	160	
46%HSiW/SiO_2	143	0.5	146	0.56	15	157	3.7
44%HSiW/SiO_2(m)	152	0.4	105	0.33	18	168	
71%HSiW/SiO_2	87	0.3	118	0.96	20	160	3.5
65%HSiW/SiO_2(m)	91	0.2	97	0.57	20	169	
HSiW	8.01	0.01	68	3.50	43	177	2.9
HSiW (300 °C)						(138)[k]	3.2

[a] HSiW/SiO_2 catalysts prepared by impregnation from water and HSiW/SiO_2(m) from MeOH, both calcined at 150°C/10^{-3} kPa for 1.5 h; HPA loading from ICP analysis (nominal HPA loading in HSiW/SiO_2 catalysts: 5, 10, 15, 25, 40 and 60%); water content in the catalysts 5–7%; prior to BET analysis, the catalysts pre-treated at 250 °C in a vacuum. [b] BET surface area per gram of catalyst. [c] Single point total pore volume at p/p_o = 0.97 per gram of catalyst. [d] Average BET pore diameter. [e] Bulk density of catalyst powder. [f] From XRD, calculated from the Scherrer equation. [g] Initial enthalpy of NH_3 adsorption from NH_3-MC at 150 °C, average values from 2–3 measurements (±6 kJ mol^{-1}); the catalysts pre-treated at 150 °C. [h] Molecules of NH_3 adsorbed per Keggin unit from TGA–DSC; the catalysts pre-treated at 150 °C. [i] Aerosil 300 silica compacted by wetting with water and dried at 150°C/10^{-3} kPa for 1.5 h. [j] Aerosil 300 silica compacted by wetting with MeOH and dried at 150°C/10^{-3} kPa for 1.5 h. [k] ΔH_o from TGA–DSC at 150 °C; prior to TGA–DSC, HPW pre-treated at 300 °C.

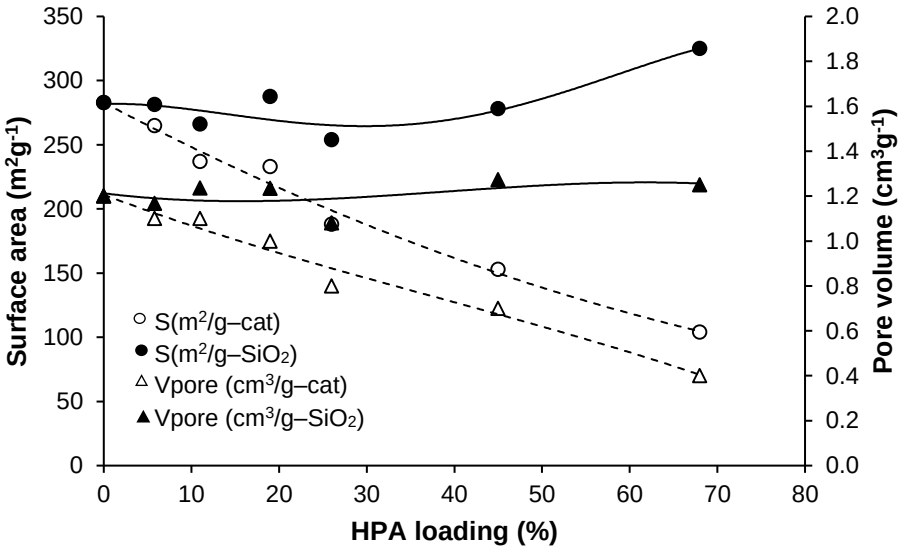

Figure 3.3. Effect of HPW loading on surface area and pore volume of HPW/SiO_2 catalysts (open markers represent the values per gram of catalyst, solid markers per gram of SiO_2).

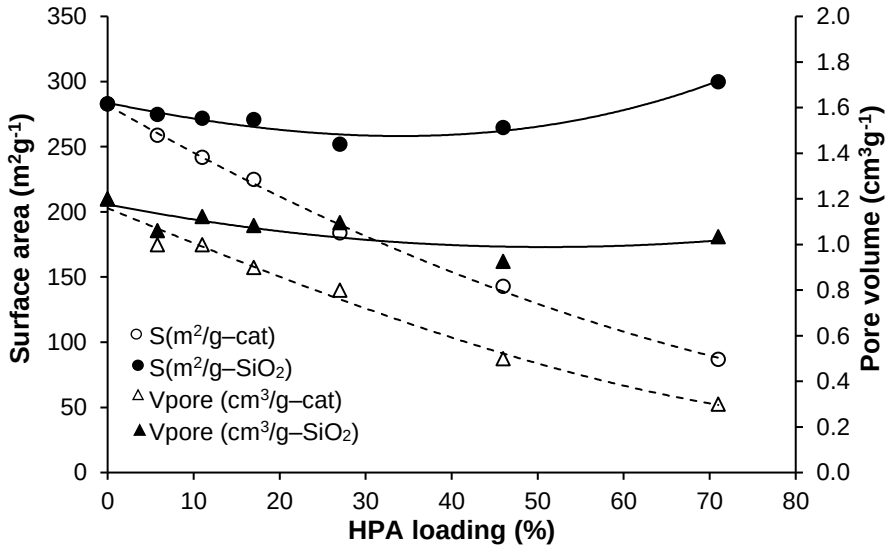

Figure 3.4. Effect of HSiW loading on surface area and pore volume of HSiW/SiO_2 catalysts (open markers represent the values per gram of catalyst, solid markers per gram of SiO_2).

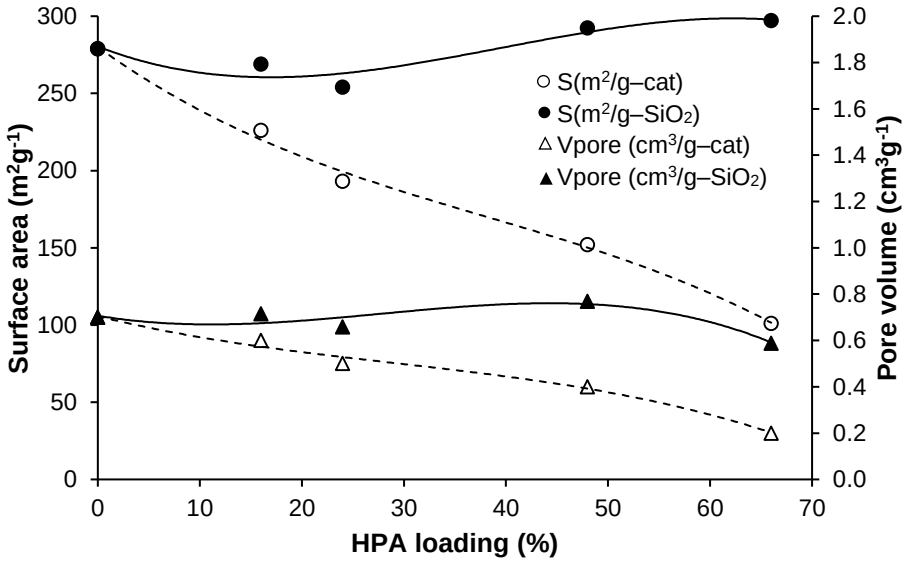

Figure 3.5. Effect of HPW loading on surface area and pore volume of HPW/SiO_2(m) catalysts (open markers represent the values per gram of catalyst, solid markers per gram of SiO_2).

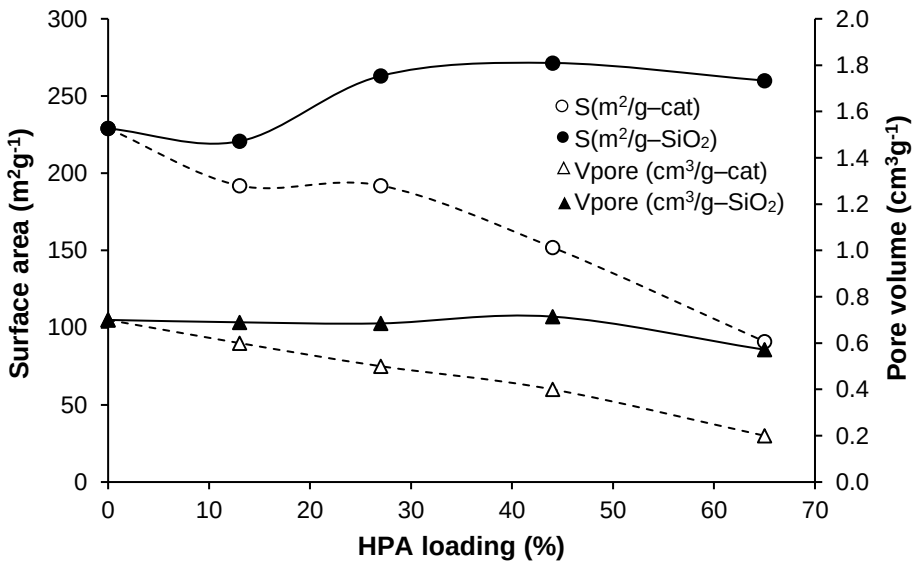

Figure 3.6. Effect of HSiW loading on surface area and pore volume of HSiW/SiO_2(m) catalysts (open markers represent the values per gram of catalyst, solid markers per gram of SiO_2).

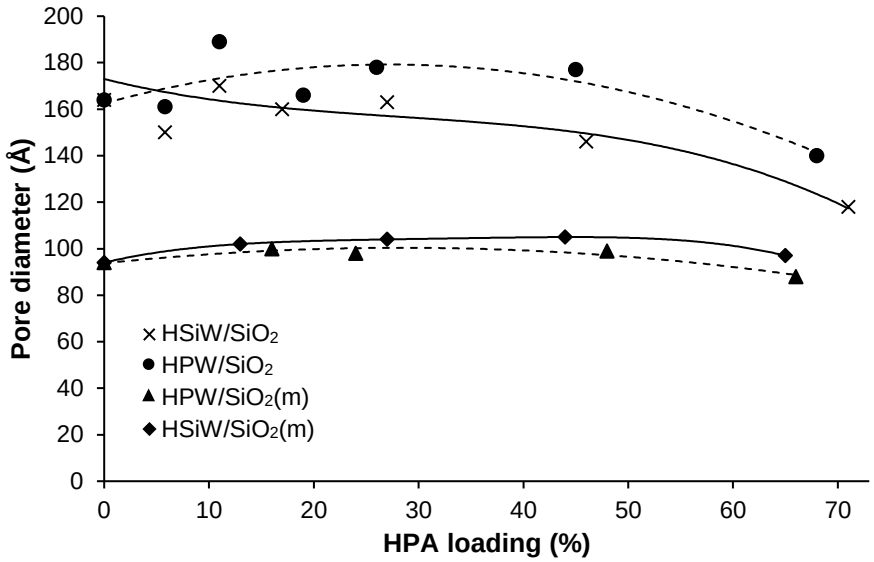

Figure 3.7. Effect of HPA loading on pore diameter of HPA/SiO_2 catalysts.

Figures 3.8–3.10 represent the nitrogen adsorption-desorption isotherms for compacted silica support (Aerosil 300), 26%HPW/SiO_2 and 27%HSiW/SiO_2 catalysts. All three are type IV isotherms indicating a mesoporous material [34,35]. In addition, the isotherms have a H2 hysteresis loop, which indicates non-uniform pores in size and/or shape [36,37] as presented in Figure 2.4 (Chapter 2). Silica has the pores that fall in the macro/mesoporous range [34,37,38]. Figure 3.11 displays the pore size distribution of compacted SiO_2, 26%HPA/SiO_2 and 27%HSiW/SiO_2 obtained by the BJH method from desorption isotherms. All pore size distributions peak at 239–329 Å pore diameter (mesopores) [39,40]. Similar results were observed for all HPA/SiO_2 and HPA/SiO_2(m) catalysts (see Figures 7.6–7.9 in Appendix). From these results, it appears that supporting HPA practically did not affect silica pores, which confirm the conclusions made above.

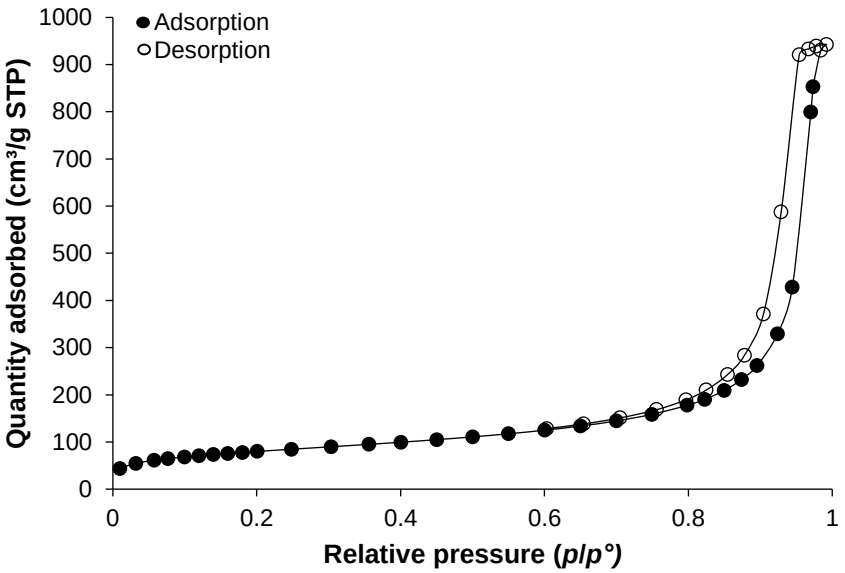

Figure 3.8. N_2 adsorption-desorption isotherm for compacted SiO_2 support.

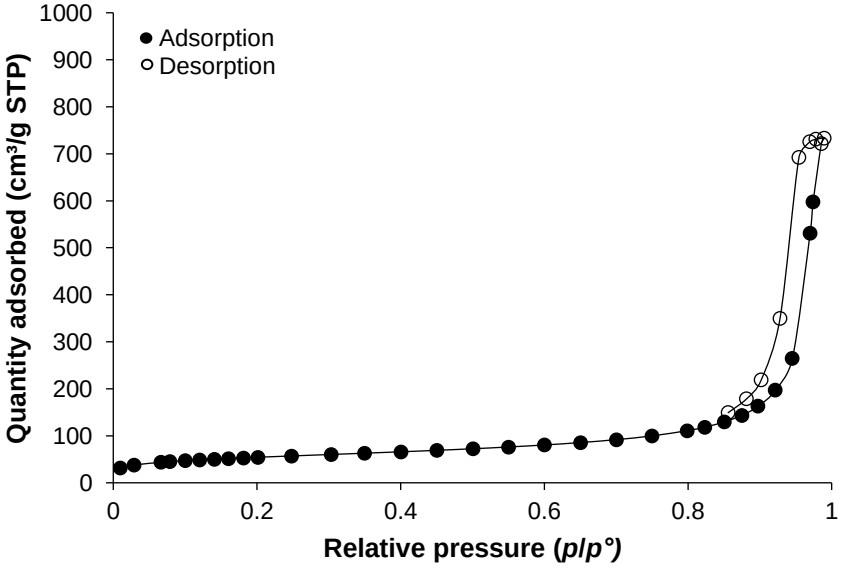

Figure 3.9. N_2 adsorption-desorption isotherm for 26%HPW/SiO_2 catalyst.

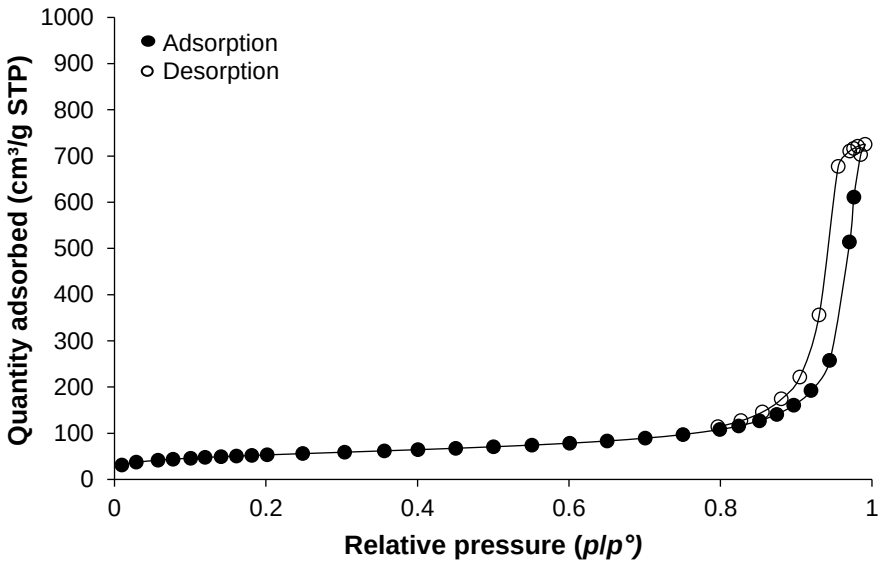

Figure 3.10. N_2 adsorption-desorption isotherm for 27%HSiW/SiO_2 catalyst.

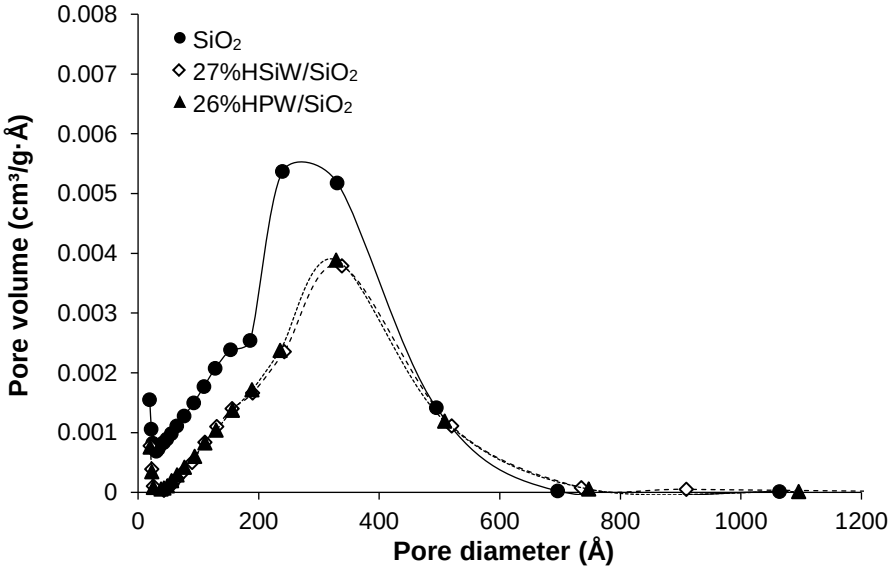

Figure 3.11. Pore size distribution for silica and HPA/SiO_2.

XRD patterns for HPW/SiO_2, HSiW/SiO_2, HPW/SiO_2(m) and HSiW/SiO_2(m) are shown in Figures 3.12–3.15. In HPW/SiO_2 catalysts, HPW crystal phase appears from 11%HPW loading, whereas in HSiW/SiO_2 catalysts, HSiW crystallites are seen from a higher HSiW loading of 17%. The HPA crystal phase in supported catalysts exhibits the diffraction patterns exactly matching those for the bulk HPAs [13–15,30,32,36,41–44]. This confirms the structural integrity of HPW and HSiW on the silica surface, i.e., the same crystal structure of bulk and supported HPA crystallites. The average size of HPA crystallites on the silica surface (Tables 3.1 and 3.2) was evaluated from the Scherrer equation, with FWHM (full width at half maximum) calculated using the Origin software (Chapter 2).

As expected, the size of HPW and HSiW crystallites increases with HPA loading. HPW and HSiW crystallites formed from aqueous and methanol solutions at similar HPA loadings have a similar size (Table 3.1 and 3.2), which suggests that these solvents make little difference to HPA crystallization [20]. Notably, the HSiW crystallites are smaller than the HPW ones at similar HPA loadings, indicating a higher HSiW dispersion on the silica surface compared to HPW.

Therefore, from the BET and XRD data, it can be concluded that in silica-supported catalysts HPA is mainly localized on the external surface and in macropores rather than within meso- and micropores of support. Increasing the HPA loading causes the HPA crystallites to grow without a significant increase in HPA coverage of the silica surface. Also, these results point to a higher surface proton sites density in HSiW/SiO_2 catalysts compared to HPW/SiO_2 at equal HPA loadings, which is not only because HSiW has more protons than HPW per Keggin unit, but also due to the higher dispersion of HSiW on the silica surface compared to HPW. This can affect the activity of these catalysts (see Chapters 4 and 5).

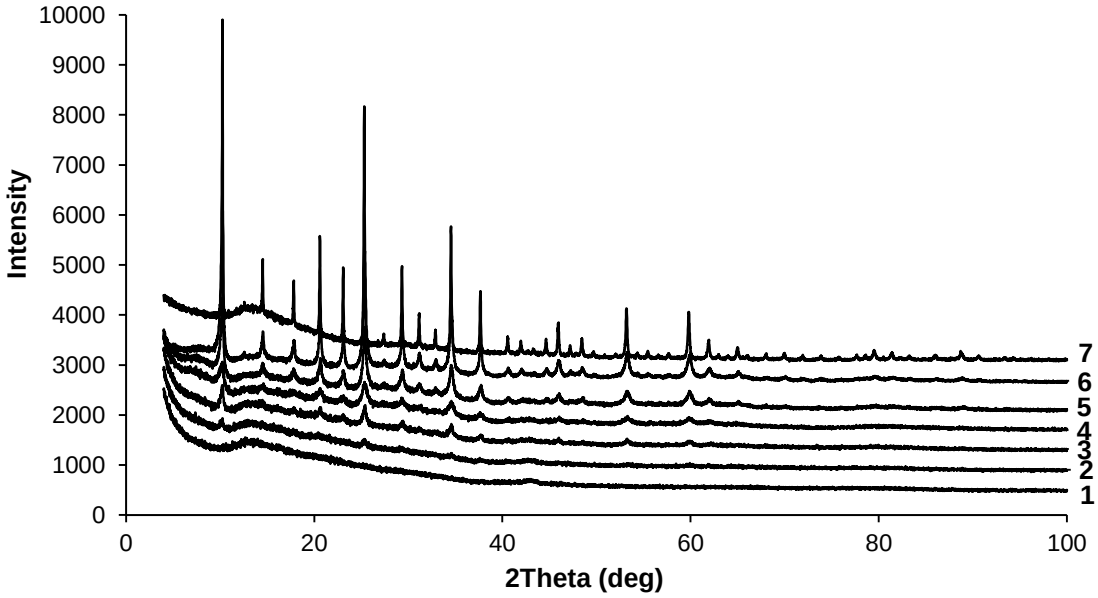

Figure 3.12. XRD patterns for HPW/SiO_2 with different HPW loadings: (1) 5.8%, (2) 11%, (3) 19%, (4) 26%, (5) 45%, (6) 68% and (7) bulk HPW.

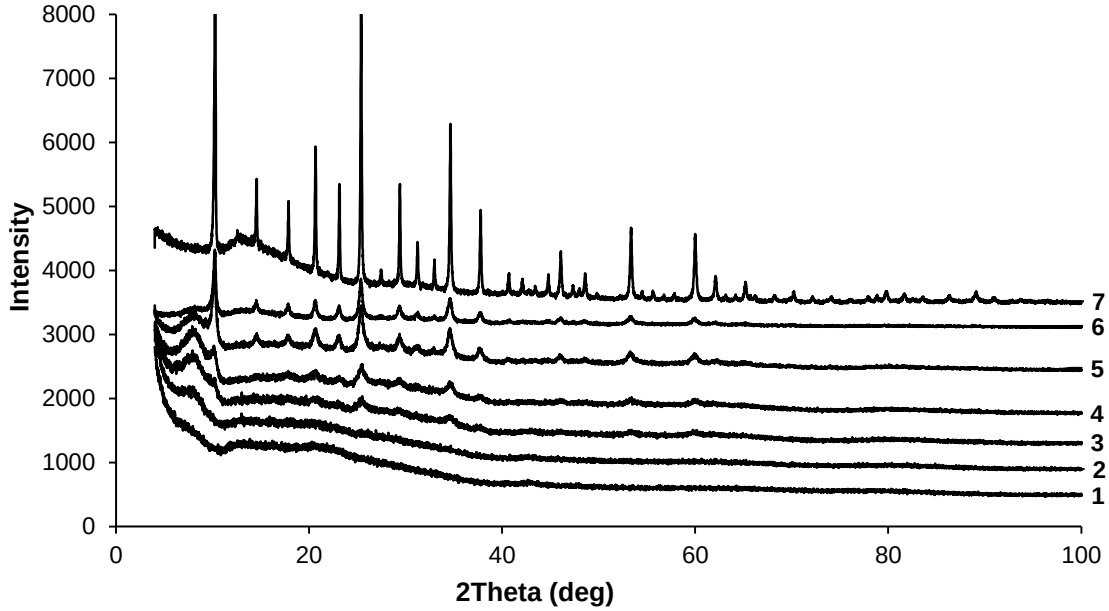

Figure 3.13. XRD patterns for HSiW/SiO_2 with different HSiW loadings (1) 5.8%, (2) 11%, (3) 17%, (4) 27%, (5) 46%, (6) 71% and (7) bulk HSiW.

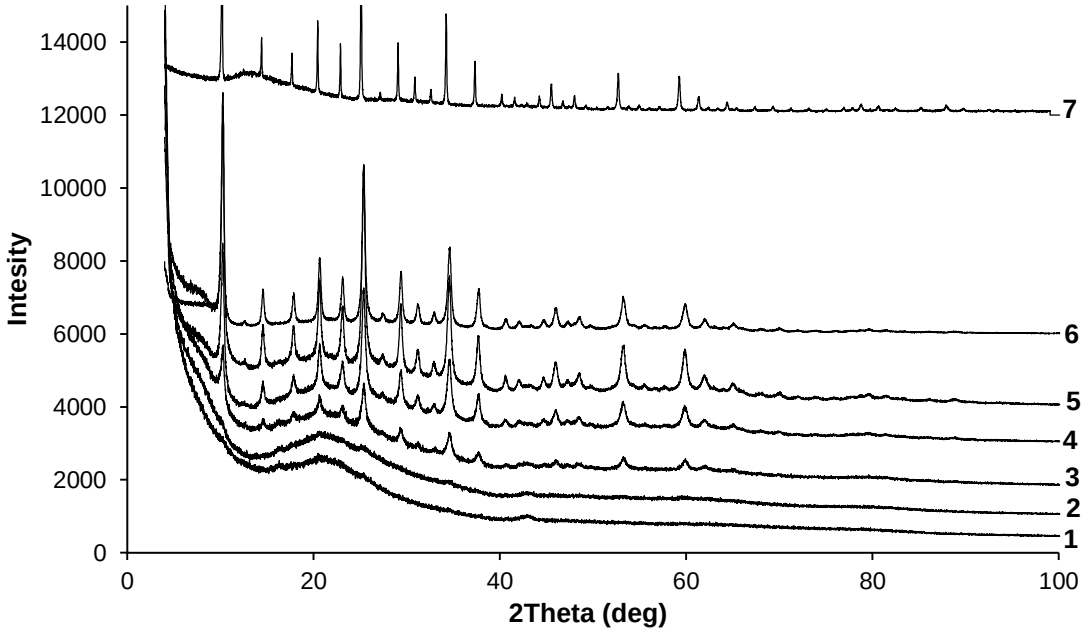

Figure 3.14. XRD patterns for HPW/SiO_2(m) with different HPW loadings: (1) 3.8%, (2) 9.7%, (3) 16%, (4) 24%, (5) 48%, (6) 66% and (7) bulk HPW.

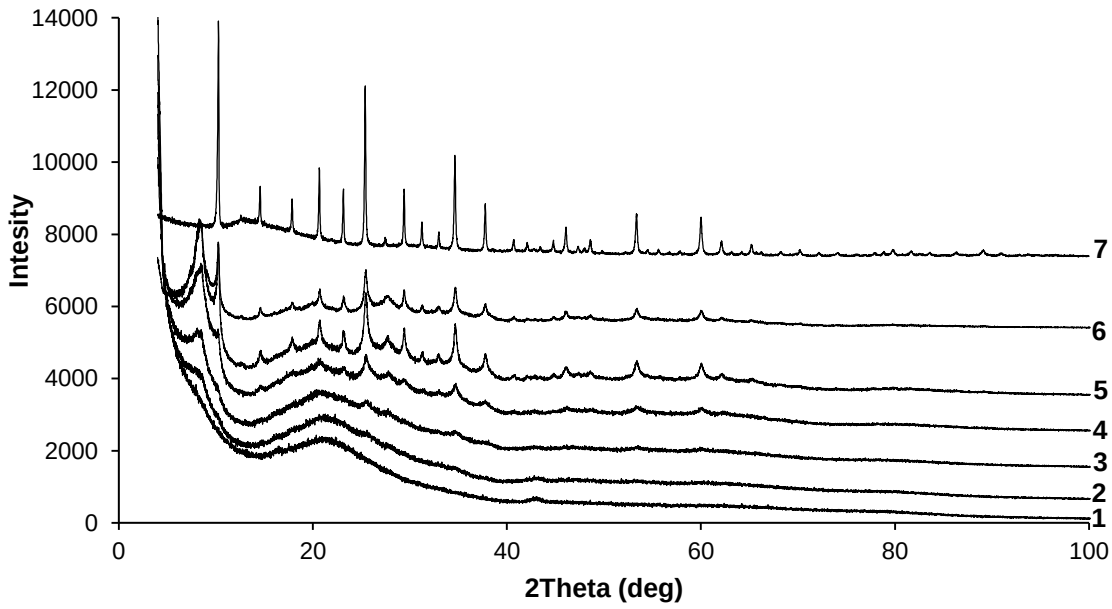

Figure 3.15. XRD patterns for HSiW/SiO_2(m) with different HSiW loadings: (1) 4.4%, (2) 8.3%, (3) 13%, (4) 27%, (5) 44%, (6) 65% and (7) bulk HSiW.

DRIFT spectra for HPW/SiO_2, HSiW/SiO_2, HPW/SiO_2(m) and HSiW/SiO_2(m) catalysts together with the reference spectra of bulk HPW and HSiW are presented in Figures 3.16–3.19. Bulk HPAs display the well-known infrared bands of metal-oxygen stretching vibrations in the range of 700–1100 cm^{-1} characteristic of Keggin heteropoly anions, in agreement with the literature [1,4,14,36,43,45,46].

Bulk HPW shows four bands at 808 cm^{-1} (W–O–W edge-sharing), 889 cm^{-1} (W–O–W corner-sharing), 984 cm^{-1} (W=O) and 1082 cm^{-1} (P–O) (Figures 3.16 and 3.18). The corresponding bands for bulk HSiW occur at 792 cm^{-1} (W–O–W edge-sharing), 881 cm^{-1} (W–O–W corner-sharing), 927 cm^{-1} (Si–O) and 980 cm^{-1} (W=O) (Figures 3.17 and 3.19). It can be seen that these bands are present unchanged in the spectra of silica-supported HPAs, except for the bands of W–O–W at 889, 808 cm^{-1} in HPW/SiO_2 and HPW/SiO_2(m) and the band of W–O–W at 792 cm^{-1} in HSiW/SiO_2 and HSiW/SiO_2(m), which are obscured by the intense bands of silica centred at 804 and 1108 cm^{-1} [36,44,47]. This shows that the structure of Keggin units (primary structure) in all HPA catalysts is largely intact, in agreement with previous reports [4,6,14,22,45].

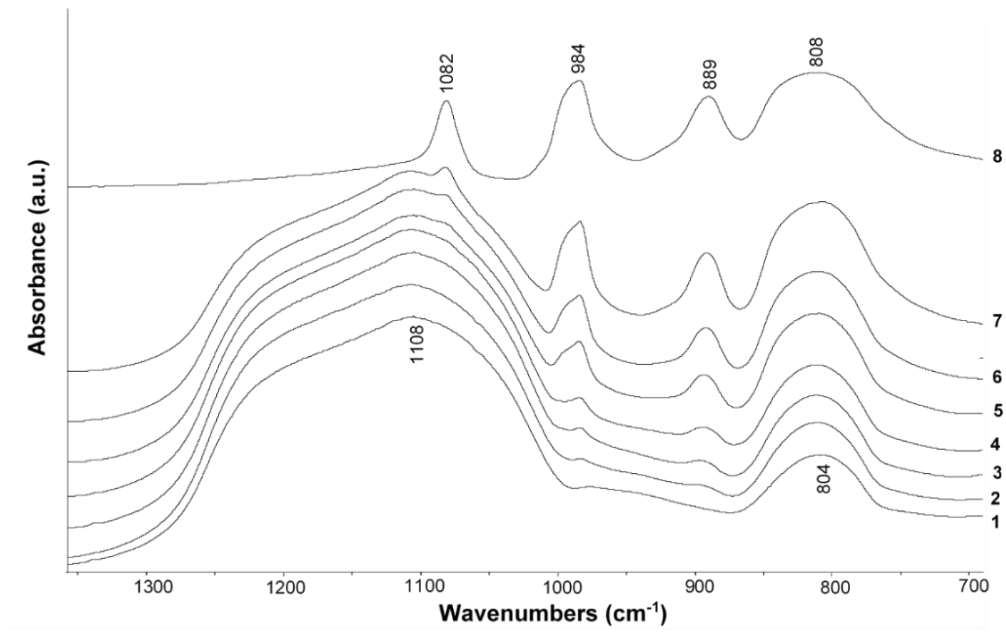

Figure 3.16. DRIFT spectra of HPW/SiO_2 catalysts (KBr mixtures): (1) SiO_2, (2) 5.8%HPW/SiO_2, (3) 11%HPW/SiO_2, (4) 19%HPW/SiO_2, (5) 26%HPW/SiO_2, (6) 45%HPW/SiO_2, (7) 68%HPW/SiO_2, (8) bulk HPW.

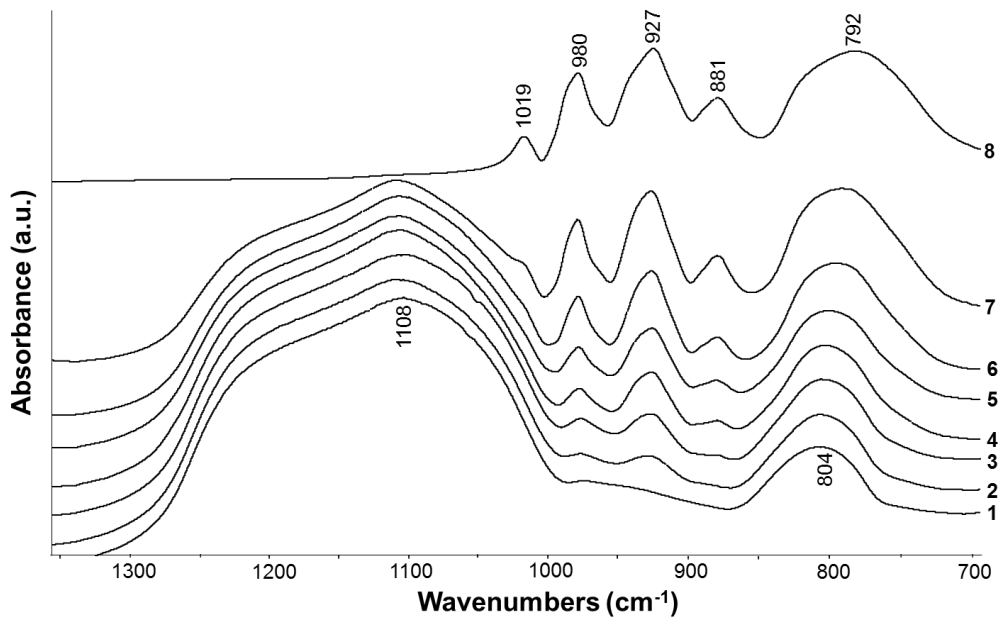

Figure 3.17. DRIFT spectra of HSiW/SiO_2 catalysts (KBr mixtures): (1) SiO_2, (2) 5.8%HSiW/SiO_2, (3) 11%HSiW/SiO_2, (4) 17%HSiW/SiO_2, (5) 27%HSiW/SiO_2, (6) 46%HSiW/SiO_2, (7) 71%HSiW/SiO_2, (8) bulk HSiW.

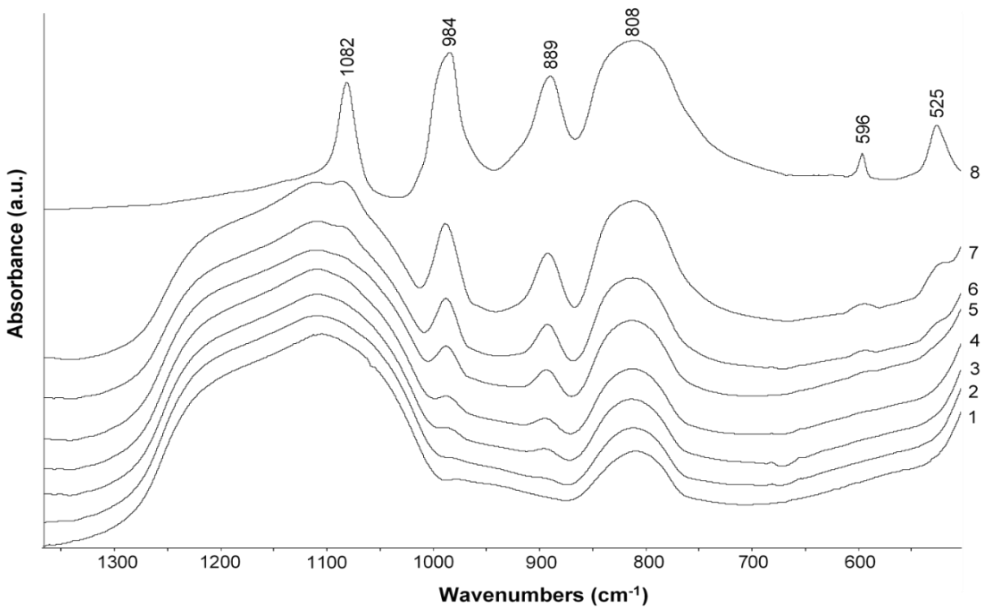

Figure 3.18. DRIFT spectra of HPW/SiO_2(m) catalysts (KBr mixtures): (1) SiO_2, (2) 3.8%HPW/SiO_2, (3) 9.7%HPW/SiO_2, (4) 16%HPW/SiO_2, (5) 24%HPW/SiO_2, (6) 48%HPW/SiO_2, (7) 66%HPW/SiO_2, (8) bulk HPW.

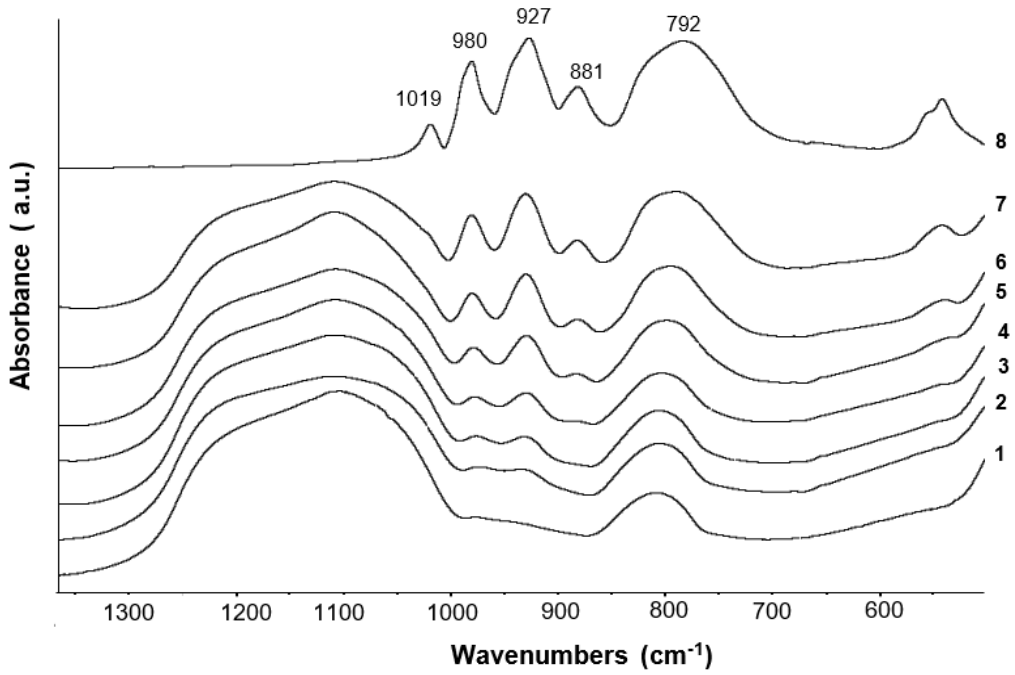

Figure 3.19. DRIFT spectra of HSiW/SiO_2(m) catalysts (KBr mixtures): (1) SiO_2, (2) 4.4%HSiW/SiO_2, (3) 8.3%HSiW/SiO_2, (4) 13%HSiW/SiO_2, (5) 27%HSiW/SiO_2, (6) 44%HSiW/SiO_2, (7) 65%HSiW/SiO_2, (8) bulk HSiW.

3.4. Acid properties of HPW and HSiW supported on silica

Initial enthalpies of NH_3 adsorption on bulk and silica-supported HPW and HSiW catalysts prepared from water and MeOH, ΔH_o, representing the strongest catalyst proton sites, are summarized in Tables 3.1 and 3.2 at different HPA loadings, including bulk HPW and HSiW. These values were obtained by extrapolating the differential enthalpy of NH_3 adsorption measured by NH_3-MC to zero NH_3 uptake. The catalysts were pre-treated at 150 °C in dry N_2 flow for 3 h, and adsorption measurements were conducted at the same temperature of 150 °C. In these measurements, the total NH_3 uptake corresponded to the neutralization of 40–100% of proton sites in the HPAs present in the catalysts. The absolute error in ΔH_o was ± 6 kJ mol^{-1}. Previously, several studies have reported the ΔH_o values for the bulk HPW and HSiW [22,24,32,48,49]. It has been firmly established that these values depend on the adsorption and pre-treatment temperature. The heat of adsorption ($-\Delta H_o$) decreases when the temperature is increased [24,32,49]. At the same time, the amount of NH_3 adsorbed increases with increasing the temperature [32]. These effects have been correlated with the amount of hydration water present in bulk HPAs. At lower temperatures, larger amounts of water present in HPA can cause hydration of NH_4^+ ions, thus increasing the heat of adsorption. Simultaneously, the water can block access for NH_3 molecules to the HPA bulk, thus reducing the amount of NH_3 adsorbed [32]. Within the temperature range of 150–200 °C, the ΔH_o values are typically close to -200±10 kJ mol^{-1} for the bulk HPW and -180±10 kJ mol^{-1} for the bulk HSiW [22,24,48,49]. Our results from NH_3-MC, ΔH_o = -203±6 kJ mol^{-1} for HPW (Table 3.1) and -177±6 kJ mol^{-1}for HSiW (Table 3.2) at the pre-treatment and NH_3 adsorption temperature of 150 °C (average of three measurements) are in good agreement with the literature values. Increasing the pre-treatment temperature to 300 °C at NH_3 adsorption temperature of 150 °C led to a decrease in

the heat of adsorption: ΔH_o = -144 kJ mol^{-1} for HPW (Table 3.1) and -138 kJ mol^{-1} for HSiW (Table 3.2), as expected.

Figure 3.20 shows the plot of differential heat of NH_3 adsorption as a function of NH_3 uptake of bulk HPW and HSiW, and Figure 3.21 shows the extrapolation of these data to zero NH_3 uptake. It can be seen in Figure 3.20 that the total NH_3 uptake is somewhat less than the stoichiometric amount, i.e., 3 NH_3 molecules per Keggin unit for HPW and 4 for HSiW, which may be due to the water present in the HPAs blocking access for NH_3 molecules.

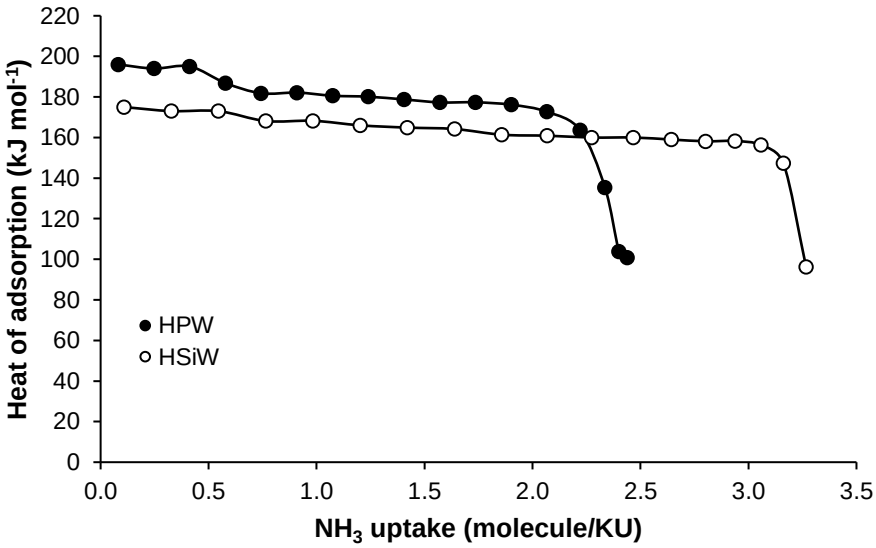

Figure 3.20. Differential heat of NH_3 adsorption on bulk HPW and HSiW as a function of NH_3 uptake at 150 °C.

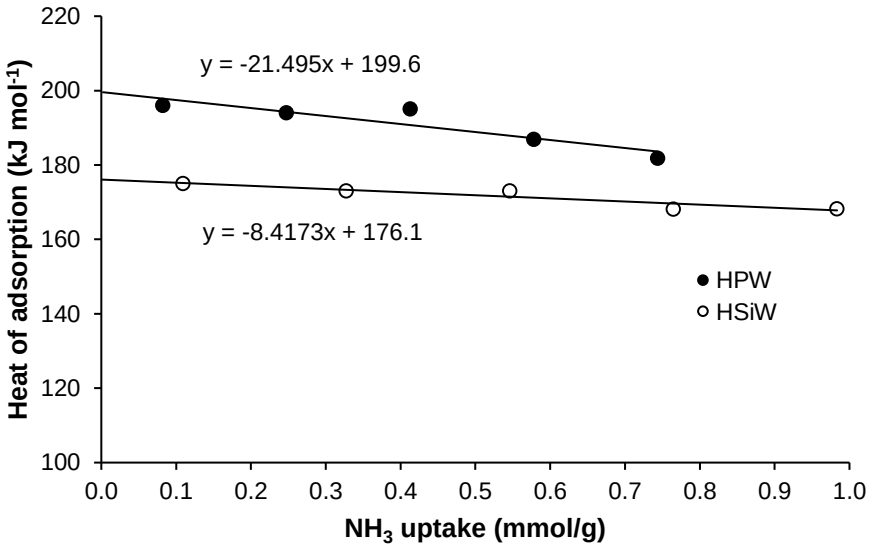

Figure 3.21. Extrapolation of differential heat of NH_3 adsorption to zero NH_3 uptake: bulk HPW (solid circles), bulk HSiW (open circles) at 150 °C.

The reproducibility of microcalorimetric measurements, including batch to batch reproducibility, for HPA/SiO_2 catalysts is illustrated in Table 3.3. For 27%HSiW/SiO_2 catalyst, as an example, the average error in a series of five measurements was ±5 kJ mol^{-1}. In general, the error was ±6 kJ mol^{-1} in a typical series of 3 measurements.

Figure 3.22 illustrations the initial heat of NH_3 adsorption ($-\Delta H_o$) as a function of HPA loading. As seen, the strength of HPA catalysts increases monotonically with HPA loading, with HPW, as expected, being stronger than HSiW at any loading. This trend can be rationalized assuming that HPA-support interaction reducing the strength of HPA proton sites should decline with increasing HPA loading, thus leading to an increase in the catalyst acid strength. The drop in the adsorption heat below 10% loading may be due to a stronger HPA-support interaction causing partial decomposition or dehydroxylation of HPA catalysts by reaction (3.1).

The plots of ΔH_o versus HPA loading above 10% HPA loading (Figure 3.22) can be represented by linear regressions (Eqs. (3.2) and (3.3)) for HPW/SiO_2 and HSiW/SiO_2,

respectively, where (HPW%) and (HSiW%) are the HPA loadings in wt%. These regressions can be used for calculating ΔH_o at any HPA loading above 10% for the catalyst system under study.

$$(-\Delta H_o) = 0.435\times(\text{HPW\%}) + 159.9 \quad \textbf{(3.2)}$$

$$(-\Delta H_o) = 0.242\times(\text{HSiW\%}) + 148.2 \quad \textbf{(3.3)}$$

The increase in adsorption heat with HPA loading is significant: by 37 kJ mol^{-1} for HPW/SiO_2 and 25 kJ mol^{-1} for HSiW/SiO_2 as the HPA loading increases from 10 to 100 %. This should affect the turnover catalyst activity (per accessible proton site), which generally scales with the catalyst acid strength obeying the Brønsted relationship. This is indeed the case, as demonstrated later in Chapter 4 for the dehydration of MeOH and EtOH.

The HPW/SiO_2 catalysts prepared from water and HPW/SiO_2(m) prepared from MeOH have practically the same acid strength at the same HPW loading (Figure 3.22). Therefore, the dimeric heteropoly acids $H_6[P_2W_{18}O_{62}]$ and $H_6[P_2W_{21}O_{71}]$, if formed [20], do not significantly affect the catalyst acid strength as these HPAs are quite strong themselves [24,25]. From NH_3-MC study [25], bulk $H_6[P_2W_{18}O_{62}]$ is weaker than bulk HPW, but silica-supported 20%$H_6[P_2W_{18}O_{62}]$/SiO_2 and 20%HPW/SiO_2 have similar acid strengths.

Table 3.3. Reproducibility of initial enthalpy of NH_3 adsorption for 27%HSiW/SiO_2[a].

Catalyst	Calcination temperature (°C)	ΔH_o[b] (kJ mol^{-1})
27.3%HSiW/SiO_2[c]	150	-159
27.3%HSiW/SiO_2	150	-156
27.3%HSiW/SiO_2	150	-151
27.1%HSiW/SiO_2[d]	150	-150
27.1%HSiW/SiO_2	150	-147
27.20±0.11% HSiW/SiO_2[e]	150	-153±5

[a] HSiW/SiO_2 catalysts prepared by impregnation from water, calcined at 150 °C/10^{-3} kPa for 1.5 h; HPA loading from ICP analysis; water content in the catalysts 5–7%; [b] Initial enthalpy of NH_3 adsorption from NH_3-MC at 150 °C; [c, d] Different batches of HSiW/SiO_2 catalyst; [e] Average results.

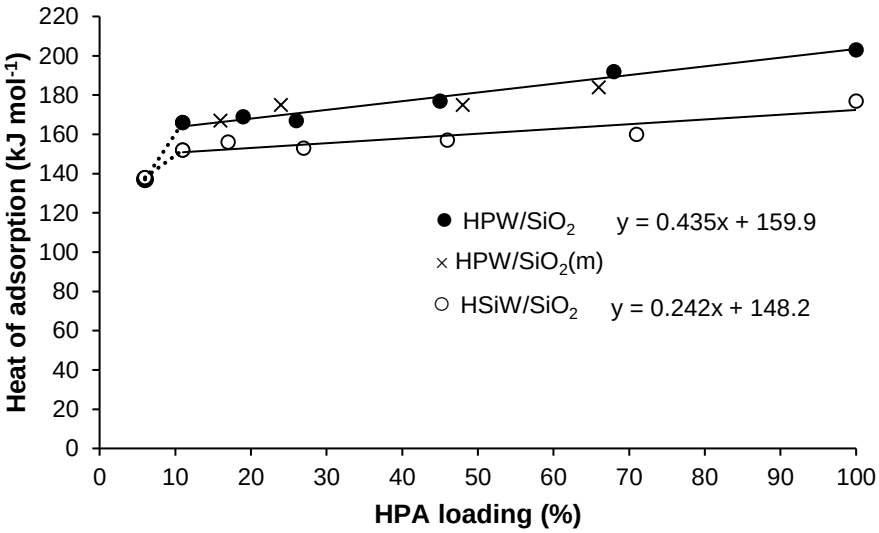

Figure 3.22. Effect of HPA loading on initial heat of NH_3 adsorption on silica supported HPAs.

The total NH_3 uptake was determined for the HPA/SiO_2 catalysts prepared from water, as well as for bulk HPW and HSiW, using TGA–DSC. The NH_3 adsorption was measured at 150 °C after catalyst pre-treatment at 150 °C. For the bulk HPAs, it was also measured at 150 °C after pre-treatment at 300 °C (TGA–DSC traces for bulk HPW and HSiW are displayed in Figures 3.23 and 3.24). Figures 3.25 and 3.26 show the TGA–DSC traces of 26%HPW/SiO_2 and 27%HSiW/SiO_2. The results are given in Tables 3.1 and 3.2 in terms of the number of NH_3 molecules adsorbed per Keggin unit, NH_3/KU. All supported HPA/SiO_2 catalysts reached NH_3 uptakes close to the stoichiometric values, i.e. 3 for HPW catalysts and 4 for HSiW catalysts, in agreement with the previous reports [15,30]. As expected, bulk HPW and HSiW adsorbed less than stoichiometric amounts of NH_3 after pre-treatment at 150 °C than after pre-treatment at 300 °C (see the last entries in Tables 3.1 and 3.2).

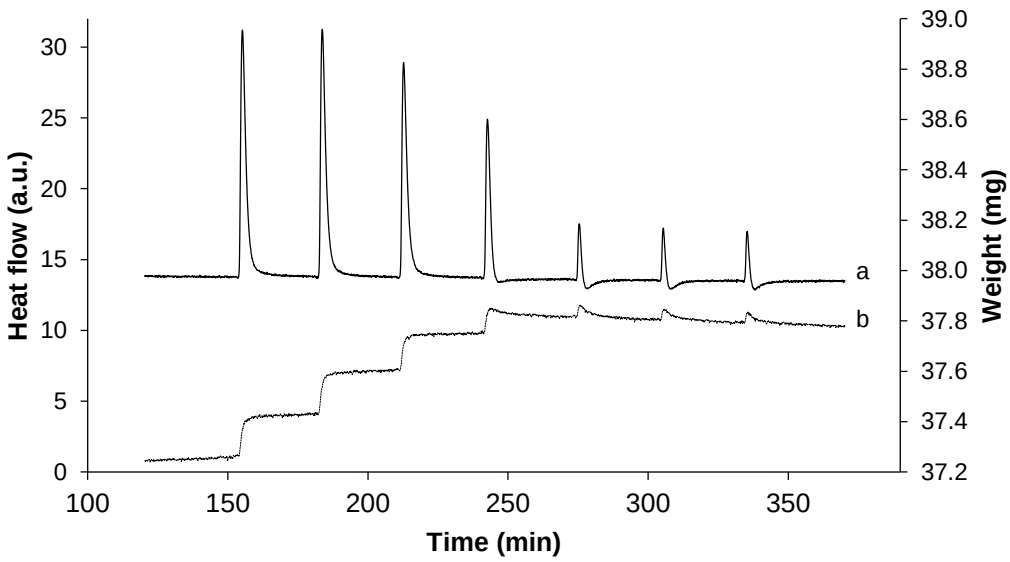

Figure 3.23. TGA–DSC for NH_3 adsorption on bulk HPW at 150 °C after pre-treatment at 300 °C: (a) heat flow, (b) weight.

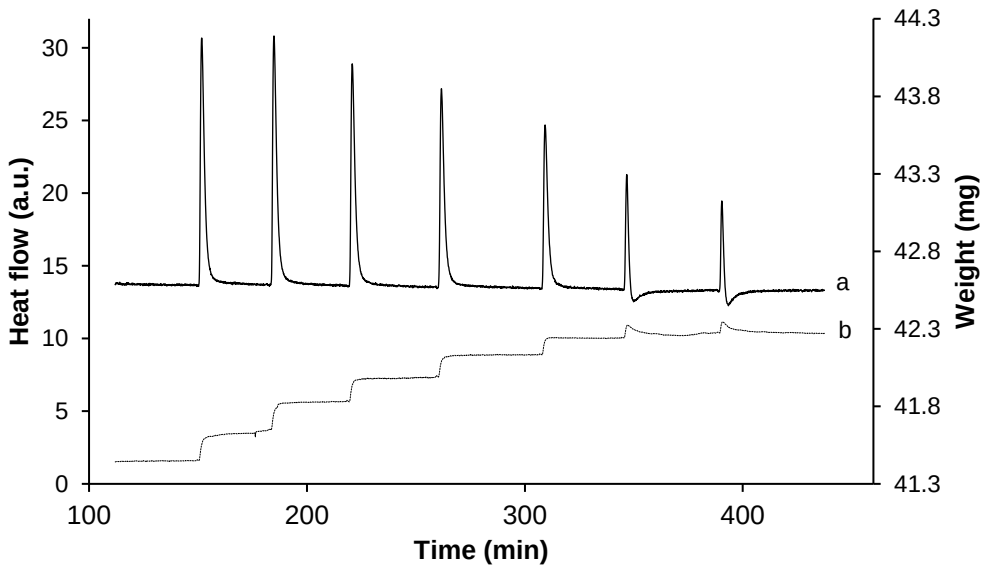

Figure 3.24. TGA–DSC for NH_3 adsorption on bulk HSiW at 150 °C after pre-treatment at 300 °C: (a) heat flow, (b) weight.

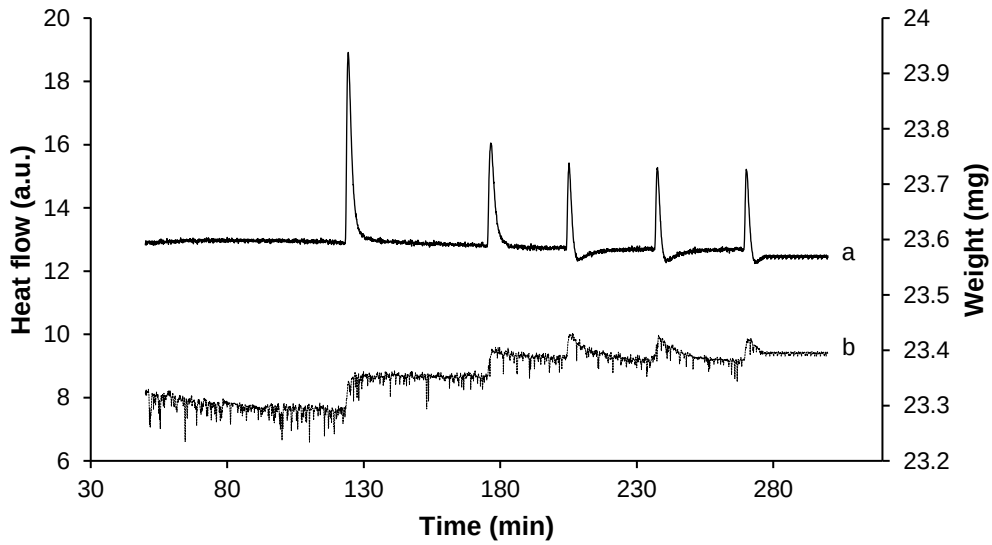

Figure 3.25. TGA–DSC for NH_3 adsorption on 26%HPW/SiO_2 at 150 °C after pre-treatment at 150 °C: (a) heat flow, (b) weight.

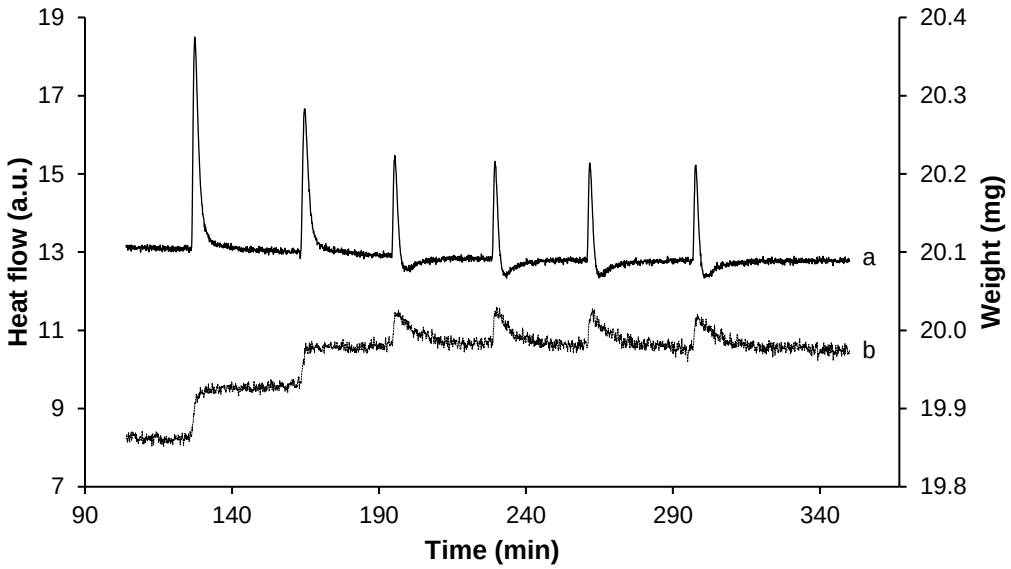

Figure 3.26. TGA–DSC for NH_3 adsorption on 27%HSiW/SiO_2 at 150 °C after pre-treatment at 150 °C: (a) heat flow, (b) weight.

In summary, our acidity characterisation demonstrates that the acid strength of silica-supported HPA catalysts increases monotonically with HPA loading all the way up to 100% loading. It might have been expected that at high loadings, ~70%, HPA-silica interaction would be minimal, and the protons would be as strong as in the bulk HPA. In fact, at 70% loading, the average HPA coverage of silica surface is only ~2 monolayers, hence the HPA-support interaction should still be significant to affect the acid strength. The question is how can the HPA-silica interaction affect the acid strength of HPA ensembles on the surface? Two mechanisms can be suggested. The first one is via dehydroxylation reaction (Eq. (3.1)) with the surface Si–OH groups. The second, and more important one, arises from the fact that protons generally tend to reside on the most basic sites. In bulk HPA, the surface protons are located on the bridging outer oxygen atoms in the Keggin anion [3,49,50]. In silica-supported HPA, the protons are expected to be located on the neighbouring oxygen atoms of the support, which are more basic than the outer oxygen atoms in the Keggin anion. Fast proton mobility in bulk HPAs is well documented; the proton mobility is accelerated by water present in HPA

[1,3–5,51]. The presence of water in HPA/SiO_2 catalysts should, therefore, enhance proton migration from the Keggin anion to the neighbouring oxygen atoms of silica. A previous ^1H MAS NMR study [17] has reported different proton locations in bulk and silica-supported HPW. Bulk HPW shows strong proton sites signal at 9.3 ppm. In the spectrum of HPW/SiO_2, only the silanol groups signal at 1.8 ppm can be seen up to 20%HPW loading. 37%HPW/SiO_2 shows a signal at 5.0 ppm from weaker proton sites. The signal of strong protons at 9.3 ppm appears only above 50%HPW loading. This demonstrates that proton sites in HPW/SiO_2 have a different chemical structure from the bulk HPW. It has been suggested that in HPW/SiO_2, the proton sites are located on silanol (A) and siloxane (B) groups of silica rather than on the outer oxygen atoms in the $PW_{12}O_{40}^{3-}$ polyanion [20,50].

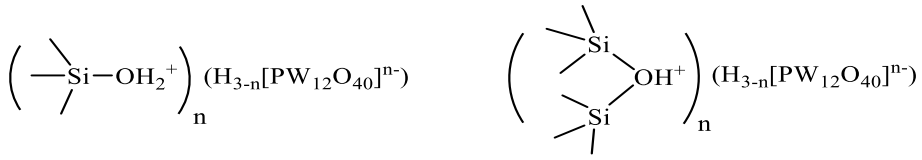

A **B**

Bulk and supported HPA catalysts exhibit different compensation effects in isopropanol dehydration, attributed to the different chemical structure of the surface proton sites in these catalysts [50].

3.5. Conclusions

Quantitative information about the acid properties of silica-supported HPA catalysts is of great significance for a host of reactions occurring in the presence of such catalysts regarding catalyst optimisation and understanding of mechanistic aspects. In this study, the acid properties of bulk and 5–70% SiO_2-supported Keggin-type HPAs (HPW, HSiW) have been systematically characterised at a gas-solid interface using NH_3 adsorption microcalorimetry, complemented by textural and structural catalyst characterisation using BET, XRD and FTIR. For these catalysts, a widely applied commercial Aerosil 300 (Degussa) has been used as the silica

support. From BET analysis, the HPA in these catalysts is mainly localized on the external surface and in macropores rather than within meso- and micropores of support. XRD shows that at similar HPA loadings, HSiW has a higher dispersion than HPW on the silica surface. As a result, HSiW/SiO_2 catalysts have a higher surface proton sites density than HPW/SiO_2; this is not only because HSiW has more protons per Keggin unit but also due to its higher dispersion on the silica surface in comparison to HPW. It is demonstrated that the acid strength of HPA/SiO_2 catalysts increases monotonically with HPA loading, with HPW being stronger than HSiW at any HPA loading.

Further, this data will be used for in-depth research into the mechanism of alcohol dehydration and related reactions in Chapter 4 and 5.

References

[1] T. Okuhara, N. Mizuno, M. Misono, Catalytic Chemistry of Heteropoly Compounds, in: D.D. Eley, Werner O. Haag, Bruce Gates (Eds.), Advances in Catalysis, Vol. 41, Academic Press, 1996: pp. 113–252.

[2] E.F. Kozhevnikova, I.V. Kozhevnikov, A calorimetric study of the acidity of bulk and silica-supported heteropoly acid $H_3PW_{12}O_{40}$, J. Catal. 224 (2004) 164–169.

[3] I.V. Kozhevnikov, Catalysis by heteropoly acids and multicomponent polyoxometalates in liquid-phase reactions, Chem. Rev. 98 (1998) 171–198.

[4] I.V. Kozhevnikov, Catalysts for Fine Chemical Synthesis Catalysis by Polyoxometalates, Vol. 2, John Wiley, Chichester, England, 2002.

[5] J.B. Moffat, Metal-Oxygen Clusters the Surface and Catalytic Properties of Heteropoly Oxometalates, Kluwer Academic Publishers, New York, 2002.

[6] Z. Wang, L. Liu, Mesoporous silica supported phosphotungstic acid catalyst for glycerol dehydration to acrolein, Catal. Today 376 (2021) 55–64.

[7] Y. Ren, B. Yue, M. Gu, H. He, Progress of the application of mesoporous silica-supported heteropolyacids in heterogeneous catalysis and preparation of nanostructured metal oxides, Materials 3 (2010) 764–785.

[8] M. Misono, A view on the future of mixed oxide catalysts The case of heteropolyacids (polyoxometalates) and perovskites, Catal. Today 100 (2005) 95–100.

[9] I.D. Dobson, Leaps of innovation, Green Chem. 5 (2003) G78–C81.

[10] https://www.ineos.com/news/ineos-group/ineos-oxide-expansion-of-saltend-site, (accessed 14 March 2022).

[11] https://www.bio.org/sites/default/files1500%20Langston.pdf, (accessed 14 March 2020).

[12] S.M. Kulikov, M.N. Timofeeva, I.V. Kozhevnikov, Adsorption of heteropoly acid

$H_4SiW_{12}O_{40}$ from solutions by porous supports, Russ. Chem. Bull. 38 (1989) 687–691.

[13] C. Peinado, D. Liuzzi, R.M. Ladera-Gallardo, M. Retuerto, M. Ojeda, M.A. Peña, S. Rojas, Effects of support and reaction pressure for the synthesis of dimethyl ether over heteropolyacid catalysts, Sci. Rep. 10 (2020) 8551.

[14] A.D. Newman, A.F. Lee, K. Wilson, N.A. Young, On the active site in $H_3PW_{12}O_{40}/SiO_2$ catalysts for fine chemical synthesis, Catal. Lett. 102 (2005) 45–50.

[15] A.D. Newman, D.R. Brown, P. Siril, A.F. Lee, K. Wilson, Structural studies of high dispersion $H_3PW_{12}O_{40}/SiO_2$ solid acid catalysts, Phys. Chem. Chem. Phys. 8 (2006) 2893–2902.

[16] J. Schnee, F. Devred, E.M. Gaigneaux, A. Vimont, Assessing the dispersion of supported $H_3PW_{12}O_{40}$ catalysts: No longer a hurdle thanks to in situ IR upon pyridine adsorption, Appl. Catal. A: Gen. 578 (2019) 116–121.

[17] V.M. Mastikhin, S.M. Kulikov, A.V. Nosov, I.V. Kozhevnikov, I.L. Mudrakovsky, M.N. Timofeeva, ^1H and ^{31}P MAS NMR studies of solid heteropolyacids and $H_3PW_{12}O_{40}$ supported on SiO_2, J. Mol. Catal. 60 (1990) 65–70.

[18] K.M. Rao, R. Gobetto, A. Iannibello, A. Zecchina, Solid state NMR and IR studies of phosphomolybdenum and phosphotungsten heteropoly acids supported on SiO_2, γ-Al_2O_3, and SiO_2-Al_2O_3, J. Catal. 119 (1989) 512–516.

[19] F. Lefebvre, ^{31}P MAS NMR Study of $H_3PW_{12}O_{40}$ supported on silica: Formation of ($\equiv SiOH_2^+$) ($H_2PW_2O_{40}^-$), J. Chem. Soc. Chem. Commun. (1992) 756–757.

[20] I.V. Kozhevnikov, K.R. Kloetstra, A. Sinnema, H.W. Zandbergen, H.V. Bekkum, Study of catalysts comprising heteropoly acid $H_3PW_{12}O_{40}$ supported on MCM-41 molecular sieve and amorphous silica, J. Mol. Catal. A: Chem. 114 (1996) 287–298.

[21] Ghanbari-Siahkali, A. Philippou, J. Dwyer, M.W. Anderson, The acidity and catalytic activity of heteropoly acid on MCM-41 investigated by MAS NMR, FTIR and catalytic tests, Appl. Catal. A: Gen.192 (2000) 57–69.

[22] A.M. Alsalme, P.V. Wiper, Y.Z. Khimyak, E.F. Kozhevnikova, I.V. Kozhevnikov, Solid acid catalysts based on $H_3PW_{12}O_{40}$ heteropoly acid: Acid and catalytic properties at a gas-solid interface, J. Catal. 276 (2010) 181–189.

[23] H. Hattori, Y. Ono, Solid Acid Catalysis from Fundamentals to Applications, Pan Stanford Publishing, Singapore, 2015.

[24] F. Lefebvre, F.X. Liu-Cai, A. Auroux, Microcalorimetric study of the acidity of tungstic heteropolyanions, J. Mater. Chem. 4 (1994) 125–131.

[25] S. Shikata, S.I. Nakata, T. Okuhara, M. Misono, Catalysis by heteropoly compounds. 32. Synthesis of methyl tert-butyl ether catalysed by heteropolyacids supported on silica, J. Catal. 166 (1997) 263–271.

[26] E. Grinenval, X. Rozanska, A. Baudouin, E. Berrier, F. Delbecq, P. Sautet, J-M. Basset, F. Lefebvre, Controlled interactions between anhydrous Keggin-type heteropolyacids and silica support: Preparation and characterization of well-defined silica-supported polyoxometalate species, J. Phys. Chem. C. 114 (2010) 19024–19034.

[27] G.I. Kapustin, T.R. Brueva, A.L. Klyachko, M.N. Timofeeva, S.M. Kulikov, I.V. Kozhevnikov, A study of the acidity of heteropoly acids, Kinet. Catal. 31 (1990) 896–898.

[28] Micek-Ilnicka, E. Bielańska, L. Lityńska-Dobrzyńska, A. Bielański, Carbon nanotubes, silica and titania supported heteropolyacid $H_3PW_{12}O_{40}$ as the catalyst for ethanol conversion, Appl. Catal. A: Gen. 421–422 (2012) 91–98.

[29] E.I. García-López, G. Marcì, I. Krivtsov, J.C. Espina, L.F. Liotta, A. Serrano, Local structure of supported Keggin and Wells-Dawson heteropolyacids and its influence on the catalytic activity, J. Phys. Chem. C 123 (2019) 19513–19527.

[30] B.B. Bardin, R.J. Davis, Effect of water on silica-supported phosphotungstic acid catalysts for 1-butene double bond shift and alkane skeletal isomerization, Appl. Catal. A: Gen. 200 (2000) 219–231.

[31] J. Zhang, M. Kanno, Y. Wang, H. Nishii, Y.K. Miura, Y. Kamiya, Changes in surface acidity of silica-supported dodecatungstosilicic acid in relation to the loading amount, J. Phys. Chem. C 115 (2011) 14762–14769.

[32] L.C. Jozefowicz, H.G. Karge, E. Vasilyeva, J.B. Moffat, A microcalorimetric investigation of heteropolyacids, Microporous Mater. 1 (1993) 313–322.

[33] Z. Buniazet, C. Lorentz, A. Cabiac, S. Maury, S. Loridant, Supported oxides catalysts for the dehydration of isobutanol into butenes: Relationships between acidic and catalytic properties, Mol. Catal. 451 (2018) 143–152.

[34] M. Szekeres, J. Tóth, I. Dékány, Specific surface area of stoeber silica determined by various experimental methods, Langmuir 18 (2002) 2678–2685.

[35] P. Unnikrishnan, D. Srinivas, Chapter 3-Heterogeneous catalysis, in: S.S. Joshi, V.V. Ranade (Eds.), Industrial Catalytic Processes for Fine and Specialty Chemicals, Elsevier, Cambridge, 2016: pp. 41–111.

[36] T. Kella, A.A. Vennathan, S. Dutta, S.S. Mal, D. Shee, Selective dehydration of 1-butanol to butenes over silica supported heteropolyacid catalysts: Mechanistic aspect, Mol. Catal. 516 (2021) 111975.

[37] P. Gupta, S. Paul, Solid acids: Green alternatives for acid catalysis, Catal. Today 236 (2014) 153–170.

[38] K. Smith, Solid Supports and Catalysts in Organic Synthesis, Ellis Horwood, London,1992.

[39] G. Leofanti, M. Padovan, G. Tozzola, B. Venturelli, Surface area and pore texture of catalysts, Catal. Today 41 (1998) 207–219.

[40] G. Attard, C. Barnes, Surfaces, Oxford University Press Inc., New York, 1998.

[41] D.B. Taylor, J.B. McMonagle, J.B. Moffat, Cation effects on the surface and bulk structure of the salts of 12-tungstosilicic acid, J. Colloid Interface Sci.108 (1985) 1.

[42] Y. Yamamoto, S. Hatanaka, K. Tsuji, K. Tsuneyama, R. Ohnishi, H. Imai, Y. Kamiya, T. Okuhara, Direct addition of acetic acid to ethylene to form ethyl acetate in the presence of $H_4SiW_{12}O_{40}/SiO_2$, Appl. Catal. A: Gen. 344 (2008) 55–60.

[43] F.J. Berry, G.R. Derrick, M. Mortimer, Identification and characterisation of stable phases of silicotungstic acid, $H_4SiW_{12}O_{40}{\cdot}nH_2O$, Polyhedron 68 (2014) 17–22.

[44] R.M. Ladera, J.L.G. Fierro, M. Ojeda, S. Rojas, TiO_2-supported heteropoly acids for low-temperature synthesis of dimethyl ether from methanol, J. Catal. 312 (2014) 195–203.

[45] C. Rocchiccioli-Deltcheff, M. Fournier, R. Franck, R. Thouvenot, Vibrational investigations of polyoxometalates. 2 Evidence for anion-Anion interactions in Molybdenum (VI) and Tungsten (VI) compounds related to the Keggin structure, Inorg. Chem. 22 (1983) 207–216.

[46] Micek-Ilnicka, The role of water in the catalysis on solid heteropolyacids, J. Mol. Catal. A: Chem. 308 (2009) 1–14.

[47] S. Siddiqui, M.U. Khan, Z.N. Siddiqui, Synthesis, characterization, and application of silica-supported copper-doped phosphotungstic acid in claisen-schmidt condensation, ACS Sustain. Chem. Eng. 5 (2017) 7932–7941.

[48] W. Alharbi, E. Brown, E.F. Kozhevnikova, I.V. Kozhevnikov, Dehydration of ethanol over heteropoly acid catalysts in the gas phase, J. Catal. 319 (2014) 174–181.

[49] B.B. Bardin, S. V. Bordawekar, M. Neurock, R.J. Davis, Acidity of Keggin-type heteropolycompounds evaluated by catalytic probe reactions, sorption

microcalorimetry, and density functional quantum chemical calculations, J. Phys. Chem. B102 (1998) 10817–10825.

[50] G.C. Bond, S.J. Frodsham, P. Jubb, E.F. Kozhevnikova, I.V. Kozhevnikov, Compensation effect in isopropanol dehydration over heteropoly acid catalysts at a gas-solid interface, J. Catal. 293 (2012) 158–164.

[51] D.I. Kolokolov, M.S. Kazantsev, M. V. Luzgin, H. Jobic, A.G. Stepanov, Direct ^{2}H NMR observation of the proton mobility of the acidic sites of anhydrous 12-tungstophosphoric acid, ChemPhysChem 14 (2013) 1783–1786.

Chapter 4: Dehydration of methanol and ethanol catalysed by silica-supported heteropoly acids in the gas phase：Surface-type versus bulk-type catalysis mechanism

Chapter 4 : Dehydration of methanol and ethanol catalysed by silica supported heteropoly acids in the gas phase: Surface-type versus bulk-type catalysis mechanism

4.1. Introduction

Dehydration of MeOH to DME and EtOH to DEE and ethene (Eqs. (4.1)–(4.3)) is of significant interest in relation to sustainable development [1–3]. DME is a multimarket product, which has attracted interest as a supplement to LPG and a clean diesel alternative [4,5]. Ethene is considered as one of the essential precursors in synthesising a variety of polymers and chemicals [6], and DEE is an aprotic solvent, anesthetic and a green fuel alternative [7].

$$2CH_3OH \rightarrow CH_3OCH_3 + H_2O \quad \textbf{(4.1)}$$

$$CH_3CH_2OH \rightarrow CH_2{=}CH_2 + H_2O \quad \textbf{(4.2)}$$

$$2CH_3CH_2OH \rightarrow (CH_3CH_2)_2O + H_2O \quad \textbf{(4.3)}$$

HPAs are one of the most extensively investigated catalysts in these reactions [8-21]. Bulk HPAs have a low surface area (1–10 m^2g^{-1}), hence a low density of surface acid sites [8,22–25]. For this reason, supported HPA catalysts are mainly used in heterogeneous acid catalysis. It has been recently demonstrated that SiO_2 supported heteropoly acids exhibit higher catalytic activities in EtOH and MeOH dehydration reactions [9,12,15].

Kinetics and mechanism of MeOH and EtOH dehydration in the gas phase over HPA catalysts has been the subject of several studies ([9,12,15–18] and references therein). Rigorous mechanistic investigation of MeOH and EtOH dehydration over a series of highly dispersed silica-supported HPAs (5 wt% HPA loading), including reaction kinetics and DFT analysis of elementary steps, has been published [15–17]. Typically, at 100–140 °C, these reactions follow

the Langmuir-type rate equation and are zero-order in alcohol at a not too low alcohol partial pressure due to saturation of surface acid sites with alcohol molecules.

In contrast to the finely dispersed supported HPAs, bulk and heavily loaded supported HPAs could catalyse the dehydration of light C1–C4 alcohols via a bulk-type (pseudo-homogeneous) mechanism, with all HPA protons, bulk and surface, being catalytically active sites [8]. This is backed by the ability of bulk HPAs to absorb alcohol molecules in large quantities into interstitial space [10,26–28]. It has been argued, however, that the bulk-type process would be diffusion controlled [25,29], hence inconsistent with high activation energies (E_a) of alcohol dehydration. The reported E_a values for MeOH dehydration over bulk HPW and HSiW are 82 and 85 kJ mol^{-1} [12]; for i-PrOH dehydration over bulk HPW, E_a = 90 kJ mol^{-1} [30]. Linear Brønsted-type correlations between the turnover rates, ln(TOF), and catalyst acid strengths, represented by the initial enthalpies of NH_3 adsorption, have been established for MeOH, EtOH and i-PrOH dehydration over HPA catalysts, which hold for both bulk and supported HPAs [9,12,30]. For MeOH-to-DME dehydration, this correlation holds for bulk and supported HPAs (15% loading) as well as for HZSM-5 zeolite catalysts, which suggests that the reaction with all these catalysts occurs via the mechanism of surface acid catalysis [12].

On the other hand, it has been reported recently that the bulk-type mechanism may be realized for the dehydration of MeOH over bulk HPW if the HPA is thermally pre-treated to remove crystallisation water from the interstitial space thus making it available for absorption of MeOH [10,29].

The aim of this work is to provide new mechanistic insights concerning the role of the bulk-type and surface-type HPA catalysis in MeOH and EtOH dehydration over silica-supported HPA catalysts, HPW/SiO_2 and HSiW/SiO_2, prepared by HPA impregnation from water and MeOH. We looked at the effect of HPA loading and acid strength on the dehydration

reactions at conditions relevant to practice (5–100% HPA loading). The acid properties of these catalysts were systematically characterised at a gas-solid interface using ammonia adsorption calorimetry (NH_3-MC and TGA–DSC) complemented by BET, XRD and IR spectroscopic characterisation of catalyst texture and HPA structural integrity (Chapter 3). The stability of HPA/SiO_2 catalysts during alcohol dehydration was also examined. The activity of HPA/SiO_2 catalysts was compared with the activity of zeolite HZSM-5.

4.2. Activity testing and reproducibility studies

Silica-supported HPA catalysts, 5–70%HPA/SiO_2, were prepared by wet impregnation of silica with aqueous and MeOH HPA solutions and dried at 150 °C/10^{-3} kPa for 1.5 h as described in Chapter 2. Previously, it was found that such catalyst pre-treatment provided the best performance in alcohol dehydration [9,12,30] and in other low-temperature reactions of polar molecules [23] in terms of both activity and catalyst stability. Moreover, the catalysts that had been dried at higher temperatures (250 °C/10^{-3} kPa/1.5 h) showed a significant decline in activity before reaching a steady state, which may be attributable to the adsorption of water formed during the alcohol dehydration. The acid properties of these catalysts, together with their textures, are given in Tables 3.1 and 3.2 in Chapter 3. The structural integrity of HPA on the silica surface was confirmed by DRIFT spectroscopy and XRD (Chapter 3). The dehydration reactions were investigated through use of the fixed-bed microreactor with on-line GC analysis. The reactor set-up is presented in Figure 2.16 (Chapter 2).

Typically, gas-phase dehydration of MeOH and EtOH was examined over SiO_2-supported HPA catalysts at 120 °C for 4 h time on stream. The reproducibility of these results was studied by repeating the reaction 2–3 times under the same conditions (reaction temperature and alcohol partial pressure). In some cases, catalyst preparation was also repeated in order to examine batch-to-batch reproducibility. The representative results are given in Table

4.1. These results show that the reproducibility of conversion and reaction selectivity in the repeated runs as well as the batch-to-batch reproducibility were generally good.

Table 4.1. Reproducibility of results for MeOH dehydration over HPA catalysts.[a]

HPA catalyst	Conversion (%)	DME selectivity (mol %)
26%HPW/SiO_2	28.9	100
26%HPW/SiO_2	27.6	100
24%HPW/SiO_2	31.8	100
24%HPW/SiO_2	30.3	100
24%HPW/SiO_2	27.6	100
13%HSiW/SiO_2(m)	23.8	100
13%HSiW/SiO_2(m)	22.4	100
27%HSiW/SiO_2(m)	33.0	100
27%HSiW/SiO_2(m)	29.5	100

[a] HPA/SiO_2 catalysts prepared by impregnation from water and HPA/SiO_2(m) from MeOH. Reaction conditions: 0.20 g catalyst, 120 °C, 3.83 kPa MeOH partial pressure, 20 mL min^{-1} N_2 flow rate, 4 h time on stream.

4.3. Stability of catalyst performance

The stability of HPA/SiO_2 catalysts were investigated during MeOH dehydration at different alcohol partial pressures at 120 °C. It was found that MeOH conversion decreased as the MeOH partial pressure was increased from 3.38 to 21.8 kPa. At the same time, catalyst stability improved, with practically no catalyst deactivation at 16.7 and 21.8 kPa MeOH partial pressures for 24 h on stream (Figure 4.1). The amount of coke that was formed in MeOH dehydration was also found to decrease with increasing MeOH partial pressure (Table 4.2).

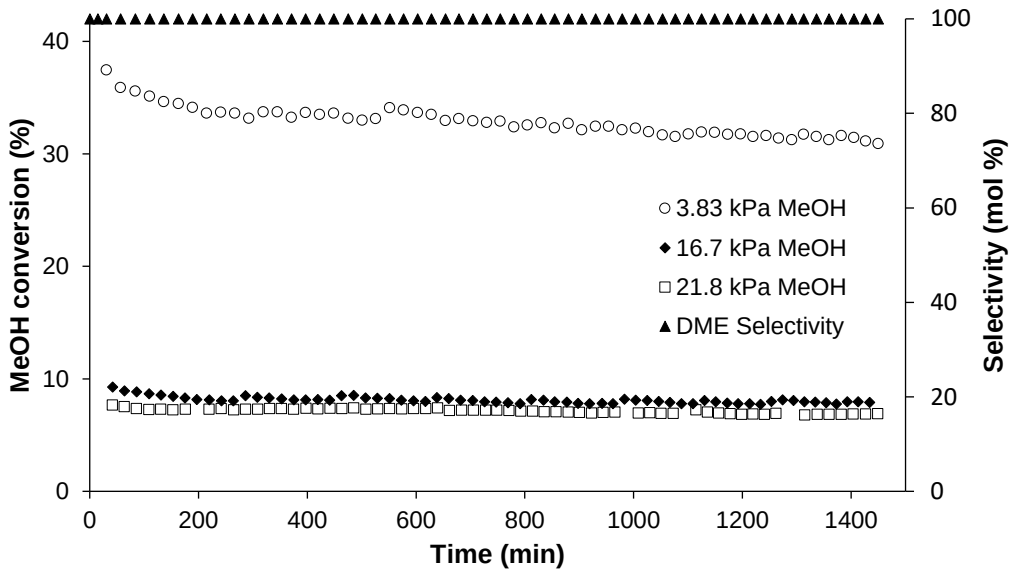

Figure 4.1. Time course of MeOH dehydration to DME over 26%HPW/SiO_2 (0.20 g catalyst, 20 ml min^{-1} N_2 flow rate, 120 °C and 3.83–21.8 kPa MeOH partial pressure, contact time *W/F* = 105–18.4 g h mol^{-1}).

Table 4.2. C and H combustion analysis of spent catalysts after use in MeOH dehydration at different MeOH pressures.

Spent catalyst	MeOH pressure (kPa)	C (wt%)	H (wt%)
26%HPW/SiO_2	3.83	0.21	0.40
26%HPW/SiO_2	16.7	0.10	0.50
26%HPW/SiO_2	21.8	0.10	0.50
27%HSiW/SiO_2	3.83	0.35	0.43
27%HSiW/SiO_2	16.7	-	0.50
27%HSiW/SiO_2	21.8	0.10	0.48

Reaction conditions: 0.20 g catalyst, 120 °C, 20 mL min^{-1} N_2 flow rate and 24 h time on stream.

A similar stable performance was also detected in EtOH dehydration over 27%HSiW/SiO_2 at a higher EtOH partial pressure of 13.6 kPa at 160 °C (Figure 4.2). This can be explained by the inhibition of catalyst coking at high alcohol pressures. From combustion analysis (CHN) of the spent 27%HSiW/SiO_2 catalyst, it was found that less than 0.2% coke was formed in EtOH dehydration during 24 h on stream.

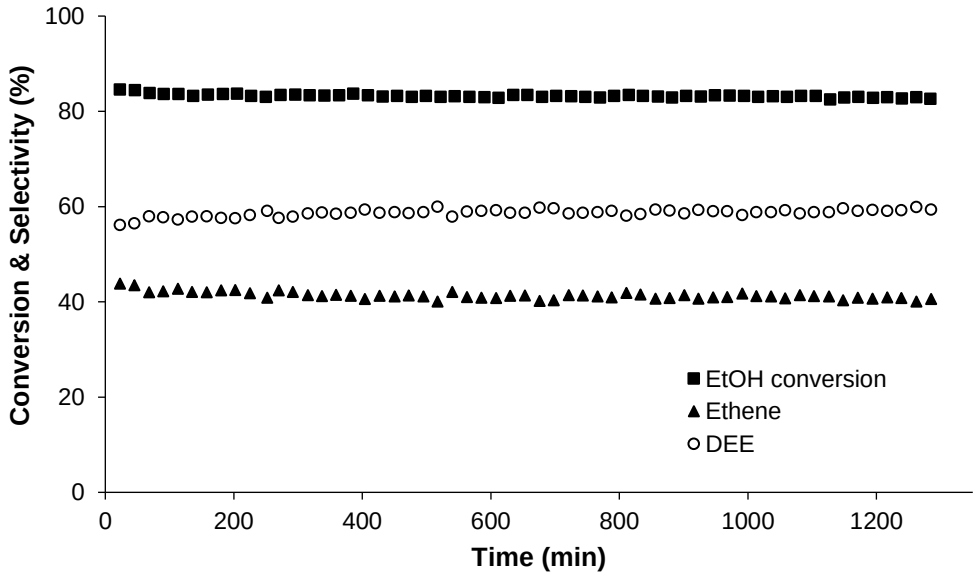

Figure 4.2. Time course of EtOH dehydration to DEE and ethene over 27%HSiW/SiO_2 (0.20 g catalyst, 20 ml min^{-1} N_2 flow rate, 160 °C, 13.6 kPa EtOH partial pressure, contact time *W/F* = 29.4 g h mol^{-1}).

Figure 4.3 shows a long-term test of MeOH dehydration over 27%HSiW/SiO_2 catalysts at 140 °C at a high MeOH partial pressure of 28 kPa. The catalyst exhibited excellent stability without any deactivation during 160 h on stream.

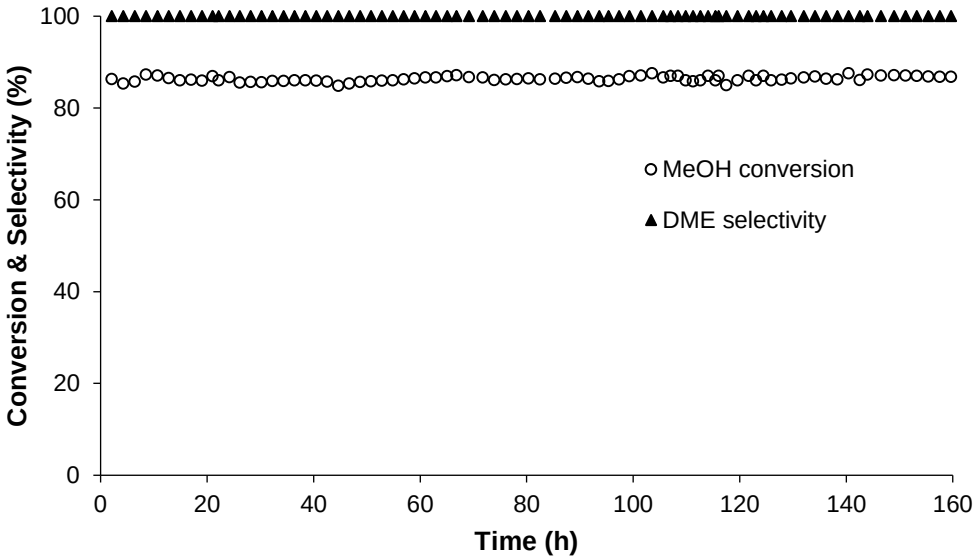

Figure 4.3. Time course of MeOH dehydration to DME over 27%HSiW/SiO_2 (0.40 g catalyst, 10 ml min^{-1} N_2 flow rate, 140 °C and 28.1 kPa MeOH pressure, contact time *W/F* = 57.0 g h mol^{-1})**.**

We also examined the effect of water on the stability of HPA/SiO_2 catalysts in MeOH and EtOH dehydration. The dehydration of MeOH was carried out over 27%HSiW/SiO_2 at 120 °C with the use of a MeOH-H_2O (0.18:0.82 mol) solution for feeding MeOH and water into the reactor by bubbling a N_2 flow through at 30 ºC. This provided a gas mixture containing MeOH (3.84 kPa partial pressure) and water (3.50 kPa H_2O partial pressure) (calculated from Raoult's law [31]) for the dehydration reaction. The results were compared with those obtained with pure MeOH (Figure 4.4). As expected, the MeOH conversion in the MeOH-H_2O system decreased (by 18%) compared with that of pure MeOH. At the same time, catalyst stability significantly improved, with practically no deactivation observed during 24 h reaction time. Less than 0.1% of coke was detected in the catalyst after the reaction. It should be noted that the presence of H_2O in the system did not influence the selectivity of DME.

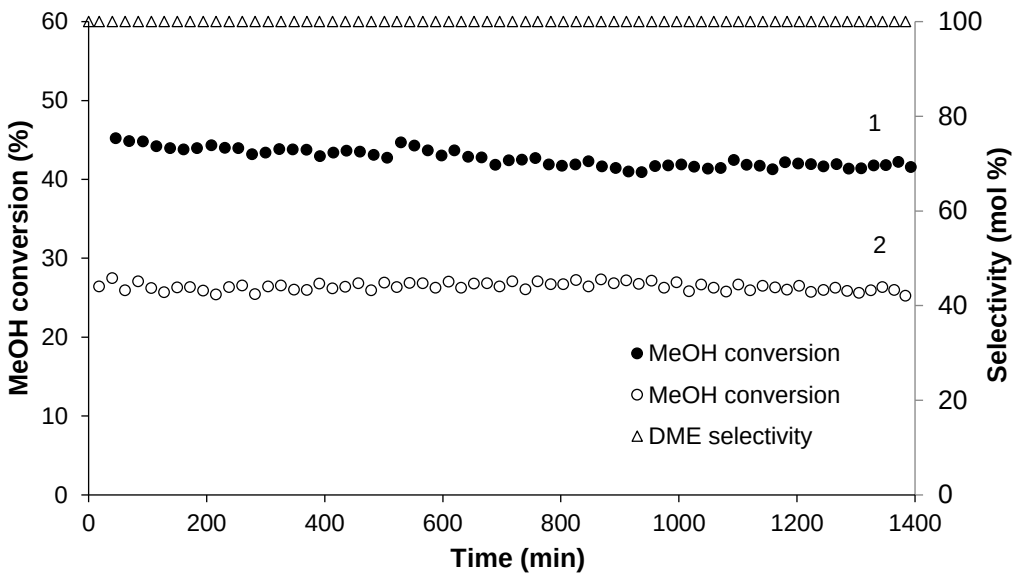

Figure 4.4. Effect of water on MeOH dehydration over 27%HSiW/SiO_2 (0.20 g catalyst, 20 ml min^{-1} N_2 flow rate, 120 °C): (1) pure MeOH (3.83 kPa) and (2) MeOH (3.84 kPa) + H_2O (3.50 kPa); DME selectivity was 100% in both cases.

Addition of water also improved the stability of the HPA/SiO_2 catalysts in the dehydration of EtOH to ethene and DEE. In this case, EtOH-H_2O (2.08:0.25 mol) azeotrope was used to feed EtOH and water instead of pure EtOH. Comparison of the dehydration of EtOH over a 26%HSiW/SiO_2 catalyst with and without addition of H_2O at 140 °C and 13.6 kPa EtOH partial pressure is presented in Figure 4.5. In both cases, a good catalyst stability was observed, yet it was slightly better in the presence of water. As expected, in the presence of water, the conversion of EtOH (48%) was lower compared with that for pure EtOH (64%). Also as expected, the DEE selectivity increased at the expense of ethene. This may be attributed to the competitive adsorption of H_2O and EtOH on active sites [21,32,33]. A very stable performance was observed in the long-term stability test for 24 h on stream when the EtOH azeotrope was used over a 26%HPW/SiO_2 catalyst at 13.6 kPa EtOH partial pressure and 160 °C (Figure 4.6). Less than 0.1% coke was found in the catalyst after this reaction. These results indicate that H_2O inhibits catalyst coking and thus improves catalyst stability [34,35].

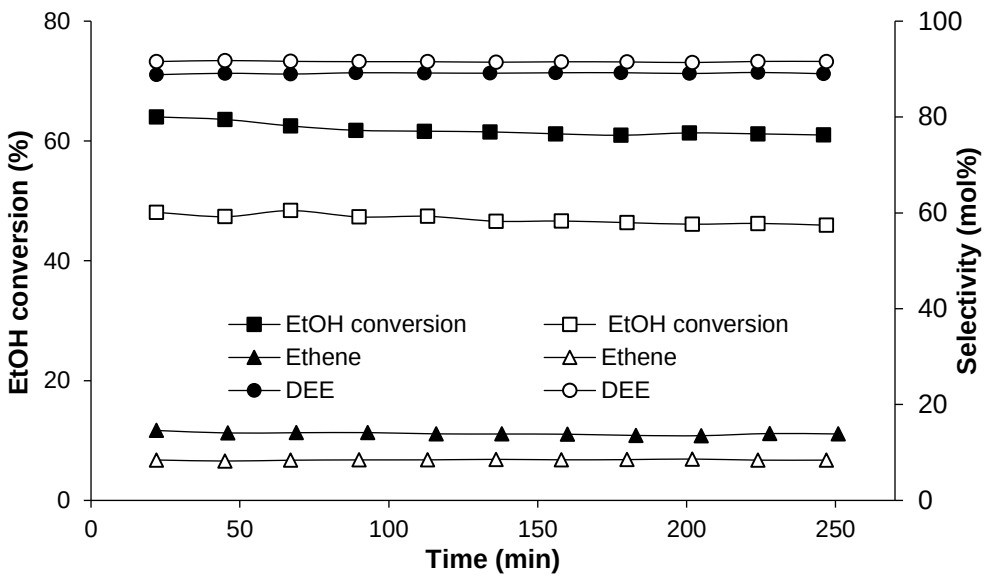

Figure 4.5. Effect of water on the conversion of EtOH to DEE and ethene over 26%HSiW/SiO_2 (0.20 g catalyst, 20 ml min^{-1} N_2 flow rate, 140 °C, 13.6 kPa EtOH partial pressure, contact time *W/F* = 29.4 g h mol^{-1}): pure EtOH (solid markers) and EtOH-H_2O azeotrope (open markers).

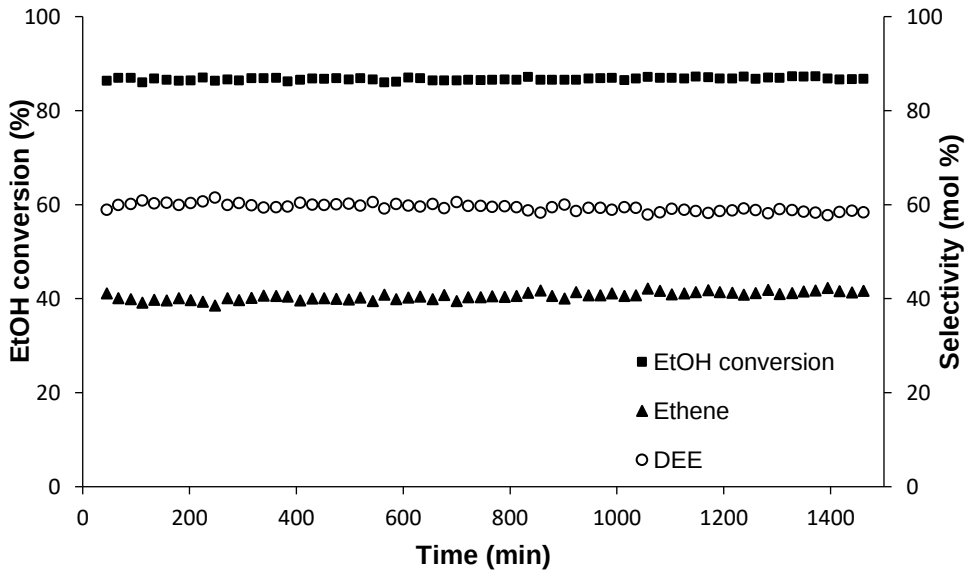

Figure 4.6. Time course of EtOH dehydration (EtOH-H_2O azeotrope) over 26%HPW/SiO_2 (0.20 g catalyst, 20 ml min^{-1} N_2 flow rate, 160 °C, 13.6 kPa EtOH pressure, contact time *W/F* = 29.4 g h mol^{-1}).

4.4. Effect of HPA loading in dehydration of methanol and ethanol over HPA/SiO_2 catalysts

Here we examined the effect of HPA loading and acid strength on alcohol conversion and product selectivity in the dehydration of MeOH to DME and EtOH to DEE and ethene (Eqs. (4.1)–(4.3)) at the gas-solid interface over HPA/SiO_2 catalysts over a wide range of HPA loadings (5–100%), seeking to provide new mechanistic insights regarding the role of bulk-type and surface-type HPA catalysis in these reactions. The dehydration reactions were mainly carried out 120 °C at low to medium alcohol conversions to keep the reactions under kinetic control. Typically, the reaction time was 4 h, during which practically no catalyst deactivation was detected (see reaction time courses in Figures 4.7–4.9). HPW and HSiW retained the Keggin structure after reaction, as shown by DRIFT spectroscopy and XRD patterns of spent HPA/SiO_2 catalysts (Table 7.1 and Figures 7.10–7.15 in Appendix).

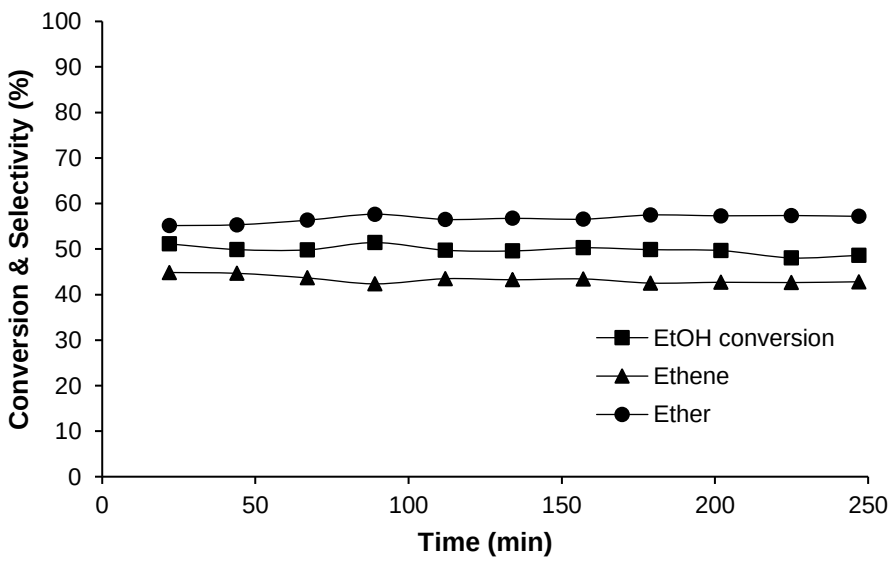

Figure 4.7. Time course for dehydration of EtOH over 19%HPW/SiO_2 (0.20 g catalyst, 120 °C, 1.48 kPa EtOH partial pressure, 20 mL min^{-1} N_2 flow rate, contact time *W/F* = 271 g h mol^{-1}, 4 h time on stream).

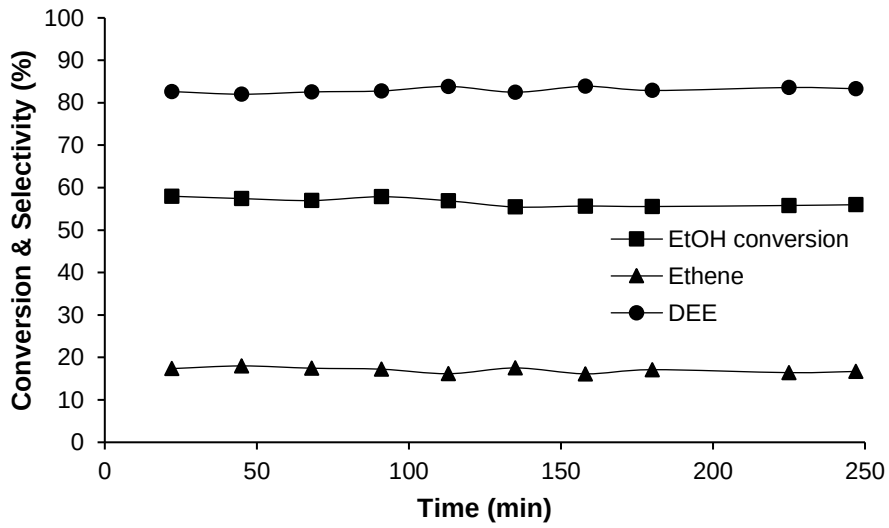

Figure 4.8. Time course for dehydration of EtOH over 17%HSiW/SiO_2 (0.20 g catalyst, 120 °C, 1.48 kPa EtOH partial pressure, 20 mL min^{-1} N_2 flow rate, contact time *W/F* = 271 g h mol^{-1}, 4 h time on stream).

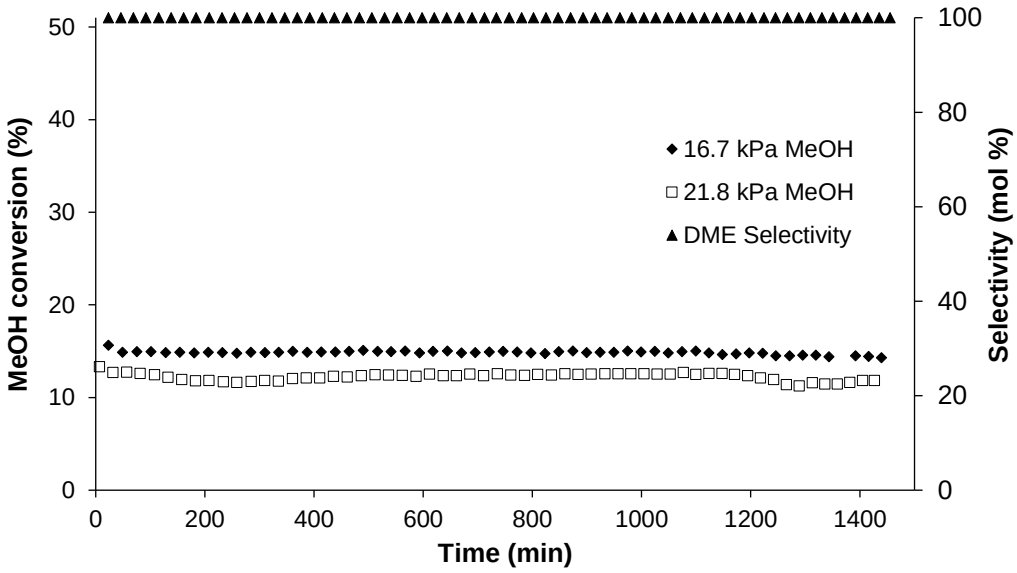

Figure 4.9. Effect of MeOH partial pressure (16.7–21.8 kPa) on conversion of MeOH to DME over 26%HSiW/SiO_2 (0.20 g catalyst, 20 ml min^{-1} N_2 flow rate, 120 °C).

Representative results on the effect of HPA loading on steady-state alcohol conversion and product selectivity at a constant contact time *W/F* are shown in Figures 4.10–4.14. As can be seen from Figure 4.10, MeOH conversion for both HPW and HSiW catalysts passes through a maximum at an HPA loading between 25 and 70%. This shows that catalyst activity scales with the number of surface proton sites in HPA/SiO_2 catalysts, which follows a similar trend passing a maximum at 40–50% HPA loading [36]. Notably, HSiW catalysts have a slightly higher activity than HPW catalysts in terms of the conversion per gram of catalyst despite the opposite order of their acid strength. For both catalysts, the selectivity to DME was 100%, no other products were observed. Similar results were obtained for HPA/SiO_2(m) catalysts prepared from MeOH (Figure 4.11).

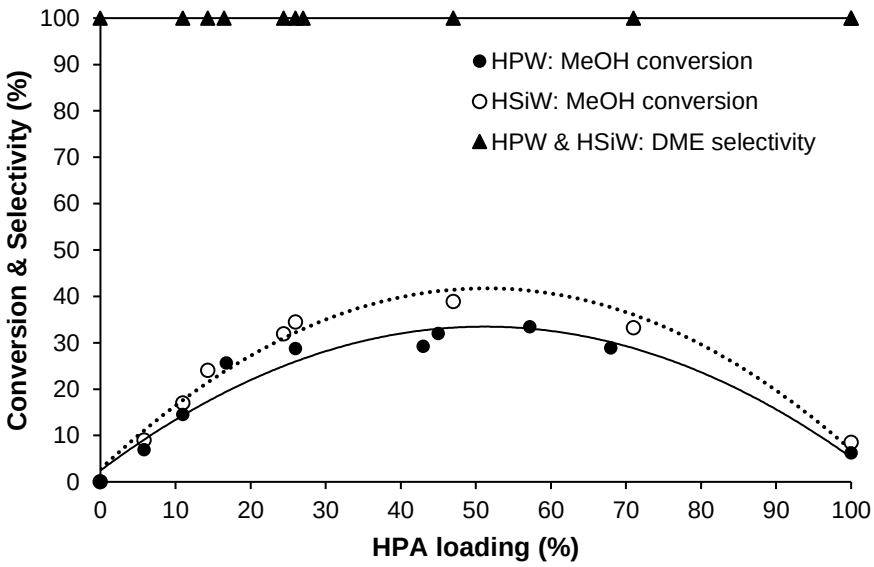

Figure 4.10. Effect of HPA loading on MeOH-to-DME conversion over silica-supported HPA (0.20 g catalyst, 120 °C, 3.83 kPa MeOH pressure, 20 mL min^{-1} N_2 flow rate, contact time *W/F* = 105 g h mol^{-1}, 4 h time on stream; 100% DME selectivity in all cases).

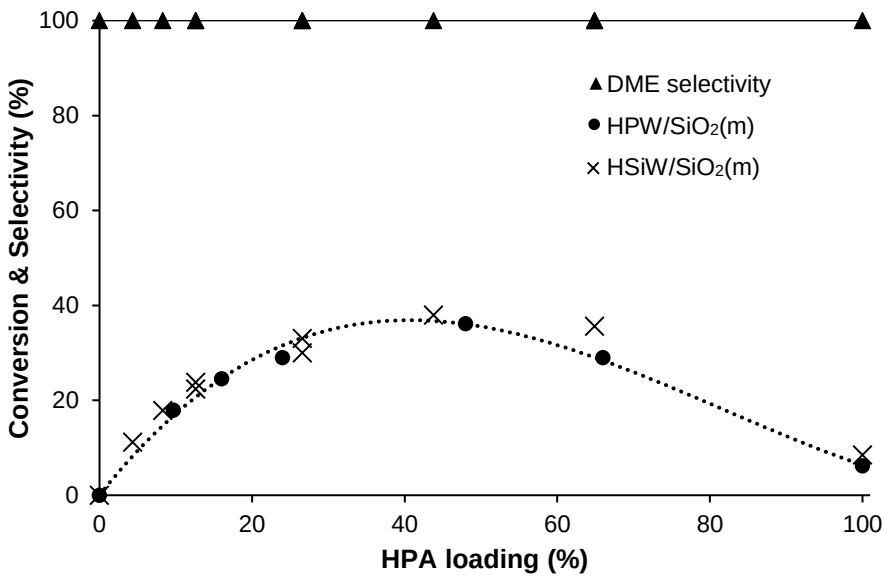

Figure 4.11. Effect of HPA loading on MeOH-to-DME conversion over HPA/SiO_2(m) prepared from MeOH (0.20 g catalyst, 120 °C, 3.83 kPa MeOH pressure, 20 mL min^{-1} N_2 flow rate, contact time *W/F* = 105 g h mol^{-1}, 4 h time on stream; 100% DME selectivity in all cases).

The higher activity of HSiW compared to HPW per catalyst weight can be explained by the larger density of accessible proton sites in HSiW catalysts in comparison to HPW ones. This is because HSiW has the larger number of protons per Keggin unit and a higher dispersion on the silica surface compared to HPW (see Chapter 3). The turnover reaction rate for HPW catalysts, however, was higher than for HSiW catalysts in agreement with their acid strength (see below).

HPW/SiO_2(m) catalysts prepared from MeOH exhibited similar activities to HPW/SiO_2 prepared from water (Figure 4.12) in agreement with their similar acid strengths (Figure 3.22, Chapter 3); the same was observed for HSiW/SiO_2(m) and HSiW/SiO_2 catalysts (Figure 4.13).

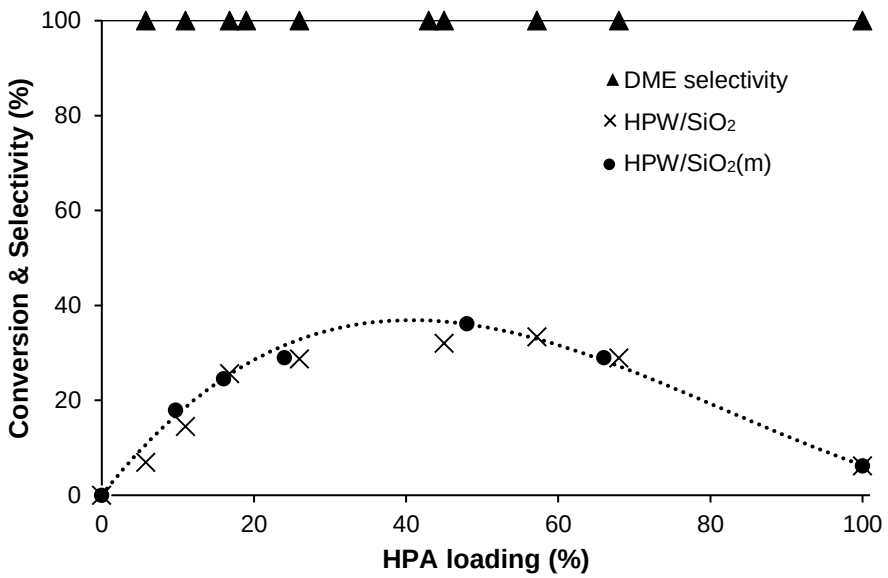

Figure 4.12. Effect of HPA loading on MeOH-to-DME conversion over HPW/SiO_2 prepared from water and HPW/SiO_2(m) prepared from MeOH (0.20 g catalyst, 120 °C, 3.83 kPa MeOH pressure, 20 mL min^{-1} N_2 flow rate, contact time *W/F* = 105 g h mol^{-1}, 4 h time on stream; 100% DME selectivity in all cases).

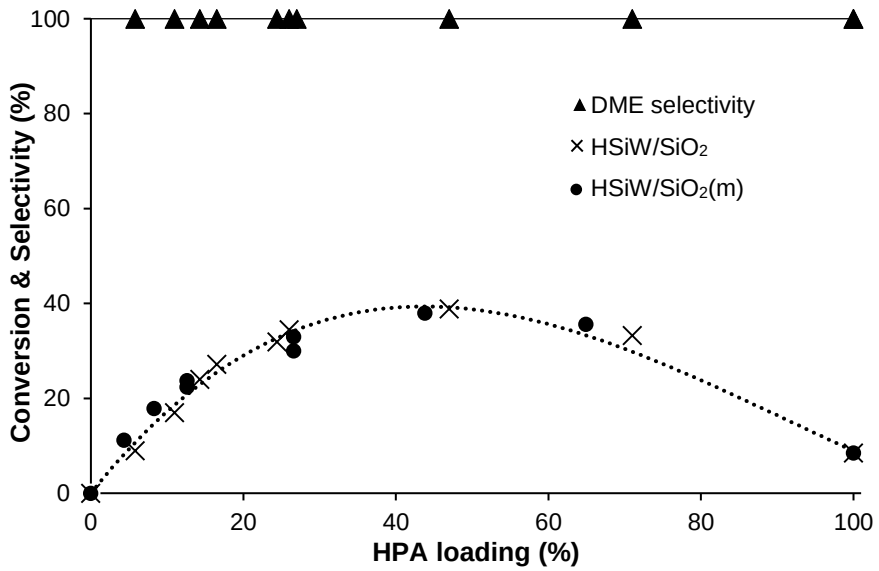

Figure 4.13. Effect of HPA loading on MeOH-to-DME conversion over HSiW/SiO_2 prepared from water and HSiW/SiO_2(m) prepared from MeOH (0.20 g catalyst, 120 °C, 3.83 kPa MeOH pressure, 20 mL min^{-1} N_2 flow rate, contact time *W/F* = 105 g h mol^{-1}, 4 h time on stream; 100% DME selectivity in all cases).

EtOH dehydration showed similar activity trends to MeOH dehydration (Figure 4.14 A), with HSiW being also more active than HPW per catalyst weight. The selectivity to ethene scaled with EtOH conversion (Figure 4.14 B), passing a maximum, whereas the selectivity to DEE, as expected, was a mirror image of the ethene selectivity. HPW catalysts gave a higher ethene selectivity than HSiW catalysts despite the higher EtOH conversion for the HSiW catalysts. In this regard, it has been shown that the selectivity depends not only on the catalyst acid strength and the number of accessible proton sites, but also on the geometry of, and local charges in, the transition states, which are likely to be different for HPW and HSiW catalysts [17].

A similar behavior was also observed for HPA/SiO_2 catalysts at higher alcohol partial pressures 13.6 kPa for EtOH and 16.7 kPa for MeOH, indicating that the accessible surface protons on HPA catalysts were unaffected by the alcohol pressure (Figures 4.15 and 4.16).

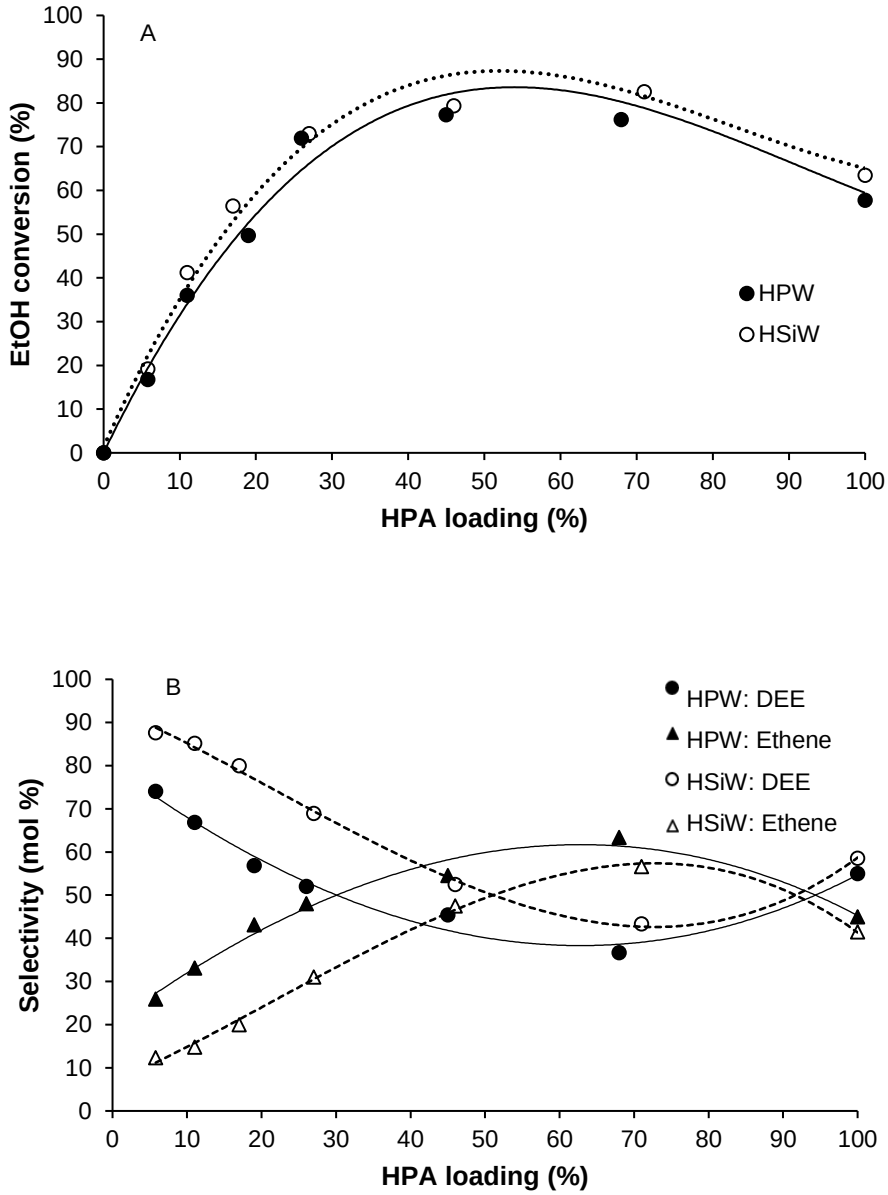

Figure 4.14. Effect of HPA loading on EtOH conversion (A) and DEE and ethene selectivity (B) over silica-supported HPA (0.20 g catalyst, 120 °C, 1.48 kPa EtOH partial pressure, 20 mL min^{-1} N_2 flow rate, contact time *W/F* = 271 g h mol^{-1}, 4 h time on stream).

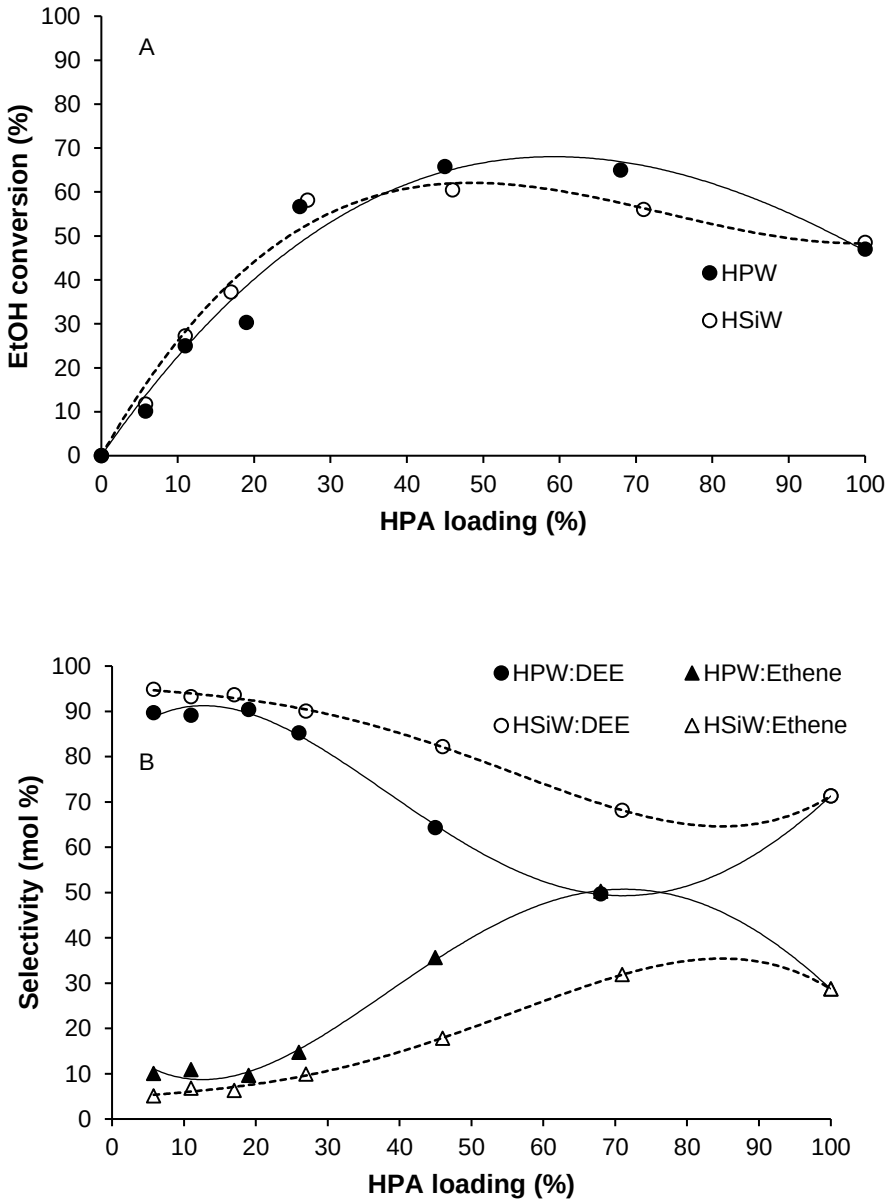

Figure 4.15. Effect of HPA loading on EtOH conversion (A) and DEE and ethene selectivity (B) over silica-supported HPA (0.20 g catalyst, 140 °C, 13.6 kPa EtOH partial pressure, 20 mL min^{-1} N_2 flow rate, contact time *W/F* = 29.5 g h mol^{-1}, 4 h time on stream).

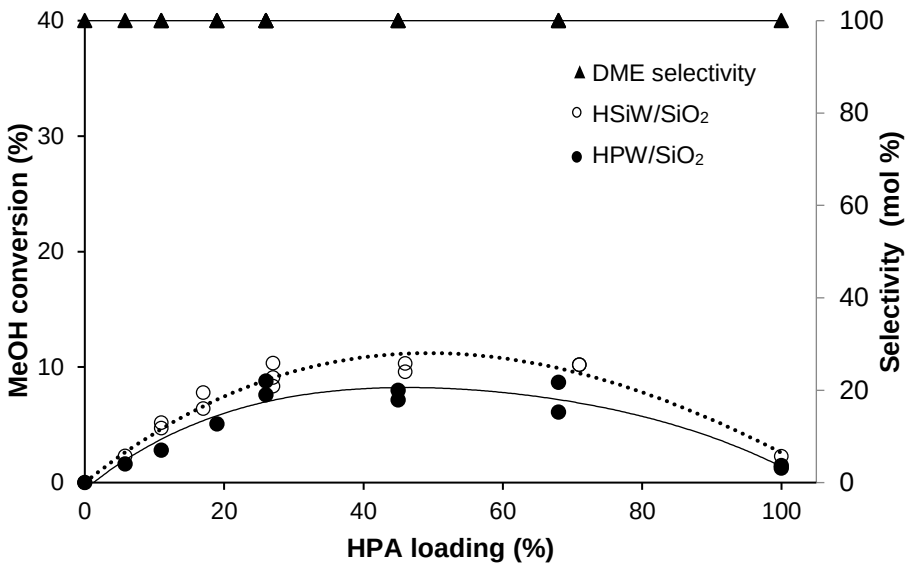

Figure 4.16. Effect of HPA loading on MeOH-to-DME conversion over HPA/SiO_2 (0.20 g catalyst, 120 °C, 16.7 kPa MeOH pressure, 20 mL min^{-1} N_2 flow rate, contact time *W/F* = 24 g h mol^{-1}, 4 h time on stream: 100% DME selectivity in all cases).

Overall, these results show that HPA loading of about 25% is an optimum one to achieve the maximum MeOH and EtOH conversion; further increase in HPA loading gives no significant rise in alcohol conversion. However, ethene selectivity in EtOH dehydration peaks at about 70% HPA loading (Figure 4.14 B). In these experiments performed at 120 °C, the maximum ethene selectivity was 60% at 80% EtOH conversion. The selectivity to ethene reached 100% at 100% EtOH conversion (100% ethene yield) at 160 °C and *W/F* = 271 g h mol^{-1} for 26%HPW/SiO_2 and 27%HSiW/SiO_2 catalysts (see below). For comparison, one of the most active zeolites, HZSM-5 (Si/Al = 12.5), gives 98% ethene yield at 220 °C [37].

4.5. Reaction kinetics

With the optimum HPA loadings, 26%HPW/SiO_2 and 27%HSiW/SiO_2, the dehydration of MeOH and EtOH was close to zero order in alcohol at 120 °C and 1.48–21.8 kPa alcohol partial pressure.

Figure 4.17 displays the logarithmic plot of the rate of MeOH dehydration over 27%HSiW/SiO_2 catalyst versus MeOH partial pressure demonstrating the order in MeOH of 0.1±0.1.

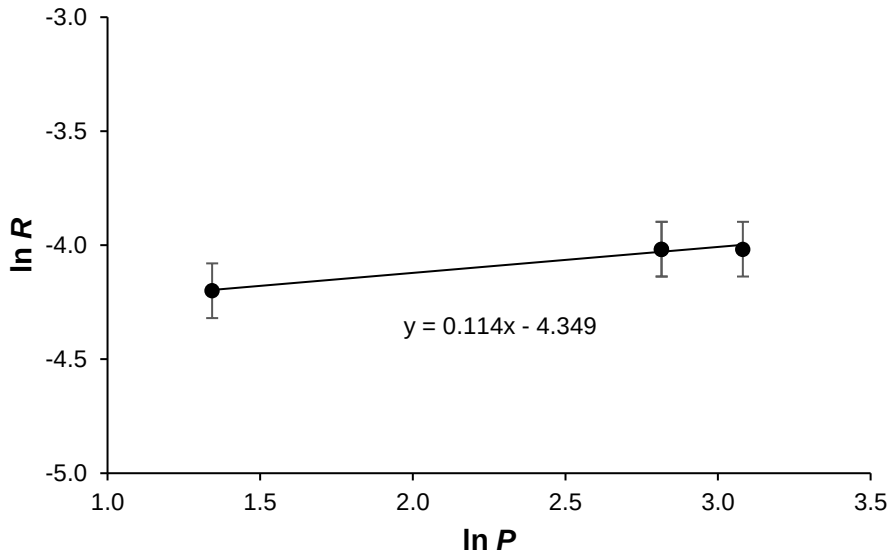

Figure 4.17. Logarithmic plot of the rate of MeOH dehydration over 27%HSiW/SiO_2 (mol $g^{-1}h^{-1}$ per HPA weight) versus MeOH partial pressure (kPa) at 120 °C, 0.20 g catalyst weight, 10–20 mL min^{-1} N_2 flow rate and 3.83–21.8 kPa MeOH partial pressure.

From zero-order kinetics, MeOH dehydration had a true activation energy (E_a) of 79 kJ mol^{-1} for 26%HPW/SiO_2 and 74 kJ mol^{-1} for 27%HSiW/SiO_2 in the temperature range of 110–140 °C (see the Arrhenius plots in Figure 4.18). EtOH dehydration had the same activation energy E_a = 72 kJ mol^{-1} for both catalysts in this temperature range. The high E_a values indicate no diffusion limitations in these dehydration systems, which is also supported by the Weisz–Prater analysis reported previously [9]. These findings agree with previous reports on alcohol dehydration on supported HPA catalysts with sub-monolayer HPA loadings [9,12].

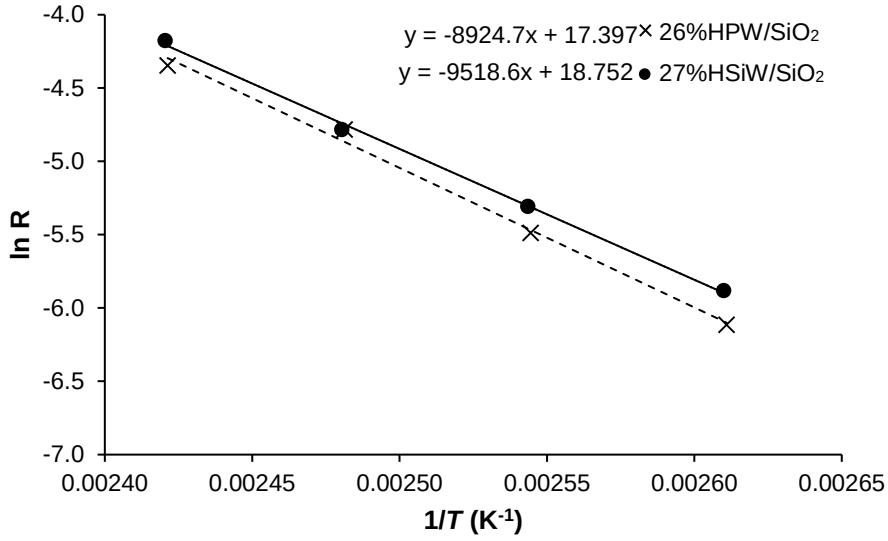

Figure 4.18. Arrhenius plots for MeOH dehydration over 26%HPW/SiO_2 (dotted line) and 27%HSiW/SiO_2 (solid line) (HPA/SiO_2 catalysts (0.05 g) diluted with SiO_2 (0.15 g), 3.83 kPa MeOH partial pressure, 20 mL min^{-1} N_2 flow rate, W/F = 26.2 g h mol^{-1}; R is the reaction rate in mol $g^{-1}h^{-1}$); E_a = 79 kJ mol^{-1} for 26%HPW/SiO_2 and 74 kJ mol^{-1} for 27%HSiW/SiO_2.

4.6. Mechanistic considerations

The finding that the steady-state alcohol conversion passes a maximum upon increasing the HPA loading at a constant contact time (Figures 4.10–4.16) has an important mechanistic implication. It shows that the catalyst activity scales primarily with the number of surface proton sites (H^+ surface site density) rather than with HPA loading or HPA acid strength (the latter increases with HPA loading (Figure 3.22, Chapter 3). The H^+ surface site density in HPA/SiO_2 catalysts is well known to go through a maximum at a medium HPA loading; it increases with loading of HPA up to 40–50% and then declines at higher HPA loadings due to the sharp decrease in catalyst surface area to less than 10 m^2g^{-1} for bulk HPA [36]. Thus in HSiW/SiO_2 catalysts, the proton surface site density peaks at 50% HSiW loading, as found using adsorption of benzonitrile, which adsorbs only on the surface proton sites [36].

The activity of this catalyst in n-butane isomerization and 1-butene double bond migration occurring via surface-type catalysis correlates with the proton surface site density [36].

The number of surface proton sites accessible for alcohol molecules in HPA/SiO_2 catalysts was determined by in-situ titration with 2,6-di-tert-butylpyridine (DTBP) during alcohol dehydration using a modified pulse method based on the titration procedure previously applied for finely dispersed HPA/SiO_2 and zeolites [15–17,38,39]. Sterically hindered DTBP, unable to penetrate into HPA bulk, titrates only surface H^+ sites in HPA [15–17]; it does not titrate Lewis acid sites. Previous studies [15,17] have found an under a stoichiometric number of active H^+ in 5%HPA/SiO_2 for dehydration of MeOH and EtOH: 2.0–2.5 and 1.9–3.0 per HPW and HSiW Keggin unit, respectively. The loss of HPA protons may be explained by the dehydroxylation reaction (Eq. (3.1), Chapter 3) [15]. At a higher HPW loading, in 10%HPW/SiO_2, all three HPW protons have been found active in EtOH dehydration, and the result did not depend on the alcohol partial pressure [17].

Here, the DTBP titration was used to assess the number of active proton sites in HPA/SiO_2 catalysts accessible for alcohol dehydration over a wide range of HPA loading. The number of active H^+ sites found was close to the stoichiometric values for 10–30%HPA loading. Figure 4.19 B shows the DTBP titration during EtOH dehydration over 26%HPW/SiO_2. The reaction was completely suppressed at a titrant uptake DTBP/HPW = 3.0 mol/mol, which means that all three protons in HPW were active and accessible for the reaction. The same result was obtained for MeOH dehydration. Interestingly, in EtOH dehydration, after the first DTBP pulse, a step change in reaction selectivity occurred showing an increase in DEE selectivity at the expense of ethene (Figure 4.19 A). Evidently, DTBP primarily inhibited the more demanding pathway of ethene formation.

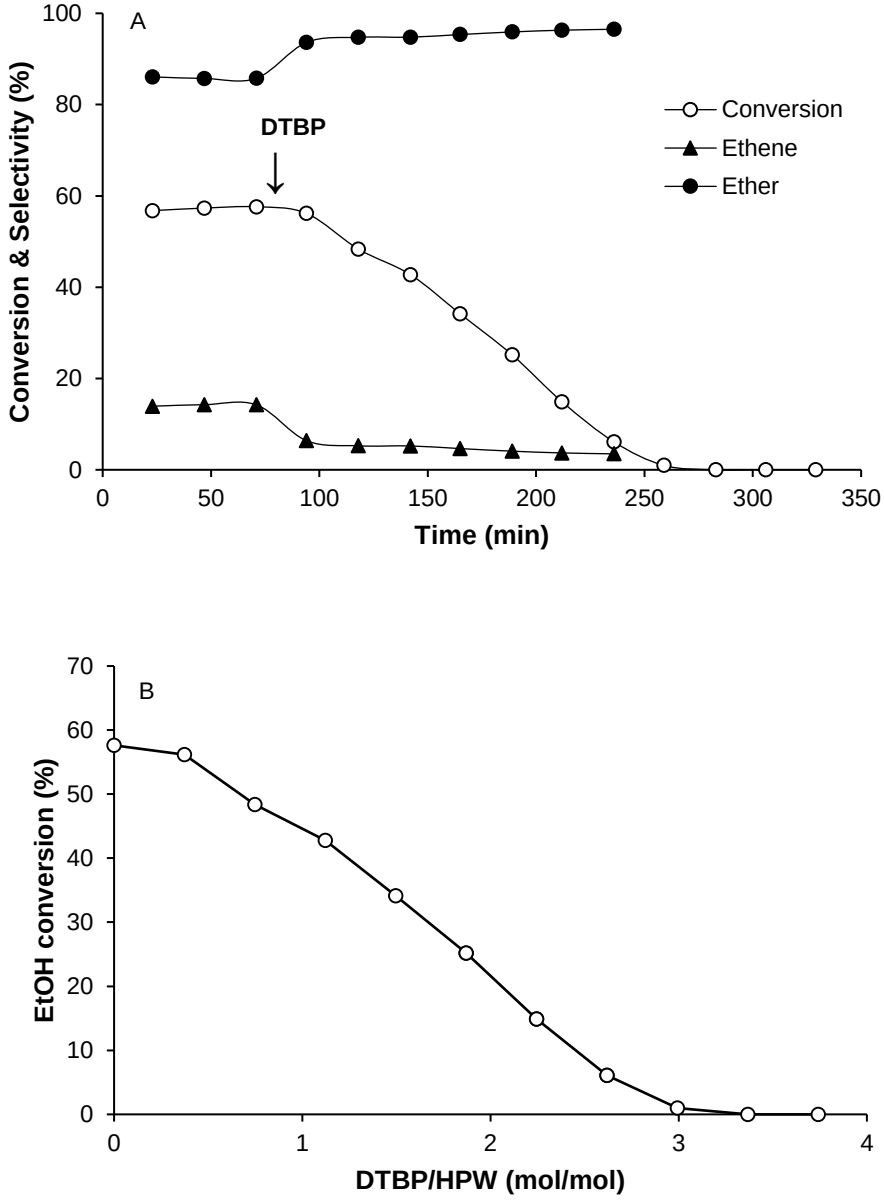

Figure 4.19. Titration with 2,6-di-tert-butylpyridine (6.5 µmol DTBP injections at each point starting at 100 min time on stream) during EtOH dehydration over 26%HPW/SiO_2 (0.20 g catalyst, 140 °C, 13.6 kPa EtOH pressure, 20 mL min^{-1} N_2 flow rate); reaction time course (A) and DTBP uptake per mole of HPW (B).

A similar effect on reaction selectivity was also observed for 27%HSiW/SiO_2 catalyst. The DTBP titration during EtOH dehydration over 27%HSiW/SiO_2 (Figure 4.20) gave an extrapolated titrant uptake DTBP/HSiW = 2.8, which tailed further beyond DTBP/HSiW ≈ 4 to completely terminate the reaction. This may indicate that initially all four protons in $H_4SiW_{12}O_{40}$ were equivalent and accessible for the reaction. But the last titrated proton in $[HSiW_{12}O_{40}]^{3-}$ may be weaker than the first three and/or less accessible for DTBP, hence required more DTBP for neutralization.

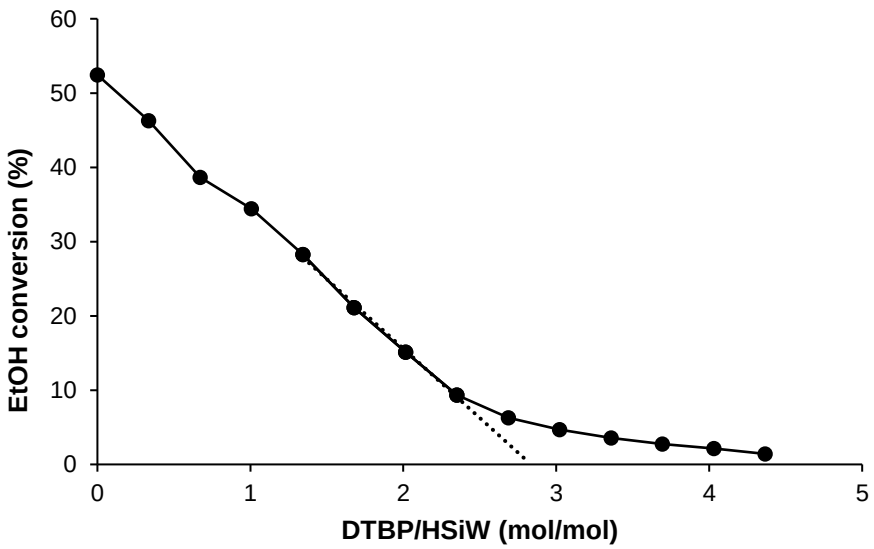

Figure 4.20. Titration with 2,6-di-tert-butylpyridine (6.5 µmol DTBP injections at each point) during EtOH dehydration over 27%HSiW/SiO_2 (0.20 g catalyst, 140 °C, 13.6 kPa EtOH pressure, 20 mL min^{-1} N_2 flow rate).

In the case of bulk and supported HPA catalysts with higher HPA loadings (> 40%), the addition of DTBP, although greatly reduced alcohol conversion, did not completely terminate the reaction (Figures 4.21–4.23). Probably alcohol molecules could penetrate through the layer of adsorbed DTBP and react with the protons underneath. Hence for these catalysts it was not possible to accurately measure the number of active proton sites.

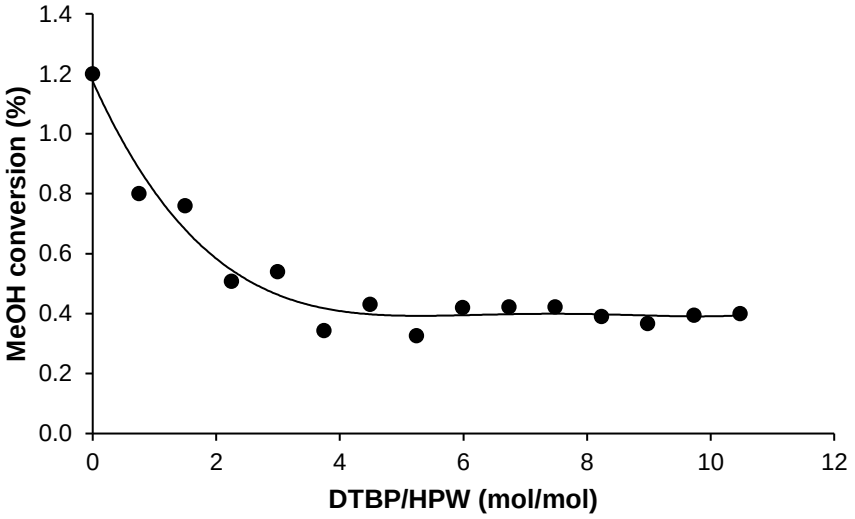

Figure 4.21. Titration with 2,6-di-tert-butylpyridine (13 µmol DTBP injections at each point) during MeOH dehydration over bulk HPW (0.05 g) + SiO_2 (0.15 g) showing MeOH conversion versus DTBP uptake per mole of HPW (120 °C, 3.83 kPa MeOH pressure, 20 mL min^{-1} N_2 flow rate).

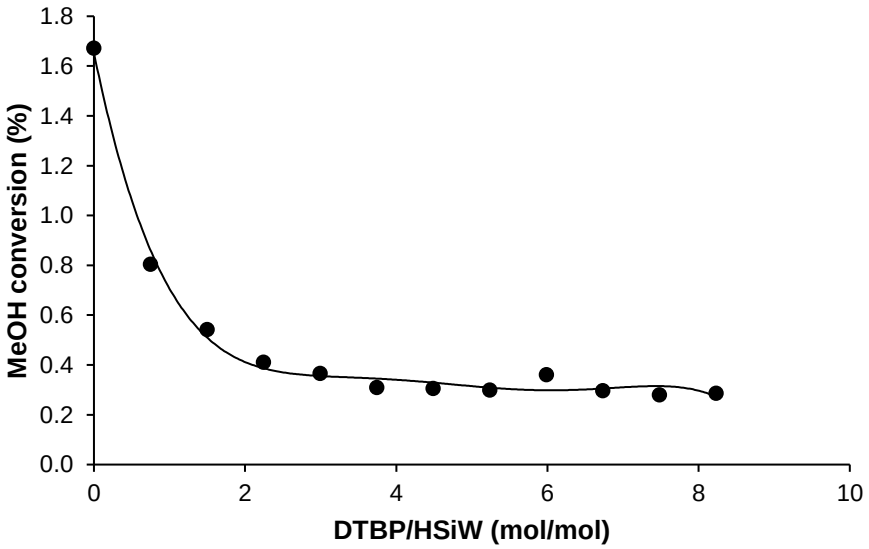

Figure 4.22. Titration with 2,6-di-tert-butylpyridine (13 µmol DTBP injections at each point) during MeOH dehydration over bulk HSiW (0.05 g)+ SiO_2 (0.15 g) showing MeOH conversion versus DTBP uptake per mole of HSiW (120 °C, 3.83 kPa MeOH pressure, 20 mL min^{-1} N_2 flow rate).

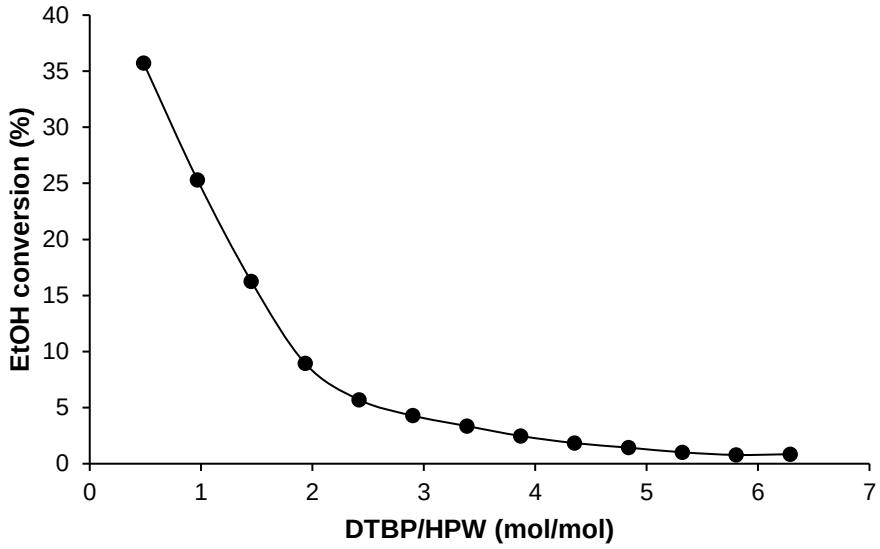

Figure 4.23. Titration with 2,6-di-tert-butylpyridine (6.5 µmol DTBP injections at each point) during EtOH dehydration over bulk HPW (0.05 g) + SiO_2 (0.15 g) showing EtOH conversion versus DTBP uptake per mole of HPW (140 °C, 13.6 kPa EtOH pressure, 20 mL min^{-1} N_2 flow rate).

DRIFT spectrum of bulk HPW catalyst after titration with DTBP during EtOH dehydration (Figure 4.24) shows the bands at 1530, 1616 and 3370 cm^{-1} characteristics of the protonated DTBP [38,39]. The same bands are seen in the spectrum of DTBP adsorbed on bulk HPW.

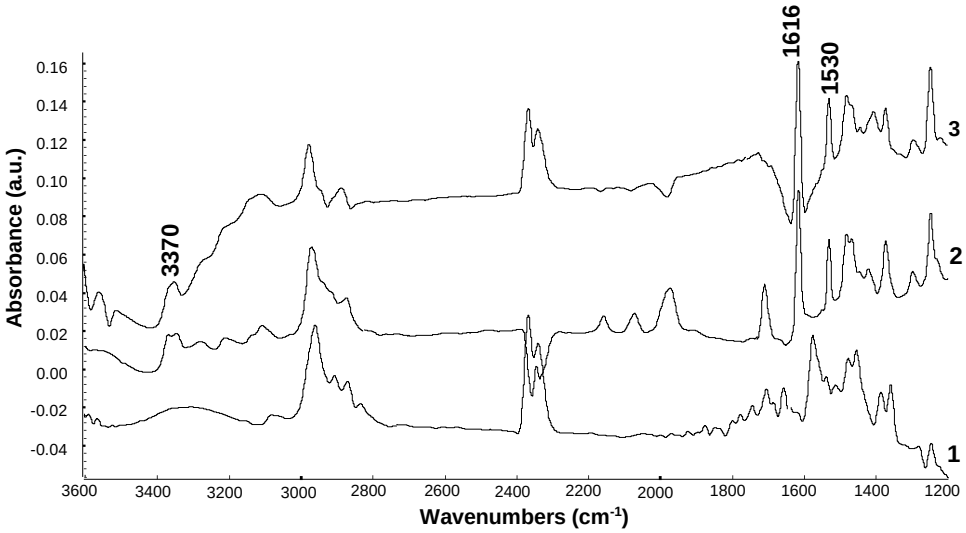

Figure 4.24. DRIFT spectra: (1) DTBP (KBr mixture), (2) DTBP adsorbed on bulk HPW (KBr mixture versus KBr + HPW background) and (3) spent bulk HPW catalyst after titration with DTBP during EtOH dehydration (KBr mixture versus KBr + HPW background; see reaction details in Figure 4.23). The labelled bands at 1530, 1616 and 3370 cm^{-1} are attributed to the protonated DTBP.

Tables 4.3 and 4.4 show the density of H^+ surface sites and the initial enthalpies of NH_3 adsorption for the bulk and SiO_2-supported HPW and HSiW catalysts together with turnover frequencies (TOF) for MeOH and EtOH dehydration. The H^+ density for 11–27%HPA loading was calculated assuming that all protons of HPA were accessible, as follows from the DTBP titration. The H^+ density for the bulk HPAs was calculated using the Keggin unit cross-section of 144 A^2 [8,12,23,24] and the HPA surface area from Table 3.1 and 3.2 (Chapter 3). The H^+ surface site density increases from 0.12 to 0.27 mmol g^{-1} for HPW/SiO_2 and from 0.15 to 0.38 mmol g^{-1} for HSiW/SiO_2 with increasing HPA loading in the range 11–27%. For bulk HPAs, the proton site density is 10-fold lower (0.020 and 0.037 mmol g^{-1} for HPW and HSiW) - only ~2% of the total number of HPA protons.

Table 4.3. Dehydration of MeOH over HPA/SiO_2 catalysts.[a]

Catalyst	HPA loading %	Surface H^{+} [b] mmol g^{-1}	Conversion %	10^3 R[c] mol $g^{-1}h^{-1}$	TOF[d] h^{-1}	$-\Delta H_o$[e] kJ mol^{-1}
HPW/SiO_2	11	0.115	15	1.4	12	166
	17	0.177	26	2.5	14	167[f]
	26	0.271	29	2.8	10	167
	100	0.020	6.2	0.59	30	203
HSiW/SiO_2	11	0.153	17	1.6	12	152
	14	0.195	24	2.3	11	152[f]
	27	0.375	35	3.3	8.9	153
	100	0.037	8.5	0.81	22	177

[a] 0.20 g catalyst, 120 °C, 3.83 kPa MeOH partial pressure, 20 mL min^{-1} N_2 flow rate, contact time W/F = 105 g h mol^{-1}. [b] Proton surface site density per gram of catalyst. [c] Reaction rate $R = XF/W$, where X is the fractional alcohol conversion, F is the inlet molar flow rate of alcohol and W is the catalyst weight. [d] TOF per H^+ surface site. [e] Initial enthalpy of NH_3 adsorption ±6 kJ mol^{-1}. [f] Calculated from Eqs. (3.2) and (3.3), Chapter 3.

The TOF values for MeOH and EtOH dehydration, determined from zero-order kinetics, are almost constant at lower HPA loadings between 10–30%, where the catalyst acid strength changes very little. The TOF values increase significantly for bulk HPAs: almost 3-fold for MeOH and 10-fold for EtOH dehydration, which is consistent with the catalyst acid strength represented by the enthalpy of NH_3 adsorption. HPW catalysts have greater turnover rates than HSiW catalysts, especially for the bulk HPAs, in agreement with their acid strength. From the TOF values, the reactivity of MeOH and EtOH is very close at relatively low HPA loadings of 10–30%. Unexpectedly, in the case of bulk HPAs, EtOH is 3–4 times more reactive than MeOH. This could be caused by a different adsorption geometry of these alcohols on the surface of bulk crystalline HPAs.

Table 4.4. Dehydration of EtOH over HPA/SiO_2 catalysts.[a]

Catalyst	HPA loading %	Surface H^+ [b] mmol g^{-1}	Conversion %	10^3 R[c] mol $g^{-1}h^{-1}$	TOF[d] h^{-1}	$-\Delta H_o$[e] kJ mol^{-1}
HPW/SiO_2	11	0.115	36	1.3	12	166
	19	0.201	50	1.9	9.3	169
	26	0.271	72	2.7	9.8	167
	100	0.020	58	2.1	110	203
HSiW/SiO_2	11	0.153	41	1.5	9.9	152
	17	0.236	56	2.1	8.8	156
	27	0.375	72	2.7	7.1	153
	100	0.037	64	2.4	64	177

[a] 0.20 g catalyst, 120 °C, 1.48 kPa EtOH partial pressure, 20 mL min^{-1} N_2 flow rate, contact time W/F = 271 g h mol^{-1}. [b] Proton surface site density per gram of catalyst. [c] Reaction rate $R = XF/W$, where X is the fractional alcohol conversion, F is the inlet molar flow rate of alcohol and W is the catalyst weight. [d] TOF per H^+ surface site. [e] Initial enthalpy of NH_3 adsorption ±6 kJ mol^{-1}.

The results obtained clearly show that the steady-state activity of silica-supported HPA catalysts in alcohol dehydration correlates with the density of HPA surface proton sites since both the activity and the proton site density change in parallel with HPA loading. This indicates that under the reaction conditions studied, MeOH and EtOH dehydration over bulk and silica-supported HPA catalysts, prepared from water as well as from MeOH, occurs via the mechanism of surface-type HPA catalysis within the whole range of HPA loading rather than via the bulk-type (pseudo-homogeneous) HPA catalysis. For the bulk-type mechanism, the conversion is expected to scale directly with the HPA loading.

This conclusion applies to the typical HPA/SiO_2 catalysts i.e., those prepared and pre-treated by conventional methods. Such catalysts contain variable quantities of water within the HPA interstitial space resulting from both catalyst preparation and alcohol dehydration. Bulk

anhydrous HPAs might absorb alcohol molecules into the interstitial space and possibly initially react through the bulk-type mechanism as claimed elsewhere [10], although once a steady state is reached, the interstitial space would be filled with water formed in the dehydration reaction. Most of our catalytic activity tests was carried out at 120 °C to keep reactions under kinetic control; at higher reaction temperatures, more relevant to practice, the bulk-type mechanism appears even less likely due to reduction in total adsorption of alcohol molecules as well as possible diffusion limitations.

Previously, a linear relationship between the turnover frequency of EtOH dehydration over HPW and HSiW catalysts and the initial enthalpy of NH_3 adsorption, ΔH_o, has been reported [9]. This relationship includes HPW supported on, TiO_2, SiO_2, Nb_2O_5 and ZrO_2 at a sub-monolayer coverage of 15%. Acidic salts $Cs_{2.5}H_{0.5}PW_{12}O_{40}$ and $Cs_{2.25}H_{0.75}PW_{12}O_{40}$, as well as 15%HSiW/$SiO_2$ all operate via the surface-type mechanism [9]. Figure 4.25 shows this plot, with our new results for bulk HPW and HSiW from Table 4.4 added. Excellent fit of these results into the relationship further strengthens the conclusion about the surface-type mechanism of HPA catalysis in alcohol dehydration.

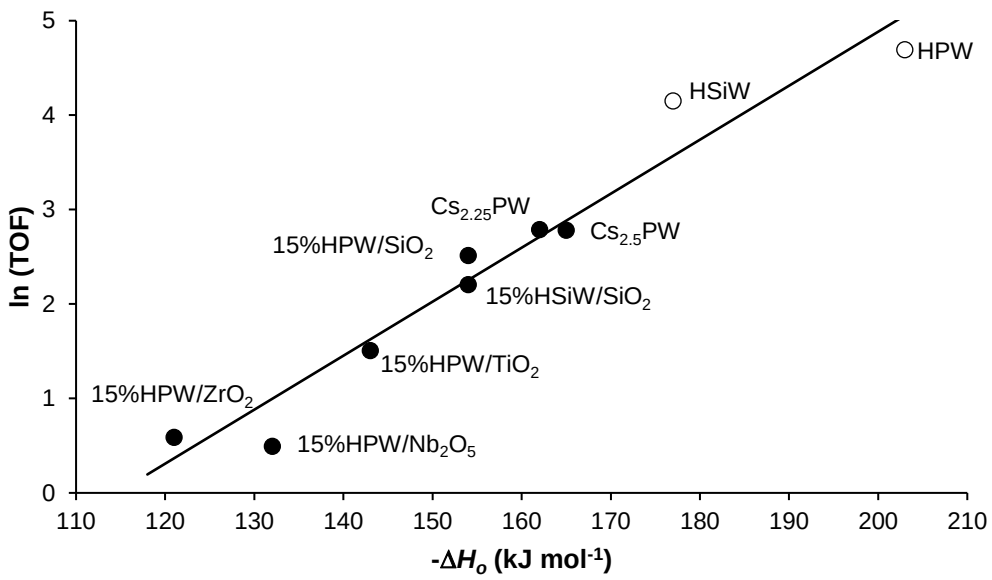

Figure 4.25. A plot of ln (TOF) for EtOH dehydration (TOF in h^{-1}) over HPA catalysts vs initial heat of NH_3 adsorption (120 °C, 0.20 g catalyst, 1.48 kPa EtOH partial pressure, 20 mL min^{-1} N_2 flow rate) [9]. The added data for bulk HPW and HSiW (open circles) are from the present work.

4.7. Comparison of activity of HPA/SiO_2 catalysts and zeolites

Zeolites are widely applied as solid acid catalysts. Zeolites are crystalline aluminosilicate materials comprising $[SiO_4]^{4-}$ and $[AlO_4]^{5-}$ tetrahedra connected by oxygen atoms to form a three-dimensional structure with uniform channels and cages of 3 to 13 Å size and high surface areas (400–800 m^2g^{-1}) [40–42]. Proton forms of zeolites have a high proton site density, relatively strong acid strength, large surface area and high thermal stability [43].

Numerous studies have demonstrated the high catalytic activity of zeolites for EtOH dehydration, including HZSM-5, BEA, Faujasite, Ferrierite and Mordenite [3,37,44–50]. Among zeolite catalysts, HZSM-5 has attracted the most attention owing to its high acidity and ability to catalyse reactions at relatively low temperatures [3,37,44,45]. Hence, it was important to compare the activity of HPA and HZSM-5 catalysts in EtOH dehydration.

For comparison, we chose 26%HPW/SiO_2, 27%HSiW/SiO_2 and commercial HZSM-5 zeolites (47 and 12). The Si/Al ratios were determined using ICP-OES analysis and found to be close to those specified by the manufacturer. The surface area and porosity of the HZSM-5 zeolites are gived in Table 7.2 and their XRD patterns are shown in Figure 7.16 in Appendix. The HZSM-5 zeolite (47) had a proton site density of 0.35 mmol g^{-1}, which was similar to the total number of protons in 27% HSiW/SiO_2 (0.38 mmol g^{-1}) and 26% HPW/SiO_2 (0.27 mmol g^{-1}) while HZSM-5 (12) had a 4-fold greater proton site density (1.28 mmol g^{-1}).

Figure 4.26 (A–C) shows the light-off tests for these catalysts and demonstrates the effect of reaction temperature on EtOH conversion and DEE and ethene selectivity. As seen, the two HPA catalysts performed very similarly; both reached 100% conversion and 100% ethene selectivity at 160 °C. HZSM-5 (47) exhibited lower activity despite similar proton site density; it reached 100% EtOH conversion at 200 °C with an ethene selectivity of 99% (1% of C_1–C_3 hydrocarbons also formed). HZSM-5 (12) with a four-fold greater proton site density reached 98.6% EtOH conversion and 94.8% ethene selectivity at 200 °C (5% C_1–C_3 hydrocarbons also formed).

Therefore, the HZSM-5 catalyst was significantly less active than 26%HPW/SiO_2 and 27%HSiW/SiO_2 per unit catalyst weight. Also, HPAs have been reported to be superior in activity over zeolites with different Si/Al ratios in MeOH dehydration [12].

The difference in catalyst performance can be explained in terms of the weaker acid strength of HZSM-5 zeolite compared to HPA catalysts, as determined by NH_3-MC ($-\Delta H_o$ = 120–140 kJ mol^{-1} for HZSM-5) [12]. Diffusion limitations in zeolite micropores could also contribute to its inferior catalytic activity [47]. However, zeolites (Si/Al = 47) exhibited good performance stability in EtOH dehydration for 20 h on stream, as shown in Figure 4.27.

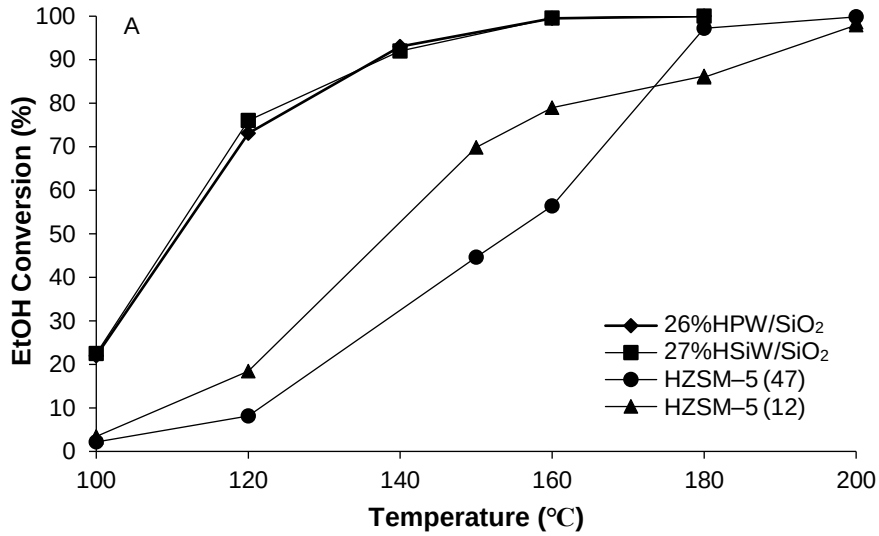
A
EtOH Conversion (%)
Temperature (°C)
26%HPW/SiO2
27%HSiW/SiO2
HZSM–5 (47)
HZSM–5 (12)

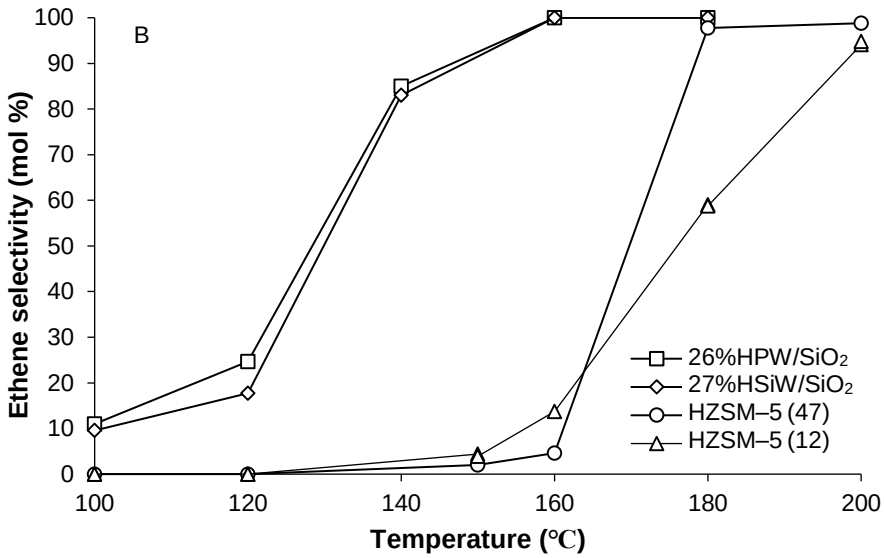
B
Ethene selectivity (mol %)
Temperature (°C)
26%HPW/SiO2
27%HSiW/SiO2
HZSM–5 (47)
HZSM–5 (12)

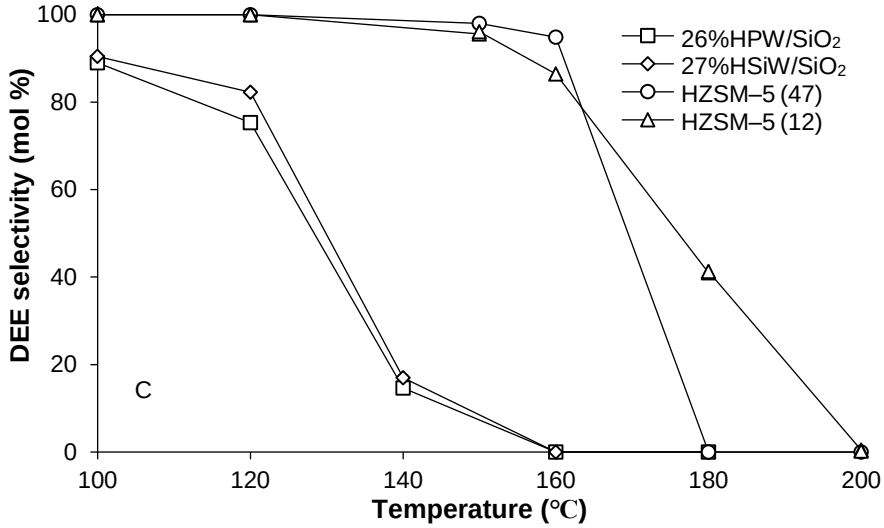

Figure 4.26. Effect of temperature on (A) EtOH dehydration, (B) ethene selectivity and (C) DEE selectivity over HPA/SiO_2 and HZSM-5 (0.20 g catalyst, 20 ml min^{-1} N_2 flow rate, 1.48 kPa EtOH pressure, contact time *W/F* = 271 g h mol^{-1}**).**

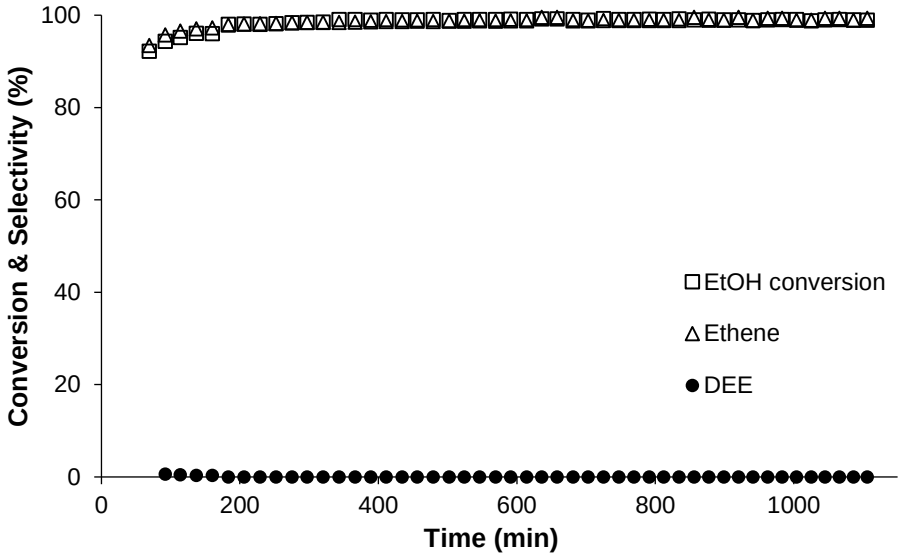

Figure 4.27. Time course for dehydration of EtOH over HZSM-5 (47) (0.20 g catalyst, 20 ml min^{-1} N_2 flow rate, 180 °C, 1.48 kPa EtOH pressure, contact time *W/F* = 271 g h mol^{-1}).

4.8. Conclusions

In this study, we have examined the effect of HPA loading and acid strength in the dehydration of MeOH and EtOH over HPA/SiO_2 catalysts with a wide range of HPA loadings 5–100% prepared by HPA impregnation from water and MeOH. HSiW and HPW catalysts show close catalytic activities per HPA weight, with HSiW having a slightly higher activity despite its weaker acid strength. This can be elucidated by the larger number of protons per Keggin unit and the higher dispersion of HSiW compared to HPW. The turnover reaction rate for HPW catalysts is higher than that for HSiW catalysts in agreement with their acid strength. The catalysts prepared from water and MeOH had a very close acid strength and exhibited similar activities in alcohol dehydration. Besides, HPA catalysts based on SiO_2 have been shown to have greater catalytic activity than zeolites HZSM-5.

It has been established that the steady-state catalyst activity correlates with the surface proton site density of silica-supported HPA catalysts rather than with the HPA loading or HPA acid strength. This indicates that alcohol dehydration occurs via the mechanism of surface-type HPA catalysis at the gas-solid interface rather than the bulk-type (pseudo-homogeneous) HPA catalysis. This conclusion is further strengthened by fitting the activity of bulk HPW and HSiW into the activity-acid strength relationship for supported HPA catalysts operating via the surface-type catalysis.

References

[1] A. Corma, S. Iborra, A. Velty, Chemical routes for the transformation of biomass into chemicals, Chem. Rev. 107 (2007) 2411–2502.

[2] Z. Buniazet, C. Lorentz, A. Cabiac, S. Maury, S. Loridant, Supported oxides catalysts for the dehydration of isobutanol into butenes: Relationships between acidic and catalytic properties, Mol. Catal. 451 (2018) 143–152.

[3] D. Fan, D-J. Dai, H-S. Wu, Ethylene formation by catalytic dehydration of ethanol with industrial considerations, Materials 6 (2013) 101–115.

[4] T.H. Fleisch, A. Basu, R.A. Sills, Introduction and advancement of a new clean global fuel: The status of DME developments in China and beyond, J. Nat. Gas Sci. Eng. 9 (2012) 94–107.

[5] F. Pontzen, W. Liebner, V. Gronemann, M. Rothaemel, B. Ahlers, CO_2-based methanol and DME-efficient technologies for industrial scale production, Catal. Today 171 (2011) 242–250.

[6] K. Weissermel, H-J. Arpe, Industrial Organic Chemistry, fourth ed., Wiley–VCH Verlag GmbH & Co. KGaA, Weinheim, 2003.

[7] T. Kito-Borsa, D.A. Pacas, S. Selim, S.W. Cowley, Properties of an ethanol-diethyl ether-water fuel mixture for cold-start assistance of an ethanol-fueled vehicle, Ind. Eng. Chem. Res. 37 (1998) 3366–3374.

[8] T. Okuhara, N. Mizuno, M. Misono, Catalytic Chemistry of Heteropoly Compounds, in: D.D. Eley, Werner O. Haag, Bruce Gates (Eds.), Advances in Catalysis, Vol. 41, Academic Press, 1996: pp. 113–252.

[9] W. Alharbi, E. Brown, E.F. Kozhevnikova, I.V. Kozhevnikov, Dehydration of ethanol over heteropoly acid catalysts in the gas phase, J. Catal. 319 (2014) 174–181.

[10] J. Schnee, E.M. Gaigneaux, Lifetime of the $H_3PW_{12}O_{40}$ heteropolyacid in the methanol-to-DME process: A question of pre-treatment, Appl. Catal. A: Gen. 538 (2017) 174–180.

[11] J. Schnee, A. Eggermont, E.M. Gaigneaux, Boron nitride: A support for highly active heteropolyacids in the methanol-to-DME reaction, ACS Catal. 7 (2017) 4011–4017.

[12] W. Alharbi, E.F. Kozhevnikova, I.V. Kozhevnikov, Dehydration of methanol to dimethyl ether over heteropoly acid catalysts: The relationship between reaction rate and catalyst acid strength, ACS Catal. 5 (2015) 7186–7193.

[13] A. Ciftci, D. Varisli, K. Cem, N.A. Sezgi, T. Dogu, Dimethyl ether, diethyl ether & ethylene from alcohols over tungstophosphoric acid based mesoporous catalysts, Chem. Eng. J. 207–208 (2012) 85–93.

[14] R.M. Ladera, J.L.G. Fierro, M. Ojeda, S. Rojas, TiO_2-supported heteropoly acids for low-temperature synthesis of dimethyl ether from methanol, J. Catal. 312 (2014) 195–203.

[15] R.T. Carr, M. Neurock, E. Iglesia, Catalytic consequences of acid strength in the conversion of methanol to dimethyl ether, J. Catal. 278 (2011) 78–93.

[16] A.J. Jones, R.T. Carr, S.I. Zones, E. Iglesia, Acid strength and solvation in catalysis by MFI zeolites and effects of the identity, concentration and location of framework heteroatoms, J. Catal. 312 (2014) 58–68.

[17] W. Knaeble, E. Iglesia, Kinetic and theoretical insights into the mechanism of alkanol dehydration on solid Brønsted acid catalysts, J. Phys. Chem. C 120 (2016) 3371–3389.

[18] M.C.H. Clemente, G.A. V. Martins, E.F. de Freitas, J.A. Dias, S.C.L. Dias, Ethylene production via catalytic ethanol dehydration by 12-tungstophosphoric acid@ceria-zirconia, Fuel 239 (2019) 491–501.

[19] P.G. Moses, J.K. Nørskov, Methanol to dimethyl ether over ZSM-22: A periodic density functional theory study, ACS Catal. 3 (2013) 735–745.

[20] J. Haber, K. Pamin, L. Matachowski, B. Napruszewska, J. Połtowicz, Potassium and silver salts of tungstophosphoric acid as catalysts in dehydration of ethanol and hydration of ethylene, J. Catal. 207 (2002) 296–306.

[21] V.V. Bokade, G.D. Yadav, Heteropolyacid supported on montmorillonite catalyst for dehydration of dilute bio-ethanol, Appl. Clay Sci. 53 (2011) 263–271.

[22] E.F. Kozhevnikova, I.V. Kozhevnikov, A calorimetric study of the acidity of bulk and silica-supported heteropoly acid $H_3PW_{12}O_{40}$, J. Catal. 224 (2004) 164–169.

[23] I.V. Kozhevnikov, Catalysis by heteropoly acids and multicomponent polyoxometalates in liquid-phase reactions, Chem. Rev. 98 (1998) 171–198.

[24] I.V. Kozhevnikov, Catalysts for Fine Chemical Synthesis Catalysis by Polyoxometalates, Vol. 2, John Wiley, Chichester, England, 2002.

[25] J.B. Moffat, Metal-Oxygen Clusters the Surface and Catalytic Properties of Heteropoly Oxometalates, Kluwer Academic Publishers, New York, 2002.

[26] M. Misono, Chapter 4-Catalysis of Heteropoly Compounds (Polyoxometalates), in: M. Misono (Eds.), Studies in Surface Science and Catalysis, Elsevier B.V., Oxford, 2013: pp. 97–155.

[27] M. Misono, Unique acid catalysis of heteropoly compounds (heteropolyoxometalates) in the solid state, Chem. Commun. 1 (2001) 1141–1153.

[28] T. Kella, A.A. Vennathan, S. Dutta, S.S. Mal, D. Shee, Selective dehydration of 1-butanol to butenes over silica supported heteropolyacid catalysts: Mechanistic aspect, Mol. Catal. 516 (2021) 111975.

[29] C. Lang, J. Schnee, B.J.T. Mba, F. Devred, E.M. Gaigneaux, Ammonium-substitution for successfully activating the bulk of Keggin acid salts in 1-butanol dehydration, Catal. Sci. Technol. 10 (2020) 6244–6256.

[30] A.M. Alsalme, P.V. Wiper, Y.Z. Khimyak, E.F. Kozhevnikova, I.V. Kozhevnikov, Solid acid catalysts based on $H_3PW_{12}O_{40}$ heteropoly acid: Acid and catalytic properties at a gas-solid interface, J. Catal. 276 (2010) 181–189.

[31] W.D.T. Dale, P.A. Flavelle, P. Kruus, Concentration fluctuations in water-methanol mixtures as studied by ultrasonic absorption, Can. J. Chem. 54 (1976) 355–366.

[32] S. Kim, Y.T. Kim, C. Zhang, G. Kwak, K-W. Jun, Effect of reaction conditions on the catalytic dehydration of Methanol to dimethyl ether over a K-modified HZSM-5 catalyst, Catal. Lett. 147 (2017) 792–801.

[33] D. Varisli, T. Dogu, G. Dogu, Ethylene and diethyl-ether production by dehydration reaction of ethanol over different heteropolyacid catalysts, Chem. Eng. Sci. 62 (2007) 5349–5352.

[34] Y. Saito, P.N. Cook, H. Niiyama, E. Echigoya, Dehydration of alcohols on/in heteropoly compounds, J. Catal. 95 (1985) 49–56.

[35] I.V. Kozhevnikov, Sustainable heterogeneous acid catalysis by heteropoly acids, J. Mol. Catal. A: Chem. 262 (2007) 86–92.

[36] J. Zhang, M. Kanno, Y. Wang, H. Nishii, Y.K. Miura, Y. Kamiya, Changes in surface acidity of silica-supported dodecatungstosilicic acid in relation to the loading amount, J. Phys. Chem. C 115 (2011) 14762–14769.

[37] C-Y. Wu, H-S. Wu, Ethylene Formation from Ethanol Dehydration Using ZSM-5 Catalyst, ACS Omega 2 (2017) 4287–4296.

[38] A. Corma, V. Fornés, L. Forni, F. Márquez, J. Martínez-Triguero, D. Moscotti, 2,6-Di-tert-butyl-pyridine as a probe molecule to measure external acidity of zeolites, J. Catal. 179 (1998) 451–458.

[39] H. Hattori, Y. Ono, Solid Acid Catalysis from Fundamentals to Applications, Pan Stanford Publishing, Singapore, 2015.

[40] C.S. Cundy, P.A. Cox, The hydrothermal synthesis of zeolites: History and development from the earliest days to the present time, Chem. Rev. 103 (2003) 663–701.

[41] P. Zarrintaj, G. Mahmodi, S. Manouchehri, A.H. Mashhadzadeh, M. Khodadadi, M. Servatan, M.R. Ganjali, B. Azambre, S-J. Kim, J.D. Ramsey, S. Habibzadeh, M.R. Saeb, M. Mozafari, Zeolite in tissue engineering: Opportunities and challenges, MedComm. 1 (2020) 5–34.

[42] A. Al-nayili, Novel Lewis acidic zeolites as heterogeneous catalysts for liquid phase chemistry, Doctoral dissertation, Cardiff Catalysis Institute, Cardiff, 2017.

[43] D. Masih, S. Rohani, J.N. Kondo, T. Tatsumi, Low-temperature methanol dehydration to dimethyl ether over various small-pore zeolites, Appl. Catal. B: Environ. 217 (2017) 247–255.

[44] H. Xin, X. Li, Y. Fang, X. Yi, W. Hu, Y. Chu, F. Zhang, A. Zheng, H. Zhang, X. Li, Catalytic dehydration of ethanol over post-treated ZSM-5 zeolites, J. Catal. 312 (2014) 204–215.

[45] R. Batchu, V. V. Galvita, K. Alexopoulos, T.S. Glazneva, H. Poelman, M.F. Reyniers, G.B. Marin, Ethanol dehydration pathways in H-ZSM-5: Insights from temporal analysis of products, Catal. Today 355 (2020) 822–831.

[46] M. Zhang, Y. Yu, Dehydration of ethanol to ethylene, Ind. Eng. Chem. Res. 52 (2013) 9505–9514.

[47] T.K. Phung, L. Proietti Hernández, A. Lagazzo, G. Busca, Dehydration of ethanol over zeolites, silica alumina and alumina: Lewis acidity, Brønsted acidity and confinement effects, Appl. Catal. A: Gen. 493 (2015) 77–89.

[48] J.C. Soh, S.L. Chong, S.S. Hossain, C.K. Cheng, Catalytic ethylene production from ethanol dehydration over non-modified and phosphoric acid modified Zeolite H-Y (80) catalysts, Fuel Process. Technol. 158 (2017) 85–95.

[49] H. Chiang, A. Bhan, Catalytic consequences of hydroxyl group location on the rate and mechanism of parallel dehydration reactions of ethanol over acidic zeolites, J. Catal. 271 (2010) 251–261.

[50] A.D. Reviere, D. Gunst, M.K. Sabbe, M-F. Reyniers, A. Verberckmoes, Dehydration of butanol towards butenes over MFI, FAU and MOR: Influence of zeolite topology, Catal. Sci. Technol. 11 (2021) 2540–2559.

Chapter 5: Diethyl ether conversion to ethene and ethanol catalysed by heteropoly acids

Chapter 5 : Diethyl ether conversion to ethene and ethanol catalysed by heteropoly acids

5.1. Introduction

The dehydration of EtOH is a promising reaction for the production of ethene (Eq. (5.1)) and DEE (Eq. (5.2)) from renewable non-petroleum resources [1–4]. This reaction can be carried out in the gas phase over solid acid catalysts such as zeolites, metal oxides and HPAs (HPW, HSiW) [5–17]. HPAs, having a stronger acidity ([18–23] and references therein), exhibited high activity in this reaction [7–9,17,24,25].

$$CH_3CH_2OH \rightarrow CH_2{=}CH_2 + H_2O \quad \textbf{(5.1)}$$

$$2CH_3CH_2OH \rightarrow (CH_3CH_2)_2O + H_2O \quad \textbf{(5.2)}$$

$$(CH_3CH_2)_2O \rightarrow CH_3CH_2OH + CH_2{=}CH_2 \quad \textbf{(5.3)}$$

DEE is a key intermediate in the EtOH-to-ethene dehydration [8,13–16]. In the presence of an acid catalyst, DEE undergoes elimination to produce ethene and EtOH (Eq. (5.3)); the latter, in turn, dehydrates to ethene (Eq. (5.1)). The mechanism of ethene formation from EtOH dehydration is debated ([13] and references therein). DEE forms in EtOH dehydration at low temperatures, whereas ethene forms at higher temperatures, either directly from EtOH or via DEE elimination or both [13]. Therefore, knowledge about the acid-catalysed elimination of DEE can shed the light on the mechanism of the EtOH-to-ethene dehydration and help in optimising the production of ethene. DEE elimination is also of interest in its own right to convert spent DEE into useful products such as ethene and EtOH [14,16].

The EtOH-to-ethene dehydration is suggested to proceed via the bimolecular elimination mechanism E2. This mechanism involves simultaneous cleavage of C–H and C–O bonds in alcohol by a pair of acid H^+ and base B^- catalyst sites (Scheme 5.1) [24,26]. From the

general concept of heterolytic 1,2-elimination reactions [27], a similar E2 mechanism may be assumed for the acid-catalysed DEE elimination to form ethene and EtOH (Scheme 5.1). E2 mechanism has been suggested for the elimination of DEE on γ-Al_2O_3 from DFT modelling [13].

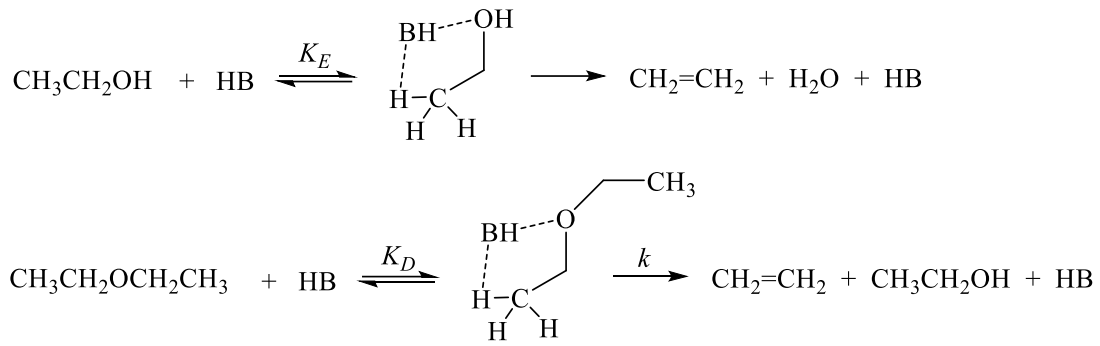

Scheme 5.1. E2 elimination of EtOH and DEE by a pair of acid H^+ and base B^- sites.

Several studies on DEE elimination over γ-alumina have been published [13–16] including kinetics [15] and DFT analysis of reaction mechanism [13]. Phung and Basca [14] have reported the elimination of DEE in the presence of zeolite and oxide catalysts at 150–450 °C, with the catalyst activity decreasing in the order: HZSM-5 > USY > γ-Al_2O_3 ≈ SiO_2-Al_2O_3. The most active catalyst HZSM-5 gives 90% ethene selectivity at 100% DEE conversion at 350 °C; 10% of higher hydrocarbons is also formed [14]. Little has been published, however, on the elimination of DEE over HPA catalysts so far, except for a brief report by Bokade and Yadav [8] on DEE elimination over HPW supported on clay at 150–250 °C with a moderate ethene yield of 58% at 250 °C.

In this work, we investigate the elimination of DEE to ethene and EtOH in the presence of bulk and supported Brønsted solid acid catalysts based on tungsten Keggin HPAs (HPW and HSiW) at a gas-solid interface. Our primary goal is to compare the activity and selectivity of HPA catalysts with that of conventional catalysts such as zeolites and metal oxides. We also

aim to establish a relationship between the turnover activity of HPA catalysts and their acid strength and gain an insight into the reaction mechanism.

5.2. Catalysts and reaction conditions

The Brønsted acid catalysts used in this work included bulk and supported HPA catalysts: (i) bulk HPW, HSiW and acidic heteropoly salt CsPW; and (ii) silica-supported HPW and HSiW with a wide range of HPA loadings from 5.8 to 71%. The emphasis was put on the HPA/SiO_2 catalysts that are most interesting for practical applications. For comparison, HPW supported on TiO_2 and ZrO_2 at a sub-monolayer loading of ~15% were also included. The HPA catalysts were synthesised by wet impregnation of oxide supports (SiO_2, TiO_2 and ZrO_2) with an aqueous HPA solution as described in Section 2.2.2. and dried at 150 °C/10^{-3} kPa for 1.5 h [28,29]. CsPW was prepared using the procedure in the literature [30], which was described in Section 2.2.5. From TGA, the finished catalysts contained 5–7% of H_2O; further drying was not practical because the reaction under study yielded H_2O as a by-product. The HPA catalysts that are studied in this work have been thoroughly characterised previously regarding their texture, structural integrity and acid properties (acid strength and acid site density) using BET analysis, DRIFT spectroscopy and XRD, microcalorimetry and TGA–DSC of NH_3 adsorption, respectively (see Chapter 3 and ref. [28,29,31]). The acid properties of these catalysts together with their texture are summarised in Table 5.1. Tungsten Keggin HPAs are well known to be the purely Brønsted acids, as demonstrated by IR spectroscopy of adsorbed pyridine, with their strength close to super acidity (([18–23] and references therein). The initial enthalpies of NH_3 adsorption on bulk and supported HPW and HSiW catalysts extrapolated to zero NH_3 coverage, ΔH_o, represent the strongest catalyst proton sites. The acid strength of HPA catalysts under study declines in the order HPW > HSiW > CsPW for bulk catalysts and HPW/SiO_2 > HSiW/SiO_2 > HPW/TiO_2 > HPW/ZrO_2 for supported catalysts [28,29]. The acid strength

decreases in the following sequence: SiO_2 > TiO_2 > ZrO_2, which has been attributed to the increasing interaction between the support and HPA [28,29].

Previously, in Chapter 3, it has been shown that the strength of HPA/SiO_2 catalysts increases monotonically with HPA loading up to 100% loading, as illustrated in Figure 3.22 presenting the ΔH_o values from Table 5.1. This trend has been explained by HPA-support interaction reducing the strength of HPA proton sites at lower HPA loadings. From TPD of benzonitrile, there is no strong surface Brønsted acid sites in HSiW/SiO_2 with low HSiW loadings 5–10%; strong acid sites form at higher loadings, probably in the second layer of HSiW on the SiO_2 surface [32].

The conversion of DEE to ethene and EtOH was carried out at 150–250 °C under atmospheric pressure in a Pyrex fixed-bed reactor fitted with on-line GC analysis as explained in detail in Section 2.5.3 (Chapter 2). The DEE pressure was varied from 6–24 kPa [33] by diluting the downstream flow with N_2. The reactor set-up is presented in Figure 2.16.

Prior to reaction, the catalysts (typically 0.20 g) were pre-treated in situ at the reaction temperature for 1 h in N_2 flow. The downstream gas flow was analyzed by the on-line GC to obtain DEE conversion and product selectivity. Each catalyst test was carried out at least twice. Typically, the reactions were conducted for 4 h time on stream (TOS) unless stated otherwise.

Table 5.1. Catalyst characterisation.

Catalyst[a]	Surface area[b] m^2g^{-1}	Pore volume[c] cm^3g^{-1}	Pore diameter[d] Å	$-\Delta H_o$[e] kJ mol^{-1}
ZrO_2	95	0.1	31	
TiO_2	44	0.1	90	
SiO_2	283	1.2	164	
HPW	5.7	0.01	74	203
HSiW	8.01	0.01	68	177
CsPW	130	0.1	27	164
14%HPW/ZrO_2	69	0.1	29	121
15%HPW/TiO_2	46	0.2	164	143
5.8%HPW/SiO_2	265	1.1	161	137
11%HPW/SiO_2	237	1.1	189	166
17%HPW/SiO_2	226	0.9	158	167 [f]
26%HPW/SiO_2	188	0.8	178	167
43%HPW/SiO_2	150	0.6	150	179 [f]
57%HPW/SiO_2	94	0.3	139	185 [f]
5.8%HSiW/SiO_2	259	1.0	150	138
11%HSiW/SiO_2	242	1.0	170	152
14%HSiW/SiO_2	222	1.0	183	152[f]
25%HSiW/SiO_2	191	0.8	167	154 [f]
46%HSiW/SiO_2	143	0.5	146	157
71%HSiW/SiO_2	87	0.3	118	160

[a] HPA loading from ICP-OES analysis. [b] BET surface area. [c] Single point total pore volume at p/p_o = 0.97. [d] Average BET pore diameter. [e] Initial enthalpy of NH_3 adsorption extrapolated to zero NH_3 coverage from NH_3 adsorption microcalorimetry at 150 ºC (±6 kJ mol^{-1}) (Chapter 3, [28,29]). [f] Calculated from Eqs. ((3.2) and (3.3), Chapter 3).

5.3. Diethyl ether elimination: Thermodynamic analysis

The thermodynamic analysis includes determining the Gibbs free energy, equilibrium constant and equilibrium conversion for DEE elimination (Eqs. (5.3) and (5.4)) and EtOH-to-ethene dehydration (Eq. (5.1)) in the ideal gas system at 1 bar pressure. Initial thermodynamic data on

the formation functions $\Delta_f G^o$ and $\Delta_f H^o$, as well as S^o and C_p at standard conditions (298.15 K and 1 bar) are shown in Table 5.2.

$$DEE = EtOH + C_2H_4 \quad \textbf{(5.3)}$$

$$DEE = 2C_2H_4 + H_2O \quad \textbf{(5.4)}$$

$$EtOH = C_2H_4 + H_2O \quad \textbf{(5.1)}$$

Table 5.2. Initial thermodynamic data (298.15 K, 1 bar, ideal gas phase). [a]

Compound	$\Delta_f G^o$ kJ mol^{-1}	$\Delta_f H^o$ kJ mol^{-1}	S^o J mol^{-1}K^{-1}	C_p J mol^{-1}K^{-1}
H_2O	-228.6	-241.8	188.8	33.6
C_2H_4	68.4	52.4	219.3	42.9
EtOH	-167.9	-234.8	281.6	65.6
Et_2O		-252.1	342.7	119.5

[a] CRC Handbook of Chemistry and Physics, 84th ed., 2003–2004.

Equations (5.5–5.10) used for the calculations are given below, where K_p is the equilibrium constant, and x is the equilibrium conversion. ΔC_p was assumed to be independent of temperature, i.e., $\Delta C_p = \Delta C_p^o$. Tables 5.3, 5.4, and 5.5 summarise the results.

$$\Delta H = \Delta H^o + \Delta C_p^o (T - 298.15) \quad \textbf{(5.5)}$$

$$\Delta S = \Delta S^o + \Delta C_p^o \ln (T/298.15) \quad \textbf{(5.6)}$$

$$\Delta G = \Delta H - T\Delta S \quad \textbf{(5.7)}$$

$$K_p = \exp\{-\Delta G/RT\} \quad \textbf{(5.8)}$$

For Eq. (5.1) and (5.3):

$K_p = x^2P/(1-x^2)$, where P is the total pressure (1 bar).

$$x = \sqrt{K_p/(P + K_p)} \quad \textbf{(5.9)}$$

For Eq. (5.4):

$$K_p = \frac{4x^3P^2}{(1-x)(1+2x)^2} \quad \textbf{(5.10)}$$

From this equation, x was calculated by the trial and error method.

Table 5.3. Thermodynamics of DEE elimination (DEE = EtOH + C_2H_4). [a]

T	T	ΔH	ΔS	ΔG	K_p	x
°C	K	kJ mol^{-1}	J mol^{-1}K^{-1}	kJ mol^{-1}	bar	
25	298.15	69.7	158.2	22.53	1.13E-04	0.011
75	348.15	69.2	156.5	14.67	6.30E-03	0.079
125	398.15	68.6	155.0	6.88	1.25E-01	0.334
175	448.15	68.1	153.7	-0.84	1.25E+00	0.746
225	498.15	67.5	152.6	-8.49	7.78E+00	0.941
275	548.15	67.0	151.5	-16.10	3.42E+01	0.986
300	573.15	66.7	151.0	-19.88	6.48E+01	0.992

[a]At 1 bar, ΔC_p^o = -11.0 J mol^{-1}K^{-1}.

Table 5.4. Thermodynamics of EtOH-to-ethene dehydration (EtOH = C_2H_4 + H_2O). [a]

T	T	ΔH	ΔS	ΔG	K_p	x
°C	K	kJ mol^{-1}	J mol^{-1}K^{-1}	kJ mol^{-1}	bar	
25	298.15	45.4	126.5	7.68	4.51E-02	0.208
75	348.15	46.0	128.2	1.37	6.24E-01	0.620
125	398.15	46.5	129.7	-5.14	4.72E+00	0.908
175	448.15	47.0	130.9	-11.66	2.29E+01	0.979
225	498.15	47.6	132.1	-18.21	8.11E+01	0.994
275	548.15	48.1	133.1	-24.86	2.34E+02	0.998
300	573.15	48.4	133.6	-28.17	3.70E+02	0.999

[a]At 1 bar, ΔC_p^o = 10.9 J mol^{-1}K^{-1}.

The DEE dehydration (Eq. (5.4)) is the sum of reactions (5.1) and (5.3). Thermodynamic data for reaction (5.4) were obtained by combining the data from Tables 5.3 and 5.4 and shown in Table 5.5.

Table 5.5. Thermodynamics of DEE dehydration (DEE = $2C_2H_4 + H_2O$).

T	T	ΔH	ΔS	ΔG	K_p	x
°C	K	kJ mol^{-1}	J mol^{-1}K^{-1}	kJ mol^{-1}	bar^2	
25	298.15	115.1	284.7	30.22	5.08E-06	0.016
75	348.15	115.1	284.7	15.98	4.00E-03	0.10
125	398.15	115.1	284.7	1.748	5.90E-01	0.52
175	448.15	115.1	284.7	-12.49	2.85E+01	0.96
225	498.15	115.1	284.6	-26.72	6.33E+02	0.998
275	548.15	115.1	284.6	-40.95	7.99E+03	1.00
300	573.15	115.1	284.6	-48.07	2.40E+04	1.00

From the data in Tables 5.3 and 5.5, the equilibrium composition of ideal gas system containing DEE, EtOH, C_2H_4 and H_2O was calculated. The results are given in Table 5.6.

Table 5.6. Equilibrium composition of ideal gas system containing DEE, EtOH, C_2H_4 and H_2O (mol% based on C_2H_4) as a function of temperature at ambient pressure starting from pure DEE.

T	T	Equilibrium composition				Comment
°C	K	DEE	EtOH	C_2H_4	H_2O	
0	273.15	50.0	0	0	0	
25	298.15	49.0	0.5	0.5	0	from Eq. (5.3)
75	348.15	46.0	1.5	2.5	2.5	from Eqs. (5.3), (5.1)
125	398.15	24.0	0	52.0	26.0	from Eq. (5.4)
175	448.15	2.0	0	96.0	48.0	from Eq. (5.4)
225	498.15	0.1	0	99.8	49.9	from Eq. (5.4)
275	548.15	0	0	100	50	from Eq. (5.4)
300	573.15	0	0	100	50	from Eq. (5.4)

Figure 5.1 shows the composition of an ideal gas system containing DEE, EtOH, C_2H_4 and H_2O at equilibrium as a function of temperature at ambient pressure calculated from thermodynamic data [33]. This diagram represents the DEE elimination system starting from pure DEE. Thermodynamic analysis shows that DEE elimination (Eq. (5.3)) is less favourable than EtOH-to-ethene dehydration (Eq. (5.1)), with ΔG^o = 22.53 kJ mol^{-1} (Table 5.3) and 7.7 kJ mol^{-1} (Table 5.4), respectively. The equilibrium concentration of EtOH is very small and passes a maximum at about 100 ^{o}C (Figure 5.1). Phung and Basca [14] have reported thermodynamic analysis for this system starting from pure EtOH. Our analysis is in agreement with their data.

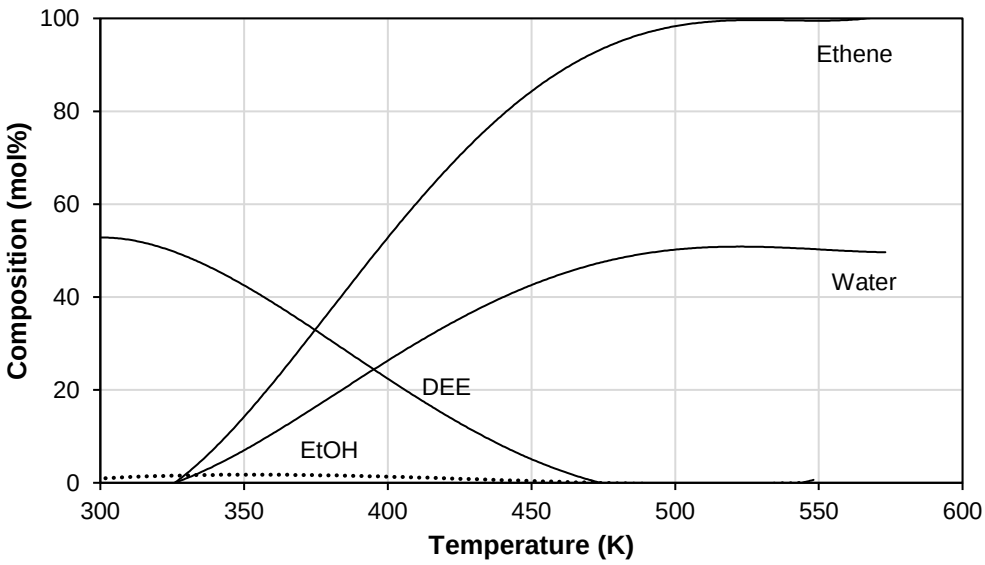

Figure 5.1. Equilibrium composition of an ideal gas system containing DEE, EtOH, C_2H_4 and H_2O as a function of temperature at ambient pressure.

5.4. DEE elimination over HPA catalysts: DEE conversion and product selectivity

Our first goal was to compare the performance of HPA catalysts in the DEE elimination with the most active catalysts reported so far such as zeolites. Since the turnover rates were not available at comparable conditions, we looked at the ethene yields per catalyst weight at comparable space velocities (WHSV).

The HPA catalysts showed stable performance in the elimination of DEE regarding both DEE conversion and product selectivity. Practically no catalyst deactivation was observed at 130–160 ^{o}C, as can be seen from Figure 5.2 showing stable performance of 14%HSiW/SiO_2 catalyst at 160 ^{o}C for 4 h TOS with 12% DEE conversion. Longer term stability tests (20 h TOS) at 200 ^{o}C showed a stable performance of 17%HPW/SiO_2 (Figure 5.3) and CsPW (Figure 5.4) at 70–75% DEE conversion. From combustion chemical analysis of spent catalysts, less than 0.1% coke was formed on the catalysts during these reactions.

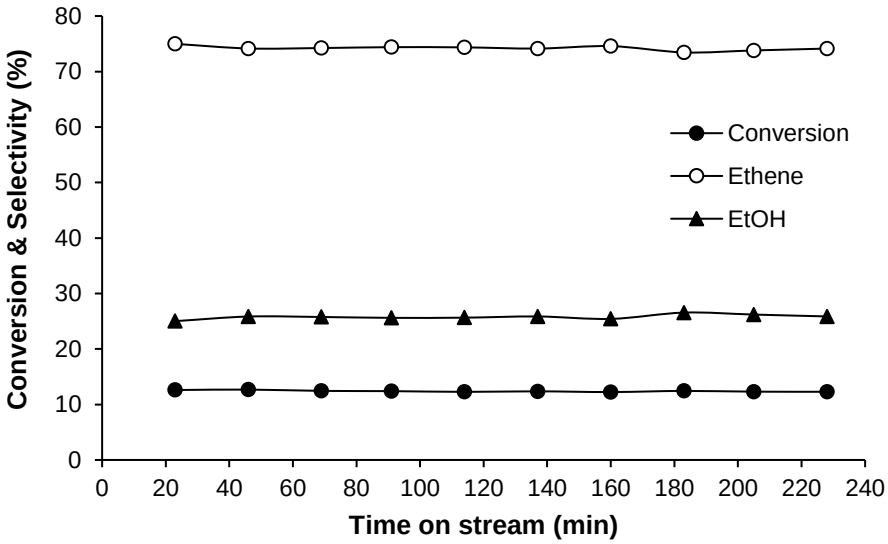

Figure 5.2. Time course for DEE elimination over 14%HSiW/SiO_2 (0.20 g catalyst, 160 ^{o}C, 12 kPa DEE partial pressure, 20 ml min^{-1} flow rate, WHSV = 2.2 h^{-1}).

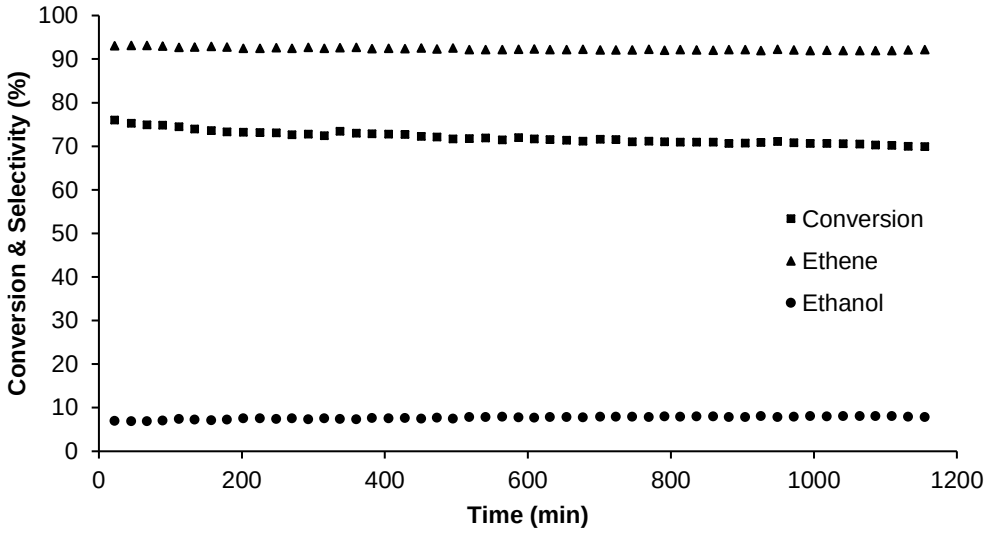

Figure 5.3. Long term stability of DEE elimination over 17%HPW/SiO_2 (0.20 g catalyst, 200 °C, 12 kPa DEE partial pressure, 20 ml min^{-1} N_2 flow rate, WHSV = 2.2 h^{-1}).

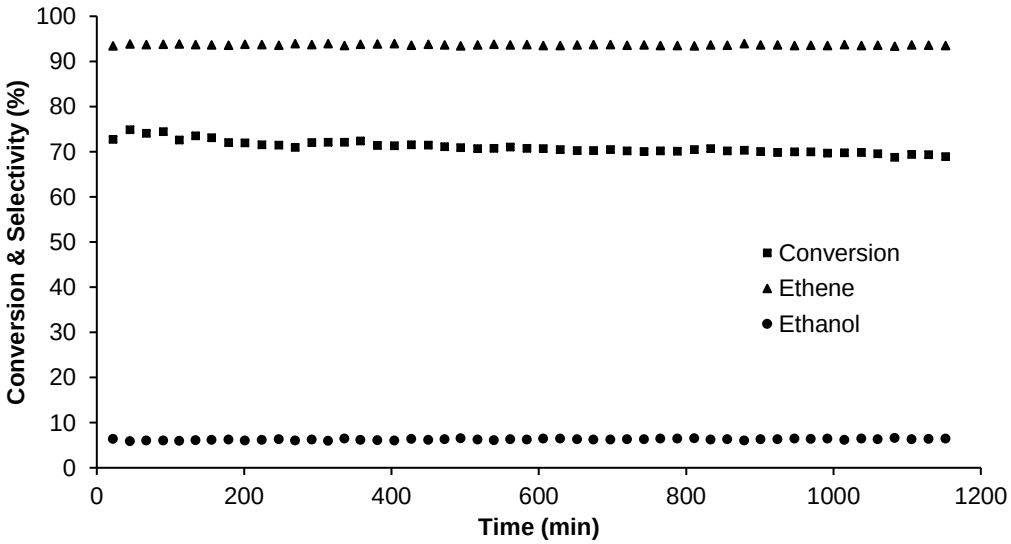

Figure 5.4. Long term stability of DEE elimination over CsPW (0.20 g catalyst, 200 °C, 12 kPa DEE partial pressure, 20 ml min^{-1} N_2 flow rate, WHSV = 2.2 h^{-1}).

Figure 5.5 displays the temperature effect on DEE conversion and product selectivity for bulk and silica-supported HPA catalysts. Only ethene and EtOH were observed among the organic reaction products. As expected from the thermodynamic analysis (Figure 5.1), the DEE conversion and ethene selectivity increase with reaction temperature, both reaching a completion at 220–250 ^{o}C, whereas EtOH selectivity decreases almost to zero. The values of DEE conversion and ethene yield at 220 ^{o}C are presented in Table 5.7. The most active HPA catalysts, CsPW, 17%HPW/SiO_2 and 14%HSiW/SiO_2, give 95, 97 and 98% ethene yield, respectively, at 97–99% DEE conversion at a space velocity WHSV = 2.2 h^{-1}. These HPA catalysts outperform the best reported zeolite catalysts [14]. Thus HZSM-5 (Si/Al = 140 mol/mol) and USY (Si/Al = 15 mol/mol) give 90 and 97% ethene yield at almost 100% conversion at 350 ^{o}C and ambient pressure [14], i.e. at a more than 100 ^{o}C higher temperature compared to the HPA catalysts. These results have been obtained at a higher WHSV = 10.4 h^{-1} [14], but the space velocity has a relatively small effect on the ethene yield at this temperature [14]. γ-Al_2O_3 and SiO_2-Al_2O_3 have been found to be less efficient than HZSM-5 and USY [14]. Previously, DEE elimination over 30%HPW/montmorillonite has been reported to give 58% ethene yield at 68% DEE conversion at 250 ^{o}C, ambient pressure and WHSV = 1.6 h^{-1} [8]. The low activity of this catalyst can be attributed to a rather basic clay support. Basic and amphoteric supports such as MgO and Al_2O_3 are known to decrease the acidity of HPAs and may even cause disintegration of HPA structure [19–21]. Silica is most frequently used for supporting HPAs because of its inertness and availability in a wide textural variety [19–21,34].

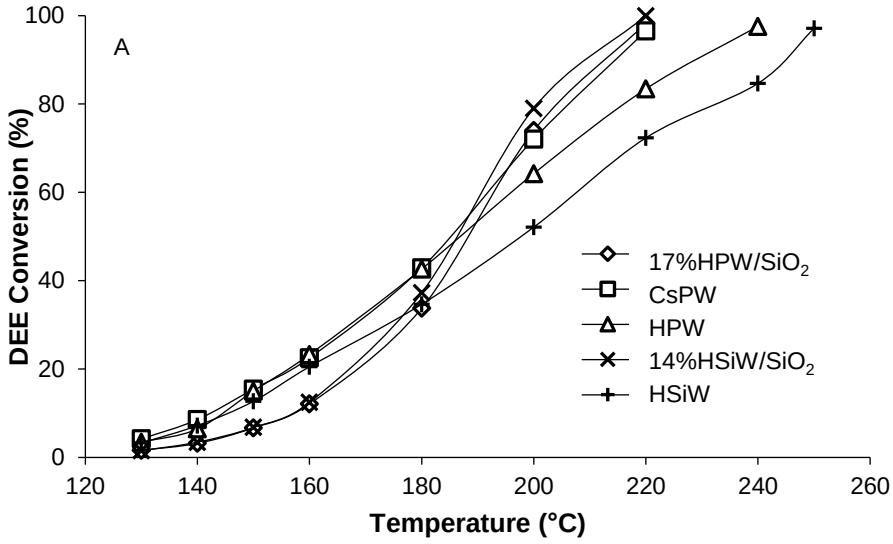
A
DEE Conversion (%)
Temperature (°C)
17%HPW/SiO2
CsPW
HPW
14%HSiW/SiO2
HSiW

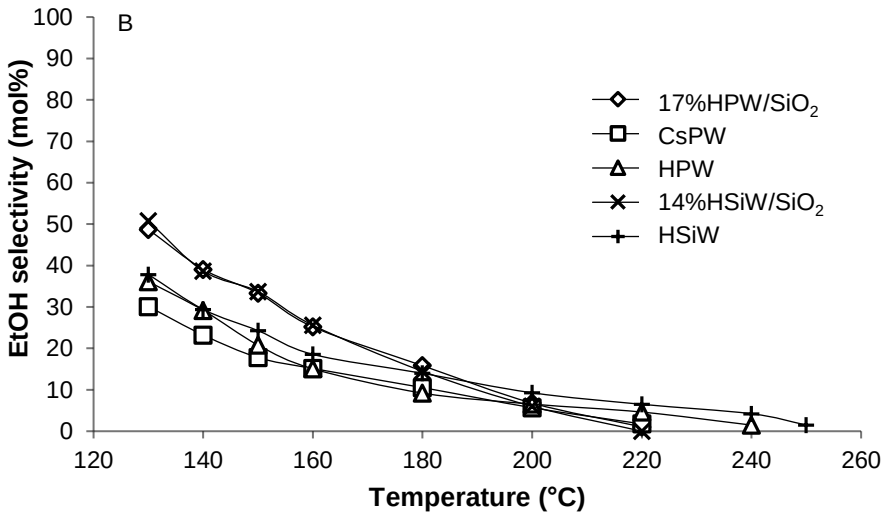
B
EtOH selectivity (mol%)
Temperature (°C)
17%HPW/SiO2
CsPW
HPW
14%HSiW/SiO2
HSiW

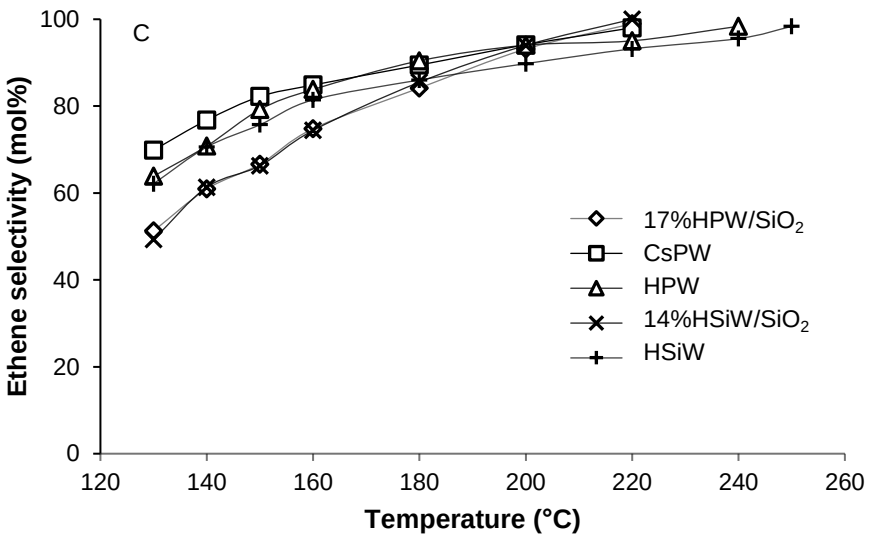

Figure 5.5. Effect of temperature on DEE conversion (A), EtOH selectivity (B) and ethene selectivity (C) (0.20 g catalyst, 12 kPa DEE partial pressure, 20 ml min^{-1} N_2 flow rate, 4 h TOS).

Table 5.7. DEE conversion and ethene yield.[a]

Catalyst	14%HSiW/SiO_2	17%HPW/SiO_2	CsPW	HPW	HSiW
DEE conversion, %	99	98	97	83	72
C_2H_4 yield, %	98	97	95	79	67

[a] 220 °C, 12 kPa DEE partial pressure, 20 ml min^{-1} flow rate, 0.20 g catalyst, WHSV = 2.2 h^{-1} (for HPW and HSiW, 0.30 g catalyst, WHSV = 1.5 h^{-1}). Proton site densities for these catalysts are given in Table 5.9.

5.5. Kinetics of DEE elimination

Kinetics of DEE elimination was studied at differential conditions (DEE conversion 2–12%), 130–160 °C and 6–24 kPa DEE partial pressure. The reactions were conducted for 4 h TOS, with practically no catalyst deactivation observed (Figure 5.2). Comparison of data in Figure 5.5 with thermodynamic data in Figure 5.1 shows that the reaction system was far from

equilibrium at 130–160 ºC. Thus, at 150 ºC (423 K), the equilibrium conversion of DEE is ~90% (Figure 5.1), whereas in our reaction system it was 7–15% (Figure 5.5 A).

For all HPA catalysts the reaction was found to be zero order in DEE as illustrated in Figure 5.6 for 14%HSiW/SiO_2, where the rate of DEE conversion remains almost constant (0.0020–0.0024 mol $g^{-1}h^{-1}$) at a 5-fold variation of DEE partial pressure (5–25 kPa). Close to zero-order logarithmic plots for all HPA catalysts are presented in Figures 5.7 and 5.8, with the order in DEE varying from -0.05 to 0.14. Assuming Langmuir-type kinetics, this would indicate that the active sites in HPA catalysts were saturated with adsorbed DEE molecules.

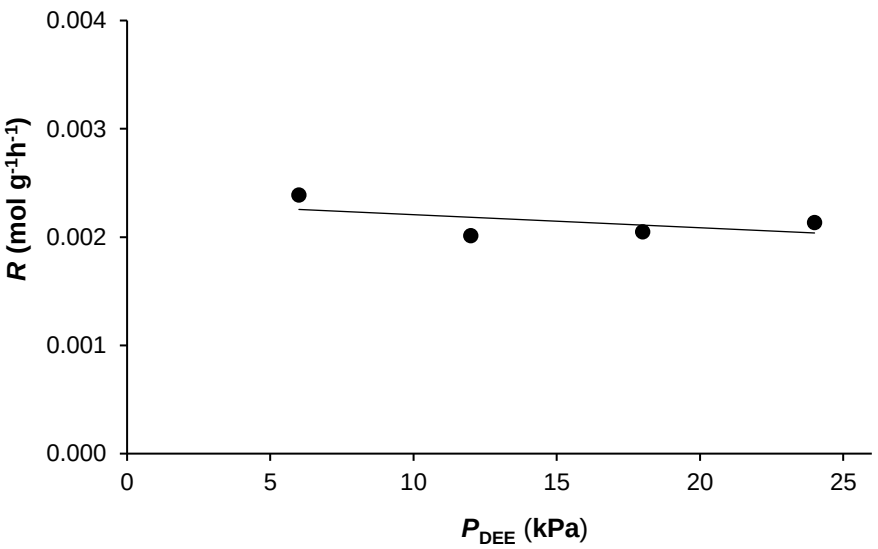

Figure 5.6. Effect of DEE partial pressure on the rate of DEE elimination over 14%HSiW/SiO_2 (0.20 g catalyst, 150 °C, 20 ml min^{-1} flow rate, 4 h TOS).

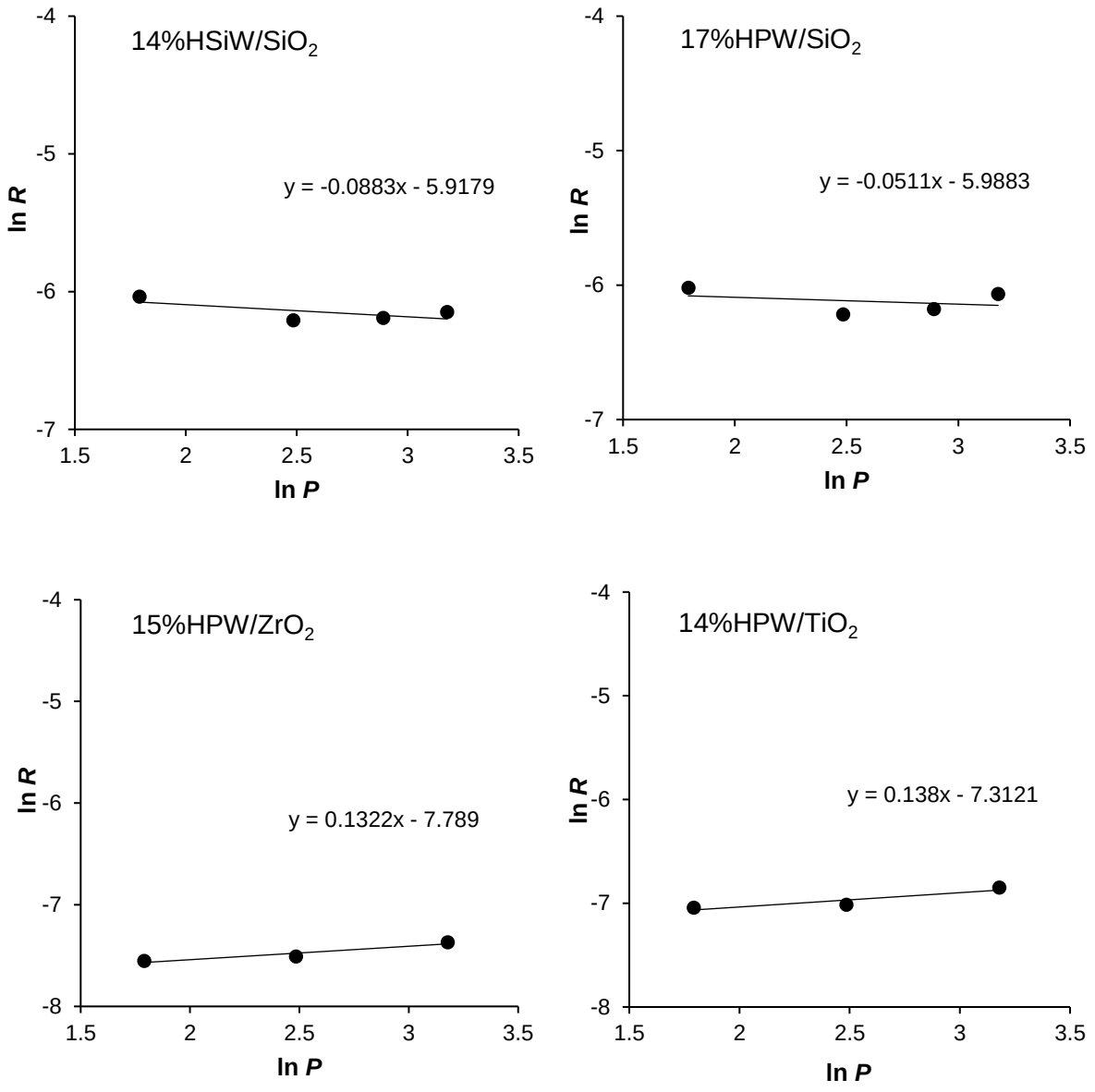

Figure 5.7. Logarithmic plot of reaction rate *R* (mol $g^{-1}h^{-1}$) vs. DEE partial pressure *P* (kPa) for DEE elimination at 150 ^{o}C and 20 ml min^{-1} flow rate over: 17%HPW/SiO_2 (0.20 g), 14%HSiW/SiO_2 (0.20 g), 14%HPW/TiO_2 (0.20 g), 15%HPW/ZrO_2 (0.20 g).

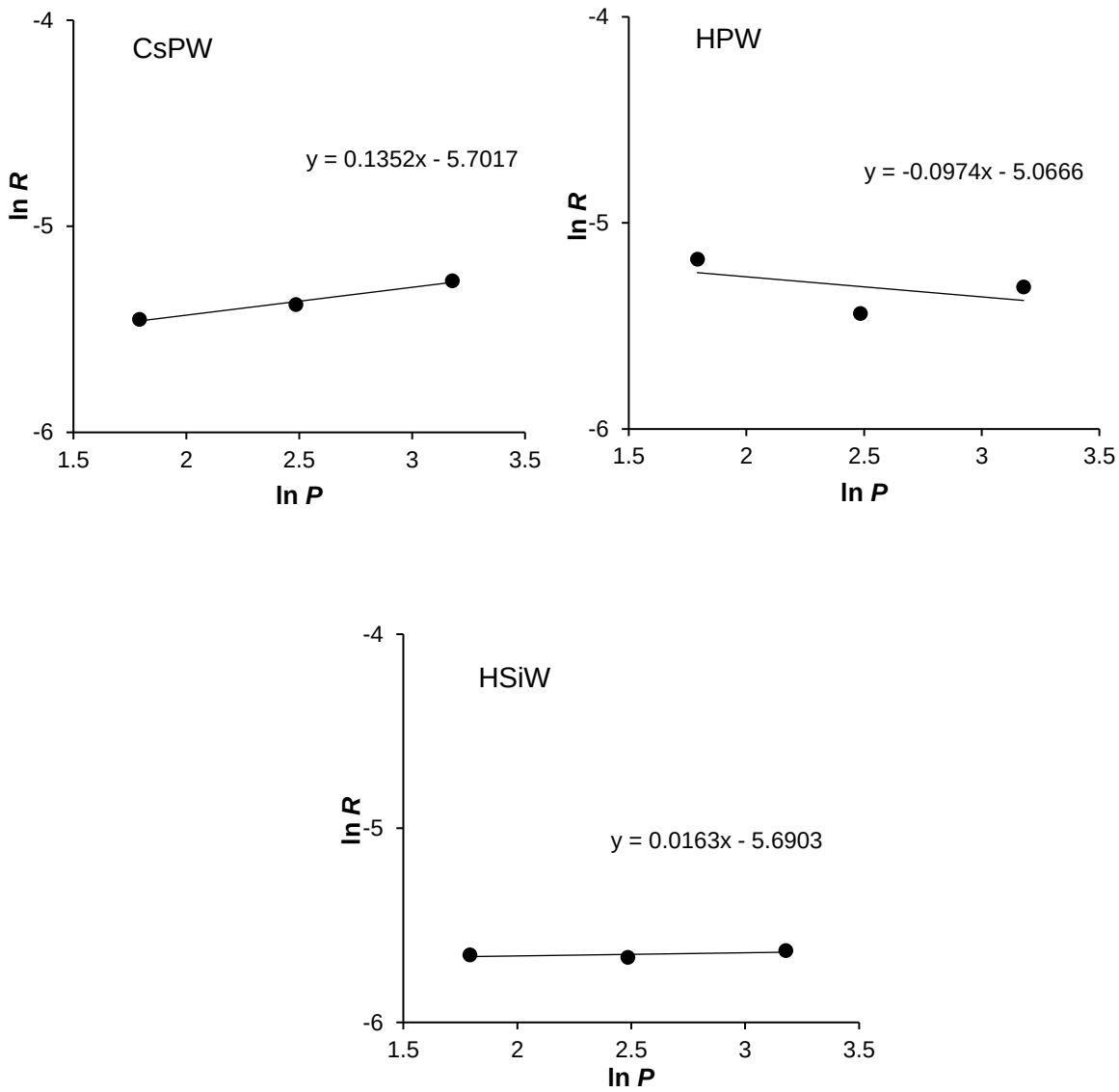

Figure 5.8. Logarithmic plot of reaction rate R (mol $g^{-1}h^{-1}$) vs. DEE partial pressure P (kPa) for DEE elimination at 150 ^{o}C and 20 ml min^{-1} flow rate over: CsPW (0.20 g), HPW (0.30 g) and HSiW (0.30 g).

Figure 5.9 shows the Arrhenius plots for bulk and silica-supported HPA catalysts. The activation energies (E) obtained were in the range of 69.5–101.5 kJ mol^{-1} (Table 5.8). Given zero reaction order in DEE, the observed activation energies are the true value E. For HPW supported on montmorillonite, E = 80.6 kJ mol^{-1} has been reported [8]. The high E values and zero order in DEE indicate that the reactions were not affected by diffusion limitations. Additionally, the Weisz-Prater analysis supports the absence of internal diffusion limitations

[35]. For example, for 17%HPW/SiO_2 at 150 °C, Weisz-Prater criterion was determined to be $C_{WP} = 1.1 \cdot 10^{-4} << 1$ indicating no internal diffusion limitations (see Appendix for details).

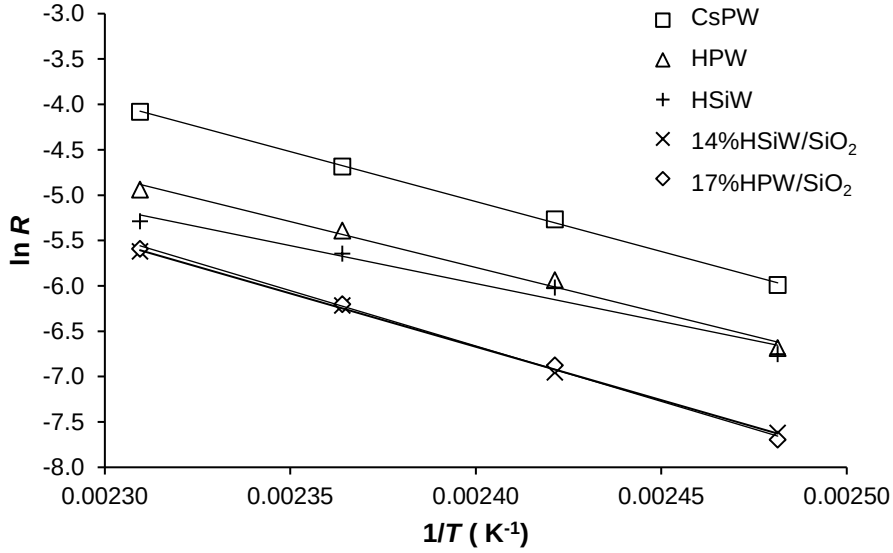

Figure 5.9. Arrhenius plot for DEE elimination over HPA catalysts (0.055–0.20 g catalyst amount, 12 kPa DEE partial pressure, 20 ml min^{-1} flow rate, WHSV = 2.2–8.0 h^{-1}, 130–160°C temperature range; *R* is the reaction rate in mol $g^{-1}h^{-1}$).

Table 5.8. Activation energies for HPA catalysts.[a]

Catalyst	17%HPW /SiO_2	14%HSiW/SiO_2	CsPW	HPW	HSiW
E, kJ mol^{-1}	101.5	97.8	91.5	84.1	69.5

[a] At 130–160 °C, 12 kPa DEE partial pressure, 20 ml min^{-1} flow rate, 0.055–0.20 g catalyst (WHSV = 2.2–8.0 h^{-1}).

Assuming that in overall DEE-to-ethene conversion the E2 elimination of DEE to ethene and EtOH (Eq. (5.3), Scheme 5.1) is an irreversible rate-limiting step, with equilibrated re-adsorption of EtOH, followed by irreversible EtOH dehydration (Eq. (5.1)), with no re-adsorption of products occurring, the observed DEE conversion rate is given by Langmuir-type equation (5.11) [15,36]:

$$R = \frac{kK_D[\mathrm{H}^+]P_D}{1+K_EP_E+K_DP_D} \quad \textbf{(5.11)}$$

Here, K_E and K_D are the equilibrium constants for EtOH and DEE adsorption on Brønsted acid sites, respectively, k is the rate constant of the rate-limiting step, $[H^+]$ is the accessible proton sites density in catalyst, P_E and P_D are the partial pressures of EtOH and DEE. At high P_D, when the active sites of the catalyst are saturated with the ether, the reaction becomes zero order in DEE, i.e., $R = k[H^+]$, in agreement with experimental data. From this data the values of turnover frequency (TOF) can be obtained as $R/[H^+]$ (see below).

5.6. Mechanistic considerations

Misono et al. [18] proposed two types of mechanism for heterogeneous acid catalysis by HPA - surface type and bulk type mechanisms. The surface type is the conventional acid catalysis involving proton sites at the surface of HPA. The bulk type (bulk type I [18]) is suggested to operate in the case of bulk HPAs with polar reactants, such as lower alcohols, ketones, ethers, etc., which are capable of being absorbed in large quantities into catalyst bulk in the interstitial space between heteropoly anions. In this case, all HPA protons, both bulk and surface ones, are thought to be accessible so that reaction occurs pseudo-homogeneously, and its rate should scale with the total number of protons or HPA weight. Bulk type catalysis has been demonstrated for MeOH dehydration over bulk HPW in a static system [20,37,38]. However, as Moffat argued [20], bulk type reaction via substrate absorption into the interstitial space would be almost inevitably diffusion-hindered in a steady-state flow system. In contrast, nonpolar reactants, e.g., hydrocarbons, that cannot penetrate HPA bulk react via the surface type mechanism [18].

DEE is a relatively polar solvent, which readily dissolves HPAs such as HPW and HSiW and is capable of absorbing into the bulk of HPA crystallites. Hypothetically, DEE might react with bulk HPA and high-loaded HPA/SiO_2 catalysts via the bulk-type mechanism.

Therefore, here we attempted to gain an insight into the DEE elimination mechanism over HPA/SiO_2 catalysts concerning the possibility of bulk-type versus surface-type catalysis.

With silica-supported HPAs at low and medium HPA loadings, both polar and nonpolar substrates typically react via the surface type catalysis, showing similar dependencies between catalyst activity and HPA loading - the activity, expressed as substrate conversion or reaction rate per total HPA/SiO_2 catalyst weight, increases with HPA loading at a constant HPA/SiO_2 catalyst weight, reaching a plateau at 25–40% loading, or passes a maximum [21,32,39]. This is the result of a trade-off between the density of surface proton sites and their strength at varying HPA loading. The proton site density (per total catalyst weight) passes a maximum at a medium HPA loading due to the sharp decrease in catalyst surface area to less than 10 m^2g^{-1} for bulk HPA (Chapter 3 [32]), whereas the acid strength increases monotonically with HPA loading (Figure 3.22). Using the TPD of benzonitrile, which interacts only with the surface acid sites in HPA, the amount of strong surface Brønsted sites in HSiW/SiO_2 has been found to pass a maximum at a HSiW loading of ~50% (Figure 5.10) [32]

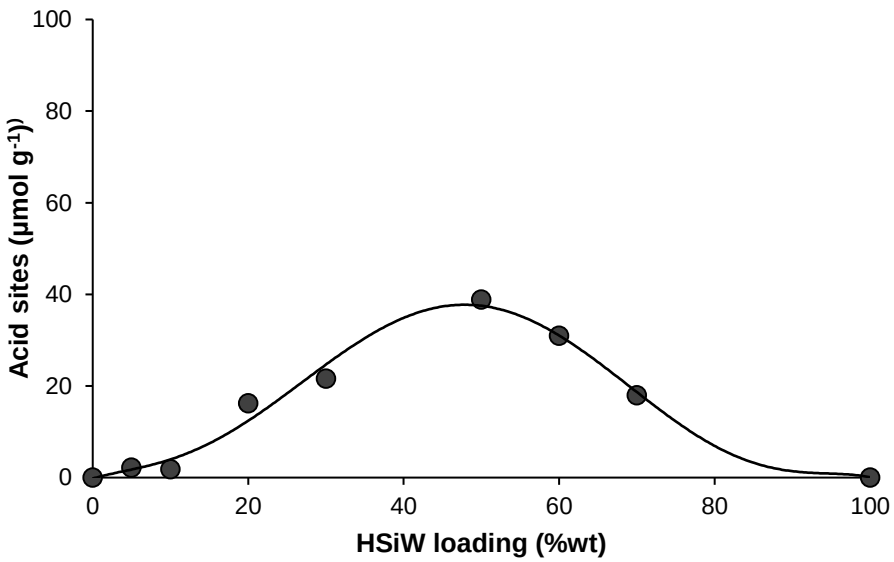

Figure 5.10. The amount of strong surface Brønsted sites in HSiW/SiO_2 as a function of HSiW loading from TPD of benzonitrile (adapted from [32]).

For the surface-type mechanism, in the case of reactions less demanding towards catalyst acid strength, the activity of supported HPA is expected to scale with the proton surface site density passing a maximum as the HPA loading increases. Such dependence has been observed for the dehydration of MeOH and EtOH over HPA/SiO_2 at 120 ^oC, which suggests the surface type mechanism in the whole range of HPA loading including high-loaded and bulk HPA catalysts (Chapter 4). Figure 5.11, compiled from the data in Chapter 4, shows that the rate of MeOH dehydration per HPA/SiO_2 catalyst weight passes a maximum as the HPA loading increases from 0 to 100% at a constant catalyst weight, whereas the rate per HPA weight decreases in parallel with decreasing the surface proton sites number per HPA weight, as expected for the surface type catalysis. The surface type mechanism for MeOH and EtOH dehydration is also supported by Brønsted relation between the catalyst activity and acid strength, which holds for both bulk HPAs and other catalysts operating via the surface type mechanism (oxide-supported HPAs with sub-monolayer HPA loadings, CsPW and zeolites (Chapter 4) [29].

On the other hand, for more demanding reactions, for example, the isomerisation of cycloalkanes over HPW/SiO_2 occurring at 300 ^oC via the surface type mechanism, the activity tends to plateau at higher HPW loadings due to the competing effect of increasing proton site strength [20,40]. Contrary to the surface type, for the bulk type one, the rate per total catalyst weight is expected to increase with HPA loading, whereas the rate per HPA weight should remain approximately constant at varying HPA loading.

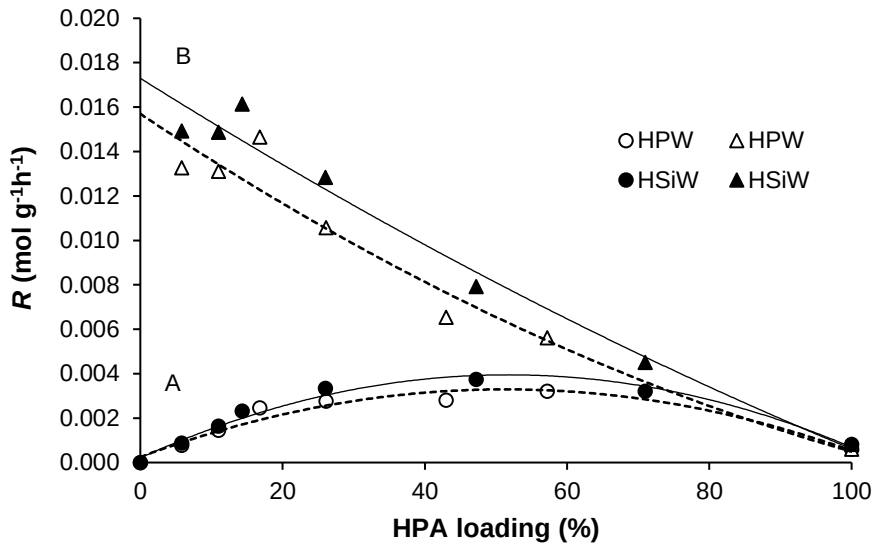

Figure 5.11. Plot of MeOH dehydration rate per total HPA/SiO_2 catalyst weight (A, open and closed circles) and per HPA weight (B, open and closed triangles) versus HPA loading (120 ^oC, WHSV = 0.30 h^{-1}) (Chapter 4).

Figure 5.12 shows the rate of DEE elimination per total HPA/SiO_2 catalyst weight as a function of HPA loading for HPW/SiO_2 and HSiW/SiO_2 catalysts at 150 ^oC. The rate increases with HPA loading up to about 25% loading and levels off at higher loadings. As seen, this plot is somewhat different from that for MeOH dehydration (Figure 5.11). In fact, it is as expected for the surface type mechanism for the more demanding DEE elimination occurring at 150 ^oC (less demanding MeOH dehydration occurs at 120 ^oC). The rate of DEE elimination per HPA weight decreases with increasing HPA loading (Figure 5.12 B), as for MeOH dehydration. Therefore, these results are consistent with DEE elimination occurring via the surface type mechanism in the whole range of HPA loading including high-loaded and bulk HPA catalysts. This cannot completely rule out the participation of bulk protons located near the surface of HPA, but these do not seem to play a significant role. This conclusion is further strengthened by Brønsted relation between the catalyst activity and acid strength (see below).

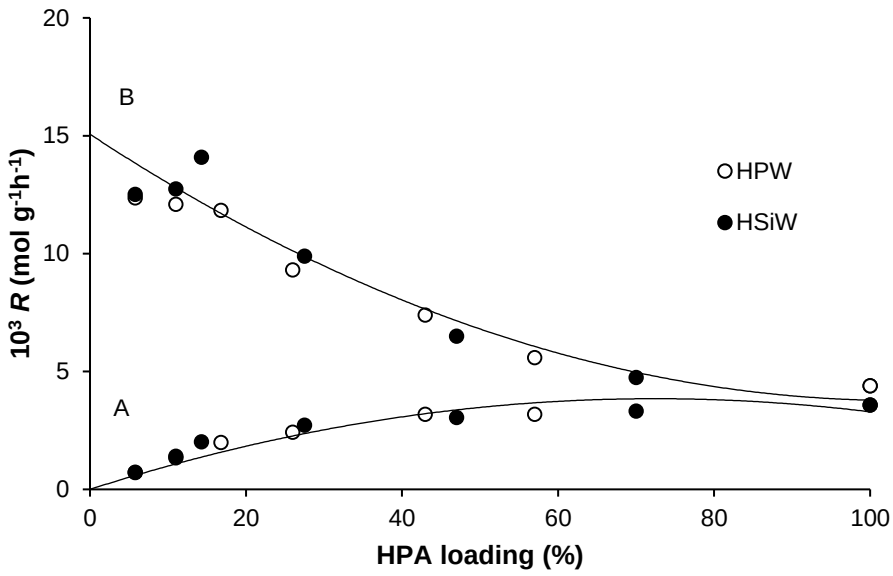

Figure 5.12. Plot of DEE elimination rate per total HPA/SiO_2 catalyst weight (A) and per HPA weight (B) versus HPA loading (0.20 g catalyst, 150 ^{o}C, 12 kPa DEE partial pressure, 20 ml min^{-1} flow rate).

It is worth noting that HPW and HSiW catalysts exhibit very close activity per catalyst weight over the whole range of HPA loading (Figure 5.12) despite HPW catalysts having stronger acid sites than HSiW ones (Table 5.1). This may be explained by the higher proton surface site density in HSiW catalysts due to the larger number of protons per Keggin unit and higher HSiW dispersion on the silica surface compared to HPW catalysts (see Chapter 3). Nevertheless, the turnover activity (TOF) of HPW catalysts was found greater than that of HSiW ones as expected from their acid strength (see below).

Figure 5.13 presents the data shown in Figure 5.12 from a different angle - as product selectivity versus DEE conversion. Both HPW/SiO_2 and HSiW/SiO_2 catalysts give practically the same ethene and EtOH selectivities. As the DEE conversion increases with increasing HPA loading, the selectivity to ethene grows at the expense of EtOH. Importantly, the extrapolation to zero conversion gives a 50:50 ethene/EtOH selectivity, which shows that the initial reaction step is DEE → C_2H_4 + EtOH. This demonstrates that the whole DEE-to-ethene process occurs

through a consecutive pathway: DEE → C_2H_4 + EtOH followed by EtOH → C_2H_4 + H_2O, where ethene is both a primary product of DEE elimination and a secondary product via dehydration of the primary product EtOH. The mechanism of ethene formation from EtOH dehydration is still debated ([13] and references therein). DEE forms in EtOH dehydration at low temperatures, whereas ethene forms at higher temperatures. The question is whether the ethene forms directly from EtOH or via DEE elimination or both [13]. Our results, therefore, show that ethene can form via the DEE elimination.

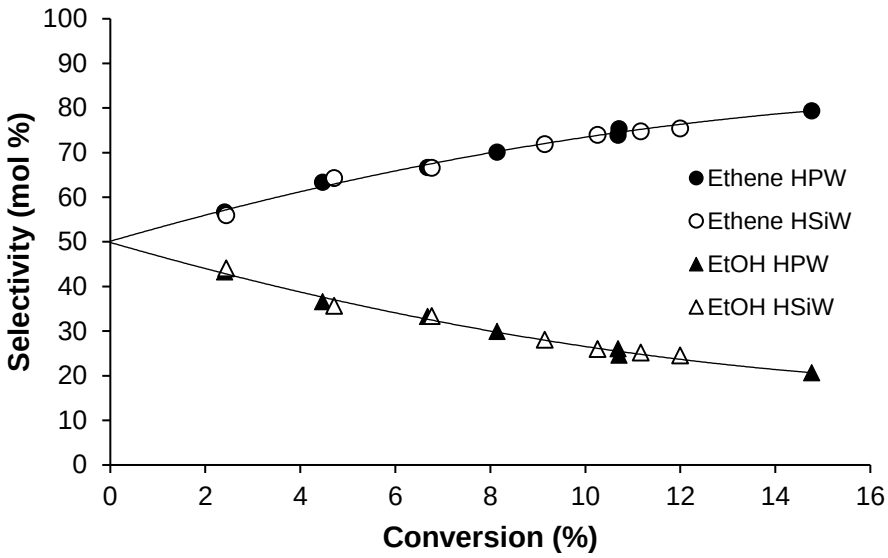

Figure 5.13. Plot of product selectivity versus DEE conversion for HPA/SiO_2 catalysts with HPA loading varied from 5.8 to 100% (0.20 g catalyst, 150 ^oC, 12 kPa DEE partial pressure, 20 ml min^{-1} flow rate).

5.7. Relationship between turnover rate and catalyst acid strength

Table 5.9 shows the density of catalyst surface proton sites and TOF values for the elimination of DEE at 150 ^oC for all the HPA catalysts studied including bulk catalysts (HPW, HSiW and CsPW) and supported catalysts at a sub-monolayer HPA loading of 14–17%. The TOF values were calculated per surface proton site from zero-order kinetics as $R/[H^+]$. The densities of

surface proton sites were evaluated as defined elsewhere (Chapter 4, [28,29]). For supported HPA catalysts with sub-monolayer HPA coverage, all stoichiometric HPA protons were assumed to be equally accessible for reaction. This is supported by NH_3 adsorption calorimetry [41] and titration with di-tert-butylpyridine [25]. For bulk catalysts, HPW, HSiW and CsPW, the number of surface protons was estimated using a Keggin unit cross section of 144 $Å^2$ and the catalyst surface areas from Table 5.1 with the stoichiometric number of protons per Keggin unit [18–21]. The TOF values thus obtained should be regarded as an approximation since the number of accessible protons could differ from the stoichiometric numbers used in the calculations. The TOF values thus calculated range from 4.3 h^{-1} for 14%HPW/ZrO_2 to 170 h^{-1} for bulk HPW demonstrating a strong impact of catalyst acid strength on the turnover reaction rate, as can be seen from the ΔH_o values for these catalysts.

Table 5.9. Proton site density and turnover frequency for HPA catalysts.

Catalyst	$[H^+]^a$ mmol g^{-1}	TOF[b] h^{-1}	$-\Delta H_o$[c] kJ mol^{-1}
HPW	0.0198	170	203
HSiW	0.0369	65	177
CsPW	0.0750	53	164
17%HPW/SiO_2	0.1751	13	167
14%HSiW/SiO_2	0.1946	11	152
15%HPW/TiO_2	0.1521	6.9	143
14%HPW/ZrO_2	0.1458	4.3	121

[a] Density of surface proton sites per total catalyst weight. [b] TOF per surface proton site at 150 °C, 24 kPa DEE partial pressure, 20 ml min^{-1} flow rate. [c] Initial enthalpy of NH_3 adsorption from NH_3 adsorption microcalorimetry at 150 °C (±6 kJ mol^{-1}) (Chapter 4 [28,29]).

Figure 5.14 shows a Brønsted linear relation between the turnover activity of HPA catalysts in DEE elimination, ln (TOF), and their acid strength determined from initial enthalpy of NH_3 adsorption, ΔH_o. Both parameters were determined at the same temperature of 150 °C

and similar flow conditions. As seen, the relation holds for the bulk HPAs as well as for the oxide-supported HPAs - all being the Brønsted acid catalysts. This implies that Brønsted acid sites play a vital role in the elimination of DEE over HPA catalysts. It also implies the same reaction mechanism for the whole series of catalysts involved [42]. Since this relation holds for the oxide-supported HPAs with sub-monolayer HPA loadings and CsPW operating via the surface-type mechanism, on the one hand, and for the bulk HPAs, on the other, it suggests that the bulk HPW and HSiW would also largely operate through the mechanism of surface catalysis, in agreement with our conclusion in Section 5.6.

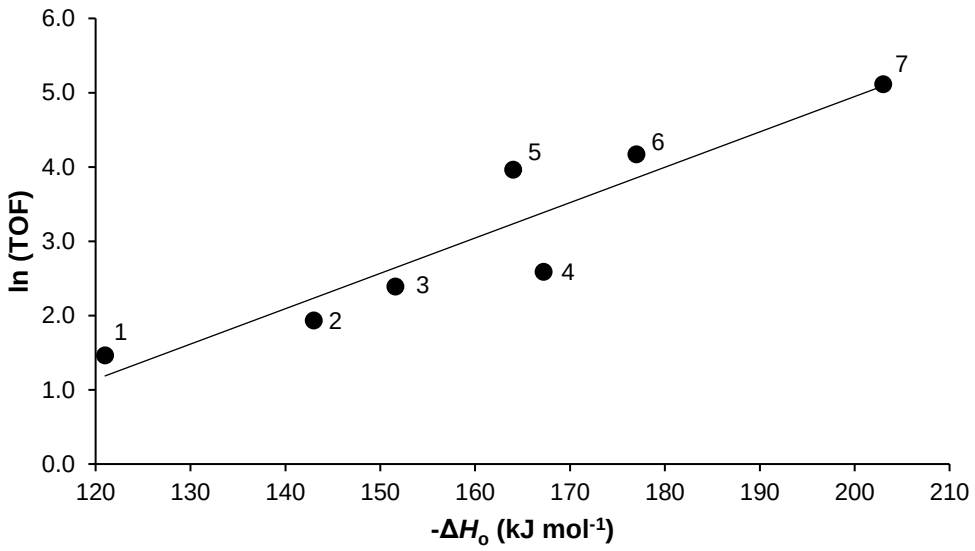

Figure 5.14. Plot of ln (TOF) for DEE elimination (TOF in h^{-1}) over HPA catalysts versus initial heat of NH_3 adsorption (150 ^oC, 0.20 g catalyst, 24 kPa DEE partial pressure, 20 ml min^{-1} flow rate): (1) 14%HPW/ZrO_2, (2) 15%HPW/TiO_2, (3) 14%HSiW/SiO_2, (4) 17%HPW/SiO_2, (5) CsPW, (6) HSiW, (7) HPW.

5.8. Conclusions

Diethyl ether (DEE) is the key intermediate of EtOH-to-ethene dehydration. In the presence of acid catalysts, DEE undergoes elimination to produce ethene and EtOH; the latter dehydrates

to ethene. Knowledge about the elimination of DEE can shed the light on the mechanism of the EtOH-to-ethene dehydration and help to optimise the production of ethene.

In this work, the elimination of DEE has been examined at a gas-solid interface over a various bulk and supported Brønsted solid acid catalysts based on tungsten Keggin HPAs in a fixed-bed reactor at 130–250 °C and ambient pressure. The most active HPA catalysts are silica-supported HPW and HSiW and bulk heteropoly salt CsPW giving 95–98% ethene yield at 220 ^{o}C and WHSV = 2.2 h^{-1}. The HPA catalysts outperform the best reported zeolite catalysts such as HZSM-5 and USY, which give the same yield but at temperatures about 100 ^{o}C higher compared to the HPA catalysts.

A Brønsted correlation between the turnover catalyst activity and the acid strength of catalyst has been established, which indicates that Brønsted acid sites play a significant role in the elimination of DEE over HPA catalysts. The results obtained point to the DEE conversion occurring through the consecutive reaction pathway: DEE → C_2H_4 + EtOH followed by EtOH → C_2H_4 + H_2O, where ethene is both a primary product of DEE elimination and a secondary product via dehydration of the primary product EtOH. Evidence is provided that DEE elimination over bulk HPA and high-loaded HPA/SiO_2 catalysts proceeds via the surface-type mechanism.

References

[1] D. Fan, D-J. Dai, H-S. Wu, Ethylene formation by catalytic dehydration of ethanol with industrial considerations, Materials 6 (2013) 101–115.

[2] J.M.R. Gallo, J.M.C. Bueno, U. Schuchardt, Catalytic transformations of ethanol for biorefineries, J. Braz. Chem. Soc. 25 (2014) 2229–2243.

[3] A. Corma, S. Iborra, A. Velty, Chemical routes for the transformation of biomass into chemicals, Chem. Rev. 107 (2007) 2411–2502.

[4] T. Doğu, D. Varişli, Alcohols as alternatives to petroleum for environmentally clean fuels and petrochemicals, Turkish J. Chem. 31 (2007) 551–567.

[5] S. Golay, L. Kiwi-minsker, R. Doepper, A. Renken, Influence of of the catalyst acid/base properties on the catalytic ethanol dehydration under steady state and dynamic conditions. In situ surface and gas-phase analysis, Chem. Eng. Sci. 54 (1999) 3593–3598.

[6] T. Zaki, Catalytic dehydration of ethanol using transition metal oxide catalysts, J. Colloid Interface Sci. 284 (2005) 606–613.

[7] D. Varisli, T. Dogu, G. Dogu, Silicotungstic acid impregnated MCM-41-like mesoporous solid acid catalysts for dehydration of ethanol, Ind. Eng. Chem. Res. 47 (2008) 4071–4076.

[8] V.V. Bokade, G.D. Yadav, Heteropolyacid supported on montmorillonite catalyst for dehydration of dilute bio-ethanol, Appl. Clay Sci. 53 (2011) 263–271.

[9] A. Ciftci, D. Varisli, K. Cem, N.A. Sezgi, T. Dogu, Dimethyl ether, diethyl ether & ethylene from alcohols over tungstophosphoric acid based mesoporous catalysts, Chem. Eng. J. 207–208 (2012) 85–93.

[10] Takahara, M. Saito, M. Inaba, K. Murata, Dehydration of ethanol into ethylene over solid acid catalysts, Catal. Lett.105 (2005) 249–252.

[11] K. Yasunaga, F. Gillespie, J.M. Simmie, H.J. Curran, Y. Kuraguchi, H. Hoshikawa, M. Yamane, Y. Hidaka, A multiple shock tube and chemical kinetic modeling study of diethyl ether pyrolysis and oxidation, J. Phys. Chem. A 114 (2010) 9098–9109.

[12] K. Ramesh, Y.L.E. Goh, C.G. Gwie, C. Jie, T.J. White, A. Borgna, Ethanol dehydration activity on hydrothermally stable LaP_xO_y catalysts synthesized using CTAB template, J. Porous Mater. 19 (2012) 423–431.

[13] M.A. Christiansen, G. Mpourmpakis, D.G. Vlachos, Density functional theory-computed mechanisms of ethylene and diethyl ether formation from ethanol on γ-Al_2O_3(100), ACS Catal. 3 (2013) 1965–1975.

[14] T.K. Phung, G. Busca, Diethyl ether cracking and ethanol dehydration: Acid catalysis and reaction paths, Chem. Eng. J. 272 (2015) 92–101.

[15] J.F. DeWilde, A. Bhan, Kinetics and site requirements of ether disproportionation on γ-Al_2O_3, Appl. Catal. A: Gen. 502 (2015) 361–369.

[16] G. Garbarino, R. Prasath, P. Vijayakumar, P. Riani, E. Finocchio, G. Busca, R. Prasath Parameswari Vijayakumar, P. Riani, E. Finocchio, G. Busca, Ethanol and diethyl ether catalytic conversion over commercial alumina and lanthanum-doped alumina: Reaction paths, catalyst structure and coking, Appl. Catal. B: Environ. 236 (2018) 490–500.

[17] J. Haber, K. Pamin, L. Matachowski, B. Napruszewska, J. Połtowicz, Potassium and silver salts of tungstophosphoric acid as catalysts in dehydration of ethanol and hydration of ethylene, J. Catal. 207 (2002) 296–306.

[18] T. Okuhara, N. Mizuno, M. Misono, Catalytic Chemistry of Heteropoly Compounds, in: D.D. Eley, Werner O. Haag, Bruce Gates (Eds.), Advances in Catalysis, Vol. 41, Academic Press, 1996: pp. 113–252.

[19] I.V. Kozhevnikov, Catalysis by heteropoly acids and multicomponent polyoxometalates in liquid-phase reactions, Chem. Rev. 98 (1998) 171–198.

[20] J.B. Moffat, Metal-Oxygen Clusters the Surface and Catalytic Properties of Heteropoly Oxometalates, Kluwer Academic Publishers, New York, 2002.

[21] I.V. Kozhevnikov, Catalysts for Fine Chemical Synthesis Catalysis by Polyoxometalates, Vol. 2, John Wiley, Chichester, England, 2002.

[22] M. Misono, A view on the future of mixed oxide catalysts The case of heteropoly acids (polyoxometalates) and perovskites, Catal. Today 100 (2005) 95–100.

[23] I.V. Kozhevnikov, Heterogeneous acid catalysis by heteropoly acids: Approaches to catalyst deactivation, J. Mol. Catal. A: Chem. 305 (2009) 104–111.

[24] W. Alharbi, E. Brown, E.F. Kozhevnikova, I.V. Kozhevnikov, Dehydration of ethanol over heteropoly acid catalysts in the gas phase, J. Catal. 319 (2014) 174–181.

[25] W. Knaeble, E. Iglesia, Kinetic and theoretical insights into the mechanism of alkanol dehydration on solid Brønsted acid catalysts, J. Phys. Chem. C 120 (2016) 3371–3389.

[26] H. Noller, P. Andréu, M. Hunger, The mechanism of contact elimination, A contribution to understanding the function of polar catalysts, Angew. Chemie Int. Ed. 10 (1971) 172–181.

[27] C.K. Ingold, Structure and Mechanism in Organic Chemistry, in: second ed, Cornell University Press, London, 1969.

[28] A.M. Alsalme, P.V Wiper, Y.Z. Khimyak, E.F. Kozhevnikova, I.V. Kozhevnikov, Solid acid catalysts based on $H_3PW_{12}O_{40}$ heteropoly acid: Acid and catalytic properties at a gas-solid interface, J. Catal. 276 (2010) 181–189.

[29] W. Alharbi, E.F. Kozhevnikova, I.V. Kozhevnikov, Dehydration of methanol to dimethyl ether over heteropoly acid catalysts: The relationship between reaction rate and catalyst acid strength, ACS Catal. 5 (2015) 7186–7193.

[30] Y. Izumi, M. Ono, M. Kitagawa, M. Yoshida, K. Urabe, Silica-included heteropoly compounds as solid acid catalysts, Microporous Mater. 5 (1995) 255–262.

[31] Z. Buniazet, C. Lorentz, A. Cabiac, S. Maury, S. Loridant, Supported oxides catalysts for the dehydration of isobutanol into butenes: Relationships between acidic and catalytic properties, Mol. Catal. 451 (2018) 143–152.

[32] J. Zhang, M. Kanno, Y. Wang, H. Nishii, Y.K. Miura, Y. Kamiya, Changes in surface acidity of silica-supported dodecatungstosilicic acid in relation to the loading amount, J. Phys. Chem. C 115 (2011) 14762–14769.

[33] D.R. Lide, Handbook of chemistry and physics, eightieth ed., CRC Press, 2007.

[34] T. Kella, A.A. Vennathan, S. Dutta, S.S. Mal, D. Shee, Selective dehydration of 1-butanol to butenes over silica supported heteropolyacid catalysts: Mechanistic aspect, Mol. Catal. 516 (2021) 111975.

[35] P.B. Weisz, C.D. Prater, Interpretation of measurements in experimental catalysis, Adv. Catal. 6 (1954) 143–196.

[36] G.C. Bond, S.J. Frodsham, P. Jubb, E.F. Kozhevnikova, I.V. Kozhevnikov, Compensation effect in isopropanol dehydration over heteropoly acid catalysts at a gas-solid interface, J. Catal. 293 (2012) 158–164

[37] J. Schnee, E.M. Gaigneaux, Elucidating and exploiting the chemistry of Keggin heteropolyacids in the methanol-to-DME conversion: Enabling the bulk reaction thanks to operando Raman, Catal. Sci. Technol. 7 (2017) 817–830.

[38] J.G. Highfield, J.B. Moffat, Elucidation of the mechanism of dehydration of methanol over acid using infrared photoacoustic spectroscopy, J. Catal. 95 (1985) 108–119.

[39] Y. Izumi, K. Urabe, M. Onaka, Zeolite, Clay and Heteropoly Acid in Organic Reactions, Kodansha/VCH, Tokyo, 1992.

[40] S. Gao, C. Rhodes, J.B. Moffat, Ring-expansion of methylcyclopentane to cyclohexane and ring-contraction of cyclohexane to methylcyclopentane on silica-supported 12-

tungstophosphoric acid and stoichiometric and nonstoichiometric microporous silver 12-tungstophosphate, Catal. Lett. 55 (1998) 183–188.

[41] E.F. Kozhevnikova, I.V. Kozhevnikov, A calorimetric study of the acidity of bulk and silica-supported heteropoly acid $H_3PW_{12}O_{40}$, J. Catal. 224 (2004) 164–169.

[42] R.P. Bell, Chapter 10-Rates, equilibria, and structures in proton-transfers, in: R.P. Bell, The Proton in Chemistry, second ed., Springer US, 1973: pp. 194–225.

Chapter 6: Conclusions and future Work

Chapter 6 : Conclusions and future work

6.1. General conclusions

Dehydration of MeOH to dimethyl ether and EtOH to diethyl ether and ethene is of significant interest in relation to sustainable development. DME is a multimarket product, which has attracted interest as a supplement to liquefied petroleum gas (LPG) and a clean diesel alternative. The dehydration of EtOH has long been of interest to produce ethene and DEE from non-petroleum renewable feedstock. Ethene is the feedstock for about 30% of all petrochemicals, and DEE is a valuable chemical and a green fuel alternative.

In recent years, heteropoly acids have attracted much attention as catalysts for alcohol dehydration. HPAs exhibit higher catalytic activities than traditional acid catalysts such as zeolites and mixed oxides. Silica has been demonstrated to be the effective support for HPAs due to its neutral nature, large surface area, porosity and availability in a wide textural diversity. However, the knowledge about the silica-supported HPA catalysts has been limited, especially about the effect of HPA loading on the strength of proton sites in the SiO_2-supported HPA catalysts and their catalytic performance in alcohol dehydration and related reactions. Such information is very important for catalyst and process optimisation as well as for gaining mechanistic insights, for example, regarding the role of bulk versus surface catalysis in alcohol dehydration over HPA catalysts.

The aim of this study is to gain a more detailed knowledge of the acid properties of the silica-supported HPA catalysts, containing the strongest Keggin-type heteropoly acids, namely, HPW and HSiW, with a wide range of relevant to practice HPA loadings from 5 to 100%. This knowledge has been used for the investigation of dehydration of methanol and ethanol over HPA/SiO_2 catalysts in order to optimise catalyst performance and gain new mechanistic

insights. In addition, DEE elimination to ethanol and ethene, which is a step-in ethanol dehydration, has been studied in the presence of HPA/SiO_2 catalysts.

In Chapter 3 of this thesis, the acid properties of bulk and 5–70% SiO_2-supported HPAs HPW and HSiW were elucidated. The acidity of the catalysts was systematically characterised at a gas-solid interface through use of NH_3-MC, and these results were complemented by textural and structural catalyst characterisation through use of BET, XRD and FTIR. BET analysis showed that the HPA in these catalysts was mainly localised on the external surface and in macropores rather than within meso- and micropores of the support. Use of XRD showed that, at similar HPA loadings, HSiW was more widely dispersed on the silica surface than HPW. As a result, HSiW/SiO_2 catalysts were understood to have a higher density of surface proton sites than HPW/SiO_2 due to the higher dispersion of HSiW and because HSiW has more protons per Keggin unit. It was demonstrated that the acid strength of HPA/SiO_2 catalysts increased monotonically with HPA loading, with HPW being stronger than HSiW at any HPA loading. Moreover, the acid strength increased linearly above 10% HPA loading and could be determined using a linear regression for HPA loadings.

In Chapter 4, the effects of HPA loading and acid strength were examined in the dehydration of MeOH and EtOH over HPA/SiO_2 catalysts at a wide range of HPA loadings (5–100%). The catalysts were prepared by HPA impregnation from water and MeOH. HSiW and HPW catalysts showed close catalytic activities per HPA weight; HSiW showed slightly higher activity than HPW despite its weaker acid strength. This can be described in terms of its larger number of protons per Keggin unit and the higher dispersion of HSiW compared with HPW. The turnover reaction rate for HPW catalysts was higher than that for HSiW catalysts, in agreement with their acid strength. The catalysts that were prepared from water and MeOH had very close acid strengths and exhibited similar activities in alcohol dehydration.

It was established that the steady-state catalyst activity correlated with the surface proton-site density of silica-supported HPA catalysts rather than with the HPA loading or HPA acid strength. This indicates that alcohol dehydration occurs via the mechanism of surface-type HPA catalysis at the gas-solid interface rather than bulk-type (pseudo-homogeneous) HPA catalysis. This conclusion was further strengthened by fitting the activity of bulk HPW and HSiW into the activity-acid strength relationship for supported HPA catalysts operating via surface-type catalysis.

The work described in Chapter 5 concluded that DEE is the key intermediate of EtOH-to-ethene dehydration. In the presence of acid catalysts, DEE undergoes elimination to produce ethene and EtOH; the latter dehydrates to ethene. The elimination of DEE was examined at the gas-solid interface at 130–250 °C and ambient pressure over various bulk and supported Brønsted solid-acid catalysts that were based on tungsten Keggin HPAs. The most active HPA catalysts were found to be silica-supported HPW and HSiW and the bulk heteropoly salt CsPW provided a 95–98% ethene yield at 220 ^{o}C and a WHSV of 2.2 h^{-1}. The HPA catalysts outperformed the best reported zeolite catalysts such as HZSM-5 and USY; these have been shown to produce the same yield but at temperatures about 100 ^{o}C higher than the temperatures required for best performance of the HPA catalysts.

A Brønsted correlation between the turnover catalyst activity and the acid strength of each catalyst was established. This correlation indicated that Brønsted acid sites played a significant role in the elimination of DEE over HPA catalysts. The results obtained point to the occurrence of the DEE conversion through the consecutive reaction pathway DEE → C_2H_4 + EtOH followed by EtOH → C_2H_4 + H_2O, in which ethene is both a primary product of DEE elimination and a secondary product via dehydration of the primary product EtOH. Evidence

was provided that DEE elimination over bulk HPA and high-loaded HPA/SiO_2 catalysts proceeded via the surface-type mechanism.

6.2. Future work

Despite the compelling data that are presented in this thesis, additional characterisation is required to understand the precise structure and composition of surface species on the HPA/SiO_2 catalysts. Such characterisation would also be beneficial to clarify the precise nature of the acid sites in HPA/SiO_2 catalysts.

This study has increased our understanding of the Brønsted acid catalysts HPA/SiO_2. However, the work that was performed for this thesis was focused on silica-supported HPA catalysts that used one silica support-commercial Aerosil 300 from Degussa. In the future, it would be interesting to expand the range of silica supports to include materials that show different textural properties, in particular those with various surface areas and pore sizes. In this context, we could prepare these catalysts by the wet impregnation method at optimum loading that was found in this study (25-30%). In addition, we could investigate the acid properties of these catalysts and explain how the textural variety of support affected the acidity and activity of the catalysts.

Moreover, since HPA/SiO_2 is an efficient catalyst for dehydration of EtOH and MeOH, it could be tested with other alcohol substrates, e.g., butanol. The application of HPA/SiO_2 for dehydration of butanol to butene may also be attractive as a route to fulfil demand for petrochemical feedstock and fuel additives.

On the other hand, the 15% TiO_2 and ZrO_2-supported HPW catalysts that were studied did not show high activity in the DEE elimination and alcohol dehydration reactions [1,2]. This may have occurred due to a low density of available surface protons and/or weak catalyst acidity. It would be interesting to carry out a systematic investigation of the acidic and catalytic

properties of these catalysts (HPW, HSiW) with a wide range of HPA loadings that are relevant to practice.

Reference

[1] W. Alharbi, E. Brown, E.F. Kozhevnikova, I.V. Kozhevnikov, Dehydration of ethanol over heteropoly acid catalysts in the gas phase, J. Catal. 319 (2014) 174–181.

[2] W. Alharbi, E.F. Kozhevnikova, I.V. Kozhevnikov, Dehydration of methanol to dimethyl ether over heteropoly acid catalysts: The relationship between reaction rate and catalyst acid strength, ACS Catal. 5 (2015) 7186–7193.

Appendix

Chapter 7 : Appendix

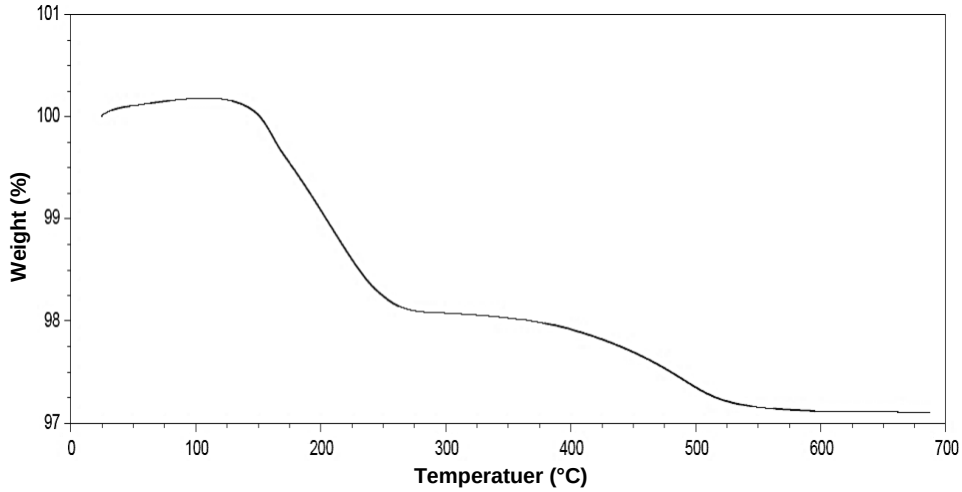

Figure 7.1. TGA of bulk $H_3PW_{12}O_{40}$ after pre–treatment at 150 °C/10^{-3} kPa for 1.5 h (3% weight loss to 600 °C).

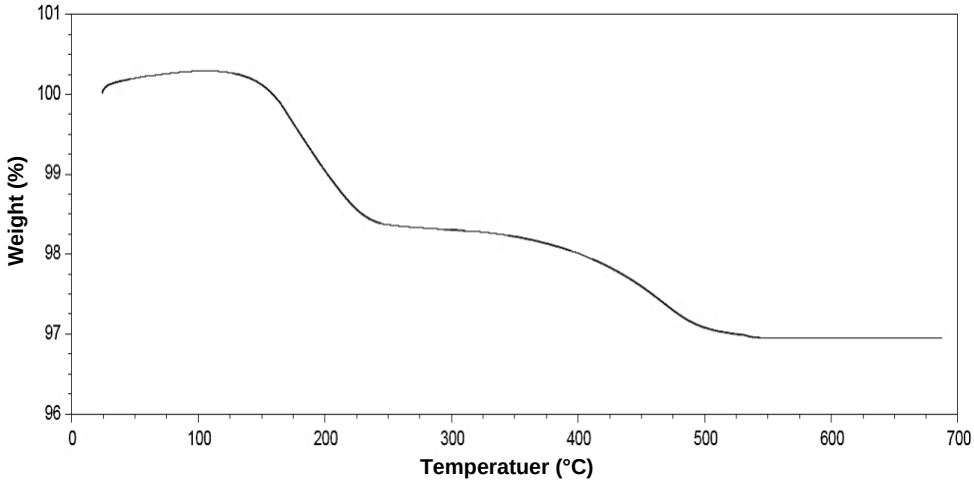

Figure 7.2. TGA of bulk $H_4SiW_{12}O_{40}$ after pre–treatment at 150 °C/10^{-3} kPa for 1.5 h (3% weight loss to 600 °C).

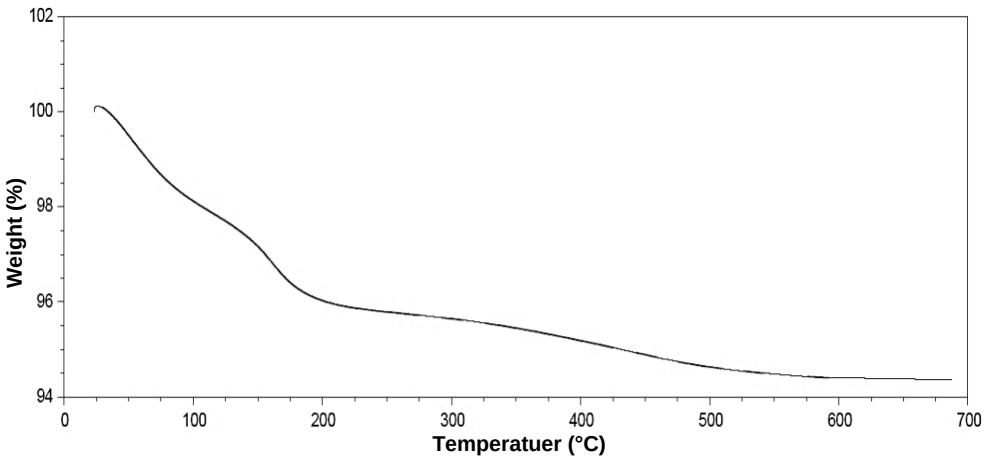

Figure 7.3. TGA of 45%HPW/SiO_2 after pre–treatment at 150 °C/10^{-3} kPa for 1.5 h (5.7% weight loss to 600 °C).

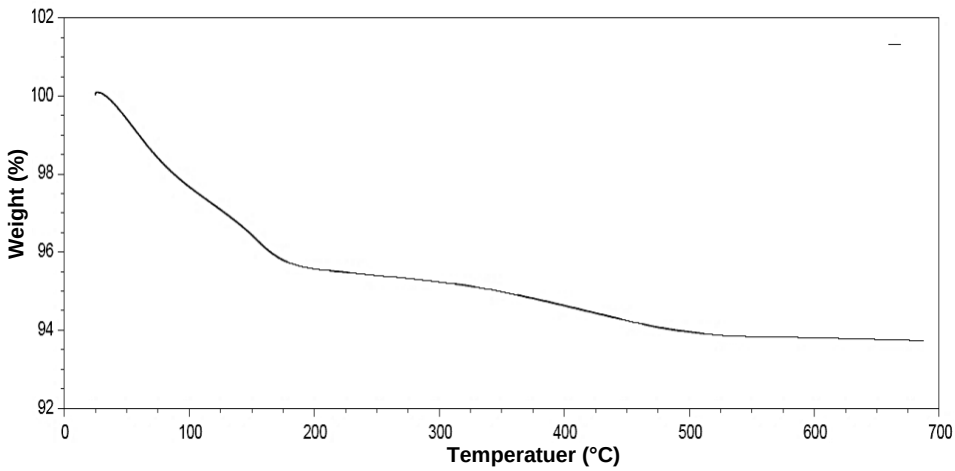

Figure 7.4. TGA of 46%HSiW/SiO_2 after pre–treatment at 150 °C/10^{-3} kPa for 1.5 h (6% weight loss to 600 °C).

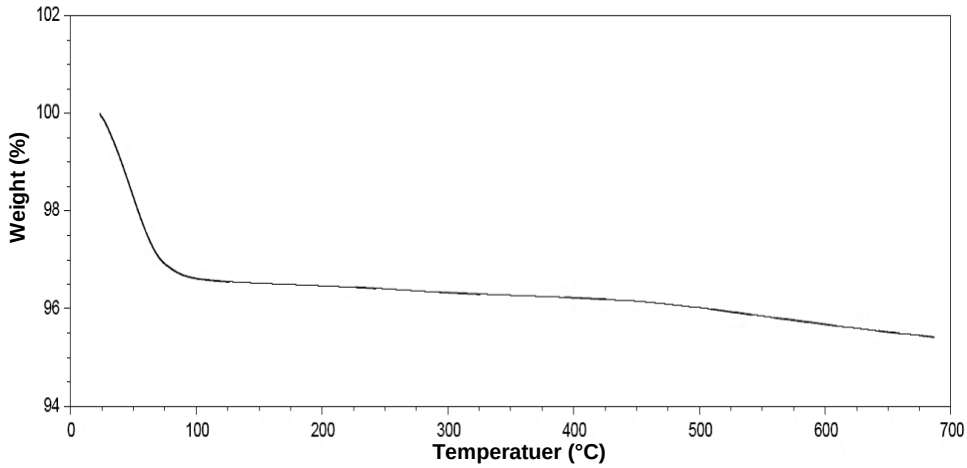

Figure 7.5. TGA of pure compacted SiO_2 under N_2 flow after pre–treatment at 150 °C/10^{-3} kPa for 1.5 h (4% weight loss to 600 °C).

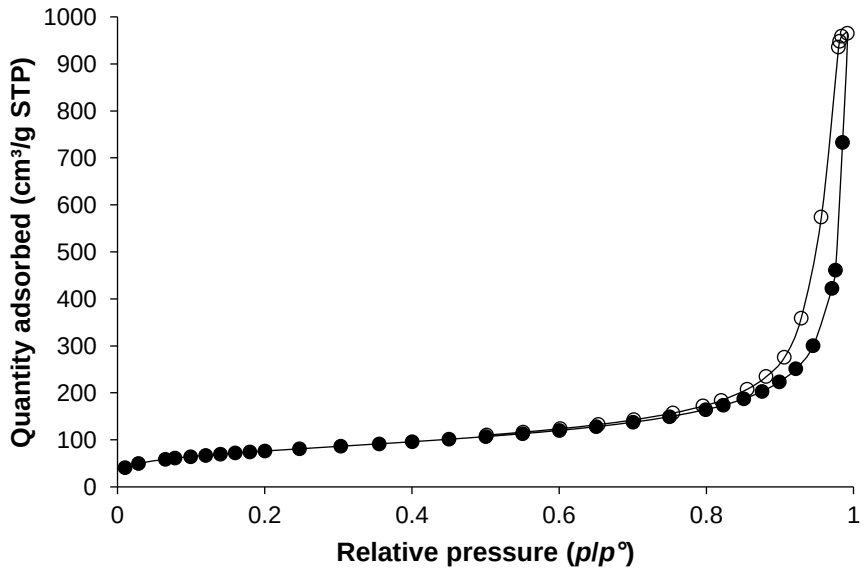

Figure 7.6. N_2 adsorption (solid circles) and desorption (open circles) isotherms of SiO_2(m).

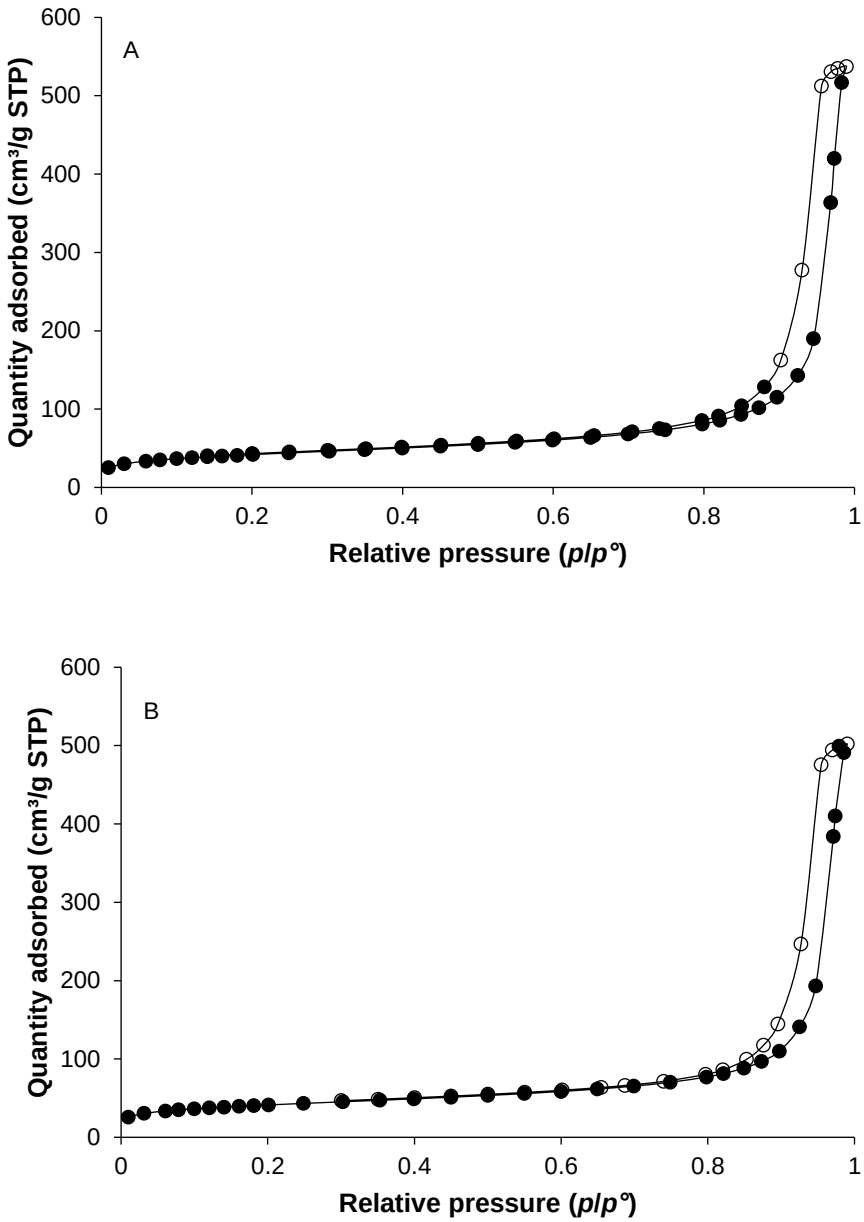

Figure 7.7. N_2 adsorption (solid circles) and desorption (open circles) isotherms of: (A) 45%HPW/SiO_2 and (B) 46%HSiW/SiO_2.

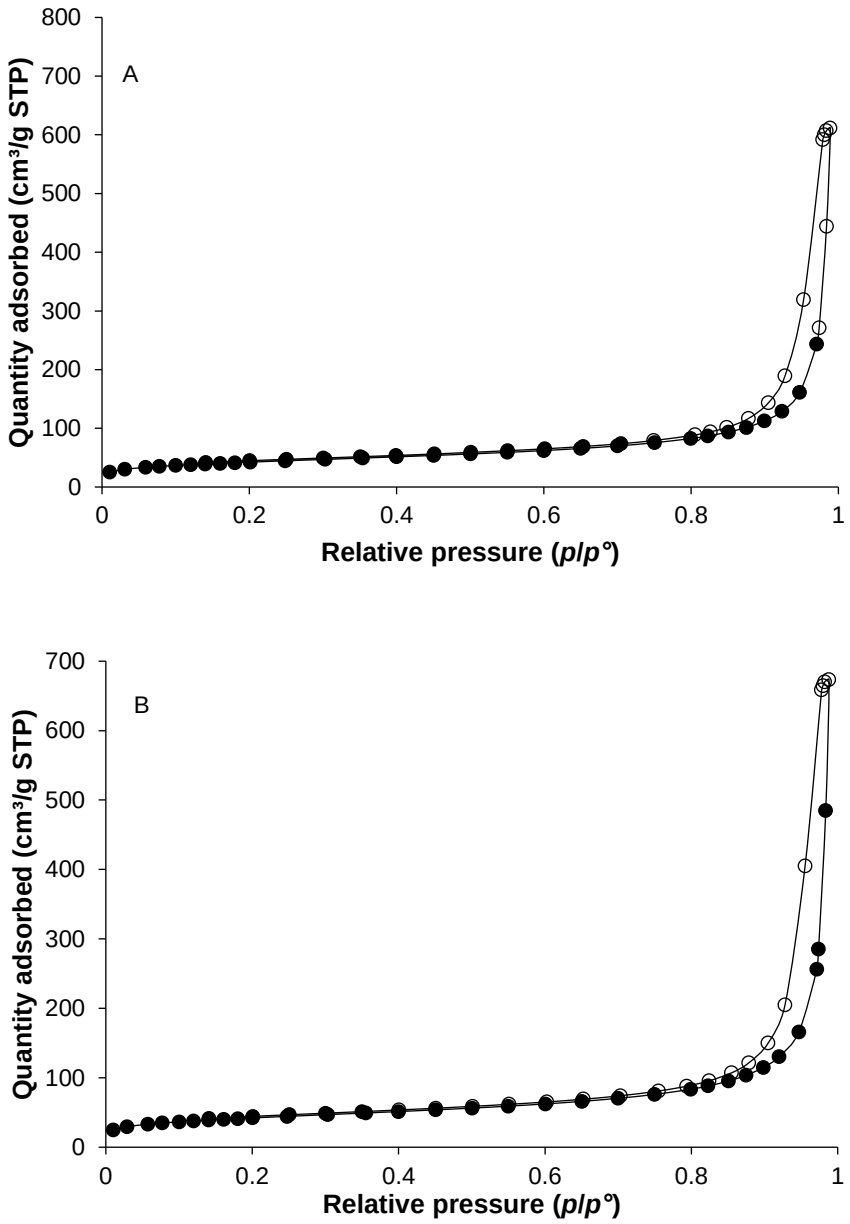

Figure 7.8. N_2 adsorption (solid circles) and desorption (open circles) isotherms of (A) 48%HPW/SiO_2(m) and (B) 44%HSiW/SiO_2(m).

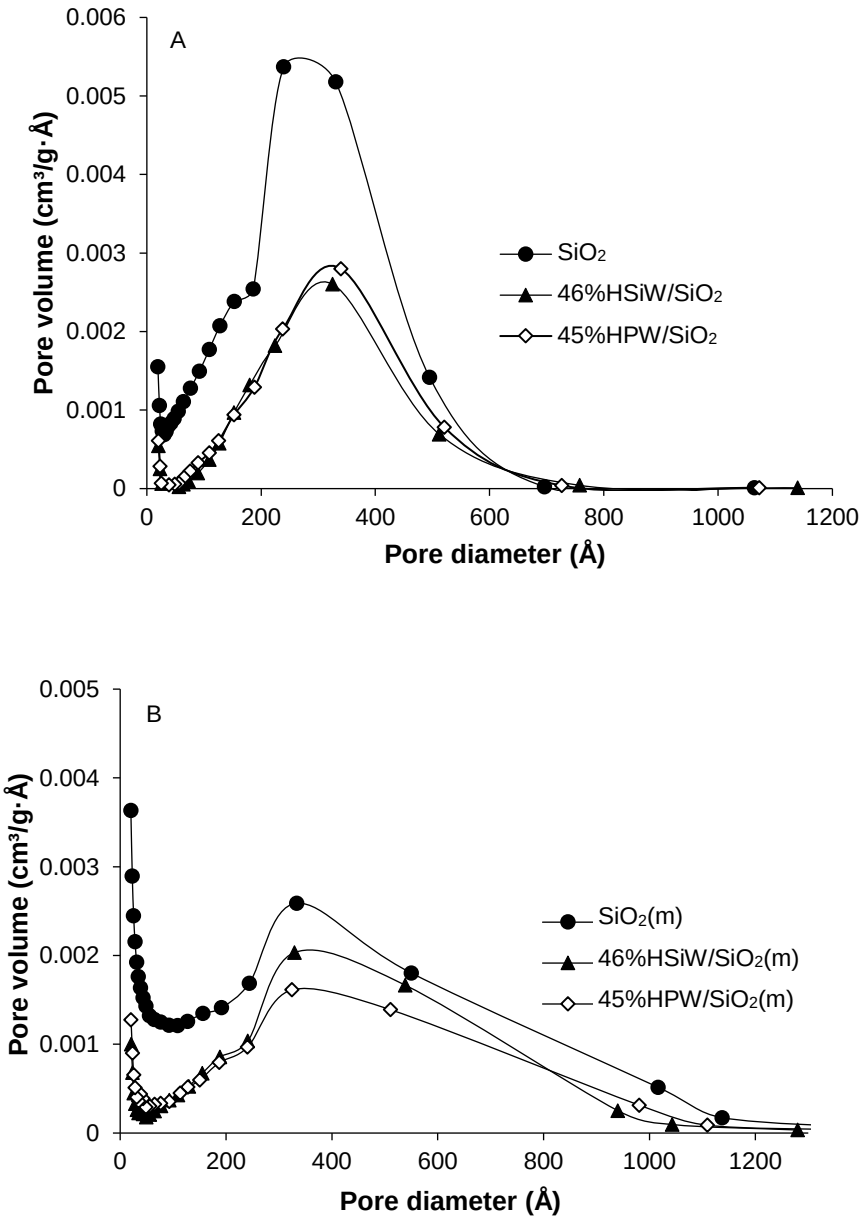

Figure 7.9. Pore size distribution for (A) HPA/SiO_2 and (B) HPA/SiO_2(m) catalysts.

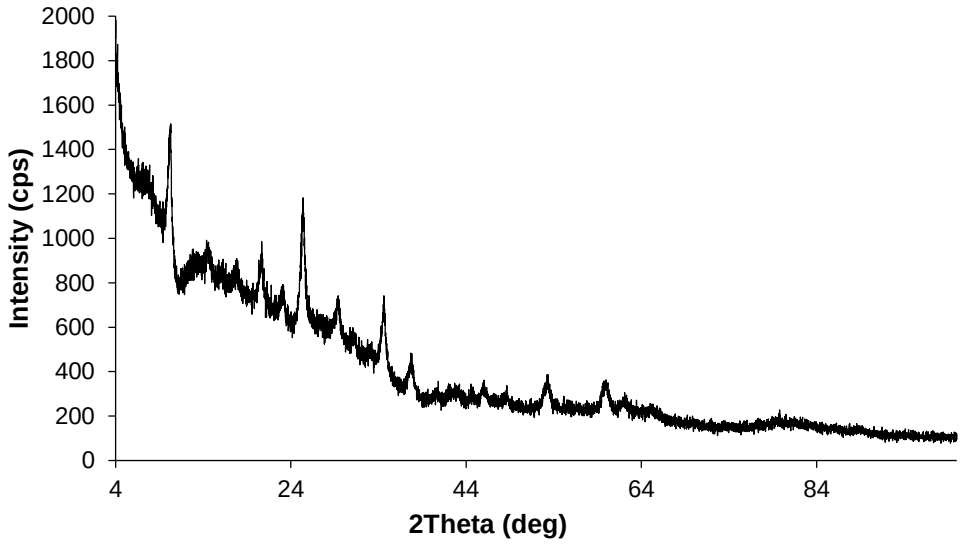

Figure 7.10. XRD patterns of spent 26%HPW/SiO_2 catalyst after MeOH dehydration at (0.20 g catalyst, 120 °C, 3.83 kPa MeOH pressure, 20 mL min^{-1} N_2 flow rate, contact time W/F = 105 g h mol^{-1}, 4 h time on stream: 100% DME selectivity in all cases).

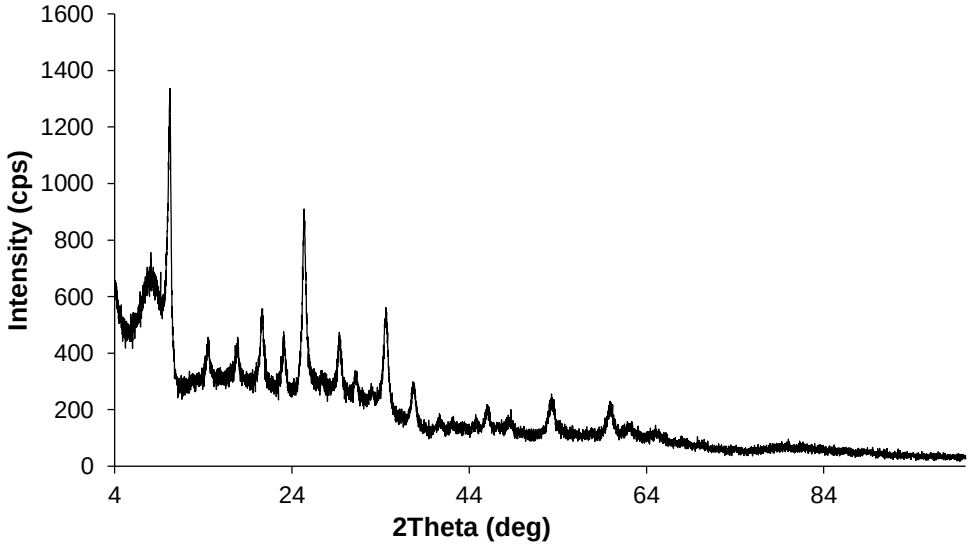

Figure 7.11. XRD patterns of spent 46%HSiW/SiO_2 catalyst after MeOH dehydration at (0.20 g catalyst, 120 °C, 3.83 kPa MeOH pressure, 20 mL min^{-1} N_2 flow rate, contact time *W/F* = 105 g h mol^{-1}, 4 h time on stream: 100% DME selectivity in all cases).

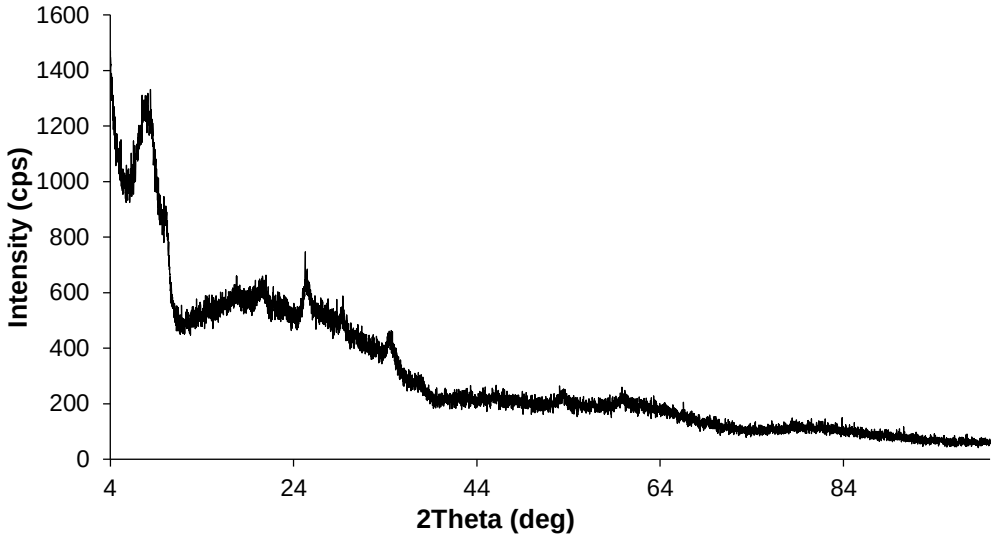

Figure 7.12. XRD patterns of spent 27%HSiW/SiO_2 catalyst after MeOH dehydration at (0.20 g catalyst, 120 °C, 3.83 kPa MeOH pressure, 20 mL min^{-1} N_2 flow rate, contact time *W/F* = 105 g h mol^{-1}, 4 h time on stream: 100% DME selectivity in all cases).

Table 7.1. Particle size of spent HPA/SiO_2 catalysts after MeOH dehydration.[a]

Catalyst	HPA particle size (± 1 nm)
Spent 26%HPW/SiO_2	14
Spent 27%HSiW/SiO_2	10
Spent 46%HSiW/SiO_2	16

[a] (0.20 g catalyst, 120 °C, 3.83 kPa MeOH pressure, 20 mL min^{-1} N_2 flow rate, contact time *W/F* = 105 g h mol^{-1}, 4 h time on stream: 100% DME selectivity in all cases).

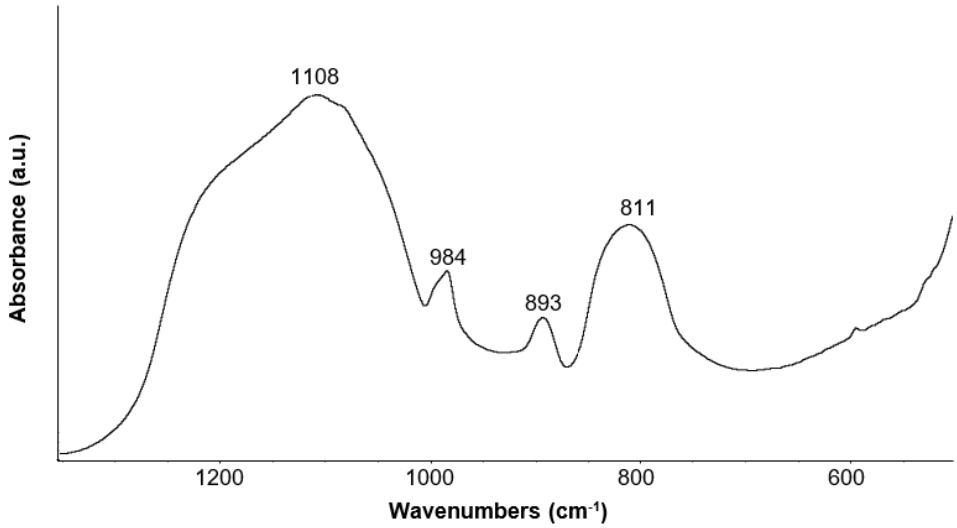

Figure 7.13. DRIFT spectra of spent 26%HPW/SiO_2 catalyst after MeOH dehydration (0.20 g catalyst, 120 °C, 3.83 kPa MeOH pressure, 20 mL min^{-1} N_2 flow rate, contact time *W/F* = 105 g h mol^{-1}, 4 h time on stream: 100% DME selectivity in all cases).

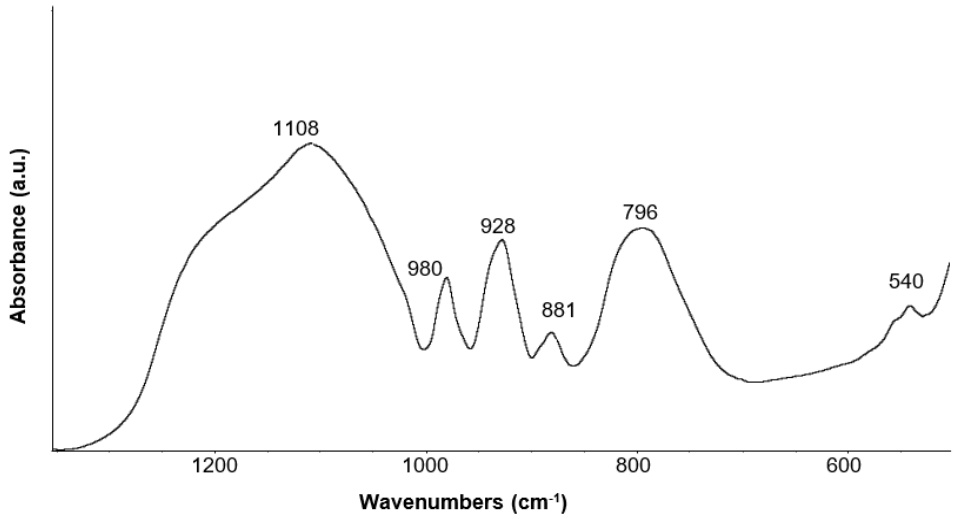

Figure 7.14. DRIFT spectra of spent 46%HSiW/SiO_2 catalyst after MeOH dehydration (0.20 g catalyst, 120 °C, 3.83 kPa MeOH pressure, 20 mL min^{-1} N_2 flow rate, contact time *W/F* = 105 g h mol^{-1}, 4 h time on stream: 100% DME selectivity in all cases).

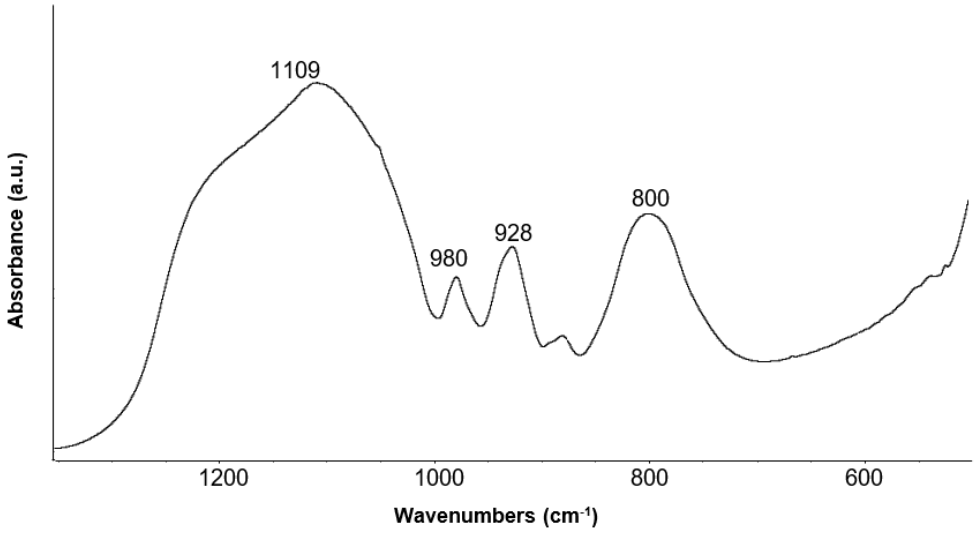

Figure 7.15. DRIFT spectra of spent 27%HSiW/SiO_2 catalyst after MeOH dehydration (0.20 g catalyst, 120 °C, 3.83 kPa MeOH pressure, 20 mL min^{-1} N_2 flow rate, contact time *W/F* = 105 g h mol^{-1}, 4 h time on stream: 100% DME selectivity in all cases).

Table 7.2. Texture of commercial zeolites.

Catalyst[a]	Surface area[b] (m^2/g)	Pore volume[c] (cm^3/g)	Pore diameter[d] (Å)
HZSM-5 (47)	411	0.26	26
HZSM-5 (12)	378	0.22	24

[a] Zeolites were calcined for 2 h at 500 °C in air; prior to BET analysis, the catalysts pre–treated at 250 °C in vacuum [b] BET surface area [c] Single point total pore volume [d] Average BET pore diameter.

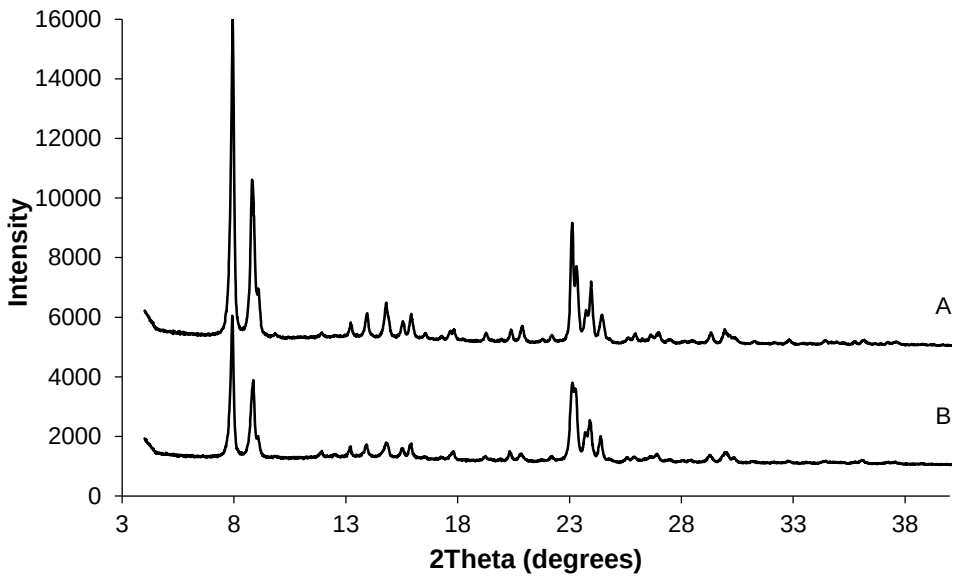

Figure 7.16. XRD patterns for HZSM-5 with Si/Al: (A) 47, (B) 12.

Weisz–Prater analysis

The Weisz–Prater criterion, C_{WP} (Eq. (7.1)), uses measured values of reaction rate to determine if internal diffusion is limiting the reaction [1]. If $C_{WP} << 1$, there are no diffusion limitations; when $C_{WP} >> 1$, internal diffusion strongly limits the reaction.

$$C_{WP} = \frac{r\rho l^2}{DC_b} \quad \textbf{(7.1)}$$

Here, r is the reaction rate per unit catalyst weight (mol $g^{-1}s^{-1}$), ρ is the bulk density of catalyst (g cm^{-3}), l is the radius of catalyst particle (cm), D is the effective diffusion coefficient (cm^2s^{-1}) and C_b is the bulk concentration of substrate in the feed (mol cm^{-3}).

For DEE elimination on 17%HPW/SiO_2 at 150 ºC and 12 kPa DEE partial pressure, the rate $r = XF/W = 1.99\cdot10^{-3}$ mol $g^{-1}h^{-1} = 5.53\cdot10^{-7}$ mol $g^{-1}s^{-1}$ (Figure 5.12 in Chapter 5). Other parameters are as follows: $\rho = 0.39$ g cm^{-3} , $l = 0.56\cdot10^{-2}$ cm (average particle radius for the catalyst with 45–180 µm diameter of catalyst particles) and $C_b = 3.5\cdot10^{-6}$ mol cm^{-3} at 150 ºC. The catalyst had a pore diameter of 15.8 nm in mesoporous range (Table 5.1). The Knudsen

diffusion coefficient D for transport of DEE molecules into the pore was calculated using Eq. (7.2) [2]:

$$D = \left(\frac{d}{3}\right)\left(\frac{8RT}{\pi M}\right)^{1/2} \quad \textbf{(7.2)}$$

where R is the gas constant (8.314 J $K^{-1}mol^{-1}$), T is the temperature (423.15 K), M is the DEE molecular mass (0.074 kg mol^{-1}) and d is the mean pore diameter ($15.8 \cdot 10^{-9}$ m). From this equation, $D = 1.8 \cdot 10^{-7}$ m^2s^{-1} = $1.8 \cdot 10^{-2}$ cm^2s^{-1}. Overall, from Eq. (7.1) this gives $C_{WP} = 1.1 \cdot 10^{-4} << 1$, which indicates no internal diffusion limitations.

References

[1] P.B. Weisz, C.D. Prater, Interpretation of measurements in experimental catalysis, Adv. Catal. 6 (1954) 143–196.

[2] M.B. King, J.M. Winterbottom, Kinetics of homogeneous reactions and of reactions on solid catalyst surfaces, in: J.M. Winterbottom, M.B. King (Eds.), Reactor Design for Chemical Engineer, CRC Press, London, 1999: p. 77.